# Photodestruction and Growth of Interstellar Polycyclic Aromatic Hydrocarbons

von
Dipl.–Phys. Thierry Allain
aus Oran (Algerien)

Vom Fachbereich 04 (Physik)
der Technischen Universität Berlin
zur Erlangung des akademischen Grades

Doktor der Naturwissenschaften (Dr. rer. nat.)

genehmigte Dissertation

Berlin 1996

D 83

Promotionsausschuß:
Prof. Dr. Wolfgang Richter (Vorsitzender)
Prof. Dr. Erwin Sedlmayr (Berichter)
Priv.-Doz. Dr. Jens Peter Kaufmann (Berichter)
Dr. Sydney Leach (Berichter)
Prof. Dr. Philippe Bréchignac

Tag der mündlichen Prüfung: 26. 4. 1996

*A Ulrike et à notre petite Julie*

# Zusammenfassung

Die Entdeckung einer Reihe von Emissionsbanden in den Infrarot–Spektren von verschiedenen Quellen, die durch ein starkes UV Strahlungsfeld charakterisiert sind (Aktive Galaxien, Reflektionsnebel, Planetarische Nebel, HII Regionen, ...), gaben den Anlaß zu einem der aufregendsten Rätsel der modernen Astrophysik (Gillet et al. 1973). Bis 1984 konnten keine überzeugenden Szenarien zur Erklärung des kompletten Satzes von Emissionsbanden gefunden werden und so wurden diese Emissionsbanden in der Astrophysik bekannt unter dem Namen "Unidentified Infrared" (UIR) Banden. Als erste bemerkten Léger und Puget (1984) sowie Allamandola et al. (1985) die Übereinstimmung zwischen den infrarot Vibrationsmoden der Polyaromatischen Kohlenwasserstoffe (PAHs) und den UIR Banden. Sie schlugen daher vor, daß freie PAHs die Träger der UIR Banden seien. Ausgehend von dieser Annahme leiteten diese Autoren eine hohe Häufigkeit von PAHs im Interstellaren Medium (ISM) ab. Jedoch ist die Zuordnung der UIR Banden zu den Vibrationsbanden freier PAHs immer noch fraglich und es wurden auch andere Vorschläge zur Erklärung der UIR Banden gemacht. Mit anderen Worten ist die Existenz großer Mengen an PAHs im Universum immer noch eine nicht entschiedene Streitfrage in der astrophysikalischen Gemeinschaft.

Das Anliegen der vorliegenden Dissertation ist es, unabhängig von astronomischen Beobachtungen neue Informationen über interstellare PAHs zu bekommen. Es sollen ausschließlich experimentelle Ergebnisse und theoretische Rechnungen verwendet werden, mit dem Ziel die charakteristischen Eigenschaften von PAHs zu bestimmen, die in der Lage sind, unter den physikalischen Bedingungen des ISM zu überleben. Die Rechnungen werden einerseits für die Regionen in denen die UIR Banden beobachtet sind, und andererseits für die zirkumstellaren Hüllen (ZSH) von C-Sternen, für die seit 1983 bekannt ist, daß sich dort PAHs bilden (Keller & Sedlmayr 1983), durchgeführt.

Im ersten Teil der Arbeit werden Photozerstörungsraten für PAHs in der ISM berechnet, wobei experimentelle Ergebnisse von Jochims et al. (1994) verwendet werden. Dabei werden astrophysikalisch relevante Raten, d.h. integriert über das interstellare Strahlungsfeld, für die Photodissoziation von Wasserstoff und Azethylen von PAH Molekülen abgeleitet.

Da häufig angenommen wird, daß PAHs unter den Bedingungen in der ISM möglicherweise ionisiert und teilweise dehydriert sind, wird eine Methode entwickelt, die simultan die Wasserstoffsättigung sowie den Ionisationsgrad der PAHs berechnen kann. Dieses Verfahren wird für die astrophysikalischen Bedingungen angewendet, unter denen UIR Banden beobachtet werden.

Um die Photodissoziation dieser ionisierten und teilweise dehydrierten PAHs zu studieren, wird ein Modell entwickelt, das den Ansatz, der für PAH Moleküle benutzt wird, auf PAH Kationen und PAHs mit geringer Wasserstoffsättigung erweitert. Es wird gezeigt, daß die Photodissoziation von Wasserstoff und Kohlenstoffteilchen von ionisierten und teilweise dehydrierten PAHs größer ist als die ihrer entsprechenden Moleküle. Dies gilt insbesondere für teilweise dehydrierte PAHs, die sehr instabil gegenüber Photozerstörung sind. Vergleicht man die Rate für Photodissoziation von Azethylen mit der ihrer Rückrate, d.h. Anlagerung von Kohlenstoffteilchen, so kann man daraus schließen, daß nur PAHs mit mehr als 50 Kohlenstoffatomen in der Lage sind, das UV Strahlungsfeld in den Regionen zu überleben, die UIR Banden zeigen.

Da PAHs mit 50 und mehr Kohlenstoffatomen in der ISM möglicherweise überleben können, ist es sinnvoll die Regionen zu studieren, in denen sie sich bilden und in denen sie wachsen. Der zweite Teil dieser Dissertation befaßt sich daher mit PAHs in zirkumstellaren Hüllen. Zur Untersuchung diese Problems werden die stationären Windmodelle für staubbildende zirkumstellare Hüllen um späte C–Sterne verwendet, die am Institut für Astronomie und Astrophysik der TU Berlin entwickelt wurden. Insbesondere wird dabei ein Model für IRC+10216 verwendet (Winters et al. 1994, Winters 1994), dem nächsten und am häufigsten untersuchten kohlenstoffreichen Roten Riesen.

Alle Prozesse, die PAH Bildung begünstigen, werden untersucht. Auf der Basis dieser Untersuchungen wird dann die Dichte kleiner PAHs abgeschätzt. Es wird dabei bestätigt, daß PAHs durch aufeinanderfolgende Wasserstoffabstreif– sowie Azethylenanlagerungsreaktionen bis zu makroskopischer Größe wachsen. Der Übergang von PAHs zu Staubteilchen wird numerisch untersucht, mit dem Ergebnis, daß PAHs möglicherweise die Keime für Staubteilchen darstellen.

Außerdem werden die Prozesse untersucht, denen die PAHs unterliegen, wenn sie die äußeren Bereiche der zirkumstellaren Hülle erreichen. Um verläßliche Berechnungen zu ermöglichen, werden neue Werte für die optische Tiefe im Staub sowie in den Molekülen in den Hüllen von C–Sternen berechnet. Unter Verwendung dieser Ergebnisse werden die PAH–Ionisation und Hydrierungszustände für IRC+10216 abgeschätzt. Das Wachstum durch die Anlagerung von $C^+$ sowie die Photozerstörung von PAHs werden mit dem Ziel untersucht, die Größenverteilung der PAHs abzuschätzten, die an die ISM abgegeben werden. Obwohl gezeigt werden kann, daß die Wachstums– und Zerstörungsprozesse schnell genug erfolgen, um die PAH Größenverteilung auf dem Weg vom Innern der Hülle bis zur ISM zu modifizieren, kann aufgrund des Fehlens von Daten bzgl. der Prozesse, die nach dem Stoß zwischen PAHs und $C^+$ auftreten, nicht endgültig entschieden werden, wie die Größenverteilungsfunktion der PAHs am Übergang in die ISM aussieht.

Eine direkte Anwendung dieser Arbeit ist die theoretische Abschätzung der Dichte von PAHs in der ISM. Dies ergibt sich einfach aus dem Gleichgewicht der Prozesse, die zum Anreichern mit PAHs (Bildung und Wachstum in situ, Beiträge von C–Sterne, Stoß wellen) bzw. zum Verschwinden von PAHs (Photozerstörung, Stoß mit Gasteilchen, sputtering) führen. Mit Hilfe dieser Arbeit und weiterer experimenteller Untersuchungen wird es möglich sein zu entscheiden, ob PAHs so ein allgegenwärtiger und häufiger Bestandteil der ISM sind, wie es die Beobachtungen implizieren.

# Abstract

The discovery of a series of emission bands in the infrared spectra of various sources characterized by a strong ultraviolet radiation field (active galaxies, reflexion nebulae, planetary nebulae, HII regions, ...) has recently given rise to one of the most exciting puzzle of modern Astrophysics (Gillet et al. 1973). Until 1984 there were indeed no convincing explanation to account for the complete set of emission bands and they have therefore become famous in Astrophysics under the appellation of "Unidentified InfraRed" (UIR) Bands. Léger & Puget (1984) and Allamandola et al. (1985) first noticed the good match between the infrared vibrational modes of polycyclic aromatic hydrocarbons (PAHs) and the UIR bands and, thus, concluded that free PAHs could be the carriers of the UIR bands. With this assumption these authors deduced a large abundance of PAHs in the interstellar medium (ISM). However, the assignement of the UIR bands to the vibrational modes of free PAHs is still questioned and some other valuable proposals have been made to account for the UIR bands. In other words, the presence of large amounts of PAHs in space is still a matter of debate in the astrophysical community.

The philosophy of the present thesis is to get new information about interstellar PAHs independently of astronomical observations. Only experimental results and theoretical calculations are used with the purpose to determine the characteristical properties of the PAHs capable to survive under the conditions of the ISM. The calculations are carried out, in a first part, in the regions where the UIR bands are seen, and in a second part, in the circumstellar envelopes (CSE) of C–stars where it is known since 1983 that PAHs favourably form and grow (Keller & Sedlmayr 1983).

In the first part PAH photodestruction rates in the ISM are calculated by use of the experimental results of Jochims et al. (1994). As a result, astrophysically relevant rates – that is to say, integrated over the interstellar radiation field – are derived for the photoejection of hydrogen and acetylene from PAH molecules.

Since it is usually argued that PAHs are probably ionized and partially dehydrogenated under the conditions of the ISM, a method for evaluating simultaneously the hydrogen coverage and the degree of ionization of interstellar PAHs is developed and applied to the astrophysical media where the UIR bands are observed.

In order to study the photoejection rates of these ionized and partially dehydrogenated PAHs, a model is developed by extending the approach used for PAH molecules to PAH cations and to PAH with low hydrogen coverage. The rates for photoejection of hydrogen and carbon particles from ionized and partially dehydrogenated PAHs are proved to be

higher that those of their parent molecules, especially for the partially dehydrogenated PAHs which are very unstable against photodestruction. Comparing the rate for photoejection of acetylene to that of the reverse process, accretion of carbon particles, leads to the conclusion that only PAHs containing more than 50 carbon atoms are able to resist the ultraviolet radiation field in the regions showing the UIR bands.

Since PAHs with more than 50 carbon atoms can possibly survive in the ISM, it is worth studying the regions where they form and grow. It is therefore the aim of the second part of this thesis to deal with PAHs in circumstellar environments. For this purpose, the stationary models for dust forming circumstellar shells of C–giants developed at the Institute of Astronomy and Astrophysics of the Technical University Berlin are used, especially the model for the shell of IRC+10216, which is the nearest and most studied carbon–rich red giant (Winters et al. 1994, Winters 1994).

The physical processes which could favour PAH formation in the CSEs of carbon–rich red giants are analyzed. On the basis of these results, the density of small PAHs are evaluated. Thereby, it is also confirmed that PAHs rapidly growth by succesive hydrogen abstraction and addition of acetylene molecules, up to macroscopic sizes. The link between PAHs and dust particles is studied numerically, with the result that PAHs could possibly be the seeds for dust grains.

The processes undergone by PAHs when they reach the outer part of the circumstellar envelopes are also investigated. To allow for reliable calculations, new values are calculated for the dust and molecular optical depths in the envelopes of C–stars. Using these results, the PAH ionization and hydrogenation states are estimated in the envelope of IRC+10216. The growth via $C^+$ accretion and the photodestruction of PAHs are also studied with the aim of estimating the size distribution of the PAHs ejected into the ISM. Although it is demonstrated that the growth and destruction processes are rapid enough to modify the PAH size distribution along their way from the star outwards to the ISM, no definite conclusions can be drawn because of the lack of data concerning the yields of the processes which occur after the collision between PAHs and $C^+$.

A direct application of the present work is the theoretical estimate of the density of PAHs in the ISM. This simply results from the balance of all the processes contributing to the input of PAHs (formation and growth in situ, contribution of C–stars, of shock waves) and to the disappearance of PAHs (photodestruction, collision with dust particles, sputtering). This work and further experimental investigation will make such a study possible and, thus, will allow to test whether PAHs are as ubiquitous and abundant as observations imply.

# Résumé

La découverte d'une série de bandes d'émission dans le spectre infrarouge de différents objets astronomiques associés à de forts rayonnements ultraviolets (galaxies actives, nébuleuse à réflexion, nébuleuses planétaires, régions HII, ... ) a donné naissance à l'une des plus passionnantes énigme de l'astrophysique contemporaine. Jusqu'en 1984, aucun candidat convaincant n'a pu être trouvé qui explique l'ensemble des bandes d'emission et, pour cette raison, elle sont devenues célèbres en astrophysique sous le nom de bandes InfraRouge Non–identifiées (UIR). Léger & Puget (1984) et Allamandola et al. (1985) ont été les premiers à constater la bonne correspondance entre les bandes UIR et les modes de vibrations des Hydrocarbures Polycycliques Aromatiques (PAHs), et ainsi, à conclure que les PAHs pourraient être les porteurs des bandes UIR. Sous cette hypothèse, ils déduisirent une forte abondance de PAHs dans le milieu interstellaire (MIS). Pourtant, l'attribution des bandes UIR aux modes de vibration des PAHs est encore mise en doute et d'autres propositions ont été faites pour rendre compte des bandes UIR. En d'autres termes, la présence de grandes quantités de PAHs dans l'espace reste un vif sujet de discussion dans la communauté astronomique.

La philosophie de la présente thèse est d'acquérir de nouvelles connaissances sur les PAHs interstellaires indépendamment des observations astronomiques. Seuls des résultats expérimentaux et des calculs théoriques sont employés dans le but de déterminer les propriétés caractéristiques des PAHs capables de survivre dans les conditions du MIS. Les calculs sont menés, dans une première partie, dans les régions où les bandes UIR ont été observées, et dans une seconde partie, dans les envelopes circumstellaires (ECSs) d'étoiles de type C, où il est reconnu depuis 1983 que les PAHs peuvent se former et croitre (Keller & Sedlmayr 1983).

Dans la première partie les taux de photodestruction des PAHs dans le MIS sont calculés sur la base des résultats expérimentaux de Jochims et al. (1994). Ainsi, les premiers taux de photodestruction directement utilisables en astrophysique – c'est à dire intégrés sur le champ de radiation interstellaire – sont calculés pour l'éjection d'hydrogène et d'acétylène par des PAHs.

Comme il est souvent soutenu qu'une partie des PAHs interstellaires sont éventuellement ionisés et déhydrogénés, une méthode de calcul est développée qui permet d'évaluer simultanément le taux d'hydrogènation et d'ionisation das PAHs interstellaires. Cette méthode est appliquée au cas des milieux où les bandes UIR sont observées.

Afin d'étudier les taux de photodestruction des PAHs ionisés et des PAHs partiellement

déhydrogènés, un modèle est proposé qui reprend la même approche que celle employée dans le cas des molécules de PAHs en l'étendant aux cations et aux PAHs peu hydrogénés. Les taux de photodestruction obtenus pour les PAHs ionisés et déhydrogénés sont plus grands que ceux des molécules correspondantes, en particulier pour les PAHs déhydrogénés qui sont très fragiles lorsqu'ils sont soumis aux photons ultraviolets. La comparaison des taux de photodestruction et des taux du processus inverse, à savoir l'accrétion de particule de carbone, conduit à la conclusion que seuls les PAHs contenant plus de 50 atomes de carbone sont capables de résister aux radiations ultraviolettes dans les régions où sont observées les bandes UIR.

Puisque les PAHs possèdant plus de 50 atomes de carbone peuvent éventuellement survivre dans le MIS, il est intéressant d'étudier les régions où ils peuvent se former et croitre. C'est précisément le sujet de la deuxième partie de cette thèse que d'étudier les PAHs dans les enveloppes circumstellaires (ESCs). Dans ce but, les modèles stationnaires d'ECSs riches en poussière récemment dévelopés à l'Institut d'Astronomie et d'Astrophysique de l'Université Technique de Berlin sont exploités, et plus particulièrement le modèle pour IRC+10216, qui est l'étoile géante rouge riche en carbon la plus proche et la mieux connue (Winters et al. 1994, Winters 1994).

L'ensemble des processus pouvant favoriser la formation des PAHs dans les ESCs est analysé. A partir de ces résultats, la densité des plus petits PAHs est calculée. Il est ainsi confirmé que les PAHs croissent rapidement jusqu'à des tailles macroscopiques, par succésives abstractions d'hydrogène et additions d'acétylène. Le lien entre les PAHs et les grains de poussière est étudié numériquement et il est établi que les PAHs pourraient bien être les précurseurs des grains de poussière.

Les processus subis par les PAHs lorsqu'ils atteignent la partie extérieure des ESCs sont également examinés. Pour permettre des calculs corrects, de nouvelles valeurs sont calculées pour les épaisseur optiques de la poussière et des molécules de $H_2$ et CO. A l'aide de ces résultats, les taux d'ionisation et d'hydrogènation des PAHs dans l'envelope de IRC+10216 sont estimés. La croissance par accrétion de $C^+$ et la photodestruction des PAHs sont aussi étudiées, dans le but d'évaluer la distribution en taille des PAHs éjectés dans le MIS. Bien qu'il soit démontré que les processus de croissance et de destruction sont assez rapides pour modifier la distribution des PAHs pendant leur trajet de l'étoile jusqu'au MIS, il n'est pas possible de tirer des conclusions définitives en raison du manque de données concernant les rendements des processus qui suivent la collision entre les PAHs et les cations $C^+$.

Une application directe du présent travail est l'estimation de la densité des PAHs dans le MIS. Cela résulte simplement de l'équilibre entre la formation de PAHs (par formation *in situ*, contribution des étoiles de type C, des ondes de choc) et la disparition des PAHs (par photodestruction, collisions avec les grains, éffritement). Grâce aux résultats obtenus ici et à de futures expériences, une telle étude sera possible et devrait permettre de répondre définitivement à la question de l'abondance et de l'ubiquité des PAHs dans l'espace.

# Contents

# List of Figures

# List of Tables

La nature ordonna ces choses sagement:
J'en dirai quelque jour les raisons amplement.
J'aperçois le Soleil: quelle en est la figure ?
Ici–bas ce grand corps n'a que trois pieds de tour;
Mais si je le voyais là–haut dans son séjour,
Que serait-ce à mes yeux que l'oeil de la nature ?
Sa distance me fait juger de sa grandeur;
Sur l'angle et les côtés ma main la détermine.
L'ignorant le croit plat: j'épaissis sa rondeur;
Je le rends immobile, et la terre chemine.
Bref je démens mes yeux en toute sa machine:
Ce sens ne me nuit point par son illusion.
    Mon âme en toute occasion
Développe le vrai caché sous l'apparence

La Fontaine, *Un animal dans la Lune.*

# Chapter 1

# Introduction

## 1.1 The intrusion of PAHs in Astrophysics

A captivating puzzle has recently originated in astrophysics with the discovery of a series of emission bands in the infrared spectra of various sources characterized by a strong ultraviolet radiation field. Two bands were first detected in the early seventies in the 8–13 $\mu$m spectrum of the planetary nebula NGC 7027 (Gillet et al. 1973). In the following years an array of five bands at 3.3, 6.2, 7.7, 8.6 and 11.3 $\mu$m was found in the spectra of active galaxies, reflexion nebulae and HII regions (for a review see Aitken(1981) and references therein). More recently, the infrared emission bands have also been observed in the spectra of high mass Wolf–Rayet stars, C–rich protoplanetary nebulae and R Coronae Borealis (Cohen et al. 1989; Buss et al. 1990,1993; Geballe et al. 1992). Figures 1.1 and 1.2 show the 2–12 $\mu$m spectra of two objects which exhibit the bands. In 1982, Willner (1984) noted that "the ingredients necessary to produce the emission features seem to be dusty neutral material and ultraviolet radiation". By that time there were indeed no convincing candidates to account for the complete set of emission bands. For that reason, they have become famous in astrophysics under the appellation of "Unidentified Infra–Red" (UIR) bands.

The first successful proposal to fathom the mystery of the UIR bands was due to Duley & Williams (1981), who assigned the bands at 3.3 and 11.3 $\mu$m, respectively, to the stretching and bending modes of C–H bonds in aromatic rings. They proposed that carbon grains with a graphitic or an amorphous structure and hydrogen atoms at their edge, forming so–called Hydrogenated Amorphous Carbon (HAC), might be the carriers of these bands. Shortly thereafter, it was noted that the emission around 3 $\mu$m required higher temperatures than could be attained by a "classical" grain in radiative equilibrium (Sellgren 1984). Sellgren (1984) therefore proposed that the source of the UIR bands could be very small grains with a diameter of some 10 Å heated by absorption of a single photon. As already pointed out by Donn (1968), following the pioneering work of Platt (1956) such small graphitic grains probably consist of one atomic monolayer and thereby ressemble polycyclic aromatic hydrocarbons (PAHs). Since 1983, PAHs were already known to grow

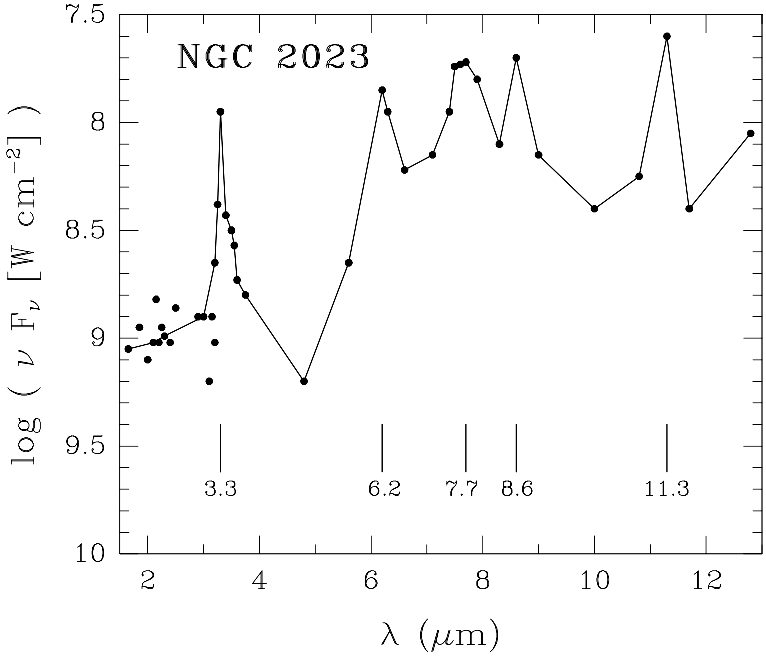


Figure 1.1: Near–infrared spectrum of the reflection nebula NGC 2023 (from Sellgren et al. 1985).

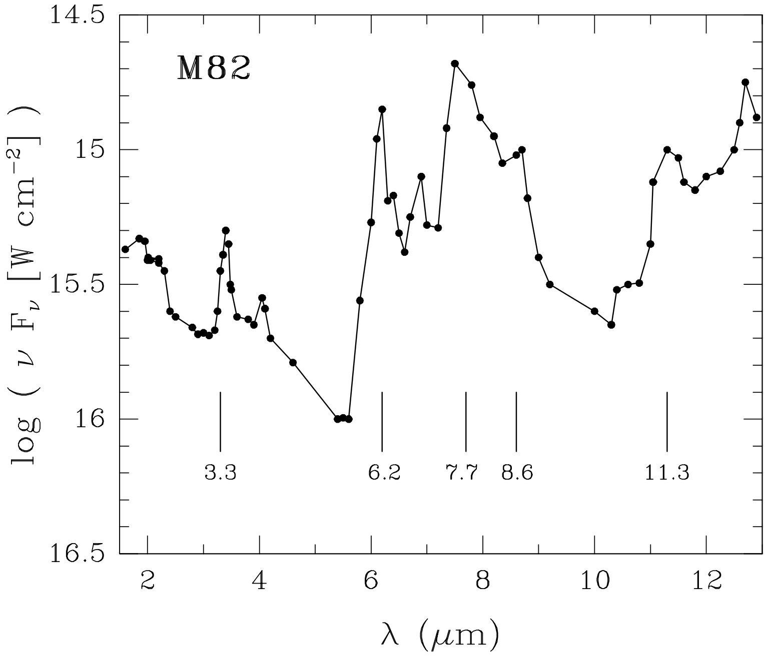


Figure 1.2: Near–infrared spectrum of the active galaxy M82 (from Willner et al. 1977).

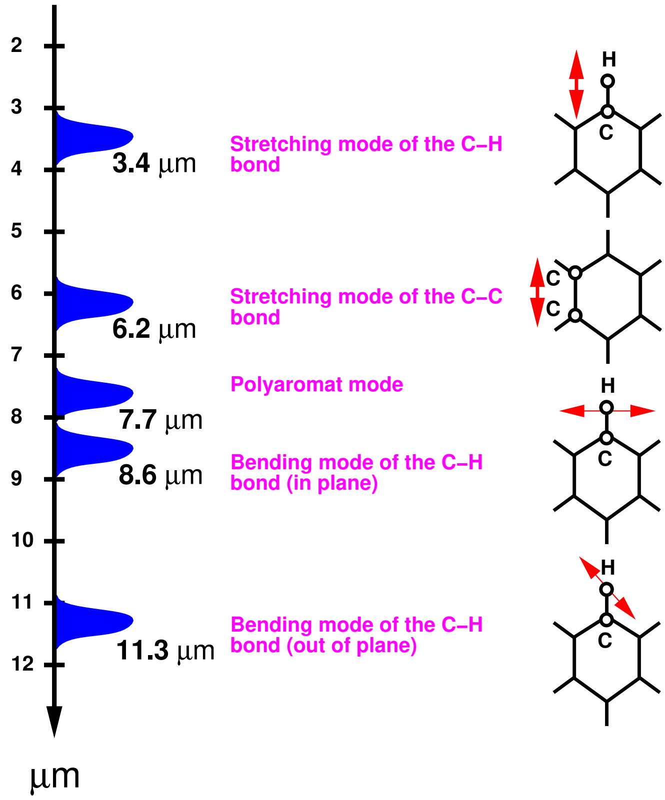


Figure 1.3: Vibrational modes of PAHs (from Gail & Sedlmayr 1987).

in the circumstellar envelopes of carbon–rich late type stars, the so–called C–stars, where they are thought to constitute the first step in the formation of dust particles (Keller & Sedlmayr 1983). However, PAHs definitely gained in popularity when Léger & Puget (1984) and Allamandola et al. (1985) noticed the striking match between the PAH infrared vibrational modes and the five UIR bands (see Fig. 1.3) and thus first concluded that free PAHs could be the carriers of the UIR bands. In the following years, the study of interstellar PAHs has become an increasingly active field of astrophysics.

However, there has been much controversy on the unambiguity of the assignment of the UIR bands to PAHs. In their "Critical assessement of the PAH hypothesis" Donn et al. (1989) reviewed the deficiencies of the proposal of PAHs as carriers of the UIR bands and called for more experimental work before drawing definitive conclusions. Moreover, some other proposals have been made to account for the UIR bands. Sakata et al. (1984) have studied the condensates of a discharge in methane at room temperature, which they called quenched carbonaceous composite (QCC), and measured bands similar to the UIR bands. A better match has even been obtained with oxidized QCC (Sakata et al. 1987). Borghesi et al. (1987) have measured the infrared emission of amorphous carbon grains obtained by striking an arc between carbon electrodes in argon and observed bands in good match with the UIR bands. According to Duley & Williams (1988) the bands could originate from individual aromatic molecular groups loosely bound to amorphous carbon grains. Coal has also been more recently proposed as carrier of the UIR bands (Papoular et al. 1989). Despite the apparently large variety of candidates, it should be recalled that all these materials contain aromatic rings, which is likely the reason for the good match of their infrared spectra with observations. The differences between the spectra of these materials probably arise from their different preparation in the laboratory (Duley 1994) and do not contradict the assignment of the UIR bands to vibrational modes of aromatic rings.

## 1.2 Properties of interstellar PAHs

Since the proposal of Léger & Puget (1984) that PAHs could be the carriers of the UIR bands, the study of PAH properties in the interstellar medium (ISM) has steadily developed. Assuming that PAHs alone are responsible for the UIR bands, Léger & Puget (1984) and Allamandola et al. (1985) first calculated their abundance by comparing the emission in the UIR bands with the emission of dust particles in the far infrared continuum and assuming ultraviolet absorption cross–sections for the PAHs and the dust. These authors deduced that the fraction of carbon in small PAHs ($\simeq$ 25 carbon atoms) could vary between 3 and 15 % in the regions showing the UIR bands. The fraction of carbon locked up in PAHs hence corresponds to an abundance of PAHs per H nuclei of about $10^{-7}$ in the regions where the UIR bands are seen. Since the emission band at 3.3 $\mu$m has also been seen in the diffuse medium (Giard et al. 1988), it has been claimed that PAHs could be an ubiquitous component of the ISM. The value of $10^{-7}$ has consequently become a standard value for the PAH abundance relative to hydrogen in the ISM. In agreement with this value Léger et al. (1989b) noticed that PAHs could therefore constitute the most abundant molecules in the ISM after $H_2$ and CO.

Because of the presumably large PAH abundance, PAHs have been introduced in models of interstellar dust in order to account for the extinction and/or emission of the ISM (Puget & Léger 1989; Désert et al. 1990; Tielens 1990; Schutte et al. 1993). Puget & Léger (1989) and Désert et al. (1990) considered an empirical dust model with three components: big grains, very small grains with a 3-dimensional configuration and radius between $\simeq$ 1 and 10 nm and PAHs. These models reproduce both the emission and extinction of the ISM for a size–distribution based on the MNR size distribution (Mathis et al. 1977) with a smooth continuation towards the molecular domain of PAHs. On the other hand, replacing the very small grains by large PAHs and PAH clusters, Tielens (1990) showed that the MRN size distribution of the interstellar dust extends out well towards the PAH domain. Schutte et al. (1993) have adopted the model of Tielens (1990) to propose a PAH size distribution which can reproduce the UIR bands observed in the ISM.

Independently of the size–distribution of PAHs, the assumption of the existence of PAHs with a large abundance in the ISM is likely to influence the chemistry of interstellar gas. This point has actually been discussed by several authors (Lepp & Dalgarno 1988; Lepp et al. 1988, Millar 1992). If PAHs are present in interstellar clouds with an abundance relative to hydrogen of $10^{-7}$, free electrons probably attach to PAH molecules and form $PAH^-$ negative anions which carry most of the electric charge (Omont 1986). Interstellar chemistry was shown to be considerably modified by the neutralization reactions of $PAH^-$ with atomic and molecular ions (Lepp & Dalgarno 1988; Lepp et al. 1988). Millar (1992) estimated that protonated PAH cations and doubly charged PAH cations could also be abundant in interstellar clouds. The presence of doubly ionized PAH molecules was previously suggested by Leach (1986). PAH cations could however be destroyed by photodestruction (Leach et al. 1989) or by electron recombination (Millar 1992). Nethertheless, all these calculations rely on experiments carried out on small PAHs ($\leq 10$ carbon atoms). The evolution of the physical and chemical rates with molecular size is still unknown for most of the involved processes and further experimental investigations are needed to obtain reliable results for the influence of PAHs on interstellar chemistry.

Because of the high ultraviolet radiation in the regions which exhibit the UIR bands, a large fraction of PAHs could be ionized and partially dehydrogenated. Indeed, there has been much work done to determine the hydrogenation and ionization states of PAHs. Spectroscopally, the hydrogenation state of PAHs can be characterized by the bands in the 11–15 $\mu$m region. The position of the bands in this spectral region are known to shift to longer wavelengths when the number of adjacent H atoms increases on an aromatic ring (Bellamy 1966). It was first thought that PAHs are partially dehydrogenated because only the band at 11.3 $\mu$m was observed in astrophysical spectra (Duley & Williams 1981, Léger & Puget 1984). However, theoretical calculations by Tielens et al. (1987) and Jochims et al. (1994) showed that the interstellar PAHs are likely to contain more than 25 carbon atoms and to be stable against photoejection of atomic hydrogen, which leads to a large hydrogen coverage of PAHs. Moreover, the 8–22 $\mu$m IRAS spectra show a plateau in emission extending to 13 $\mu$m (Cohen et al. 1985), which also supports the idea of a larger PAH hydrogenation than was first expected by Duley & Williams (1981) and Léger & Puget (1984). More recently, the presence of "superhydrogenated" PAHs, i.e. PAHs with H extra atoms at the edge of the carbon skeleton, has been proposed to explain the subfeature at 3.4 $\mu$m (Schutte et al. 1993). This confirms that the discussion about the hydrogenation state of interstellar PAHs is still open.

Concerning the PAH ionization state, estimates of the fraction of ionized PAHs in the ISM has been performed by Omont (1986) and by Verstraete et al. (1990) by balancing PAH ionization to electron recombination. A large variety of ionization fraction values has been obtained in the media where the UIR bands are seen. Moreover, PAH ionization has been proposed as explanation for the heating of the warm phase of the ISM, where temperatures reach some thousand Kelvin (Verstraete et al. 1990). As previously discussed, the existence of doubly ionized PAH molecules has also been suggested by several authors. However, most of the previous results regarding PAH ionization have been obtained using theoretical estimates for the electron recombination of PAH cations deduced from properties of graphitic grains. From the experimental point of view no support can be actually found to confirm such a theoretical approach. Indeed, the experiments of electron recombination with PAH cations have been carried out up to now only on small PAHs ( $\leq 10$

carbon atoms) where electron recombination is rather dissociative (Abouelaziz et al. 1993). Additionally, it should be noted that the infrared emission spectra of small PAH cations (naphthalene, anthracene and pyrene), which have been recently calculated, show that the vibrational modes of PAH cations have similar frequencies to the corresponding neutral PAHs but emit with different relative intensities (de Frees et al. 1993). The results of these authors tend to prove that the carriers of the UIR bands could be highly hydrogenated PAH cations.

Beside the previous studies, there has been relatively less work on the processes of formation and destruction of PAHs, which is a crucial point in order to confirm their presence in the ISM. It is now well documented that PAHs could form in the envelopes of C–stars (Keller & Sedlmayr 1983; Keller 1987; Frenklach & Feigelson 1989; Cherchneff et al. 1992; Goeres 1993; Cadwell et al. 1994; Cherchneff 1995) where the chemistry of their formation has been investigated. The growth and sputtering of PAHs have also been studied in shocked regions but the lack of exact chemical data leads to contradictory results concluding that PAHs are either a transient species or an ubiquitous component in interstellar clouds (Duley & Williams 1986; Brown et al. 1989, Flower et al. 1990). Another proposal by Herbst (1991) provides models for *in situ* formation of large hydrocarbon species in dense interstellar clouds. Nevertheless, all of these studies have been done in regions where the UIR bands are not observed because the UV radiation field is too weak to excite PAHs and make them reemit in the IR. On the other hand, in the regions showing the UIR bands photodestruction of PAHs is probably the most important destruction process (Omont 1986). No theoretical calculation has been done so far to estimate the photodestruction rate of PAHs in the ISM although it should provide a valuable approach to test the hypothesis of the existence of interstellar PAHs.

## 1.3 Aim and structure of this thesis

The aim of this thesis is to present estimates for the photodestruction rate of PAHs in space. The calculations will be carried out, first, in the regions where the UIR bands are seen and where PAHs are assumed to exist, and secondly, in the outer part of C– star circumstellar envelopes (CSEs) where the PAHs, which form near the star, are exposed to the interstellar radiation field. This study should help to determine more accurately the molecular size and the densities of the PAHs which are able to survive the interstellar radiation field.

In **Chap. 2** a model for interstellar PAHs is developed in order to estimate their rate of photodissociation in the ISM. The stability of PAHs are studied in the regions of high UV radiation where the UIR emission bands attributed to PAHs are observed (reflection nebulae, planetary nebulae, active galactic nuclei, HII regions...), by comparing the rate of acetylene loss to the rate of accretion of carbon to PAH molecules.

In **Chap. 3** the model presented in Chap. 2 for PAH molecules is extended in order to describe ionized and partially dehydrogenated PAHs and hence provide a more realistic description of these species in the ISM. A method is first developed for evaluating the ionization and hydrogenation states of PAHs in a given medium. Taking into account these ionization and hydrogenation states, the conclusions of Chap. 2 concerning the stability of interstellar PAHs against photodissociation are then revised. A minimal size of surviving PAHs is deduced in the regions with a strong ultraviolet radiation field.

In **Chap. 4** a simple modelization of PAHs is presented with the aim of estimating the interactions of gas particles with PAHs in space. The results are applied to the case of the CSEs of C–stars where PAHs are known to form and grow. Calculations of PAH drift velocity and PAH temperatures are carried out in a typical stellar envelope. Using these results, the PAH formation and growth are studied and discussed in the context of the role of PAHs for the formation of dust particles.

In **Chap. 5** dust and molecular shielding are evaluated in a typical C–star envelope in order to calculate reliable rates for the photoprocesses undergone by PAHs in the outer part of the CSE. Estimates of the ionization fraction and the hydrogene coverage of PAHs in circumstellar shells are obtained. Collisions of PAHs with $C^+$ are also studied and shown to be frequent enough to modify the size–distribution of the PAHs formed near the star.

In **Chap. 6** the conclusions of this thesis are summarized and suggestions for future work are presented.

The **Appendix A** presents the main results of a self–consistent model for stationary dust driven winds in the CSEs of C–stars. This model developed by Winters (1994) describes IRC+10216, which is the nearest and best studied carbon star.

The **Appendix B** gives the background for a discussion on timescales in the study of non equilibrium chemistry in circumstellar environments. The results discussed in Appendix A and B are used in Chap. 4 and Chap. 5.

The **Appendix C** presents the integrated absorption cross–sections of CO and $H_2$ molecules used in Chap. 5 to calculate the molecular shielding.

L'esprit humain est organisé pour percevoir, dans l'espace et dans la durée, des rapports qui existent effectivement hors de lui et indépendamment de lui. Il pénètre ainsi dans la réalité, mais dans une réalité relative, phénoménale, dont la connaissance suffit aux besoins et au rôle de l'homme dans le monde. Lorsqu'il tente de l'outrepasser et d'ériger cette réalité relative en réalité absolue, il cède sans doute à un penchant de sa nature, mais ce penchant le trompe, et la raison l'en avertit, en lui montrant des abimes sans fond et des contradictions sans issue.

Antoine Augustin Cournot, *Essai sur les fondements de nos connaissances* .

# Chapter 2

# PAH Photodissociation rates

**abstract**

A model for interstellar polycyclic aromatic hydrocarbons (PAHs) is developed in order to estimate their rate of photodissociation in the interstellar medium. These photoreactions include the loss of atomic and molecular hydrogen and the loss of the acetylene molecule. The stability of PAHs against photodissociation is studied in the regions of high UV radiation where the infrared emission bands attributed to PAHs are observed (reflection nebulae, planetary nebulae, active galactic nuclei, HII regions...) by comparing the rate of acetylene loss to the rate of accretion of carbon to PAHs. This comparison shows that only PAH molecules with more than 50 carbon atoms may survive the UV radiation field of these regions, whereas smaller PAHs such as coronene or ovalene are destroyed within a few years.

———————————————

## 2.1 Introduction

The regions where the "Unidentified Infra–Red (UIR) emission bands are seen (reflection nebulae, planetary nebulae, active galactic nuclei, HII regions...) are usually associated with a strong UV radiation field. This UV radiation field may be an important factor for destruction of Polycyclic Aromatic Hydrocarbons (PAHs), which are thought to be good candidates as carriers of the UIR bands (Léger & Puget 1984, Allamandola et al. 1985). It is therefore of great interest to precisely study the stability of PAHs against photodestruction in the regions which exhibit the UIR bands.

A recent study on unimolecular photoreactions of PAHs has been done by Jochims et al. (1994) which provides the rates of photodissociation of PAHs for given values of their excitation energy. These results argue against the theoretical and semi–empirical results which have been used so far to estimate the photostability of PAHs (Barker 1983; Omont 1986; Allamandola *et al.* 1989; Léger et al. 1989a; Buch 1989) and prove that for the typical energy of photons in the interstellar medium (ISM) only PAHs with more than 30 – 40 carbon atoms may have infrared radiative rates larger than the photodissociation rates and can therefore survive the interstellar UV field.

To subsist, these PAHs nevertheless have to undergo a rate of growth by accretion of carbon atoms or ions greater than the rate of photodissociation integrated over the interstellar UV spectrum. The determination of such an integrated photodissociation rate is a difficult task because it has to take into account all the possible processes following the absorption of a photon: ionization, dissociation, IR and visible luminescence. It is however worth calculating because it is the only way to estimate the size of the interstellar PAHs and their density independently of the observational determinations. Such calculations could hence improve our understanding of the existence of interstellar PAHs.

It is the aim of this chapter to calculate the photodestruction rate of PAH molecules in the ISM. In Sect. 2.2, the physical and chemical properties of PAHs are reviewed and the yields of the processes occuring after absoption of a photon by a PAH are calculated. From these yields, the rates for photoionization and photoejection of hydrogen and acetylen are derived in Sect. 2.3 for interstellar PAH molecules. Finally, in Sect. 2.4, the implications for the surviving of PAHs in the regions which exhibit the UIR bands are discussed.

## 2.2 PAH Photophysics and photochemistry

In this section we first make some comments on the state of knowledge concerning the photophysics and photochemistry of interstellar PAHs. We then propose a model for these PAHs which describes in a simplified way their behaviour using some relations deduced from both theory and experiment. In the last subsection we apply this model to determine the yields of the more important processes following the absorption of a photon by a PAH in the interstellar medium.

### 2.2.1 Photophysics

Omont (1986) has shown that in the ISM the rates of collision of the most abundant particles with a typical PAH are never larger than $10^{-4}$ s$^{-1}$. Since the smallest rates of PAHs unimolecular processes are of the order of $10^{2}$ s$^{-1}$ (Allamandola et al. 1989; Léger et al. 1989a, 1989b; Jochims et al. 1994) they are highly isolated in space. Léger & Puget (1984) have first shown that PAHs can reach transitory vibrational temperatures up to 1000 K after absorption of a photon, whereas it has been demonstrated that their rotational temperature always remains around 100 K (Rouan et al. 1992). In the interstellar medium PAHs therefore have the possibility to evolve as free molecules from states of high vibrational excitation. Accounting for these results we use for the description of interstellar PAHs a step ladder model that only specifies the electronic and vibrational states of the species. Figure 2.1 represents the case of an aromatic molecule whose electronic states can be singlets or triplets.

UV photon absorption is in many interstellar situations the dominant excitation process of such a molecule. When absorption occurs, the molecule is in most cases in the lowest singlet electronic state, $S_0$, from which it reaches an upper level. The main absorption features of PAH molecules are due, on the one hand, to the $S_0$—$S_1$, $S_0$—$S_2$, $S_0$—$S_3$,... transitions,

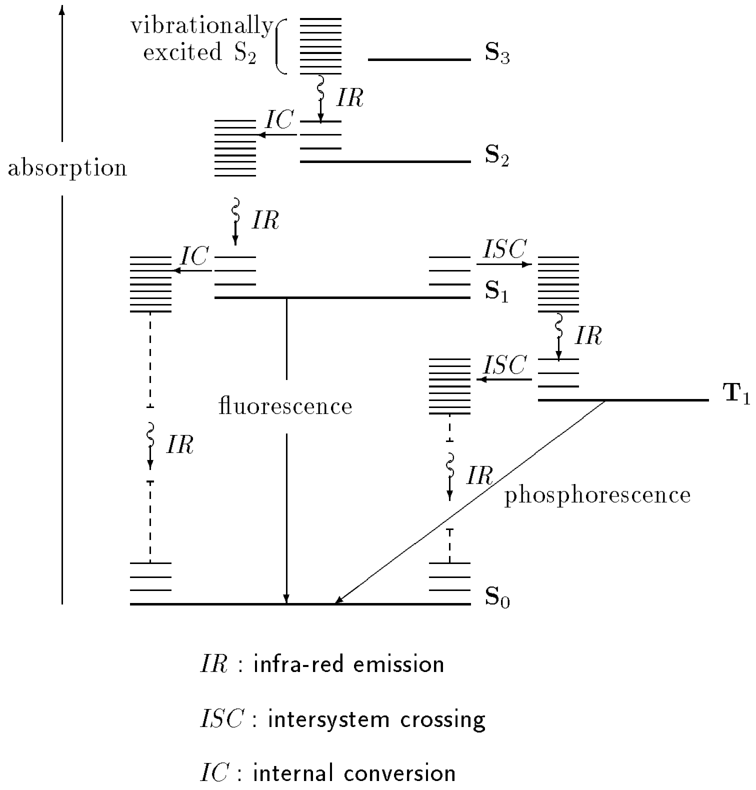


Figure 2.1: Radiative and radiationless decay processes in a typical PAH molecule.

which are spin allowed, and, on the other hand, to the $\sigma \rightarrow \sigma^*$ and the $\sigma \rightarrow \pi^*$ transitions (Koch & Otto 1972, Koch et al. 1972; Pantos et al. 1978) and to direct ionization (Verstraete et al. 1990), which explain the very strong far-UV band around 16 eV [See also the recent spectra of Joblin (1992) obtained in the gas phase at low pressure].

The processes following photoabsorption are electronic and vibrational transitions, ionization and photodissociation. The transition processes of PAHs have been extensively described in the literature especially by Birks (1970). The transitions are either radiative, described as fluorescence when they take place between states of same multiplicity and phosphorescence between states of different multiplicity, or radiationless. The radiationless transitions take place between isoenergetic vibrational levels of different electronic states and are described as internal conversion (IC) between states of same multiplicity or intersystem crossing (ISC) otherwise (see Fig. 2.1). After absorption of a photon, $S_p$—$S_{p-1}$ ,..., $S_2$—$S_1$ internal conversions usually occur rapidly ($10^{-12} - 10^{-10}$ s) and result in a practically complete conversion of the absorbed energy to vibrationally excited levels of the $S_1$ and $S_0$ electronic states.

### 2.2.2 Photochemistry

Several theoretical calculations have been performed to study the photodissociation of PAH molecules. The results obtained by Barker (1983), Tielens et al. (1987) and Allamandola et al. (1989) using QRRK (Quantum Rice, Ramsperger, and Kassel theory) calculations have not been confirmed by the more recent experimental results of Jochims et al. (1994). These experimental results also argue against the model of Buch (1989) who predicted direct photodissociation of C—H bonds for all PAHs at energies less than 13.6 eV by absorption to a repulsive $\sigma^*$ molecular orbital. The experiment shows on the contrary that for large PAHs rapid intramolecular redistribution of the absorbed energy among the vibrational modes considerably limits the yield of such a dissociation process.

Omont (1986) has used a modified RRKM theory (Rice, Ramsperger, Kassel and Marcus theory) to estimate the rate of loss of hydrogen and carbon atoms. To obtain numerical results he introduced into the calculation data from experiments not directly carried out on PAHs. A similar approach has been more recently adopted by Léger et al. (1989a) who proposed to use the following expression given by Forst (1973) for the dissociation rates:

$$k(E) = k_0 \frac{\rho(E - E_0)}{\rho(E)} \qquad \text{for } E > E_0 \; , \tag{2.1}$$

$$k(E) = 0 \qquad \text{for } E \leq E_0 \; , \tag{2.2}$$

where $E$ represents the internal energy of the molecule, $\rho$ its density of states and $E_0$ is the sum of the dissociation energy and the zero point energy $E_\mathrm{z}$. The function $\rho(E)$ can be expressed using the Whitten-Rabinovitch approximation (Whitten & Rabinovitch 1963) in the form:

$$\rho(E) = (E + aE_\mathrm{z})^{s-1} \left[ s! \prod_{i=1}^{s} h\nu_i \right]^{-1} , \tag{2.3}$$

where $\nu_i$ are the vibrational frequencies of the modes and $s$ their number, while $a$ is a correction factor ($0 < a < 1$) that varies with $E$ according to an empirical law given in Whitten & Rabinovitch (1963). Equations (2.1) are only valid if the rate of dissociation for a molecule thermalised at temperature $T$ has the form of the Arrhenius law:

$$k(T) = k_0 \, \exp\left( - \frac{E_0}{RT} \right) , \tag{2.4}$$

providing the constant $k_0$ and $E_0$ of Eq. (2.1). From indirect experimental evidence, Léger et al. (1989a) (who call this process thermo–photodissociation) have proposed to use the values $k_{0_\mathrm{H}} = 2.4\ 10^{14}\ \mathrm{s}^{-1}$ and $E_{0_\mathrm{H}} = 4.5$ eV for the loss of a hydrogen atom and $k_{0_\mathrm{C}} = 10^{17}\ \mathrm{s}^{-1}$ and $E_{0_\mathrm{C}} = 8$ eV for the loss of a carbon atom.

More recently Jochims et al. (1994) have obtained experimental results for the dissociative ionization of PAH molecules. This study led to the determination of the internal energy of the ion corresponding to the astrophysically critical rate of dissociation $10^2\ \mathrm{s}^{-1}$

Table 2.1: Parameters for the RRK expression.

| loss channel | $E_0(eV)$ | $k_0(s^{-1})$ $^{(a)}$ |
|---|---|---|
| H | 2.8 | 1 (16) |
| $H_2$ | 2.9 | 1 (16) |
| $C_2H_2$ | 2.9 | 1 (15) |

(a) Powers of ten are written inside the brackets

below which the species will preferentially relax by infrared emission. The results obtained were considered to be valid for neutral PAHs since the intramolecular dynamics and dissociation energies are closely similar for monocationic and neutral PAHs, as illustrated by the fact that vibrational frequencies are little modified in these two species which differ only by removal of a single $\pi$ electron from a "sea" of conjugated $\pi$ electrons (Leach 1987).

Jochims et al. (1994) explored experimentally three main channels corresponding to the loss of an hydrogen atom, a hydrogen molecule and an acetylene molecule. Their results have proved to be correctly interpreted on the basis of the simple Rice, Ramsperger, and Kassel (RRK) theory (for more details see for instance Forst (1973)). The rate of desintegration for a molecule of energy E is then given by the expression:

$$k(E) = k_0 \left(1 - \frac{E_0}{E}\right)^{s-1} \qquad \text{for } E > E_0 \;, \tag{2.5}$$

$$k(E) = 0 \qquad \text{for } E \leq E_0 \;, \tag{2.6}$$

where $E$ is the internal energy of the molecule and $s$ the number of degrees of freedom over which the energy $E$ can be distributed. Jochims et al. (1994) assumed that all degrees of freedom are involved; this corresponds to $s = 3N - 6$ where $N$ is the number of atoms of the molecule. $E_0$ and $k_0$ are two constants determined by fitting the results of the experiment and are given in Table 2.1 for the loss of H, $H_2$ and $C_2H_2$. We note that in the RRK model, the parameter $E_0$ is only approximately related to the bond dissociation energy (Forst 1973) and it was used as a parameter by Jochims et al. (1994).

We have plotted in Fig. 2.2 the rates of loss of carbon atoms calculated from the so–called thermo–photodissociation model and from RRK theory for benzene, naphthalene, anthracene, pyrene and coronene. In both cases the evolution of the rates with the size of the molecule are the same, leading to the conclusion that larger molecules are more stable against photodestruction. There is however a large discrepancy in the numerical values of the results which indicates that the rates from the thermo–photodissociation theory are by several orders of magnitude lower than those obtained with the RRK theory.

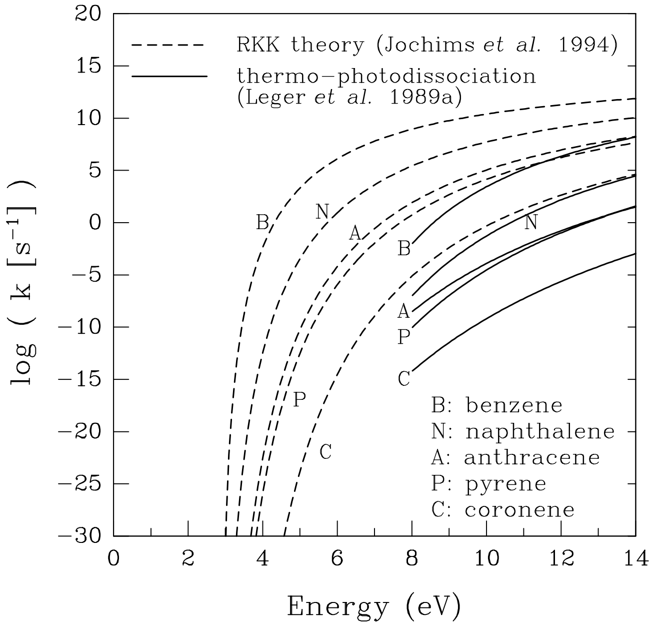


Figure 2.2: Rates of destruction for various PAHs molecules calculated from RRK and thermo–photodissociation theories.

The discrepancy is probably due to the values of the parameters $k_0$ and $E_0$ used for the thermo–photodisociation. This point shows that theoretical considerations based on experimental observations not directly based on reactions with PAHs may lead to large uncertainties in the results. On the contrary, values of the constants in the RRK model have been obtained to fit the recent experiments of Jochims et al. (1994) performed on PAHs. We therefore use the RRK results for our calculations in the remainder of this thesis. Another advantage of the RRK theory for the sake of our study is its simplicity compared to the calculation of the thermo–photodissociation rate, which supposes the use of the $3N - 6$ vibrational frequencies of the molecule. Furthermore, the lack of data about these vibrational modes, especially for PAHs containing more than 8 rings, prevents us from using thermo–photodissociation calculations for some PAHs.

### 2.2.3 A model for the study of interstellar PAHs

The model for interstellar PAHs presented in this section is based on an ensemble of equations which integrates the present knowledge on PAHs in order to describe, in a reliable and simple way, the behaviour of interstellar PAHs in the ISM after absorption of a photon.

As suggested in Sect. 2.2.1, the only electronic levels considered in the model are $S_1$, $S_0$ and $T_1$. The transitions involving upper levels are supposed to bring quasi–instantaneously the species to the level $S_1$ by internal conversion. The other transitions of the molecules ($S_1$–$S_0$, $S_1$–$T_1$ and $T_1$–$S_0$ radiationless transitions, $S_1$ fluorescence and $T_1$ phosphorescence) have been taken into account using the rates of Birks (1970) and more recent data when they exist. The references of the data we use for the calculations are presented in Table 2.2. The decay rates have been mainly determined from the lifetime $\tau_{\rm f}$ and the quantum yield of fluorescence $\Phi_{\rm f}$ of PAHs. The expressions for the radiative $k_{\rm r}$ and non-radiative $k_{\rm nr}$ transitions are simply given by the following expressions:

$$k_{\rm r} = \frac{\Phi_{\rm f}}{\tau_{\rm f}}\,, \tag{2.7}$$

$$k_{\rm nr} = \frac{1 - \Phi_{\rm f}}{\tau_{\rm f}}\,. \tag{2.8}$$

Unfortunately, these rates have often been obtained in solution and, in such a medium, a molecule excited by photoabsorption dissipates its vibrational excitation energy to its neighbours and thereby comes rapidly (typically $10^{-11}$ s) into thermal equilibrium with its environment. The values of the decay rates obtained in solution can therefore only be used for PAHs having no vibrational energy left in their $S_1$ and/or $T_1$ electronic states. To study the evolution of the rates with excess vibrational energy, we use the results of experiments on PAH vapors at low pressure and/or in molecular beams when they are available and some semi-empirical calculations otherwise.

For the radiationless transitions we use the results described in the extensive reviews of Avouris et al. (1977) and Lim (1985). To simplify the model, we always assume simple laws (linear or exponential) for the dependence of the rate on excess energy, which is in good agreement with both theory and experiment. For the non-radiative transition $S_1 - S_0$ of most PAHs we deduce for instance from Lim (1985) the following semi-empirical result:

$$k_{\rm nr} = k_0 \exp\left(\alpha E_{\rm vib}\left[{\rm cm}^{-1}\right]\right) \tag{2.9}$$

with

$$\alpha = 2\ 10^{-2} + 4.38\ 10^{-8}\left(E_{\rm S_1-S_0}\left[{\rm cm}^{-1}\right] - 25500\right)\,, \tag{2.10}$$

where $k_0$, $E_{\rm vib}$ and $E_{\rm S_1-S_0}$ represent the rate for no excess energy over the state $S_1$, the excess energy and the energy of the transition $S_1 - S_0$, respectively. Figure 2.3 shows the evolution of the non-radiative rates in the case of a naphthalene molecule. Concerning the radiative transitions of vibrationally excited PAHs, we use the yields of fluorescence and phosphorescence available in the literature, especially from molecular beam experiments (see for instance the results of Hermine (1994)). When no experimental data are available, we assume that the rates of fluorescence and phosphorescence are constant up to the quenching of luminescence set at the electronic levels $S_2$, and $T_2$.

The IR properties of large PAHs are adapted from the model PAH considerations of Léger et al. (1989b). For some smaller PAHs in the gas phase the Einstein coefficients of vibrational transitions have been directly determined from measurements of integrated absorption coefficient (Bishop and Cheung 1982) or from laser-induced dissociation studies (Dunbar et al. 1987; Klippenstein et al. 1993). For PAHs having less than N = 25 atoms we have also collected the values of the 3N-6 frequencies in the literature determined either from experiment or from theoretical calculations. For computational purposes they have

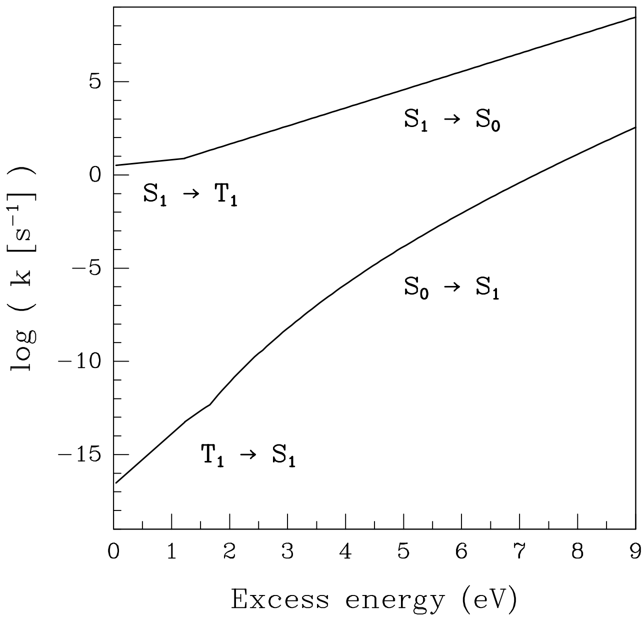


Figure 2.3: Rates of radiationless processes and reversal processes for the molecule of naphthalene.

been grouped according to their physical origin. More precisely, all the modes around 3.3 $\mu$m which correspond to stretching modes of the C–H bonds have been considered together as well as the bending modes of the C–H bonds around 11.3 $\mu$m, the stretching modes of the C–C bonds around 6.2 $\mu$m, the bending modes of the C–C bonds around 8.6 $\mu$m and finally the typical polycyclic skeleton modes around 7.7 $\mu$m. The Einstein coefficients corresponding to these IR transitions have also been modified to take into account the excess vibrational energy of the PAH. When this excitation energy is high, the emitting mode may indeed have $n$ quanta with $n > 1$ and its Einstein coefficient may therefore change. From the harmonic approximation we deduce:

$$A^{\rm n,n-1} = n\ A^{1,0}\ , \tag{2.11}$$

where $A^{\rm n,n-1}$ represents the Einstein coefficient for the $n \rightarrow (n-1)$ transition. The number of quanta of the emitting mode is calculated by assuming a complete energy distribution between all normal modes. The most probable population numbers can be calculated from the equation:

$$E_{\rm ex} = \sum_{i=1}^{3N-6} \frac{h\nu_i}{\exp\left(\frac{h\nu_i}{kT^*}\right) - 1}\ , \tag{2.12}$$

where $E_{\rm ex}$ is the excess energy, $T^*$ a parameter that is defined as a vibrational temperature and $\nu_i$ the frequency of the mode $i$.

Table 2.2: Physical data on PAH molecules.

| molecule | benzene $C_6H_6$ | naphthalene $C_{10}H_8$ | anthracene $C_{14}H_{10}$ | pyrene $C_{16}H_{10}$ | coronene $C_{24}H_{12}$ |
|---|---|---|---|---|---|
| $IP\ (eV)$ | $9.24^{(a)}$ | $8.15^{(a)}$ | $7.41^{(a)}$ | $7.41^{(a)}$ | $7.29^{(a)}$ |
| $S_1\ (eV)$ | 4.72 | 3.97 | 3.42 | 3.34 | 2.95 |
| $S_2\ (eV)$ | 6.08 | 5.77 | 3.72 | 3.71 | 3.51 |
| $T_1\ (eV)$ | 3.66 | 2.64 | 1.82 | 2.08 | 2.37 |
| $fluorescence\ rate\ (s^{-1})$ | $2.2\ (6)^{b}$ | 1.0 (7) | 4.9 (7) | $6.2\ (5)^{(c)}$ | $2.5\ (6)^{(d)}$ |
| $phosphorescence\ rate\ (s^{-1})$ | 1.0 (−15) | 2.0 (−2) | 1.1 (−7) | 5.9 (1) | 5.9 (1) |
| $S_1 \rightarrow T_1\ rate\ (s^{-1})^{(e)(f)}$ | $7.8\ (6)^{(b)}$ | $2.5\ (3)^{(g)}$ | 1.1 (7) | 3.0 (4) | 2.1 (6) |
| $S_1 \rightarrow S_0\ rate\ (s^{-1})^{(e)(f)}$ | 4.0 (4) | $2.0\ (5)^{(h)}$ | 1.0 (6) | 3.0 (5) | 4.0 (5) |
| $T_1 \rightarrow S_0\ rate\ (s^{-1})^{(e)(f)}$ | 2.9 (−2) | 3.9 (−1) | 2.2 (1) | 2.0 (0) | 1.2 (1) |
| $UV - absorption\ spectrum$ | $(i)$ | $(j)$ | $(i)$ | $(i)$ | $(i)$ |
| $IR - modes$ | $(k)\ (l)\ (m)$ | $(k)\ (l)$ | $(l)\ (n)$ | $(k)\ (o)\ (p)$ | $(k)\ (o)\ (q)$ |

Data without indication are taken from Birks (1970), (a) Eilfeld and Schmidt (1981), (b) Spears & Rice (1971), (c) Werkhoven et al. (1975a,1975b), (d) Bermudez & Chan (1986), (e) Avouris et al. (1977) and references therein, (f) Lim (1985) and references therein, (g) Fisher et al. (1971), (h) Hsieh et al. (1974), (i) Joblin (1992), (j) Koch et al. (1972b), (k) Cyvin (1982), (l) Cyvin et al. (1984), (m) Bishop & Cheung (1982), (n) Evans & Scully (1964), (o) Cyvin et al. (1979), (p) Bree et al. (1971) and (q) Léger et al. (1989b)

The occupation probability of a particular mode is then given by a Bose-type function:

$$n = \left[\exp\left(\frac{h\nu_i}{kT^*}\right) - 1\right]^{-1} . \qquad (2.13)$$

The correction to $A^{1,0}$ is larger for the smaller molecules which have fewer modes over which the absorbed energy can be distributed. The corrections to the Einstein coefficients are however always less than a factor 10 in the case of benzene. They can therefore be neglected with a good approximation for PAHs having more than 25 carbon atoms, for which the vibrational frequencies of all the modes are not available.

For the ionization of the molecule we use the value of the first ionization potential (IP) from Eilfeld and Schmidt (1981). As confirmed in the study of Verstraete et al. (1990) concerning the ionization cross-section $\sigma_{\rm ion}$ of isolated pyrene and coronene molecules, we assume that the photoionization yield $Y_{\rm ion} = \sigma_{\rm ion}/\sigma_{\rm absorption}$ does not depend on the number of carbon atoms of the molecule. In general $Y_{\rm ion}$ shows a steep increase after the first ionization potential up to a value of 0.75 at the Lyman limit. We use the following linear interpolation for the ionization yield of PAH molecules:

$$\begin{aligned}
Y_{\mathrm{ion}} &= 0.0 && \text{for } E < \mathrm{IP}\ , \\
Y_{\mathrm{ion}} &= \frac{0.10}{8.90-\mathrm{IP}}\,[(E/\mathrm{eV})-\mathrm{IP}] && \text{for } E/\mathrm{eV} \in [\mathrm{IP}, 8.9]\ , \\
Y_{\mathrm{ion}} &= 0.25\,(E/\mathrm{eV}) - 2.125 && \text{for } E/\mathrm{eV} \in [8.9, 11]\ , \\
Y_{\mathrm{ion}} &= 0.0596\,(E/\mathrm{eV}) - 0.03 && \text{for } E/\mathrm{eV} \in [11, 13.6]\ .
\end{aligned} \tag{2.14}$$

Table 2.2 shows that there exists a systematic evolution of the ionization potential with the size of the molecule. Verstraete et al. (1990) have proposed the following expression, which we use for larger PAHs whose ionization threshold is unknown

$$\mathrm{IP} = 4.8\ +\ \frac{10.9}{a\ (\text{Å})}\quad \mathrm{eV}\ , \tag{2.15}$$

where $a$ is the largest linear size of the molecule and corresponds to the radius in the case of compact PAHs. We use the following relation of Omont (1986) for the radius of such a PAH molecule containing $N_{\mathrm{C}}$ carbon atoms:

$$a = 0.9\ N_{\mathrm{C}}^{1/2}\quad \text{Å}\ . \tag{2.16}$$

No real evidence exists in the laboratory for inverse internal conversion (IIC) from a vibrational level to another corresponding to an upper electronic state, but this process may be important in the ISM. This has been proposed by Léger et al. (1988) who predict a recurrent fluorescence which they name Poincaré fluorescence, due to the possibility for a molecule in very high vibrational levels of the ground state to return to the state $S_1$. The IIC is introduced in the model and its rate $k_{\mathrm{IIC}}$ is deduced from the rate of the corresponding IC, $k_{\mathrm{IC}}$, by application of detailed balance (Léger et al. 1988):

$$k_{\mathrm{IIC}} = k_{\mathrm{IC}}\ \frac{\rho(E-\Delta E)}{\rho(E)}\ , \tag{2.17}$$

where $E$ is the vibrational energy of the molecule, $\rho$ the density of states and $\Delta E$ the energy gap between the two electronic levels involved in the transition. Figure 2.3 gives the results obtained in the case of the non-radiative transitions of naphthalene. As already noticed by Léger et al. (1988) the effect of IIC increases rapidly with the internal energy. Our calculations have also proved that, for two molecules presenting similar rates of IC, the importance of IIC could be greater in the case of the smaller molecule. Introducing IIC processes leads to some modifications of the fluorescence and phosphorescence properties. As did Léger et al. (1988) we define rates of Poincaré luminescence, by mutiplying the probability to emit a photon by phosphorescence or fluorescence with the rate at which the molecule returns to the excited emitting modes:

$$k_{\rm fluo}^{\rm Poincare} = (k_{\rm S_0 \to S_1} + k_{\rm T_1 \to S_1}) \frac{k_{\rm fluo}}{\sum k_{\rm i}} \,, \tag{2.18}$$

$$k_{\rm phos}^{\rm Poincare} = (k_{\rm S_0 \to T_1} + k_{\rm S_1 \to T_1}) \frac{k_{\rm phos}}{\sum k_{\rm i}} \,, \tag{2.19}$$

where $k_{\rm fluo}$, $k_{\rm phos}$ and $\sum k_{\rm i}$ represent the rates of fluorescence, phosphorescence and the sum of all the processes which the molecule can undergo, respectively. However, as in the case of Fig. 2.3, the IIC rates have relative low values for the smaller values of excess energy where visible and UV luminescence have the greatest yields. This largely limits the importance of Poincaré fluorescence and phosphorescence.

### 2.2.4 Redistribution of the absorbed energy

In this section we use the previous model to analyse the distribution of energy in a PAH having absorbed a photon. The energy ranges between 0 and 13.6 eV, which are the typical astrophysical values in HI region of the ISM. Using the references and data of Table 2.2 we have computed the total rate of luminescence (visible and UV fluorescence, phosphorescence and infrared emission) $k_{\rm lum}(E)$ as a function of energy, taking into account all the modifications introduced by the excess energy and the Poincaré luminescence (Eqs. (2.11) (2.13) (2.18) ). From the determination of photodissociation rates $k_{\rm diss}$ (Eq. (2.5)) and from the yield of ionization $Y_{\rm ion}$ (Eq. (2.14)), we are then able to estimate the yields of each process, assuming that there are no relaxation processes other than luminescence, photodissociation and ionization after the absorption of a photon. We can hence write:

$$\begin{aligned}
Y_{\rm fluo}(E) &= \frac{k_{\rm fluo}(E)}{k_{\rm tot}} \,, \\
Y_{\rm phos}(E) &= \frac{k_{\rm phos}(E)}{k_{\rm tot}} \,, \\
Y_{\rm IR}(E) &= \frac{k_{\rm IR}(E)}{k_{\rm tot}} \,, \\
Y_{\rm H\ loss}(E) &= \frac{k_{\rm H\ loss}^{\rm RRK}(E)}{k_{\rm tot}} \,, \\
Y_{\rm H_2\ loss}(E) &= \frac{k_{\rm H_2\ loss}^{\rm RRK}(E)}{k_{\rm tot}} \,, \\
Y_{\rm C_2H_2\ loss}(E) &= \frac{k_{\rm C_2H_2\ loss}^{\rm RRK}(E)}{k_{\rm tot}} \,,
\end{aligned} \tag{2.20}$$

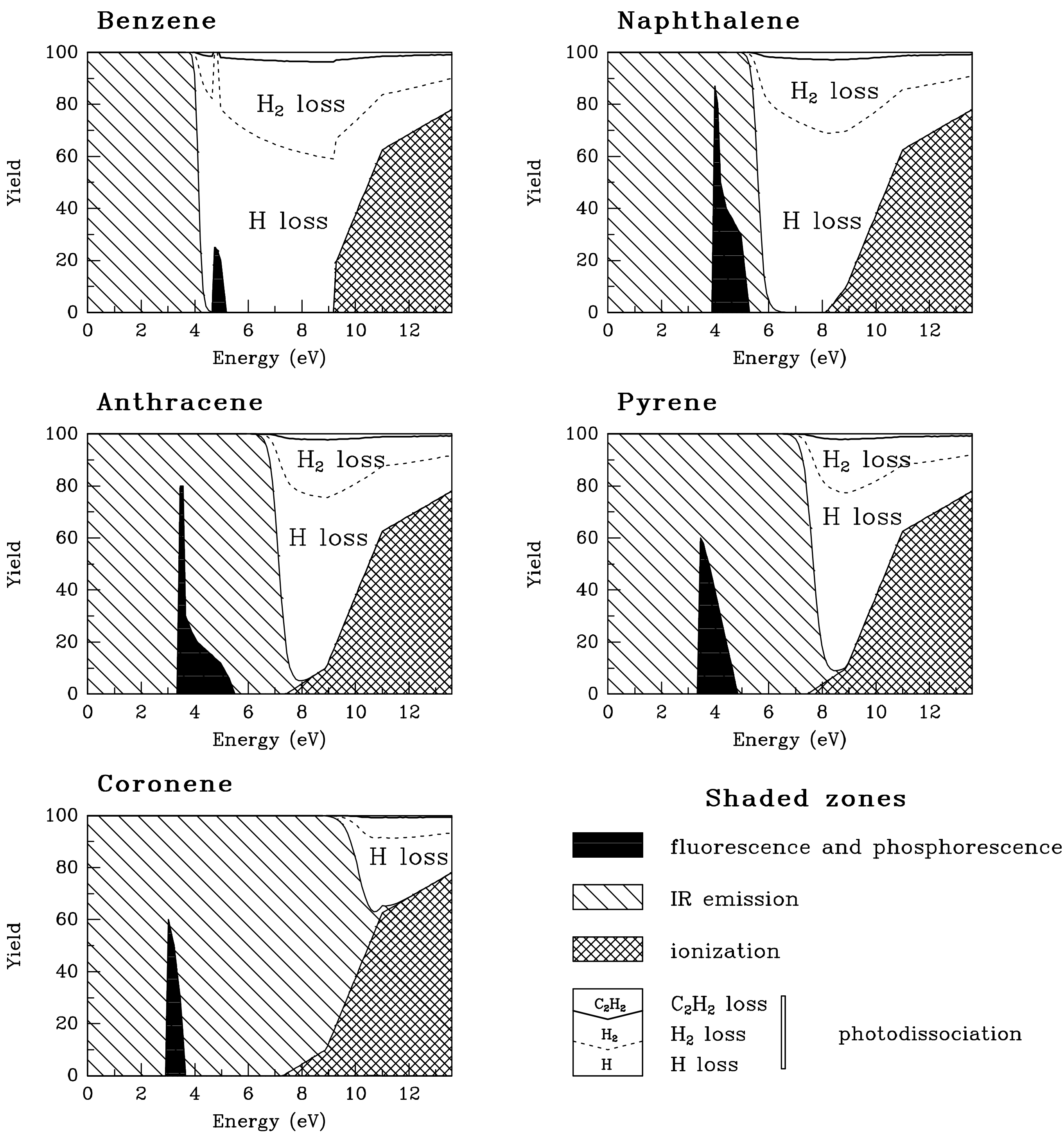


Figure 2.4: Distribution of the energy in some PAH molecules after the absorption of a photon.

where

$$\begin{aligned}
k_{\mathrm{IR}}(E) &= A_{3.3\mu\mathrm{m}} + A_{6.2\mu\mathrm{m}} + A_{7.7\mu\mathrm{m}} + A_{8.6\mu\mathrm{m}} + A_{11.3\mu\mathrm{m}} \ , \\
k_{\mathrm{lum}}(E) &= k_{\mathrm{IR}}(E) + k_{\mathrm{fluo}}(E) + k_{\mathrm{phos}}(E) \ , \\
k_{\mathrm{diss}}(E) &= k^{\mathrm{RRK}}_{\mathrm{H\ loss}}(E) + k^{\mathrm{RRK}}_{\mathrm{H_2\ loss}}(E) + k^{\mathrm{RRK}}_{\mathrm{C_2H_2\ loss}}(E) \ , \\
k_{\mathrm{tot}} &= k_{\mathrm{lum}}(E) + k_{\mathrm{diss}}(E) + k_{\mathrm{ion}}(E) \ , \\
k_{\mathrm{ion}} &= Y_{\mathrm{ion}} k_{\mathrm{tot}} \ .
\end{aligned} \tag{2.21}$$

Figure 2.4 shows that luminescence is the dominating process for all PAHs after absorption of a photon having less than 6 eV. This emission appears practically only as infrared emission although some high yields of fluorescence are observed in the vicinity of the first excited singlet state.

A striking feature is the increasing importance of infrared emission with the size of the molecule. Since the yield of ionization remains almost constant for all PAHs, this means that the larger the molecule, the smaller is its photodissociation yield. The energy for which the yield of acetylene loss is larger than 1.0 % also increases with the size of the molecule as listed in Table 2.3. The yield of acetylene loss for a coronene molecule is always less than 0.8%. This may be the reason why this reaction channel has not been observed for coronene with the experimental set–up used by Jochims et al. (1994).

Table 2.3: Minimum energy for a yield of acetylene loss greater than 0.01.

| molecule | $C_6H_6$ | $C_{10}H_8$ | $C_{14}H_{10}$ | $C_{16}H_{10}$ | $C_{24}H_{12}$ |
|---|---|---|---|---|---|
| Energy (eV) | 4.96 | 5.72 | 7.23 | 7.77 | - |

## 2.3 Photodissociation rates of PAHs in the ISM

In the next subsection we present the expressions we use for the interstellar UV radiation field. The calculations of photodissociation rates are presented in the following two subsections.

### 2.3.1 Interstellar radiation field

Estimates of the intensity of the background interstellar radiation field of the ISM and of the solar neighbourhood have been made by Habing (1968), Witt and Johnson (1973), Jura (1974), Draine (1978), Gondhalekar et al. (1980) and Mathis et al. (1983).

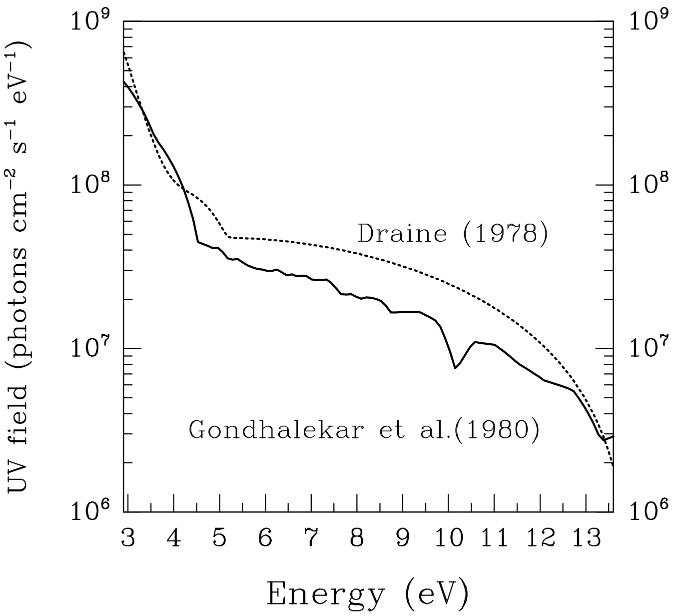


Figure 2.5: Intensity of the interstellar radiation field.

Draine (1978) has proposed an analytic expression for the angle-averaged photon flux $\lambda^3 u_\lambda / 4\pi h^2 c$ where $u_\lambda$ is the radiative energy density.

$$\begin{aligned} \frac{N_1(E)}{4\pi} &= 6.919\ 10^3 (E/\mathrm{eV})^3 - 2.152\ 10^5 (E/\mathrm{eV})^2 \\ &\quad +1.658\ 10^6 (E/\mathrm{eV}) \\ &\qquad \text{photons cm}^{-2}\text{s}^{-1}\text{eV}^{-1}\ . \end{aligned} \tag{2.22}$$

$N_1(E)$ represents the photon flux integrated over all directions. Equation (2.22) gives valid results over the range 5 – 13.6 eV. However, the energies of interest for the study of PAH photodissociation range from the threshold of fragmentation at 2.8 eV to the Lyman limit at 13.6 eV. To extend the expression (2.22) to lower energies, we use the observational results of Witt and Johnson (1973), which has been used by Draine (1978), and obtain the following expression for the total flux over the range 2.8 – 5.2 eV:

$$\begin{aligned} N_1(E) &= 4.89085\ 10^6 (E/\mathrm{eV})^4 - 9.133074\ 10^7 (E/\mathrm{eV})^3 \\ &\quad + 6.36590\ 10^8 (E/\mathrm{eV})^2 - 1.96811\ 10^9 (E/\mathrm{eV}) \\ &\quad + 2.28706\ 10^9 \\ &\qquad \text{photons cm}^{-2}\text{s}^{-1}\text{eV}^{-1}\ . \end{aligned} \tag{2.23}$$

The expressions (2.22) and (2.23) provide us a first set of values $N_1$ for the photon flux in the ISM. As did van Dishoeck (1988), we also use another set $N_2$ of more recent data. Gondhalekar et al. (1980) have indeed indicated an interstellar UV radiation field over the range 4.5 – 13.3 eV which is somewhat smaller than the previous estimates of Draine. However, they have used the first observations made over the whole sky and should therefore provide a realistic value of the total interstellar radiation field. The theoretical estimate of Mathis et al. (1983) appears to be in good agreement with the results of Gondhalekar et al. (1980) and has been used to extend the latter interstellar radiation field to the range 2.8 – 13.6 eV. The two sets of values are reported in Fig. 2.5.

### 2.3.2 Photodissociation rates

In order to compute the rate of a process $(i)$ for a given species $(s)$ in the ISM, one needs to know the yield $Y_{(s)}^{(i)}$ of the involved process, the absorption cross–section $\sigma_{(s)}$ of the species and the photon flux $N$, as a function of the energy $E$. The photodissociation rate is then given by the following relation:

$$k^{\mathrm{ISM}(i)}_{(s)} = \int_{E=E_0}^{E=13.6eV} Y_{(s)}^{(i)}(E)\ \sigma_{(s)}(E)\ N(E)\ dE\ . \tag{2.24}$$

Using the yields defined in Eq. (2.20) and the photon flux of Sect. 2.3.1 we compute the rate of photodissociation and photoionization of benzene, anthracene, pyrene and coronene, using the spectra of Joblin (1992) for the UV–absorption cross–sections.

To examine the effect of size we also calculate these rates for ovalene and for PAH molecules containing up to 100 carbon atoms. For ovalene and larger PAHs the yields were computed without taking into account IIC rates and the modifications of the Einstein coefficients for IR emission. For PAHs larger than ovalene we also omit phosphorescence and adopt a typical rate of $10^7$ s$^{-1}$ for fluorescence and the following expression of Robertson (1986) for an estimate of the energy of the first excited state

$$E_{\mathrm{S_1-S_0}} = \frac{2\beta}{N_{\mathrm{ring}}}\ , \tag{2.25}$$

where $N_{\mathrm{ring}}$ is the number of rings of the molecule and $2\beta$ a transition energy equal to 4.8 eV deduced from experiment. The UV absorption cross–section of ovalene is taken from Joblin (1992) and for the larger PAHs from Verstraete & Léger (1992). The results obtained for the two sets of interstellar field are listed in Tables 2.4 and 2.5. The two sets of results differ by a factor 1.6 with larger values for the radiation field of Draine (1978).

To have a better view of the size effect on the photoreactions we plot in Fig. 2.6 the rates as a function of the number of carbon atoms of the molecules for the values of photon flux given by Gondhalekar et al. (1980). From Fig. 2.6 we observe a slight increase of the photoionization rate with the size of the molecule. This can be easily explained when one considers that the yield of ionization is practically the same for all PAHs whereas the cross-sections of absorption vary roughly as $N_{\mathrm{C}}$ (Verstraete et al. 1990). The explanation for the lower rate of pyrene ($N_{\mathrm{C}}$ = 16) compared with the rate for anthracene ($N_{\mathrm{C}}$= 14)

Table 2.4: Photodissociation rates of PAH molecules in the ISM (unit = $s^{-1}$).

| | H loss | | $H_2$ loss | | $C_2H_2$ loss | |
|---|---|---|---|---|---|---|
| | Set 1[a] | Set 2[b] | Set 1 | Set 2 | Set 1 | Set 2 |
| benzene | 4.76 (−9) | 2.89 (−9) | 2.51 (−9) | 1.50 (−9) | 2.51 (−10) | 1.49 (−10) |
| anthracene | 6.17 (−9) | 3.40 (−9) | 2.15 (−9) | 1.19 (−9) | 2.14 (−10) | 1.89 (−10) |
| pyrene | 3.73 (−9) | 2.05 (−9) | 1.28 (−9) | 7.13 (−10) | 1.29 (−11) | 7.13 (−11) |
| coronene | 2.56 (−9) | 1.49 (−9) | 7.61 (−10) | 4.55 (−10) | 7.61 (−11)[c] | 4.55 (−11)[c] |
| ovalene | 2.07 (−10) | 1.78 (−10) | 5.58 (−11) | 4.85 (−11) | 5.59 (−12)[c] | 4.85 (−12)[c] |
| PAH 50 C | 2.27 (−16) | 2.31 (−16) | 3.51 (−17) | 3.61 (−17) | 3.49 (−18)[c] | 3.56 (−18)[c] |

(a) radiation field from Draine (1978), (b) radiation field from Gondhalekar et al. (1980), (c) results extrapolated from the experiments of Jochims et al. (1994)

Table 2.5: Photoionization rates of PAH molecules in the ISM (unit = $s^{-1}$).

| molecule | Set 1[a] | Set 2[b] |
|---|---|---|
| benzene | 2.01 (−9) | 1.23 (−9) |
| anthracene | 4.63 (−9) | 2.79 (−9) |
| pyrene | 3.84 (−9) | 2.34 (−9) |
| coronene | 7.53 (−9) | 4.54 (−9) |
| ovalene | 8.43 (−9) | 5.09 (−9) |
| PAH 50 C | 9.79 (−9) | 6.24 (−9) |

(a) radiation field from Draine (1978), (b) radiation field from Gondhalekar et al. (1980)

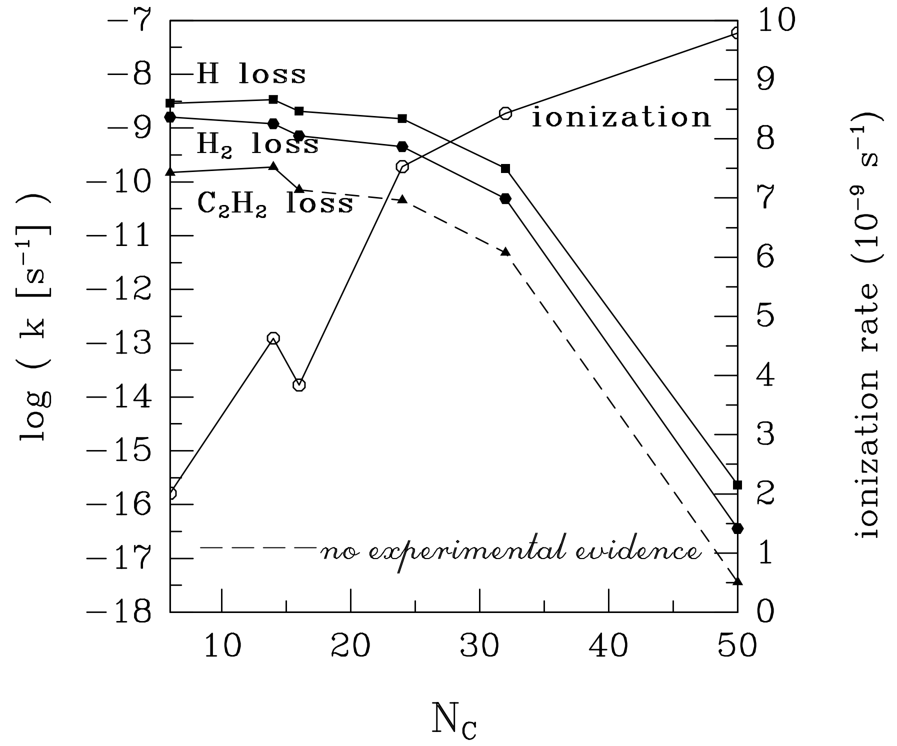


Figure 2.6: Photodissociation and photoionization rates of PAH molecules in the ISM.

may be found in the compact form of the pericondensed molecule of pyrene to be compared with the linear shape of the catacondensed molecule of anthracene.

The decrease of the photodissociation rates with size is *a priori* more difficult to predict. Larger PAHs have indeed larger absorption cross–sections and are therefore more likely to be photodissociated but the yields of photodissociation for large PAHs are much lower than for small PAHs. As has already been shown by Jochims et al. (1994), Fig. 2.6 confirms that large PAHs are more stable against photodissociation.

For PAHs having $N_{\rm C} > 50$ carbon atoms the results of photodissociation and photoionization are well reproduced by the following analytical expressions:

$$k^{(i)}_{\rm loss}(N_{\rm C}) = k^{(i)}_{\rm loss}(50)\ 10^{-0.3373(N_{\rm C}-50)}\ , \tag{2.26}$$

$$k^{(i)}_{\rm ion}(N_{\rm C}) = k^{(i)}_{\rm ion}(50)\left(\frac{N_{\rm C}}{50}\right)\ , \tag{2.27}$$

where $(i)$ represents a given choice for the interstellar field and reaction channel.

Since the parameters entering into the expression (2.5) of the RRK theory are not a direct result of the experiment but constants determined to fit the experimental results, it is worth testing the sensitivity of our results to these parameters. For the present purpose

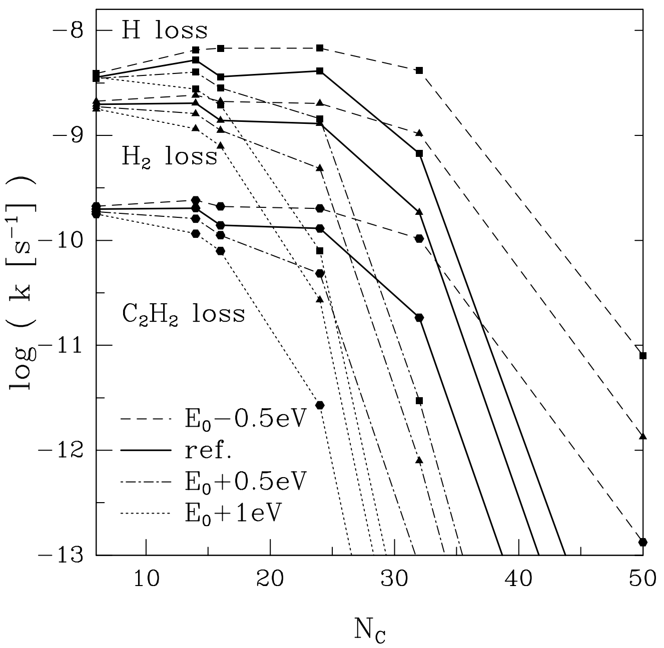


Figure 2.7: Dissociation rates in the ISM from RRK calculations with various values of the parameter $E_0$.

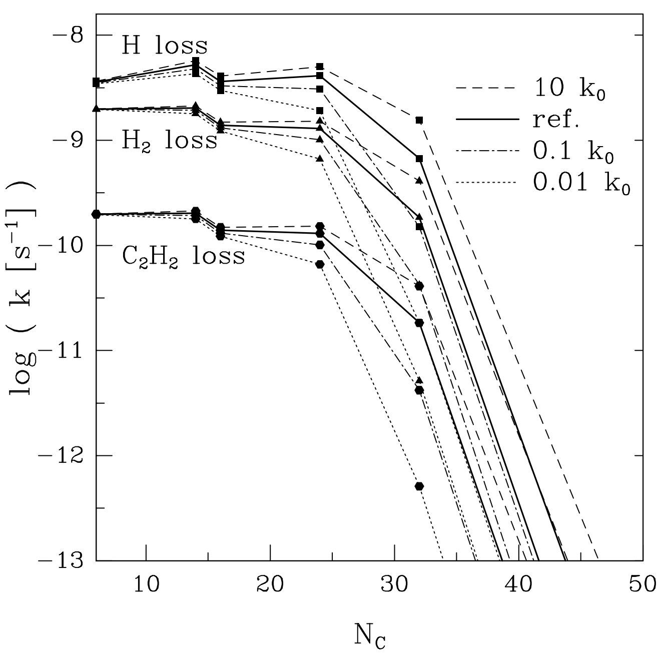


Figure 2.8: Dissociation rates from RRK calculations with various values of the parameter $k_0$.

we have used only the set of data from Gondhalekar et al. (1980) for the radiation field. We have made two series of calculations. The first was achieved by simultaneously modifying $E_0$ values for the three loss channels by increments ranging from -0.5 eV to +1 eV and keeping the values for the parameter $k_0$ unchanged. In the second calculation, $E_0$ values remained at their original values but we multiplied $k_0$ by a factor ranging from 0.01 to 10 common to the three reactions. The results of these two series of calculation are displayed in Figs. 2.7 and 2.8. The variation of $k^{\rm ISM}$ with $E_0$ and $k_0$ increases with the number of carbon atoms. This result was expected after inspection of Eq. (2.5). However, for molecules with less than 20 carbon atoms these variations remain smaller than an order of magnitude for a variation of $E_0$ of 1 eV and a variation of two orders of magnitude of $k_0$. For larger molecules the results of the calculations have to be taken with care since they are very sensitive to the parameters and since there has not always been real laboratory evidence for the photoejection of acetylene molecules from PAHs larger than pyrene (Jochims et al. 1994).

### 2.3.3 The case of an acetylenic group attached to a PAH structure

In the previous sections we have investigated the rates for the loss of an acetylene molecule from a compact PAH molecule. From the network of Frenklach & Feigelson (1989) and Cherchneff et al. (1992) who have studied the formation of PAHs in the circumstellar envelopes of carbon–rich late type red giant stars it can be seen that many species in the shells of these stars are composed of a PAH with an acetylenic group attached to its carbon skeleton (the simplest example of such molecules is phenylacetylene). It is therefore of interest to study the loss of the acetylenic group from these molecules. No experimental data addressing this question has been found in the literature. We have therefore used a theoretical approach similar to that already given in Sect. 2.2.2.

We first concentrate on the case of phenylacetylene. We use the expression (2.1) from the thermo–photodissociation theory to determine the rate of photolysis of the benzene-ethynyl group bond because the parameters entering in Eq. (2.1) may be easily evaluated. For this purpose we follow the approach of Benson (1976) and assume that the reaction of dissociation for a molecule thermalised at temperature $T$ has the form of the Arrhenius law. We estimate the frequency factor to be $k_0 = 10^{17}$ s$^{-1}$, taking the same value as that for similar reactions. To determine the activation energy $E_0$ we observe that the reverse reaction is a radical–radical recombination reaction which has no barrier energy. The activation energy of the dissociation reaction is therefore simply equal to the enthalpy of the dissociation reaction.

$$E_0 = \Delta H_{\rm r} = \Delta H_{\rm f}(\varphi\bullet) + \Delta H_{\rm f}(\equiv \bullet) - \Delta H_{\rm f}(\varphi- \equiv) \,, \tag{2.28}$$

where $\varphi$ and $\equiv$ represent the phenyl and ethynyl groups, respectively. $\Delta H_{\rm f}$ corresponds to the energy of formation which can be deduced using the group additivity theory of Benson (1976), from which we obtain the value of 5.2 eV for the activation energy $E_0$. The

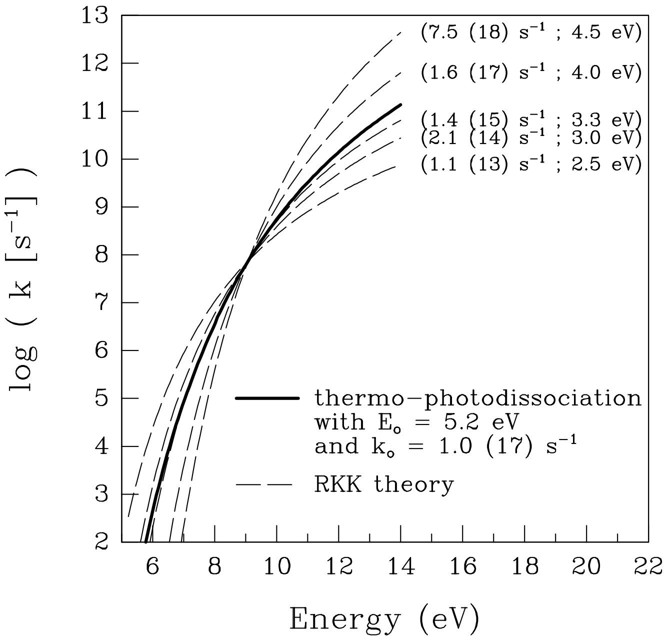


Figure 2.9: Rate of photolysis of the $\varphi$–$C_2H$ bond as a function of internal energy calculated by the thermo–photodissociation and RRK models.

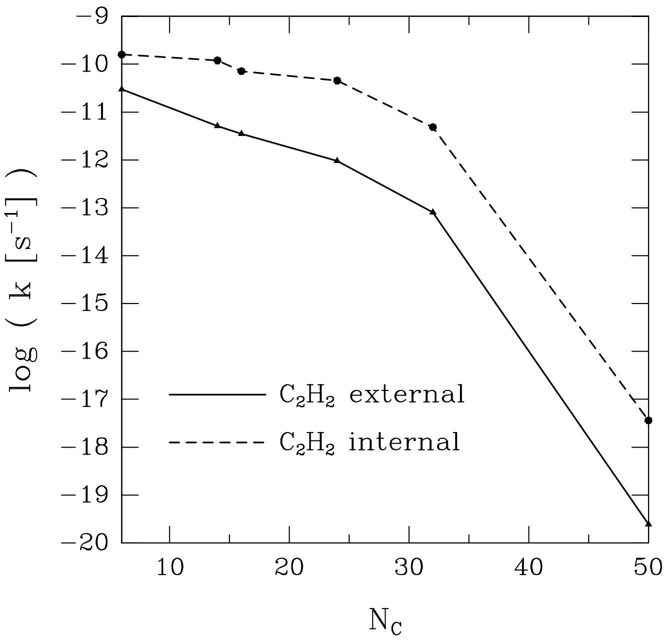


Figure 2.10: Rate of photolysis of the $\varphi$–$C_2H$ bond as a function of the number of carbon atoms of the PAH molecule bearing the acetylenic group.

vibrational modes of phenylacetylene have also to be evaluated in order to use the theory of thermo–photodissociation. They have fortunately already been calculated by Palmő *et al.* (1986), Pietilä et al. (1987) and Csàszàr et al. (1989) who have developed various force fields. We use the more recent results which are in better agreement with the observations of King & So (1970). Using all these data we compute the rate of photolysis of the $\varphi$ — $C_2H$ bond as a function of the internal energy of the molecule. The results are displayed in Fig. 2.9.

There is no data in the literature concerning vibrational states of larger PAHs bearing an ethynyl group. We therefore use the RRK theory for these molecules. In order to determine the parameters $E_0$ and $k_0$ entering in the expression (2.5) we first fit the curve provided by thermo–photodissociation calculations of phenylacetylene for the dependence of the rate with internal energy. As shown in Fig. 2.9 this is correctly achieved in the domain of interest for the pair of values:

$$E_0 = 3.3 \text{ eV} , \tag{2.29}$$

$$k_0 = 1.4 \; 10^{15} \text{ s}^{-1} . \tag{2.30}$$

We then assume that these values also give correct values for larger PAHs as has been observed by Jochims et al. (1994) for the loss of an acetylene molecule from compact PAHs.

To compute the rate of dissociation in an astrophysical environment one has to integrate, over the energy, the yield corresponding to this process multiplied by the number of absorbed photons for a given energy (see Eq. (2.24)). Unfortunately, much of the data needed concerning PAH molecules having an acetylenic group is not available. For the calculations, we have therefore assumed that the rates for fluorescence, phosphorescence and ionization of PAHs bearing an acetylenic group are equal to that of the corresponding PAHs without side chains. The UV absorption cross–section and the IR Einstein coefficient of the PAHs with an acetylenic group have been evaluated from the data of the corresponding PAHs without side chain by scaling to the number of carbon atoms (for instance in the case of the cross–section of acetylcoronene we write $\sigma(C_{24}H_{12}\text{–}C_2H) \simeq 26/24\ \sigma(C_{24}H_{12})$). This may be the crudest approximation of the calculation and may introduce the largest errors, especially for the smallest molecules whose structures are markedly changed by the addition of an acetylenic group. We also assume that the photodissociation processes leading to the loss of hydrogen and acetylene from the compact part of the PAHs can be calculated with the RKK theory using the same constants $E_0$ and $k_0$ as for compact PAHs.

To simplify the following discussion we will call internal acetylene an acetylene molecule ejected from the compact part of the PAH and refer to external acetylene when considering the loss of the attached acetylenic group. Figure 2.10 shows the results obtained for the loss of internal and external acetylene of PAHs having up to 50 carbon atoms, calculated for the radiation field of Gondhalekar et al. (1980).

The rates obtained for the loss of an external acetylenic group are relatively smaller than the rate corresponding to the loss of an internal acetylene molecule although the constants $E_0$ and $k_0$ are quite similar. This might be explained by the difference of the photodissociation reactions involved in the two processes. For the photolysis of the external acetylenic bond the vibrational energy has to be transfered to one bond of the molecule whereas the loss of an internal acetylenic group involves the vibrations of the carbon skeleton and may take place at various sites in the PAH. However, our estimate of $10^{17}$ s$^{-1}$ for the frequency factor of photo–thermodissociation from phenylacetylene is still uncertain and should be confirmed by experiment results. Finally, we note that for both ejection of internal and external acetylene the evolution of the photodissociation rate with PAH size plotted in Fig. 2.10 shows no unexpected results and confirms the stability of larger PAHs against photodestruction.

## 2.4 Astrophysical implications

The results concerning the photoejection rate of an acetylene molecule provide an estimate of the characteristic time $\tau^{\mathrm{UV}}$ of destruction of PAHs in interstellar regions where UV photodissociation is the most important cause of destruction. If we introduce the factor $\chi$ to describe a medium with a radiation field $\chi$ times larger than the mean interstellar field (for example a typical value for a planetary nebula is $\chi = 10^4$), we obtain for the destruction time:

$$\tau^{\mathrm{UV}}{}_{\mathrm{PAH}} = \frac{1}{\chi \; k^{\mathrm{ISM}}{}^{\mathrm{C_2H_2}}_{\mathrm{PAH}}} \ , \tag{2.31}$$

where $k^{\mathrm{ISM}\ \mathrm{C_2H_2}}_{\mathrm{PAH}}$ is the value for the loss of acetylene from a PAH in the ISM with $\chi = 1$. We list in Table 2.6 the corresponding destruction times for some small PAH molecules in the ISM.

The growth time of PAHs is given by:

$$\tau^{\mathrm{gr}} = \frac{1}{n_{<\mathrm{H}>} \; X(\mathrm{C}) \; k_{\mathrm{C}}} \ , \tag{2.32}$$

where $n_{<\mathrm{H}>}$, $X(\mathrm{C})$ and $k_{\mathrm{C}}$ represent respectively the total hydrogen density, the carbon abundance and reaction rate for accretion of carbon particles (carbon atoms or cations). The PAHs whose growth time is smaller than the characteristic time of photodestruction tend to grow. The accretion of carbon dominate over acetylene molecule loss so that the PAHs resist the radiation field. In contrast, the PAHs having $\tau^{\mathrm{UV}}_{\mathrm{PAH}} < \tau^{\mathrm{gr}}$ lose acetylene more rapidly than they accrete carbon and are therefore destroyed in a time of the order of $\tau^{\mathrm{UV}}_{\mathrm{PAH}}$. The smallest size of surviving PAHs is obtained for equality of $\tau^{\mathrm{UV}}_{\mathrm{PAH}}$ and $\tau^{\mathrm{gr}}$.

To have a more quantitative idea we have plotted in Fig. 2.11 the locations of the minimal size of surviving PAHs in the log($\chi$) , log($\mathrm{n}_{<\mathrm{H}>}$) plane. From Fig. 2.11 it is clear that for increasing values of $\chi$ and decreasing values of $n_{<\mathrm{H}>}$ the minimal size of surviving PAHs gradually increases. To draw Fig. 2.11 we have adopted the values of $3.10^{-4}$ for the carbon abundance and $10^{-12}$ cm$^3$s$^{-1}$ for $k_{\mathrm{C}}$ from Omont (1986). Some modifications of the value of $k_{\mathrm{C}}$ could arise from the different nature of the accreting carbon particles and a

Table 2.6: Destruction times of small PAH molecules in the ISM ($\chi = 1$).

| molecule | $k^{\mathrm{ISM}\,\mathrm{C_2H_2}}_{\mathrm{PAH}}\,(\mathrm{s}^{-1})^{(\mathrm{a})}$ | $\tau^{\mathrm{UV}}{}_{\mathrm{PAH}}$ (years) |
|---|---|---|
| benzene | 1.49 (−10) | 213 |
| anthracene | 1.89 (−10) | 168 |
| pyrene | 7.13 (−11) | 442 |
| coronene | 4.55 (−11)[b] | 692 |
| ovalene | 4.85 (−12)[b] | 6.50 (3) |
| PAH 50 C | 3.56 (−18)[b] | 8.91 (9) |

(a) data using the radiation field of Gondhalekar *et al.* (1980), (b) value not confirmed experimentally

Table 2.7: Physical properties of various astrophysical regions.

| medium | Object | $n(\mathrm{cm}^{-3})$ | $\chi$ |
|---|---|---|---|
| Planetary nebula | NGC 7027[a] | 7 (4)[b] | 4.6 (5) |
| $\mathrm{H_{II}}$ region | Orion Bar[c] | 1 (5)[d] | 4.3 (3) |
| Reflection Nebula | NGC 7023[e] | 4 (3)[f] | 2.5 (3) |
| Galactic nucleus | M82[g] | 1 (4)[h] | 2.9 (3) |
| Diffuse medium | Galactic plane[i] | 6 (-1)[j] | 1 (0) |

References to the observations and physical conditions (a) Cohen et al. (1986), (b) Allamandola et al. (1989), (c) Bregman et al. (1989), (d) Tielens and Hollenbach (1985a, 1985b), (e) Sellgren et al. (1985), (f) Chokshi et al. (1988), (g) Willner et al. (1977), (h) Wolfire et al. (1988), (i) Giard et al. (1988) and (j) Allen (1973)

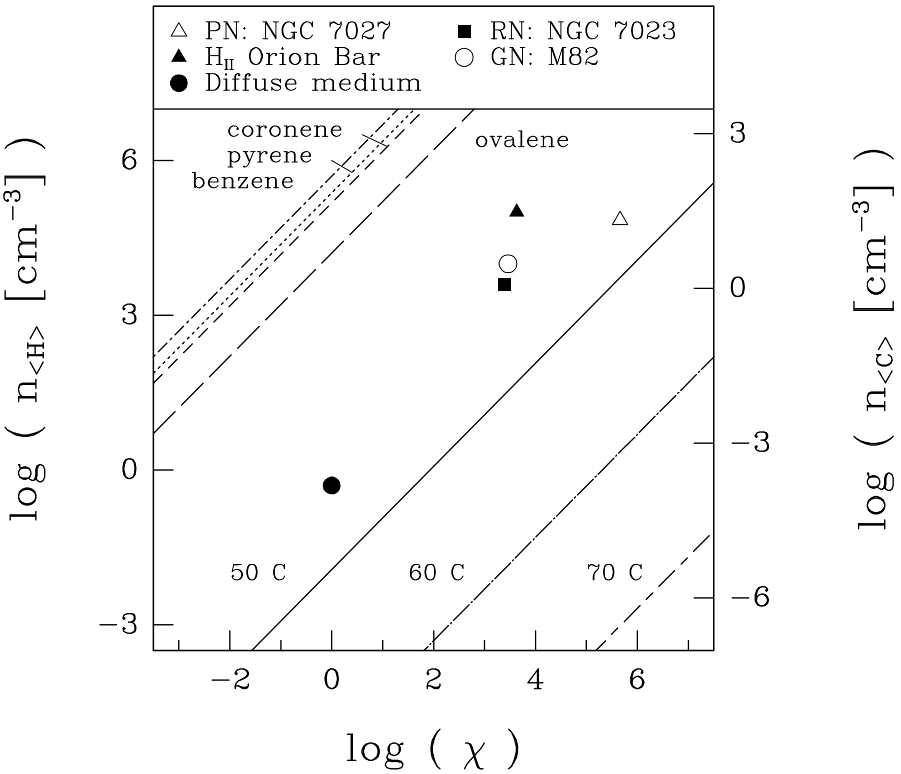


Figure 2.11: Locations of the minimal size (number of carbon atoms) of PAHs in the plane $\log(\chi)$–$\log(n_{<H>})$. The astrophysical environments mentioned are discussed in the text.

maximal value of $10^{-10}$ $cm^3s^{-1}$ could be eventually reached when one assumes a Langevin rate for collision between PAH molecules and $C^+$ cations and an accretion yield of 10 % (Bohme 1982). Indeed, the value of $10^{-12}$ $cm^3s^{-1}$ rather constitutes a low limit for the carbon accretion rate. However, we note that this value of $k_C$ is in agreement with the rate of Frenklach & Feigelson (1989) for a PAH ring closure by addition of acetylene.

We have also plotted in Fig. 2.11 the positions of some media where the UIR emission bands attributed to PAHs have been observed. The physical parameters of these media are presented in Table 2.7 with references to the observations. We have restricted our choice to some regions already studied by Omont (1986) and by Allamandola et al. (1989). As already mentioned the coefficient $\chi$ is the scaling factor to be multiplied to the radiation field of Gondhalekar et al. (1980) to describe the various environments. Allamandola et al. (1989) and Omont (1986) have used another unit for the intensity of the incident radiation field, namely the average interstellar UV field of Habing (1968) integrated between 6 and 13.6 eV and an average interstellar UV field ($10^7$ photons $s^{-1}$ $cm^{-3}$ $sr^{-1}$), respectively. The differences in the values of $\chi$ with that of these authors are therefore due to our choice of the UV interstellar radiation field. We have also included in Table 2.7 the diffuse medium where the band at 3.3 $\mu m$ has been observed (Giard et al. 1988).

Figure 2.11 demonstrates that for all media showing the UIR bands the minimal size of surviving PAHs is between 30 and 50 carbon atoms. This result is unchanged when using the value $10^{-10}$ $cm^3s^{-1}$ for the carbon accretion rate. The minimal size of PAH obtained here is quite similar to the result of Jochims et al. (1994) who compared the rate of photodissociation obtained from RRK theory to the rates of IR radiation. They concluded that, after absorption of a photon of energy 13.6 eV, PAHs having more than 30 – 40 carbon atoms should undergo relaxation via IR emission rather than photodissociation and therefore are likely to subsist in the ISM. Our approach is different: we propose here values for the rate of photoejection of an acetylene group integrated over the photon energy available in the ISM and compare this rate with the rate of the reverse process of carbon addition. Our results demonstrate that under the conditions of the interstellar radiation field, PAHs containing less than $\simeq 30--50$ carbon atoms have energy integrated photodissociation rates larger than the carbon accretion rate and are therefore eventually destroyed by the UV radiation field. This is independent of the fact that, according to Jochims et al. (1994), the larger of these PAHs ($N_C = 30 - 50$) may have photodissociation rates lower than IR emission rates for some values of the internal energy. Another point to note is that the limit–size of 50 carbon atoms is in agreement with the value obtained by Allamandola et al. (1989) for the size of interstellar PAHs from the UIR intensity observations.

For the calculations we have considered only fully hydrogenated molecules. However, it is thought that a large fraction of PAHs are ionized and partially dehydrogenated (Léger & d'Hendecourt 1985; van der Zwet & Allamandola 1985; Tielens et al. 1987; Allamandola *et al.* 1989; Geballe et al. 1989; Léger et al. 1989a,1989b; Verstraete et al. 1990). Cations are surely less stable against photodissociation than their parent molecules because they cannot lose energy through ionization as easily as the neutral PAHs. As has been shown by Leach (1986) one needs about 11 – 13 eV to ionize a PAH cation whereas the ionization potential of neutral PAHs is about 7 eV. It is also evident that dehydrogenated PAHs are less stable against photodissociation because of the lowering of the number of vibrational modes over which they can redistribute the energy and through which they can relax via IR emissions. The values of 30–50 carbon atoms we obtain for the smallest surviving PAHs are therefore a lower limit and will have to be revised to account for the exact physical state of interstellar PAHs. There is unfortunately little knowledge concerning the physical and chemical properties of PAH cations and dehydrogenated PAHs and it makes their study difficult. This question is adressed in the next chapter.

One advantage of having integrated photodissociation rates is that they may be used in the conservation equation of PAHs and therefore may help to provide estimates of the density of PAHs in the ISM. These rates are crucial for small PAHs ($N_C < 50$) for which the interstellar UV radiations are a very effective cause of destruction. Only an intensive formation *in situ* may indeed make possible their presence in UV exposed regions. Unfortunately, the rates of formation of such processes are rather uncertain, partly because the processes are largely unknown. Most of the proposed mechanisms evoke PAH formation by sputtering of dust in shocked regions (Omont 1986; Duley and Williams 1986; Waters et al. 1989; Brown et al. 1989, Flower et al. 1990). Herbst (1991) has proposed a model for the formation of hydrocarbon molecules having 30 carbon atoms in dense region. Both types of proposal unfortunately suffer from large uncertainties and a lack of experimental data and therefore prevent us from making a definitive assessment. It is however questionable whether the molecules of ovalene and coronene often presented as prototypes of interstellar PAHs and all the smaller PAHs are present in the ISM. We have shown here that in all media showing the UIR bands these molecules are indeed destroyed on a timescale of some years (see Eq. (2.31) and the values of $\chi$ in Table 2.7). Due to the lower UV radiation field in the diffuse medium this timescale is larger there (about $10^3$ years).

The case of large PAHs ($N_C > 50$) is different because they can survive the interstellar UV field in all situations. Their destruction may happen through oxidation reactions (Duley & Williams 1986) or strong shocks (Omont 1986; Flower et al. 1990). Latter (1991) has concluded that the lifetime of such PAHs is probably as large as $10^8$ years, which is also the timescale for the galactic rotation and somewhat larger than the lifetime of a typical molecular cloud. He proposed that PAHs formed in the envelopes of C–giants are distributed in the ISM where the UIR are observed and showed that the yield of formation of PAHs calculated by Frenklach & Feigelson (1989) could explain the abundances of PAHs deduced from the observations. However, more recent calculations of Cherchneff et al. (1992) argue that the yield of formation calculated in more realistic envelope models is at best not as high as $10^{-4}$ times the yield of Frenklach & Feigelson (1989). This puts into question the results of Latter (1991). Nevertheless, recent calculations by Cherchneff (1995) show that the formation yield of PAHs may be enhanced in the shocks of circumstellar red giants envelopes. Cadwell et al. (1994) show that this yield could also be enhanced following deposition of PAHs on grains. These new results are encouraging and show that further quantitative study into the formation and destruction of interstellar PAHs is required to make valid estimates of the density of PAHs in the ISM.

## 2.5 Conclusion

We have presented a model for interstellar PAHs which includes the most recent knowledge about the behaviour of these molecules in space using both theoretical and experimental results. This model has enabled us to calculate the integrated rates of photodissociation corresponding to the loss of atomic and molecular hydrogen and of acetylene molecules.

Comparing the rate of photoejection of acetylene to the rate of accretion of carbon particles to PAHs we have deduced that in all the media showing the UIR emission bands (reflection nebulae, planetary nebulae, galactic nuclei, $H_{II}$ region) only PAH molecules having more than 50 carbon atoms can survive the interstellar UV radiation field. They may also possibly grow by accretion of carbon atoms or ions.

On the contrary, in media exposed to strong UV radiation fields the time of destruction of PAHs as large as ovalene ($N_C$= 32) and smaller is not longer than a few years. As it is doubtful that any process could form PAHs more rapidly in these media we question the presence of small PAHs ($N_C \leq 32$) where the UIR bands are seen. Moreover, as a large fraction of PAHs is ionized and probably partially dehydrogenated the actual rates of photodissociation may be even larger and may therefore lead to a larger minimal size for the surviving PAHs and a quicker destruction of small PAHs.

However, with the help of the results obtained here it is at present impossible to estimate the PAH density in the ISM because there are still too many uncertainties concerning their formation and destruction processes.

A hypothesis or theory is clear, decisive and positive but is believed by no one but the man who created it. Experimental findings on the other hand, are messy, inexact things which are believed by everyone except the man who did the work

Harlow Shapley

# Chapter 3

# PAH states of ionization and hydrogenation

**abstract**

The model for interstellar polycyclic aromatic hydrocarbons (PAHs) of Chap. 2 is extended in order to describe ionized and partially dehydrogenated PAHs and hence provide a more realistic description of these species in the interstellar medium (ISM). When ionized and partially dehydrogenated, PAHs are less stable against photodestruction than their parent molecules. For instance, an ovalene cation with 32 carbon atoms has photodissociation rates 4 times greater than the corresponding molecule, whereas the corresponding totally dehydrogenated molecule has photodissociation rates 3 orders of magnitude greater. However, in the regions where the unidentified infrared (UIR) emission bands have been observed (reflection nebulae, planetary nebulae, HII regions, active galactic nuclei...) only PAHs with less than 50 carbon atoms may be considerably dehydrogenated. In contrast, the fraction of ionized PAHs is quite similar for all molecular sizes of PAHs but its value largely depends on the physical properties of the considered medium. A low ionization fraction is always found to be associated with relatively high hydrogen coverage of small PAHs. Taking into account these ionization and hydrogenation states leads to the conclusion that PAHs with more than 50 carbon atoms may survive the UV radiation field in the regions of the ISM where the UIR bands are observed. The smaller PAHs are all destroyed within some years in the media of high UV field which exhibit the UIR bands.

## 3.1 Introduction

Seven years after the first observations of the unidentified infrared (UIR) emission bands in the spectra of astrophysical sources (Gillet et al. 1977), it was proposed by Léger & Puget (1984) and by Allamandola et al. (1985) that these bands may be attributed to free polycyclic aromatic hydrocarbons (PAHs). The emission bands are mainly observed in regions associated with an intense UV radiation field (reflection nebulae, planetary nebulae, HII regions, active galactic nuclei...) and ultraviolet absorption is therefore generally thought to be the excitation process of PAHs.

Using the relative intensities of the spectra of the UIR bands and models for the excitation of PAHs, it is possible to estimate the molecular size of interstellar PAHs (Allamandola *et al.* 1987, 1989). Geballe *et al.* (1989) have for instance estimated that in the Orion Bar and the Red Rectangle PAHs should contain 15 – 20 carbon atoms, and Woodward *et al.* (1989) obtained an estimation of 13 – 27 carbon atoms in the case of NGC 7027. These results have led Duley & Jones (1990) to suggest that PAHs such as naphthalene, anthracene and tetracene are responsible for the emission of the UIR bands. These propositions have been recently questioned by the experimental results of Jochims et al. (1994) who have shown that only PAHs having more than 30 – 40 carbon atoms are expected to survive the interstellar radiation field. The theoretical study presented in Chap. 2 is based on these results and has concluded that the photodissociation rates of PAHs molecules having less than $\simeq 32$ carbon atoms are larger than the rate for accretion of carbon in the regions where the UIR bands are observed, and that these PAHs are destroyed within some years in the regions of high UV radiation field.

The photodissociation rates calculated in Chap. 2 have been obtained for fully hydrogenated PAH molecules. However, interstellar PAHs are thought to be ionized and partially dehydrogenated. (Léger & d'Hendecourt 1985; van der Zwet & Allamandola 1985; Omont 1986; Tielens et al. 1987; Allamandola *et al.* 1989; Geballe et al. 1989; Léger et al. 1989a,1989b; Verstraete et al. 1990). Cations and partially dehydrogenated PAHs are possibly less stable against photodissociation and it is the aim of this chapter to investigate their photodissociation rates in the regions showing the UIR bands. These rates are calculated in Sect. 3.2. In order to apply these rates the states of ionization and dehydrogenation of PAHs in these environments are estimated in Sect. 3.3 and, finally, the implications for the molecular size of interstellar PAHs are discussed in Sect. 3.4.

## 3.2 Photodissociation rates of PAH cations and radicals

In Chap. 2 we have developed a model in order to estimate the rates of photodissociation of PAH molecules in UV exposed regions. We propose here some modifications to take into account PAH cations and dehydrogenated PAHs. Using this modified model we calculate the rates for photodissociation of ionized and partially dehydrogenated PAHs.

### 3.2.1 Extension of the model to PAH cations

Léger & d'Hendecourt (1985), Omont (1986) and Verstraete et al. (1990) have shown that in some astrophysical environments a large fraction of PAHs are ionized. It is therefore worthwhile estimating the rates of photodestruction of PAH cations. Following the same approach as in Chap. 2, we have considered the UV and visible absorption cross–sections of PAH cations as well as their rates of UV, visible and IR luminescence, ionization and photodissociation.

The UV and visible absorption spectra of naphthalene, pyrene, perylene and coronene cations ( Salama & Allamandola 1991,1992; Lee & Wdowiak 1993a) have been recently measured in various matrices showing some differences with the spectra of their neutral precursors, especially the development of an absorption continuum. Since it is not yet clear whether the experimental set–up is responsible for this continuum, we do not take it into account in our calculations. Moreover, when no data have been found, we have assumed that the cation has the same UV absorption cross–section as its parent molecule. For large PAHs the expression of Verstraete & Léger (1992), obtained by a theoretical calculation based on the properties of graphite, was used to determine the absorption cross–section.

The electronic levels of PAH cations are doublets and quartets. Unfortunately, the results available on transition rates of PAH cations are relatively scarce and make their study difficult for PAHs larger than $C_6H_6^+$. Nevertheless, Leach (1987) has shown that internal conversion (IC) to the electronic ground state $D_0$ dominates, leaving all the excitation energy in the form of vibrational energy of the $D_0$ state. In our model for PAH cations we therefore neglect visible fluorescence and phosphorescence. The PAH cations have hence only one route for deactivation via luminescence, namely IR emission. These emissions may however differ from those of the parent molecule in a way that is still unknown for most PAHs. Dunbar (1986) has for instance reported that the infrared emission rates of the benzene cation are 4 – 5 times faster than those of neutral benzene. Few other studies of IR relaxation of PAH cations have been found in the literature. We therefore adopt the same values as those of the corresponding molecule. There are also few data about the IR frequencies of PAH cations. Klippenstein et al. (1993) have tabulated the frequencies of the benzene molecule and cation in their study of benzene cation dissociation. The two series of vibrational frequencies are quite similar and we assume that this is also the case for larger PAHs.

Concerning the ionization of PAH cations we use the values of the ionization potential (IP) from Leach (1986) and Tobita et al. (1994) and assume a linear increase of the yield of ionization with the internal energy of the PAH cation as proposed by Jochims et al. (1995). The IP of PAH cations are all about 11 – 13 eV and the contribution of ionization of cations in the 2.8 –13.6 eV range of interest for us is always found to be negligible.

In Chap. 2 we have used the experimental results of Jochims et al. (1994) to describe the processes of photodissociation of PAHs. These results have been obtained for PAH cations. In Chap. 2 we have however used them for molecules following Jochims et al. (1994) who argue that the rates are valid for both molecules and cations because they have similar intramolecular dynamics. The experimental rates are well reproduced by the RRK theory which provides the following expressions:

$$k(E) = k_0 \left(1 - \frac{E_0}{E}\right)^{3N-7} \qquad \text{for } E > E_0 \;, \tag{3.1}$$

$$k(E) = 0 \qquad \text{for } E \leq E_0 \;, \tag{3.2}$$

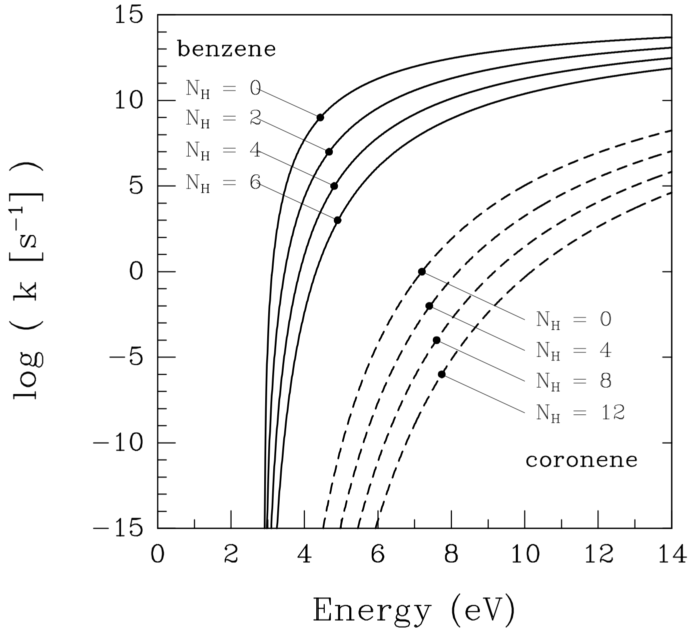


Figure 3.1: Rates of photodissociation for the loss of carbon from fully and partially dehydrogenated benzene and coronene as a function of the internal energy.

where $N$ is the number of atoms of the molecule. $k_0$ and $E_0$ are determined from the results of the experiment and are given in Table 2.1 for the loss of H, $H_2$ and $C_2H_2$.

### 3.2.2 Extension of the model to partially dehydrogenated PAHs

In astrophysical conditions, PAHs are thought to be partially dehydrogenated (van der Zwet & Allamandola 1985; Tielens et al. 1987; Allamandola et al. 1989; Geballe et al. 1989; Léger et al. 1989a,1989b). Unfortunately, there is little knowledge concerning the physical and chemical properties of dehydrogenated PAHs and we have had to make some assumptions to integrate partially dehydrogenated PAHs into our model.

For these species we first assume that photochemical processes of dissociation are still correctly described by the RRK theory and that the same constants $E_0$ and $k_0$ can be used for this purpose. In the case of a highly dehydrogenated PAH we also assume that the abstraction of carbon still happens via the loss of two neighbouring carbon atoms connected by a double bond. We therefore use the constants $E_0$ and $k_0$ presented in Table 2.1 for partially and totally dehydrogenated PAHs. We have plotted in Fig. 3.1 the rates calculated from Eq. (3.1) for the loss of an acetylene-like molecule from benzene and coronene in various hydrogenation states. From Fig. 3.1 it is evident that partially dehydrogenated PAHs are less stable than the corresponding non dehydrogenated molecules. More quantitatively, it is shown that the rates for totally dehydrogenated PAHs can be up to 5 orders of magnitude greater than the corresponding rate for the non dehydrogenated molecules. The physical explanation is that partially dehydrogenated PAHs have fewer vibrational

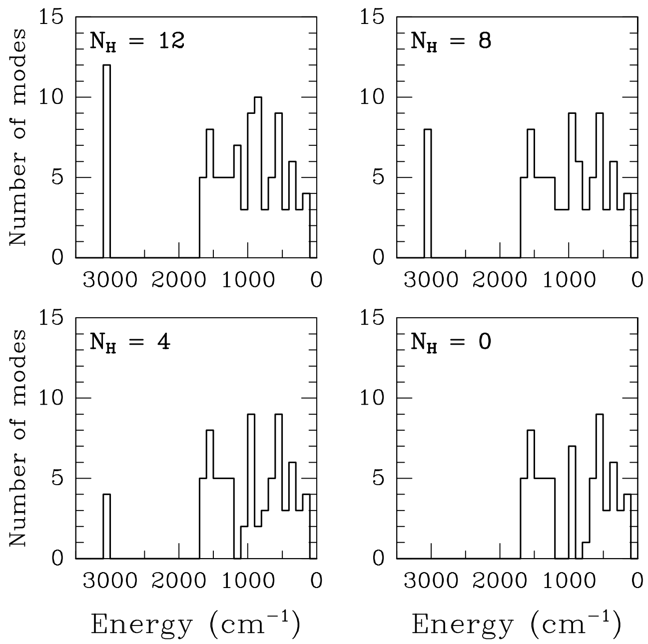


Figure 3.2: Energy distribution of vibrational modes (packed in 100 $cm^{-1}$ bins for representational convenience) for coronene ($N_H$=12) and for some dehydrogenated coronene molecules.

modes over which they can redistribute their internal energy, so that the probability that this energy may be found in the modes corresponding to the potentially broken bonds is therefore higher.

The vibrational modes of PAHs are directly affected by the loss of hydrogen atoms. In Chap. 2 we have shown that this may have an influence on the Einstein coefficients of IR emissions (see relations (2.11), (2.12) and (2.13)) and on the processes related to the density of states (relations (2.3) and (2.17)). To estimate these modifications we use the same approach as Léger *et al.* (1989b) when they calculated the specific heat of dehydrogenated PAHs. A free molecule with $N$ atoms has $3N - 6$ vibrational modes. As the number of hydrogen atoms decreases, we progressively withdraw from the distribution the modes attributed to the hydrogen atom motions (3.3 $\mu$m, 8.6 $\mu$m, 11.3 $\mu$m ) and assume that the remaining modes are not perturbed and that they have the same Einstein coefficients as those of the corresponding non dehydrogenated molecule. Figure 3.2 shows the evolution of the distribution of the vibrational modes as a function of the loss of hydrogen atoms for a molecule of coronene.

To have an idea of the effect of dehydrogenation on the physical behaviour of PAHs, in Fig. 3.3 we have plotted the vibrational temperature $T^*$ of some PAHs and of the corresponding dehydrogenated species.

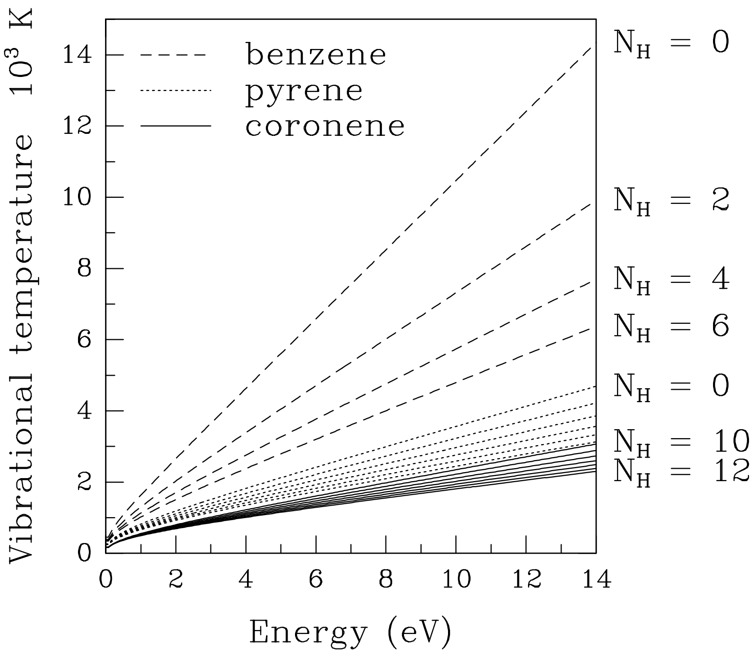


Figure 3.3: Evolution of vibrational temperature with internal energy for small PAHs and their partially dehydrogenated molecules (only PAHs with an even hydrogen number $N_H$ are represented; at a given energy these temperatures decrease with $N_H$).

This temperature is defined by assuming complete energy distribution between all normal modes and consequently the following expression for the internal energy:

$$E = \sum_{i=1}^{3N-6} \frac{h\nu_i}{\exp\left(\frac{h\nu_i}{kT^*}\right) - 1} , \tag{3.3}$$

where $N$ is the number of atoms in the species and $\nu_i$ the frequency of the mode $i$. It is clear from Fig. 3.3 that only the very small molecules have markedly different behaviour when they are dehydrogenated, which is not surprising because their hydrogen to carbon ratios, $N_H/N_C$, are larger. Coronene molecules are not very sensitive to a change of the number of hydrogen atoms and this trend surely pertains for larger PAHs. For these PAHs we therefore do not take into account the modifications of their IR properties as precisely as explained above. We only scale the Einstein coefficients of the 3.3, 8.6 and 11.3 $\mu$m IR emissions from Léger et al. (1989b) to the number of C – H bonds. For the sake of simplicity we have also neglected the variations of the emissions with the sites of the remaining hydrogen atoms. Léger et al. (1989b) and Allamandola et al. (1989) have indeed shown that solo, duo and trio hydrogen atoms may have various frequencies.

The UV absorption cross–section probably undergoes some changes due to the loss of hydrogen atoms. We make the following correction by considering the modification of the geometrical cross–section:

$$\sigma^{\mathrm{UV\ abs}}(N_{\mathrm{H}}) \simeq \sigma^{\mathrm{UV\ abs}}(N_{\mathrm{H}}^{\mathrm{o}})\ \frac{2.5N_{\mathrm{H}}\ +\ 8N_{\mathrm{C}}}{2.5N_{\mathrm{H}}^{\mathrm{o}}\ +\ 8N_{\mathrm{C}}}\ , \tag{3.4}$$

where $N_{\mathrm{H}}$ and $N_{\mathrm{C}}$ are the number of hydrogen and carbon atoms of the PAH, respectively, and $N_{\mathrm{H}}^{\mathrm{o}}$ the number of hydrogen atoms of the corresponding non dehydrogenated molecule. To establish Eq. (3.4) we have used the relation of Omont (1986) for the radius of the PAH carbon skeleton

$$a = 0.9\ N_{\mathrm{C}}^{1/2}\ \text{Å} \tag{3.5}$$

and a typical length for a the C–H bond in a PAH equal to 1.077 Å (Pulay et al. 1981).

Concerning the other physical processes of partially dehydrogenated PAHs: ionization, fluorescence, phosphorescence, internal conversion, we use the properties of the parent molecules presented in the model of Chap. 2 because of the lack of data and of the impossibility to make appropriate corrections. As these properties involve mainly the carbon skeleton of the PAHs we should not commit a large error with this assumption. The error is likely to be smaller for the larger PAHs.

### 3.2.3 Photodissociation rates of PAH cations and partially dehydrogenated molecules

As in Sect. 2.3.2, we obtained the rate of photodissociation by integrating the corresponding cross–section over the energy available in the ISM. The photodissociation cross–section for the loss of carbon for instance can be calculated according to:

$$\sigma^{\mathrm{C}}(E) = \sigma^{\mathrm{UV\ abs}}\ \frac{k^{\mathrm{C}}(E)}{\sum k_i}\ , \tag{3.6}$$

where $\sigma^{\mathrm{UV\ abs}}$, $k^{\mathrm{C}}$ and $\sum k_i$ represent the UV absorption cross–section, the rate of photodissociation for the loss of carbon from Eq. (3.1) and the sum of all the rates for the processes occuring at energy $E$ (luminescence, ionization, dissociation), respectively. Calculating the following integral:

$$k^{\mathrm{p}} = \int_{E=E_0}^{E=13.6eV} \sigma^{\mathrm{p}}(E)\ \chi\ N(E)\ dE \tag{3.7}$$

for a given PAH provides the rate of process (p) in the ISM. In Eq. (3.7) $N(E)$ represents the mean UV photon flux of the ISM at photon energy $E$, for which we have used the data of Gondhalekar et al. (1980) in the range 4.5 – 13.3 eV and of Mathis et al. (1983) for the extension over 2.8 – 13.6 eV (see Sect. 2.3.1) As in Chap. 2 $\chi$ is a scaling factor used to describe the high radiation fields of the regions showing the UIR bands.

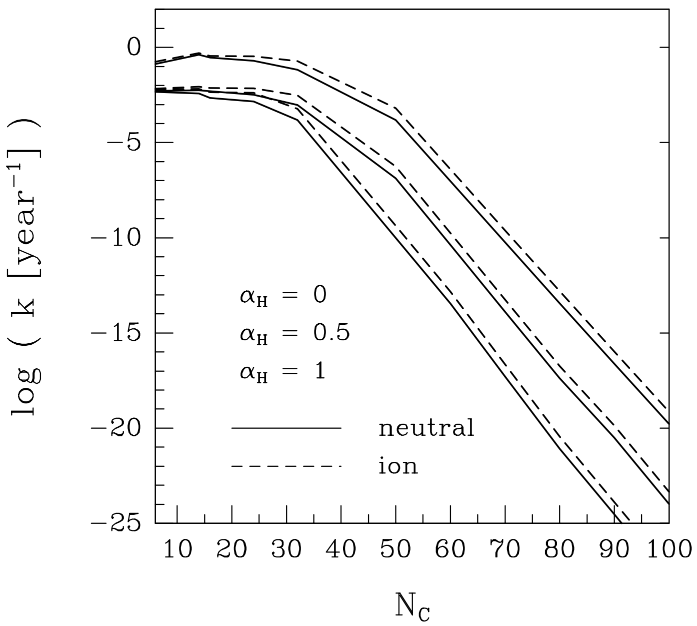


Figure 3.4: Rates of photodissociation for the loss of carbon from PAH cations and partially dehydrogenated molecules as a function of the size of the PAH.

The results concerning the photodissociation of hydrogen from PAH cations and partially dehydrogenated PAH molecules are presented in Table 3.1. The results we have obtained for the loss of carbon are in Table 3.2 and have been plotted in Fig. 3.4 as a function of the PAH size. To simplify the discussion we have defined the hydrogen coverage of a molecule by the relation:

$$\alpha_{\rm H} = \frac{N_{\rm H}}{N_{\rm H}^{\rm o}} \ , \tag{3.8}$$

where $N_{\rm H}$ is the number of hydrogen atoms borne by a PAH and $N_{\rm H}^{\rm o}$ the number of hydrogen atoms of the corresponding non dehydrogenated PAH. When we discuss the case of a PAH with a given value of $\alpha_{\rm H}$, the number of hydrogen atoms of the PAH is equal to $\mathrm{INT}(\alpha_{\rm H} N_{\rm H}^{\rm o})$ where $\mathrm{INT}(x)$ represents the integer part of $x$.

With the results of Tables 3.1 and 3.2 and Fig. 3.4 we find that PAH cations are less stable than their parent molecules against photodissociation. The explanation of this behaviour is that PAH cations cannot lose as much absorbed energy through ionization as easily as the neutrals because of their higher values of ionization potential. However, the difference with the rates of the neutrals is relatively constant for all PAHs and never much larger than an order of magnitude. In the case of dehydrogenated PAHs, the situation is totally different and we observe a slightly increasing difference with the molecular size up to 8 orders of magnitude of difference for a PAH having 100 carbon atoms.

Table 3.1: Photodissociation rates for hydrogen loss from PAH cations and dehydrogenated molecules in the interstellar field of Gondhalekar et al. (1980) (unit = year$^{-1}$)

| PAH | cation | | $\alpha_H = 0.5$ | | $\alpha_H = 0.25$ | |
|---|---|---|---|---|---|---|
| | H loss | $H_2$ loss | H loss | $H_2$ loss | H loss | $H_2$loss |
| benzene | 1.1 (-1) | 6.2 (-2) | 8.0 (-2) | 5.2 (-2) | 1.3 (-1) | - |
| anthracene | 1.7 (-1) | 6.4 (-2) | 1.5 (-1) | 5.5 (-2) | 2.9 (-1) | 9.2 (-2) |
| pyrene | 1.1 (-1) | 4.4 (-2) | 1.6 (-1) | 5.0 (-2) | 2.0 (-1) | 6.7 (-2) |
| coronene | 1.3 (-1) | 4.1 (-2) | 1.0 (-1) | 3.3 (-2) | 1.3 (-1) | 4.4 (-2) |
| ovalene | 2.2 (-2) | 6.0 (-3) | 3.2 (-2) | 9.4 (-3) | 5.7 (-2) | 1.8 (-2) |
| PAH 50 C | 2.7 (-8) | 4.2 (-9) | 6.7 (-6) | 1.4 (-6) | 1.7 (-4) | 3.9 (-5) |
| PAH 100 C | 1.4 (-25) | 4.5 (-27) | 2.3 (-22) | 1.0 (-23) | 2.2 (-20) | 1.2 (-21) |

Table 3.2: Photodissociation rates for carbon loss from PAH cations and partially dehydrogenated molecules in the interstellar field of Gondhalekar et al. (1980) (unit = year$^{-1}$)

| | PAH | cation | $\alpha_H = 0.5$ | $\alpha_H = 0$ |
|---|---|---|---|---|
| benzene | 4.7 (-3) | 6.2 (-3) | 5.2 (-3) | 1.4 (-1) |
| anthracene | 6.0 (-3) | 6.4 (-3) | 5.5 (-3) | 4.2 (-1) |
| pyrene | 2.2 (-3) | 4.4 (-3) | 5.0 (-3) | 2.8 (-1) |
| coronene | 1.4 (-3) | 4.1 (-3) | 3.3 (-3) | 2.0 (-1) |
| ovalene | 1.5 (-4) | 6.0 (-4) | 9.4 (-4) | 6.7 (-2) |
| PAH 50 C | 1.1 (-10) | 4.2 (-10) | 1.4 (-7) | 1.5 (-4) |
| PAH 100 C | 1.0 (-28) | 4.5 (-28) | 1.0 (-24) | 1.6 (-20) |

## 3.3 PAH ionization and hydrogenation states in astrophysical media

Because of the variations of the photodissociation rates of PAHs with the ionization and dehydrogenation states, it is necessary to know the ionization fraction and the hydrogen coverage of PAHs in a given astrophysical medium in order to precisely estimate the rates for photodissociation. In the present section, we therefore discuss, first, the rates of the processes governing the physical state of PAHs, and secondly, determine the PAH ionization state by balancing the processes for ionization and electron recombination, and in a similar way the PAH hydrogenation state by balancing the processes for hydrogen loss and hydrogenation.

### 3.3.1 Rates for the calculations

#### Rates for ionization and for electron recombination of PAHs

The rates for ionization have already been calculated in Chap. 2 for PAH molecules in a Gondhalekar et al. (1980) radiation field. The values for PAH ionization rates in the ISM slightly increase with molecular size but remain about $10^{-9}$ – $10^{-8}$ s$^{-1}$ for all PAHs. For partially dehydrogenated PAHs, the model presented in Sect. 3.2.2 leads to a small diminution due to the decreasing absorption cross–section (see Eq. (3.4)). On the other hand, the rates of ionization of PAH cations we have estimated are all lower than $10^{-10}$ s$^{-1}$ and we therefore do not consider doubly charged PAHs in the following discussion, although it is thought that destruction of PAHs may also occur via double ionization in the ISM (Leach 1986; Leach et al. 1989).

The reverse process of ionization is recombination with an electron, for which there are only few experimental results. Recent measurements have been performed by Abouelaziz et al. (1993) for the electron recombination of benzene and naphthalene cations at 300 K. They obtained values of $1.10^{-6}$ cm$^3$ s$^{-1}$ for $C_6H_6^+$ and $3.10^{-7}$ cm$^3$ s$^{-1}$ for $C_{10}H_8^+$. Assuming a $T^{-1/2}$ dependence (Abouelaziz et al. 1993) one can deduce an expression for the recombination rate over the temperature range of interest in astrophysics. For small PAHs electron recombination is a dissociative process (Abouelaziz et al. 1993). This is probably not the case for larger PAHs which can be stabilized after the capture process by conversion of excess electronic energy into vibrational modes, with increasing probability as the number of internal modes rapidly increases with size. However, we have not found in the literature any systematic study of the dissociative recombination of PAHs with size. We have therefore not considered electron recombination as a destructive process in the present work and leave to the future a study of the competition between electron dissociative recombination and photodestruction for small PAHs cations in the ISM.

For larger PAH cations no experimental values are available in the literature. We therefore follow the proposition of Léger & d'Hendecourt (1985) and Omont (1986) and use the approach of Spitzer (1978) in order to describe the recombination of an electron of speed $v$ with a spherical particle of radius $a$ bearing a single elementary charge $e(>0)$.

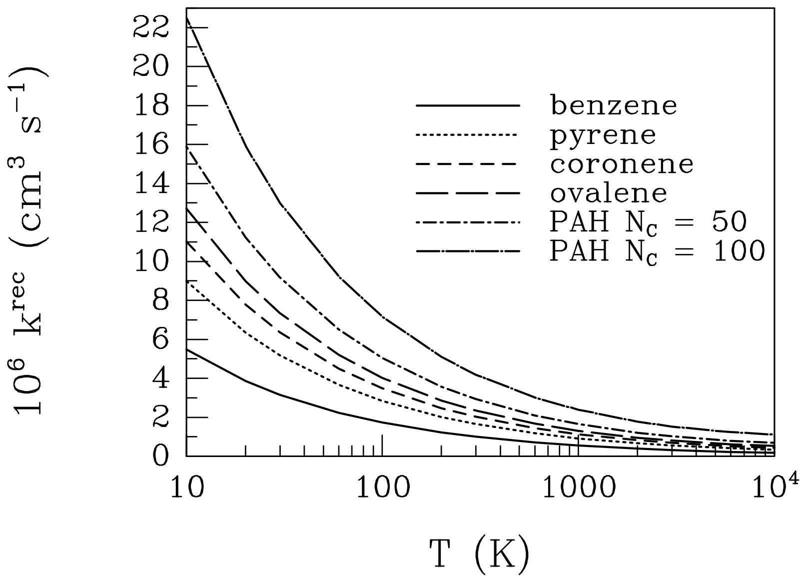


Figure 3.5: PAH cation–electron recombination rates for various PAHs as a function of temperature.

From the conservation of angular momentum one easily deduces:

$$\sigma^{\rm rec} = P\ \pi a^2 \left(1\ +\ \frac{eU(a)}{1/2m_{\rm e}v^2}\right)\ , \tag{3.9}$$

where $m_{\rm e}$ is the electron mass, $U(a) = e/a$ the electronic potential at $r = a$ and $P$ the sticking probability for recombination. The recombination rate is then obtained by averaging over a Maxwellian distribution of velocities.

$$\begin{aligned} n_{\rm e}\ k^{\rm rec} &= n_{\rm e}\ < v\sigma^{\rm rec} > \\ &= n_{\rm e}\ P\ \pi a^2 \left(\frac{8k_{\rm B}T}{\pi m_{\rm e}}\right)^{1/2} \left(1\ +\ \frac{2e^2/a}{k_{\rm B}T}\right)\ , \end{aligned} \tag{3.10}$$

where $n_{\rm e}$ is the electron density and $k_{\rm B}$ the Boltzmann constant. Verstraete et al. (1990) have shown that such an expression obtained for a sphere-shaped particle is still valid for a disk-shaped molecule of radius $a$ if one introduces a factor of 0.8. We furthermore use the relation (3.5) (Omont 1986) for the radius of a PAH molecule containing $N_{\rm C}$ carbon atoms. We then deduce the value of $P$ by ajusting the relation (3.10) to the experimental value of Abouelaziz et al. (1993) in the case of the benzene cation at 300 K (because of the geometry of the naphthalene cation, its molecular radius is not correctly described by Eq. (3.5) and we therefore do not use it to determine $P$ ). One hence obtains the value 0.30 for $P$. This value is in good agreement with the proposition of several ten percent by Omont (1986).

In so doing one finally obtains numerically:

$$n_e\, k^{\rm rec} \;=\; 2.13\;10^{-6}\; n_e\; N_{\rm C}^{1/2}\; T^{-1/2} \left[1 \;+\; 3.82\;10^{-3}\left(\frac{T}{100}\right)\left(\frac{N_{\rm C}}{50}\right)^{1/2}\right]\;{\rm s}^{-1}\;. \tag{3.11}$$

Figure 3.5 represents the evolution of the recombination rate as a function of the temperature for various PAH cations. This figure shows that the rate of recombination increases with molecular size but decreases with temperature in the range of size and temperature of interest for the present investigation.

### Rates for hydrogen loss and for hydrogenation of PAHs

The rates for photoabstraction of hydrogen particles have been calculated for PAH molecules in Chap. 2 and are presented in Table 3.1 for cations and for partially dehydrogenated PAHs.

Lee and Wdowiak (1993b) have proposed that hydrogenation of PAHs could lead to a conversion from aromatics to aliphatic compounds. They have indeed carried out electrical discharge experiments involving hydrogen and naphthalene and shown that at least one ring of the naphthalene molecule was broken and saturated. However, the experiment is still purely qualitative and involves plasma conditions. Furthemore, the experimental value of 0.5 torr for the gas pressure is very high compared with interstellar conditions. In our calculation we have therefore not considered the reactions of PAH saturation via hydrogenation in the ISM.

The hydrogenation rate has been adapted from Frenklach et al. (1985) for neutral radical PAHs (rate coefficient of their reaction (21) equal to 1.7 $10^{-11}$cm$^{-3}$ molecule$^{-1}$ s$^{-1}$). For the ionized species we follow the propositions of Tielens et al. (1987) and Allamandola et al. (1989) and assume a collision rate given by the Langevin rate constant ($\simeq 10^{-9}$ cm$^3$ s$^{-1}$) and, in the absence of experimental data, a reaction probability equal to unity. There is little knowledge about the temperature dependence of reaction rates for radiative association reactions. Some experimental results suggest that radiative association reactions are most effective at low temperatures. For the rates of rehydrogenation we have found no data in the literature and have assumed no temperature dependence.

However, the hydrogenation reaction competes with chemical attack by hydrogen atoms which may prove important at high temperature. Since data for chemical attack of large PAHs and dehydrogenated PAHs atoms are not available we use the kinetic data of the reaction with benzene.

$$C_6H_6 \;+\; H\bullet \;\longrightarrow\; C_6H_5\bullet \;+\; H_2\;. \tag{3.12}$$

Following Frenklach and Feigelson (1989) we use for the rate of this reaction the results of Kiefer et al. (1985) for temperatures above 1000 K and the chemical rate of Nicovich & Ravishankara (1984) for lower temperatures.

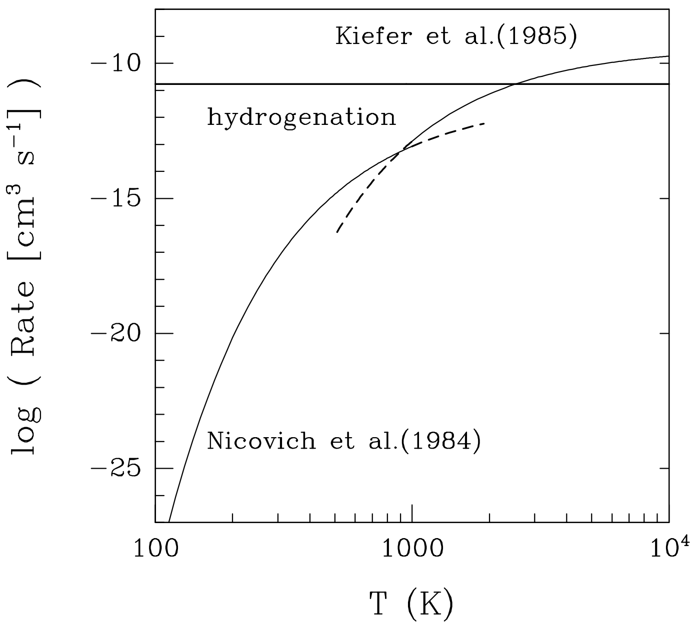


Figure 3.6: Hydrogenation and abstraction rates for reaction of a benzene molecule with an hydrogen atom as a function of temperature.

These rates take Arrhenius expressions:

$$\begin{aligned} \text{for} \quad & \mathrm{T} \geq 1000 \text{ K}, \\ & k^{\mathrm{abs}} = 4.15\ 10^{-10}\ \exp\left(-\frac{8060}{T}\right)\ \mathrm{cm}^3\ \mathrm{s}^{-1}, \\ \text{for} \quad & \mathrm{T} < 1000 \text{ K}, \\ & k^{\mathrm{abs}} = 5\ 10^{-12}\ \exp\left(-\frac{4080}{T}\right)\ \mathrm{cm}^3\ \mathrm{s}^{-1}. \end{aligned} \tag{3.13}$$

For partially dehydrogenated PAHs we also use these rates but correct them by the factor $N_{\mathrm{H}}/N_{\mathrm{H}}^{\circ}$ which accounts for the number of peripheric hydrogen atoms $N_{\mathrm{H}}$ (this factor ensures that no abstraction can occur for fully dehydrogenated PAHs). Due to the lack of data we furthermore use the previous form of the rate of hydrogen abstraction for PAH cations, for which we indeed multiplied the rate by a factor such that the ratio of abstraction to hydrogenation is the same as for neutral PAHs. Moreover, all the previously discussed rates have been used for PAHs larger than benzene ($N_{\mathrm{C}} > 6$) by correcting with a factor $\sqrt{(N_{\mathrm{C}}/6)}$ so as to account for the increase of the collision cross–section with PAH size.

However, in many astrophysical media where the characteristic PAH emission bands are observed, the UV-field can ionize hydrogen atoms so that the predominant species is there $\mathrm{H}^+$. It has indeed been observed by Woodward et al. (1989) in the case of NGC 7027 that the emission of the 3.3 $\mu$m band is present both inside and outside of the HII region.

Moreover, Giard et al. (1994) have proposed that $H^+$ sputtering could be responsible for the destruction of PAHs at the ionization front. However, no experimental results on $H^+$ chemisputtering of PAHs are available in the literature. Barlow & Silk (1977) and Draine (1979) have discussed this process for graphite and obtained contradictory results leading to a difference of four orders of magnitude for the yield of the process. As stated by Omont (1986) no definite conclusion for the destruction of PAHs by $H^+$ sputtering can be drawn yet. We have therefore not taken it into account for the present calculation.

There are unfortunately also no experimental or theoretical results concerning the recombination reactions of PAHs radicals with $H^+$. According to Omont (1986) when a proton $H^+$ arrives near a PAH, it induces on the PAH a negative charge with which it interacts in such a way that the proton is neutralized when reaching a sufficiently small distance. Therefore, we use for the rates of reactions between PAH and $H^+$ the rates we have obtained for reactions between PAH cations and hydrogen atoms. Moreover, we logically consider no reaction between PAH cations and $H^+$ because of the Coulomb repulsion.

Figure 3.6 shows the rates of rehydrogenation and chemical attack for a benzene molecule. Clearly, hydrogenation has a rate higher than chemical hydrogen abstraction for values of the temperature lower than 2000 K. With our assumptions it is also the case for larger PAH molecules and cations. In the media where the UIR bands have been observed the temperature is rarely greater than 2000 K and therefore under these conditions hydrogenation should be more effective than chemical hydrogen abstraction.

## 3.3.2 Equilibrium of ionization and of hydrogenation in the ISM

### Existence and description of the equilibrium

For an ensemble of PAHs, we consider equilibrium of ionization and of hydrogenation states to exist when ionization of PAHs is balanced by electron recombination and hydrogen abstraction by hydrogenation. For the calculations, we assume that the ensemble of PAHs is immersed in a medium characterized by the hydrogen and electron densities, the temperature and the radiation field, and that these parameters are not perturbed by the processes involving PAHs. The rates describing these processes remain therefore unchanged in the calculation. Moreover, ionization, hydrogen abstraction and recombination with electrons and hydrogen are specific to each type of PAH. Thus, a separate description of the equilibrium is required for each type of PAH.

However, such an equilibrium can be reached only in media where the time for destruction of PAHs is greater than the time needed to establish the equilibrium. The most efficient process of destruction in the media we investigate is photodestruction via the loss of an acetylene–like molecule. A typical time scale for this process is $\tau^{\rm dest} = 1/k_{\rm C}^{\rm UV}$ where $k_{\rm C}^{\rm UV}$ represents the rate for photoabstraction of carbon discussed in Sect. 3.2.3. The equilibrium of ionization is typically reached on a timescale $\tau^{\rm ion} = 1/(k^{\rm ion} + n_{\rm e}k^{\rm rec})$ where $k^{\rm ion}$ and $k^{\rm rec}$ are the rates for ionization and electron recombination presented in the previous section. Hydrogenation equilibrium occurs on a timescale $\tau^{\rm hyd} = 1/(k_{\rm H}^{\rm UV} + n_{<{\rm H}>}k^{\rm hyd} + n_{<{\rm H}>}k^{\rm abst})$ where $k_{\rm H}^{\rm UV}$, $k^{\rm hyd}$ and $k^{\rm abst}$ are the rates for photoabstraction of hydrogen, hydrogenation and chemical abstraction, respectively. Using the numerical values obtained in the previous sections shows that in all situations $\tau^{\rm dest}$ is at least one order of magnitude larger than $\tau^{\rm hyd}$ and $\tau^{\rm ion}$. This ensures the existence of the equilibrium.

To determine the ionization and the hydrogenation state of a given PAH *(P)* with $N_{\rm C}$ carbon atoms and $N_{\rm H}^{\rm o}$ hydrogen atoms in its non dehydrogenated form, we consider an ensemble of $N_{\rm PAH}$ PAHs *(P)*. For the $N_i$ neutral PAHs *(P)* bearing $i$ hydrogen atoms we introduce $n_i$, the concentration relative to the total number of PAHs ($n_i = N_i/N_{\rm PAH}$). We also define $c_i$ the concentration of the corresponding PAH cations. At equilibrium, the concentrations remain constant and we consequently infer the following conservation equations[1]:

$$
\begin{aligned}
&\text{for the neutrals} \quad i = 0,1,2,...,N_{\rm H}^{\rm o}\ , \\
\frac{dn_i}{dt} \;=\;& n_{i-1}\left(n_{\rm H}k_{{\rm H}\ \ i-1}^{\rm hyd\ (n)}\right) + \\
& n_{i+1}\left(\chi k_{{\rm H}\ \ i+1}^{\rm UV\ (n)} + n_{\rm H}k_{{\rm H}\ \ i+1}^{\rm abs\ (n)}\right) + \\
& n_{i+2}\left(\chi k_{{\rm H_2}\ i+2}^{\rm UV\ (n)}\right) + c_i\left(n_{\rm e}k^{\rm rec}\right) - \\
& n_i \sum k^{(n)} \;=\; 0\ , \qquad (3.14)
\end{aligned}
$$

$$(3.15)$$

$$
\begin{aligned}
&\text{for the cations} \quad i = 0,1,2,...,N_{\rm H}^{\rm o}\ , \\
\frac{dc_i}{dt} \;=\;& c_{i-1}\left(n_{\rm H}k_{{\rm H}\ \ i-1}^{\rm hyd\ (c)}\right) + \\
& c_{i+1}\left(\chi k_{{\rm H}\ \ i+1}^{\rm UV\ (c)} + n_{\rm H}k_{{\rm H}\ \ i+1}^{\rm abs\ (c)}\right) + \\
& c_{i+2}\left(\chi k_{{\rm H_2}\ i+2}^{\rm UV\ (c)}\right) + n_{i-1}\left(n_{\rm H+}k_{{\rm H+}\ i-1}^{\rm hyd\ (n)}\right) + \\
& n_i\left(\chi k_i^{\rm ion}\right) + n_{i+1}\left(n_{\rm H+}k_{{\rm H+}\ i+1}^{\rm abs\ (n)}\right) - \\
& c_i \sum k^{(c)} \;=\; 0\ , \qquad (3.16)
\end{aligned}
$$

where

$$
\begin{aligned}
\sum k^{(n)} \;=\;& n_{\rm H}k_{{\rm H}\ \ i}^{\rm hyd\ (n)} + n_{\rm H+}k_{{\rm H+}\ i}^{\rm hyd\ (n)} + n_{\rm H}k_{{\rm H}\ \ i}^{\rm abs\ (n)} + \\
& n_{\rm H+}k_{{\rm H+}\ i}^{\rm abs\ (n)} + \chi k_{{\rm H}\ \ i}^{\rm UV\ (n)} + \chi k_{{\rm H_2}\ i}^{\rm UV\ (n)} + \chi k_i^{\rm ion}\ , \\
\sum k^{(c)} \;=\;& n_{\rm H}k_{{\rm H}\ \ i}^{\rm hyd\ (c)} + n_{\rm H}k_{{\rm H}\ \ i}^{\rm abs\ (c)} + \chi k_{{\rm H}\ \ i}^{\rm UV\ (c)} + \\
& \chi k_{{\rm H_2}\ i}^{\rm UV\ (c)} + n_{\rm e}k^{\rm rec}\ . \qquad (3.17)
\end{aligned}
$$

In Eqs. (3.14), (3.16) and (3.17), $n_{\rm X}$ represents the density of species X, and $k_{{\rm X}\ i}^{p\ (s)}$ the rate for process $p$ involving the species X and a PAH ($P$) with $i$ hydrogen atoms in state (s)

[1] In the following equations for i=0, i=$N_{\rm H}^{\rm o}$-1 and i=$N_{\rm H}^{\rm o}$ the terms corresponding to i-1, i+2, i+1 and i+2 respectively have to be set equal to zero.

where s can be neutral (n) or cationic (c). Equations (3.14) and (3.16) constitute a system of $2(N_{\rm H}^{\rm o}+1)$ equations with $2(N_{\rm H}^{\rm o}+1)$ unknowns (the $n_i$ and $c_i$). These equations are not independent because each of them can be deduced from the sum of all the others. To solve the system, we therefore replace one of the equations by the conservation equation:

$$\sum_{i=0}^{N_{\rm H}^{\rm o}} n_i + \sum_{i=0}^{N_{\rm H}^{\rm o}} c_i = 1 \ . \tag{3.18}$$

The solution of this system provides the distribution of PAHs *(P)* in its different hydrogenated and ionized forms at equilibrium.

As in Chap. 2 we apply our calculations to some astrophysical media where the UIR emission bands attributed to PAHs have been seen. These media are presented in Table 3.3 together with their physical properties and the references to the observations. The results of the calculations are discussed in the two next subsections, which concern the ionization and hydrogenation states of PAHs, respectively.

Table 3.3: Physical properties of some astrophysical regions showing the UIR bands.

| medium | Object | $n^{(1)}_{\lt{\rm H}\gt}$ (cm$^{-3}$) | $n^{(2)}_{\rm e}$ (cm$^{-3}$) | $T$ (K) | $\chi^{(3)}$ |
|---|---|---|---|---|---|
| Planetary nebula | NGC 7027$^{(a)}$ | 7 (4)$^{(b)}$ | 7 (1) | 5 (2) | 4.6 (5) |
| Photodissociation region | Orion Bar$^{(c)}$ | 1 (5)$^{(d)}$ | 3 (1) | 5 (2) | 4.3 (3) |
| Reflection Nebula | NGC 7023$^{(e)}$ | 4 (3)$^{(f)}$ | 1 (0) | 2.5 (2) | 2.5 (3) |
| Galactic nucleus | M82$^{(g)}$ | 1 (4)$^{(h)}$ | 3 (0) | 2.5 (2) | 2.9 (3) |
| HI region | Galactic plane$^{(i)}$ | 5 (1)$^{(j)}$ | 2 (-2) | 8 (1) | 1 (0) |
| Diffuse warm medium | Galactic plane$^{(i)}$ | 5 (-1)$^{(j)}$ | 4 (-3) | 8 (3) | 1 (0) |

(1) total density of hydrogen nuclei, (2) electron density, (3) scaling factor to be multiplied to the photon flux of Gondhalekar et al. (1980) to describe the UV radiation field .
References to the observations and physical conditions (a) Cohen et al. (1986), (b) Allamandola et al. (1989), (c) Bregman et al. (1989), (d) Tielens and Hollenbach (1985a, 1985b), (e) Sellgren et al. (1985), (f) Chokshi et al. (1988), (g) Willner et al. (1977), (h) Wolfire et al. (1988), (i) Giard et al. (1988) and (j) Spitzer (1978)

### Ionization state of PAHs in the ISM

Léger & d'Hendecourt (1985) and Verstraete et al. (1990) have already discussed the state of ionization of PAHs. We likewise introduce the ionization fraction $\alpha_{\rm ion}$ to describe the state of ionization of an assembly of PAHs

$$\alpha_{\rm ion} = \frac{n_{\rm ion}}{n_{\rm ion} + n_{\rm molecule}} \; , \tag{3.19}$$

where $n_{\rm ion}$ represents the density of PAH cations and $n_{\rm molecule}$ the density of neutral molecules. With the notations previously introduced we obtain for $\alpha_{\rm ion}$ the following expression:

$$\alpha_{\rm ion} = \sum_{i=0}^{N_{\rm H}^{\circ}} c_i \; . \tag{3.20}$$

We present in Fig. 3.7 the ionization fractions calculated for the astrophysical media of Table 3.3 as a function of the molecular size. The results are in good agreement with the calculations of Verstraete et al. (1990) who have studied $\alpha_{\rm ion}$ in the case of a PAH molecule containing 80 carbon atoms, assuming however a sticking probability of 1 for the electron recombination process. Figure 3.7 shows a slight increase of the ionization fraction with the molecular size. It also reveals a large dependence of the ionization fraction with the physical parameters.

In order to study more precisely this dependence, we use an alternative expression of $\alpha_{\rm ion}$ obtained by summing the relations (3.14) and using the conservation Eq. (3.18). After some algebra, one obtains:

$$\alpha_{\rm ion} = \frac{k^{\rm ion}_{<\rm i>} + \frac{n_{\rm H+}}{\chi}\, k^{\rm hyd}_{<\rm i>}}{k^{\rm ion}_{<\rm i>} + \frac{n_{\rm H+}}{\chi}\, k^{\rm hyd}_{<\rm i>} + \frac{n_{\rm e}}{\chi}\, k^{\rm rec}(T)} \; , \tag{3.21}$$

where we have defined mean rates over the hydrogenation states:

$$k^{\rm ion}_{<\rm i>} = \frac{\sum n_i \; k^{\rm ion}_i}{\sum n_i} \; , \tag{3.22}$$

$$k^{\rm hyd}_{<\rm i>} = \frac{\sum n_i \; k^{\rm hyd}_i}{\sum n_i} \; . \tag{3.23}$$

In most regions showing the UIR bands, $n_{\rm H+}$ is low enough so that one can omit the term $n_{H+}k^{\rm hyd}/\chi$ in Eq. (3.21)[1]. Under these circumstances $\alpha_{\rm ion}$ can be written as a function of $T$ and $n_{\rm e}/\chi$ for each PAH.

In order to have some insight into the influence of the parameters $T$ and $n_{\rm e}/\chi$, we represent $\alpha_{\rm ion}$ in the plane $T$, $\log(n_{\rm e}/\chi)$. Figure 3.8 shows the results obtained for the

[1]In H II regions the term $n_{\rm H+}k^{\rm hyd}/\chi$ accounting for the PAH ionization via reaction with $\rm H^+$ has to be taken into account. However, in these media $n_{\rm e} \simeq n_{\rm H+}$ and the dominant process is electron recombination, so that $\alpha_{\rm ion} \ll 1$.

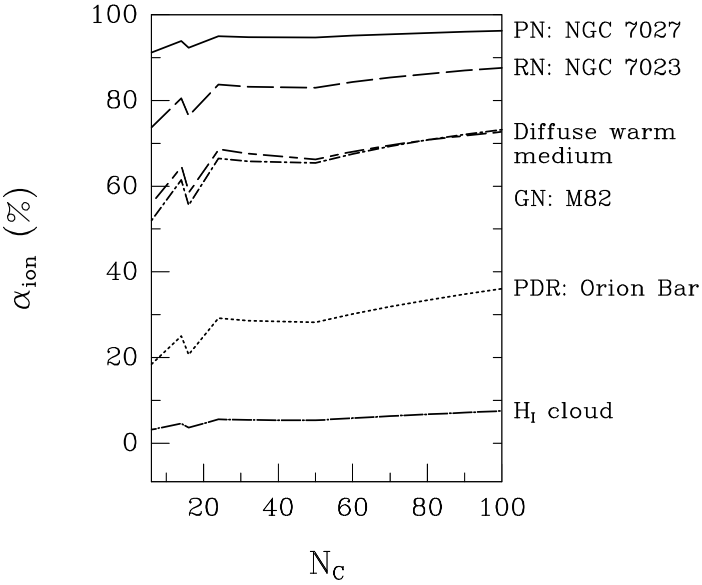


Figure 3.7: Ionization fraction of PAHs for various astrophysical media as a function of the molecular size. (PN: Planetary Nebula, RN: Reflection Nebula, GN: Galactic Nucleus, PDR Photodissociation Region)

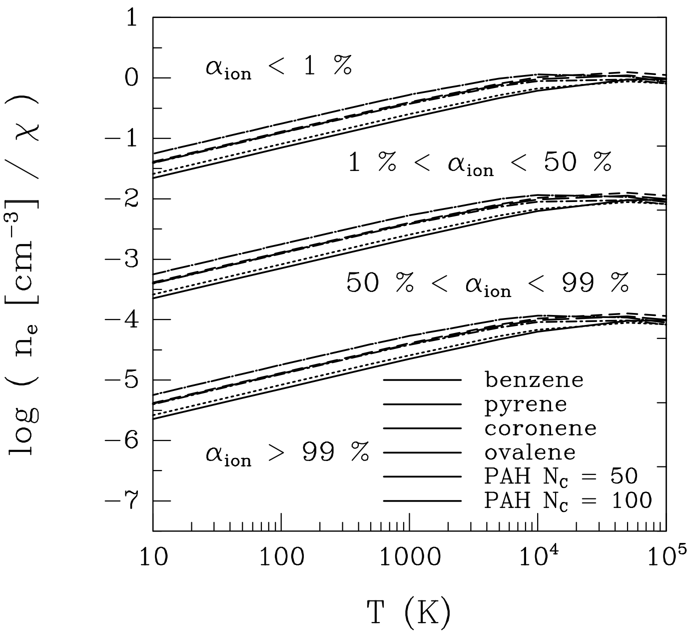


Figure 3.8: Ionization equilibrium curves in the plane $T, log(n_e/\chi)$ for various values of $\alpha_{ion}$ and for various PAHs.

values 0.01, 0.50 and 0.99 of the ionization fraction and for various PAHs. We observe again in Fig. 3.8 that all PAHs have approximatly the same ionization fraction. For a given temperature the ionization fraction decreases with the electron density (because the rate of recombination decreases) and increases with the radiation field intensity (because the ionization rate increases). More quantitatively, a decrease of the intensity of the UV-field by two orders of magnitude or an increase of the electron density by two orders of magnitude could make the ionization fraction drop from 99 % to 50 %; the same variations could cause a drop from 50 % to 1 %. The dependence on the temperature is relatively less important. More precisely, we deduce from Fig. 3.8 that full ionization ($\alpha_{\rm ion} \geq 99\%$) of PAHs is achieved for a ratio $n_{\rm e}/\chi$ lower than $n_{\rm e}/\chi_{99\%} = 10^{-6}\ T^{0.42}$ cm$^{-3}$. Neutral PAHs are to be found in large amounts ($\alpha_{ion} \leq 1\%$) in regions having a ratio $n_e/\chi$ greater than $n_{\rm e}/\chi_{1\%} = 10^{-2}\ T^{0.42}$ cm$^{-3}$.

A consequence of the sensitivity of the ionization fraction to the various physical parameters is that any attempt to determine the ionization state of PAHs will be very dependent on the quality of the evaluation of the temperature, photon flux and electron density. Moreover, as has already been seen for the media of Table 3.3, the values of $n_{\rm e}/\chi$ observed in the regions where the UIR bands have been seen range from $10^{-5}$ cm$^{-3}$ to $10^{-1}$ cm$^{-3}$. Consequently all the values of $\alpha_{\rm ion}$ may be encountered in regions showing the UIR bands.

**Hydrogenation state of PAHs**

Figure 3.9 shows the distribution of hydrogen atoms obtained for benzene and coronene type molecules and cations in two different media. Some differences can be observed **(i)** between ionic and neutral PAHs for a given PAH in a given environment, **(ii)** between the two PAHs in a given environment, and also **(iii)** between a PAH in two different media. To simplify the following discussion, we define a mean hydrogen coverage for cations and for molecules by the expression:

$$\begin{aligned} &\text{for the neutrals,} \\ &\qquad \alpha_{\rm H}(n) = \sum_{i=0}^{N_{\rm H}^{\rm o}} \frac{i}{N_{\rm H}^{\rm o}}\ n_i\ , \\ &\text{for the cations,} \\ &\qquad \alpha_{\rm H}(c) = \sum_{i=0}^{N_{\rm H}^{\rm o}} \frac{i}{N_{\rm H}^{\rm o}}\ c_i\ . \end{aligned} \tag{3.24}$$

We have presented in Fig. 3.9 $\bar{N}_{\rm H} = \alpha_{\rm H} N_{\rm H}^{\rm o}$ the mean number of hydrogen atoms borne by the PAHs. In the cases of total dehydrogenation and of high hydrogen content $\bar{N}_{\rm H}$ corresponds to the number of hydrogen atoms borne by the majority of PAHs. For medium values of $\alpha_{\rm H}$ all states of hydrogenation can be observed and $\bar{N}_{\rm H}$ (respectively $\alpha_{\rm H}$) loses its representative meaning and must really be understood as a mean value.

Figure 3.10 shows the hydrogen coverage of PAH cations and molecules as a function of the molecular size in the media of Table 3.3. Because of their larger hydrogenation

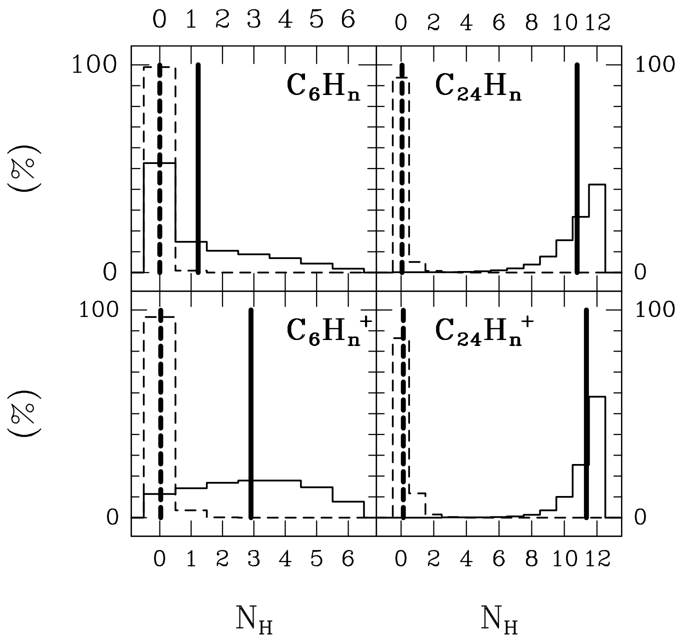


Figure 3.9: Distribution of PAHs according to their number of hydrogen atoms. The solid lines refer to the case of NGC 7027, the dashed ones to the PDR of the Orion Bar. The bold bins represent the mean number of hydrogen atoms $\bar{N}_{\rm H} = \alpha_{\rm H} N^{\rm o}_{\rm H}$.

rate, cations have larger hydrogen coverage than the neutrals but this difference tends to diminish with molecular size. In all the astrophysical environments investigated, $\alpha_{\rm H}$ increases with size up to a plateau for PAHs having more than 50 carbon atoms. The existence of this plateau can be understood from Eqs. (3.14) and (3.16) when one neglects the rate of photodissociation leading to loss of hydrogen, which considerably drops for large molecules. The remaining terms do not markedly depend on the molecular size, so that the value of $\alpha_{\rm H}$ in this plateau region depends only on the temperature. The evolution of $\alpha_{\rm H}$ with temperature for large PAHs is shown in Fig. 3.11. Up to 1000 K, $\alpha_{\rm H}$ is equal to 100 %. Since the chemical abstraction reactions are dominant for $T > 2000$ K, the hydrogen coverage drops in this temperature range, reaching a value of a few per cent for $T > 10^4$ K. Such temperatures can be reached in HII regions and shocked-regions.

Since the 3.3 $\mu$m band of the UIR features has also been observed in the HII region of NGC 7027, we also investigate the influence of the ionization fraction of hydrogen $\xi$ defined as $\xi = n_{\rm H+}/n_{\rm <H>}$ where $n_{\rm H+}$ and $n_{\rm <H>}$ represent the proton density and the total density of hydrogen nuclei, respectively. For the calculations the electron density is set equal to:

$$\begin{aligned} n_{\rm e} &= n_{\rm H^+} + n_{\rm M^+} \\ &\simeq \xi \; n_{\rm <H>} + 5.10^{-4} \; n_{\rm <H>} \ , \end{aligned} \tag{3.25}$$

where M represent the metallic species C, Si, S, Fe assumed to be present according to

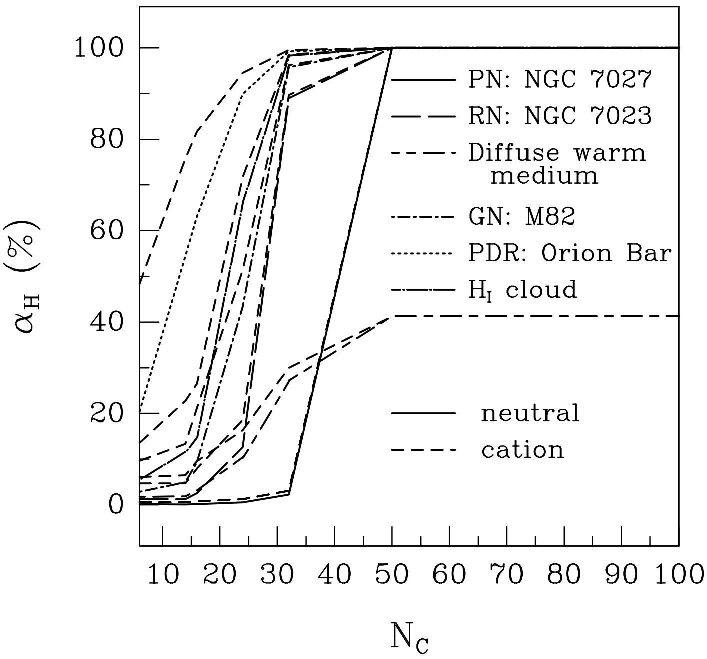


Figure 3.10: Hydrogen coverage of PAHs in some astrophysical media as a function of molecular size. For each medium the two curves represent $\alpha_H(n)$ and $\alpha_{\mathrm{H}}(c)$, hydrogen coverage for neutrals (lower curve) and for cations (upper curve), respectively.

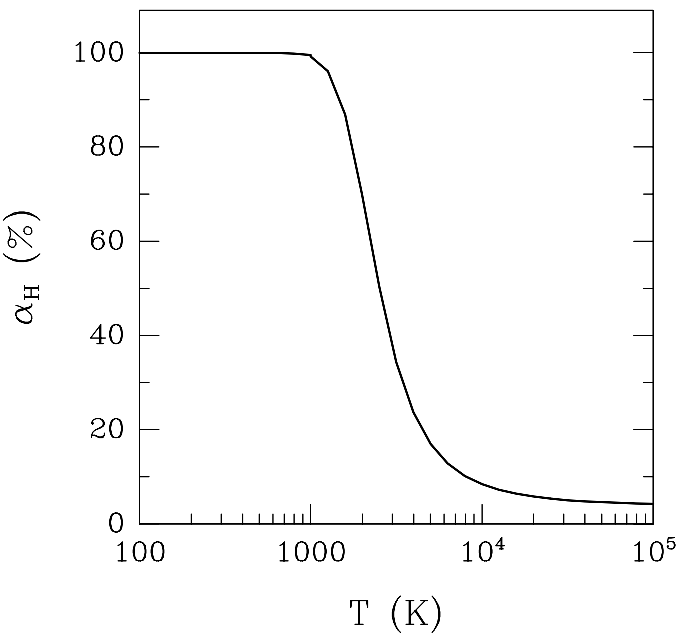


Figure 3.11: Hydrogen coverage of large PAHs ($N_C > 50$) as a function of temperature.

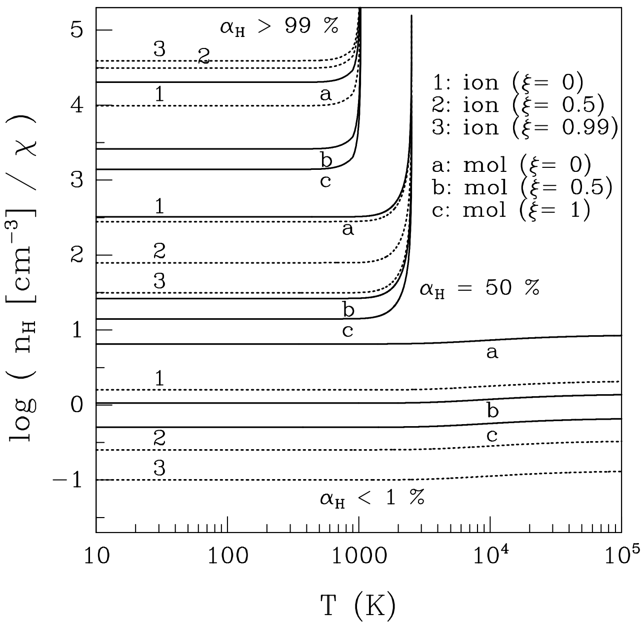


Figure 3.12: Hydrogenation equilibrium curves in the plane $T$ , $log(n_{<H>}/\chi)$ for pyrene molecules and cations in region with various values of the ionization fraction of atomic hydrogen $\xi$, and for three hydrogen coverage regimes, $\alpha_H$ = 1, 50, 99 %.

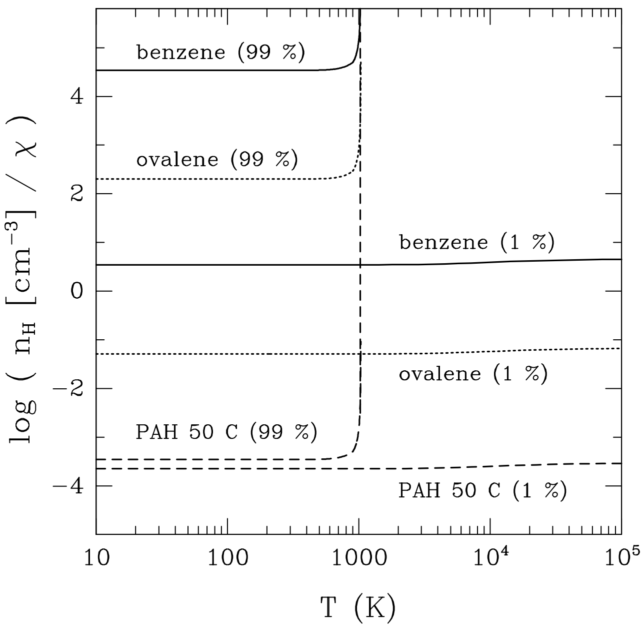


Figure 3.13: Hydrogenation equilibrium curves in the plane $T$ , $log(n_{<H>}/\chi)$ for various PAHs cations in a region with an ionization fraction of atomic hydrogen $\xi$ = 0, and for two hydrogen coverage regimes, $\alpha_H$ = 1, 99 %.

their solar abundances and fully ionized in only one ionization state.

As suggested from the study of ionization, a representation of the state of equilibrium in the plane $T$ , $\log(n_{<\mathrm{H}>}/\chi)$ may provide an interesting view of the influence of the physical parameters on the hydrogen coverage. Figure 3.12 shows the locations of the curves for $\alpha_{\mathrm{H}}$ equal to 1 %, 50 % and 99 % in the case of an ensemble of pyrene molecules and of pyrene cations for regions with various values of the ionization fraction of atomic hydrogen $\xi$. From Fig. 3.12 it can be seen that **(i)** a full hydrogen content of pyrene PAH ($\alpha_{\mathrm{H}} > 99$ %) is only possible for a temperature lower than 1000 K and a high value of $n_{<\mathrm{H}>}/\chi$ ($n_{<\mathrm{H}>}/\chi > 10^4$ cm$^{-3}$ at $T = 100$ K for pyrene cations and $\xi = 0$); **(ii)** a total dehydrogenation ($\alpha_{\mathrm{H}} < 1$ %) is reached for sufficiently low values of $n_{<\mathrm{H}>}/\chi$ whatever the value of the temperature ($n_{<\mathrm{H}>}/\chi < 2$ cm$^{-3}$ at $T = 100$ K for pyrene cations and $\xi = 0$); **(iii)** a given state of hydrogen content, that is to say a given value of $\alpha_{\mathrm{H}}$, is obtained for various ionization fractions of atomic hydrogen and states of ionization of PAHs at different values of $n_{<\mathrm{H}>}/\chi$. For instance, a total dehydrogenation of pyrene cations in a highly ionized region requires a low value of $n_{<\mathrm{H}>}/\chi$ (curve 3 in Fig. 3.12), whereas the higher value is needed in the case of pyrene molecules in a region with $\xi = 0$ (curve a in Fig. 3.12). A medium value of $n_{<\mathrm{H}>}/\chi$ is that required by pyrene cations in a region with $\xi = 0$ (curve 1 in Fig. 3.12).

In order to investigate the effect of the molecular size on situations **(i)**, **(ii)** and **(iii)** we have plotted in Fig. 3.13 the locations of the curves $\alpha_{\mathrm{H}}$ equal 1% and 99 % for various PAH cations in a region with $\xi = 0$ (these curves are equivalent to the curve 1 in Fig. 3.12). We observe in Fig. 3.13 that for a given value of $\alpha_{\mathrm{H}}$ the curves of all PAHs can be deduced from any one of them by displacement along the y axis. This leads to three interesting consequences: **(I)** the previous observations **(i)**, **(ii)** and **(iii)** can be applied to each PAH with the corresponding values of $n_{<\mathrm{H}>}/\chi$. The larger the PAH, the lower is the value of $n_{<\mathrm{H}>}/\chi$ needed to reach a given state of hydrogenation and the narrower the region in the plane $T$ , $\log(n_{<\mathrm{H}>}/\chi)$ where $1\% < \alpha_{\mathrm{H}} < 99\%$; **(II)** to have a given value of $\alpha_{\mathrm{H}}$, the temperature must not be greater than a maximum value which is the same for all PAHs and is consequently equal to that for large PAHs given in Fig. 3.11 ; **(III)** the media where the UIR bands have been seen have all values of $n_{<\mathrm{H}>}/\chi$ ranging between $10^{-1}$ and $10^2$ cm$^{-3}$, and temperatures lower than some $10^3$ K. We deduce from Figs. 3.12 and 3.13 that, in these media, PAHs having less than 50 carbon atoms are partially dehydrogenated, whereas larger PAHs have their full hydrogen content.

### Relation between hydrogenation and ionization

It was stated in Sect. 3.3.1 that hydrogenation of PAH cations is more rapid than that of their corresponding molecules. However, it can be seen by comparison of Figs. 3.7 and 3.10 that hydrogenation of small PAHs is more efficient in the media where the PAH ionization fraction is lower. The explanation for this phenomenon is that hydrogenation increases with the hydrogen density (see Figs. 3.12 and 3.13) whereas ionization decreases with the electron density (see Fig. 3.8). As the electron density practically varies as a linear function of the hydrogen density in the regions of interest here (see Eq. (3.25)), high hydrogen coverage of small PAHs are always related to low ionization fraction of PAHs. This result is confirmed in Fig. 3.14, where ionization fraction and hydrogen coverage of some PAHs are plotted as a function of $n_{<\mathrm{H}>}/\chi$ for a typical region showing the UIR bands ($T = 500$ K and $\xi = 0$) and in a typical HII region ($T = 10^4$ K and $\xi = 1$).

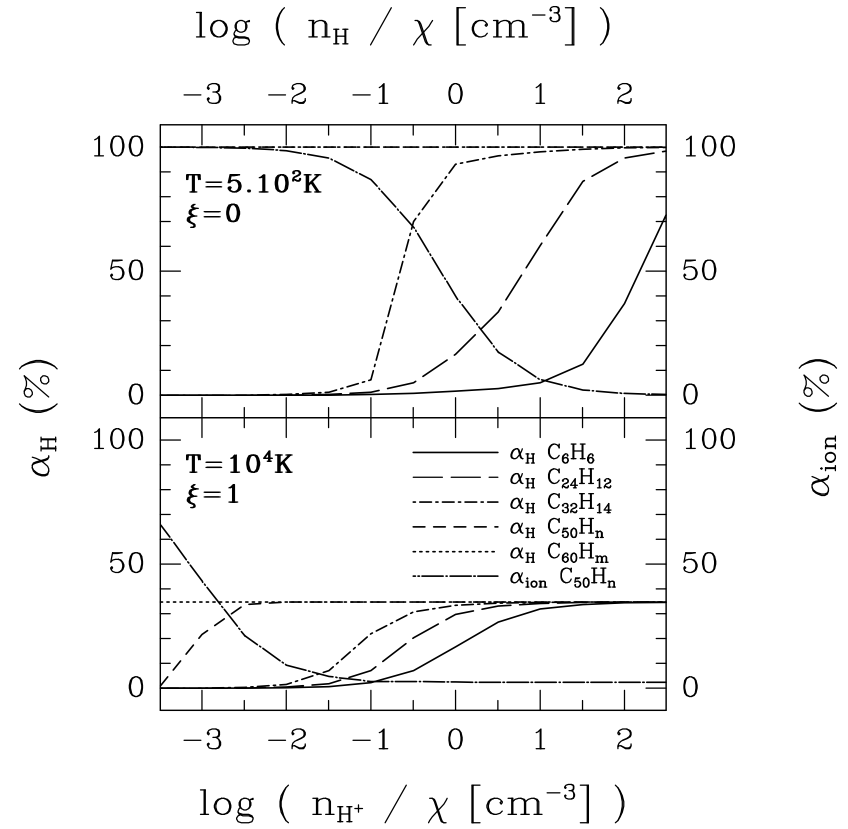


Figure 3.14: Ionization fraction and hydrogen coverage of some PAH molecules in a typical region showing the UIR bands (upper diagram) and in a HII region (lower diagram).

## 3.4 Astrophysical implications

In Chap. 2 we have introduced two characteristic times in the study of the photostability of PAHs molecules in an astrophysical medium: $\tau^{\rm UV}$, the time for photodestruction via loss of carbon and $\tau^{\rm gr}$, the time for growth by accretion of carbon particles. These times are defined as follows:

$$\tau^{\rm UV} = \frac{1}{k_{\rm C}^{\rm UV}} , \tag{3.26}$$

$$\tau^{\rm gr} = \frac{1}{n_{<{\rm C}>}\ k_{\rm C}^{\rm acc}} \simeq 10^{12} \left(\frac{n_{<{\rm C}>}}{1 \ {\rm cm}^{-3}}\right)^{-1} \quad {\rm s}, \tag{3.27}$$

where $k_{\rm C}^{\rm UV}$ is the value for the loss of carbon from a PAH and where $n_{<{\rm C}>}$ and $k_{\rm C}^{\rm acc}$ represent the density of carbon particles (carbon atoms or cations) and their rate of accretion onto PAHs.

It was established in Chap. 2 that PAHs having less than 50 carbon atoms have a characteristic time of photodissociation $\tau^{\rm UV}$ smaller than the time for growth $\tau^{\rm gr}$, and that they are consequently destroyed within a time $\tau^{\rm UV}$. We have seen here that in astrophysical environments showing the UIR bands these PAHs are probably ionized and partially dehydrogenated. Under these conditions the values of $\tau^{\rm UV}$ and $\tau^{\rm gr}$ are different from those of PAH molecules. However, we assume here that the time for accretion of carbon particles can still be used. This timescale should indeed account for accretion of both carbon atoms and carbon ions and we have therefore used a mean value in Chap. 2 for all these processes. This time may be smaller for partially dehydrogenated PAHs because of their radical sites, but also greater for PAH cations because of the Coulomb repulsion with $C^+$. We therefore keep the value of Chap. 2 for the present discussion. On the other hand, the results of Sect. 3.2.3 have shown that the rates for photodissociation of ionized and dehydrogenated PAHs are much greater than the corresponding rates for full hydrogen content molecules. The times $\tau^{\rm UV}$ are consequently lower. As in Chap. 2, we therefore conclude that $\tau^{\rm UV} < \tau^{gr}$ for small PAHs ($N_{\rm C} < 35$) in the media where the UIR bands are seen.

These results confirm the destruction of small PAHs. Moreover, we conclude here that destruction of these small PAHs is more rapid than that calculated in Chap. 2. To illustrate this result, we have presented in Table 3.4 the times of destruction of some small PAHs in their molecular and totally dehydrogenated ionized form and also for a mean state corresponding to the average ionization and hydrogen content of PAHs in the considered medium. To take into account the state of hydrogenation and ionization of PAHs we have calculated the rate for photodissociation of carbon as follows:

$$k_{\rm C}^{\rm UV} = \sum_{i=0}^{N_{\rm H}^{\circ}} \chi\ n_i\ {k_{\rm C}^{\rm UV}}_i^{(n)} + \sum_{i=0}^{N_{\rm H}^{\circ}} \chi\ c_i\ {k_{\rm C}^{\rm UV}}_i^{(c)} , \tag{3.28}$$

with the notations of Sect. 3.3.2. The values of the lifetimes in Table 3.4 put into question the existence of small free PAHs in the regions showing the UIR bands. Unless it can be

Table 3.4: Typical times for the photodestruction of PAHs in some astrophysical media (unit = year).

| Medium | benzene | | | pyrene | | | ovalene | | |
|---|---|---|---|---|---|---|---|---|---|
| | (1) | (2) | (3) | (1) | (2) | (3) | (1) | (2) | (3) |
| NGC 7027 | 1.2 (-5) | 4.7 (-4) | 1.8 (-5) | 6.0 (-6) | 9.7 (-4) | 1.7 (-5) | 1.1 (-5) | 1.4 (-2) | 1.1 (-4) |
| Orion Bar | 1.3 (-3) | 5.0 (-2) | 2.1 (-2) | 6.4 (-2) | 1.6 (-1) | 1.2 (-1) | 1.2 (-3) | 1.5 (0) | 1.2 (0) |
| NGC 7023 | 2.3 (-3) | 8.6 (-2) | 9.0 (-3) | 1.1 (-3) | 1.8 (-1) | 1.5 (-2) | 2.1 (-3) | 2.6 (0) | 7.0 (-1) |
| M82 | 2.0 (-3) | 7.4 (-2) | 1.2 (-2) | 9.6 (-4) | 1.5 (-1) | 2.4 (-2) | 1.8 (-3) | 2.3 (0) | 9.9 (-1) |
| HI region | 5.7 (0) | 2.2 (2) | 3.6 (1) | 2.8 (0) | 4.5 (2) | 8.2 (1) | 5.2 (0) | 6.5 (3) | 5.8 (3) |
| D. w. med. | 5.7 (0) | 2.2 (2) | 2.5 (1) | 2.8 (0) | 4.5 (2) | 3.9 (1) | 5.2 (0) | 6.5 (3) | 3.7 (2) |

(1) totally dehydrogenated PAH cation, (2) PAH molecule, (3) average value taking into account all hydrogen and ionized forms of the PAH according to their concentration.

shown that a more rapid formation process, such as erosion of hydrogenated amorphous carbon (HAC)(Duley 1987, 1988), could justify their presence in these environments it is indeed doubtful whether free small PAHs could be the carriers of the UIR bands as proposed by Allamandola *et al.* (1985), Geballe et al. (1989), Woodward *et al.* (1989) and more recently by Duley & Jones (1990). However, as has been suggested by Duley (1987, 1988), Duley & Jones (1990) and Allamandola (1991), IR emission could originate from PAHs loosely bonded to interstellar dust, which could therefore be more stable against photodissociation than free PAHs.

Because of their greater size, large PAHs ($N_C > 50$) also resist the UV radiation field of the ISM. For these larger PAHs a comparison shows that, in the regions where the UIR bands are seen, chemical abstraction is more efficient than photodissociation in removing hydrogen from large PAHs. However, chemical abstraction competes with hydrogenation and can lead to dehydrogenation of PAHs only in regions with a temperature higher than 2000 K. Such situations may be found in HII regions and in shocked regions (Brown et al. 1989, Flower et al. 1990).

Chemical destruction leading to a loss of carbon atoms is also probably an important factor of destruction of PAHs. Omont (1986) has estimated that this would mainly occur by reactions between $C^+$ and PAH molecules. The destruction rate should be however of the same order of magnitude or lower as the rate for carbon accretion. This means that PAHs having a photodissociation rate equal or larger than the accretion rate are likely

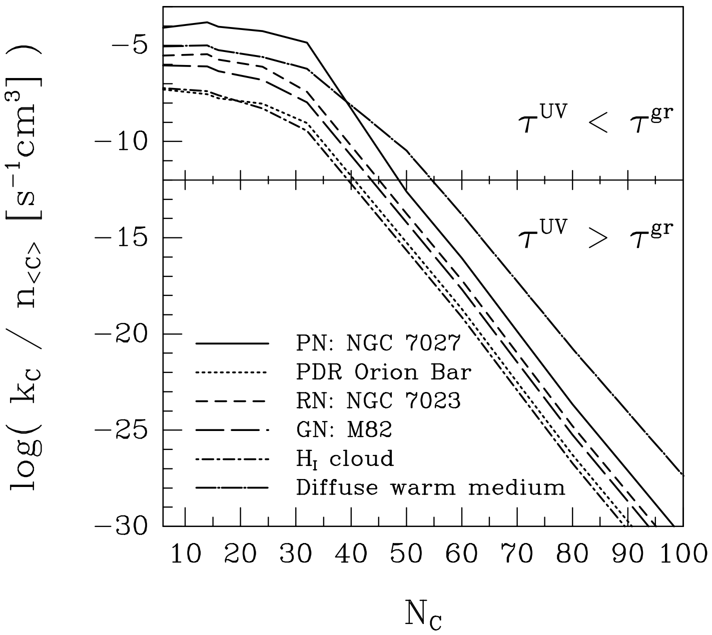


Figure 3.15: Determination of the minimal size of surviving PAHs in various astrophysical environments.

to be destroyed via UV photodissociation. On the other hand, PAHs having an accretion rate larger than the photodissociation rate are likely to resist against destruction during collision with carbon particles. In order to determine the size of the smaller PAHs which may survive in the regions showing the UIR bands we therefore compare the time for accretion $\tau^{\rm gr}$ to the time $\tau^{\rm UV}$ for photodestruction, as in Chap. 2.

For representational convenience we have plotted in Fig. 3.15 $k^{\rm acc}/n_{<\rm C>} = 1/\tau^{\rm gr} n_{<\rm C>} = 10^{-12}$ s$^{-1}$cm$^3$ and $k_{\rm C}^{\rm UV}/n_{<\rm C>} = 1/\tau^{\rm UV} n_{<\rm C>}$ for various astrophysical media. From Fig. 3.15 we observe that surviving PAHs in all these media have more than 40 carbon atoms. The smallest size is obtained for the Photodissociation Region of the Orion Bar and for the HI cloud where PAHs have a relatively high hydrogen content (see Sect. 3.3.2). On the other hand, in regions with a low hydrogen coverage small PAHs are more rapidly destroyed and the size of the smaller surviving PAHs is slightly greater: 50 carbon atoms in NGC 7027 and 55 carbon atoms in the warm diffuse medium. These conclusions are, however, not very different from those of Chap. 2 because the PAHs surviving the UV radiations do not undergo a massive loss of hydrogen in the regions showing the UIR bands and have therefore similar rates as those of the PAH molecules considered in Chap. 2. It was pointed out in Chap. 2 that is some favourable cases the carbon accretion rate could reach the maximal value of $10^{-10}$ cm$^3$s$^{-1}$, i.e. 2 orders of magnitude greater than the value assumed here (see Eq. (3.27)). Figure 3.15 shows that in such favourable cases, the minimal size of surviving PAHs would be diminished by 5 units compared to the case with an accretion rate of $10^{-12}$ cm$^3$s$^{-1}$.

The determination of the hydrogen content and ionization states of PAHs have shown some mutual influence between hydrogenation and ionization processes. Progress could be made to better analyze this coupling. At the present time it is not possible to correctly evaluate the rate of electron recombination for PAHs in various states of hydrogen content. Experimental data in this area would be of interest for astrophysicists because it is needed for precise estimate of the ionization fraction of PAHs. We note also that the results presented here have been obtained under the assumption of ionization and hydrogenation equilibrium. A dynamical calculation of the competing processes of ionization, hydrogenation and photodestruction of PAHs may provide some interesting new results.

## 3.5 Conclusion

A large fraction of interstellar PAHs are ionized and partially dehydrogenated. In the regions of the ISM where the UIR bands have been observed (reflection nebulae, planetary nebulae, HII regions, active galactic nuclei...) the ionization fraction of PAHs may indeed largely vary and it depends mainly on the intensity of the UV field and on the electron density. On the other hand, the hydrogen content is relatively similar in all the previously mentioned media. The hydrogen coverage increases with molecular size up to a value of 100 % for PAHs having more than 50 carbon atoms. For temperatures higher than some $10^3$ K this size limit decreases because of the chemical abstraction of hydrogen. A high hydrogen coverage of small PAHs is favored in regions where the ionization fraction of PAHs is relatively low, whereas marked dehydrogenation can occur at high temperatures and low hydrogen densities, which induce a high ionization fraction.

An extension of the model for interstellar PAHs of Chap. 2 to the case of PAH cations and dehydrogenated PAHs has allowed the calculation of the corresponding photodissociation rates. It is found that cations and partially dehydrogenated PAHs are less stable than their parent molecules. Cation rates are on average 5 times larger than the rates of the corresponding molecules calculated in Chap. 2. For partially dehydrogenated PAHs differences are much larger and they increase with both molecular size and degree of dehydrogenation. For a totally dehydrogenated coronene molecule there is a two orders of magnitude difference. This indicates that PAHs with less than 35 carbon atoms probably do not survive more than a year in the regions of high UV radiations where the UIR are seen. If these PAHs are really the carriers of the UIR bands it may be necessary to find a very efficient process for their formation. Most likely small PAHs emit while they are still bound in PAH clusters such as HAC. Large PAHs with more than 50 carbon atoms may also be the carriers of the UIR bands because their rates of photodissociation are lower that the rate for carbon accretion in the regions showing the UIR emission bands. Since it is now well documented that PAHs could form in the circumstellar winds of late type stars (Keller & Sedlmayr 1983; Keller 1987; Frenklach & Feigelson 1989; Cherchneff et al. 1992; Cadwell et al. 1994), it would be of great interest to precisely study their growth at least up to a size of 50 carbon atoms.

Revenons un moment à la liste des molécules qui peuplent les grands nuages interstellaires. Notons que toutes celles qui incorporent plus de trois atomes possèdent un, deux ou trois atomes de carbone. Cela, bien sûr, ne nous étonne pas. Cet atome est muni de quatre "crochets" particulièrement adaptés aux combinaisons moléculaires. Sur la Terre, il est systématiquement présent dans toutes les grandes structures moléculaires. Nous découvrons ici que cette prédominance du carbone n'est pas confinée à la biosphère. Dans le cadre de la chimie interstellaire, elle s'étend à toute la Galaxie, et, sans doute, à toutes les galaxies.

Hubert Reeves, *Patience dans l'azur* , 1981.

# Chapter 4

# PAH growth in circumstellar envelopes

**abstract**

Analytical expressions are presented to estimate the interactions of gas particles with polycyclic aromatic hydrocarbons (PAHs) described as large flat plates. This modelization enables us to determine the collision rate of gas particles with PAHs, the drag force of gas particles on PAHs and the energy exchanged between PAHs and gas particles.

These results are applied to the case of the circumstellar envelopes of C–stars where PAHs are considered to form and grow. As a result of these calculations, the drift velocities of PAHs are estimated and found to be negligible in comparison with the gas thermal velocity. The determination of PAH temperatures in the envelope is also carried out. Finally, the results are discussed in the context of the role of PAHs in the formation of dust particles.

—————————————

## 4.1 Introduction

Since Léger & Puget (1984) and Allamandola et al. (1985) first proposed polycyclic aromatic hydrocarbons (PAHs) as carriers of the so–called 'unidentified infrared (UIR) bands', it has been claimed that these molecules may be the most abundant molecules in the interstellar medium (ISM) after $H_2$ and CO (Léger et al. 1989). However, the question of their existence is still open and it is therefor of great interest to study the processes contributing to their formation and growth in astrophysical media.

It is known since 1983 that one of the more promising places for the formation of PAHs are the circumstellar envelopes (CSEs) of carbon– rich late type red giants, also known as C–stars, where the densities ($n_{\rm H} \simeq 10^{13}$ cm$^{-3}$ and $n_{\rm C_2H_2} \simeq 10^9$ cm$^{-3}$) and temperature range (500 K $\leq T \leq$ 1000 K) are favourable for the chemical reactions of formation of PAHs from acetylene (Keller & Sedlmayr 1983). It has been suggested that PAH formation constitutes the first step in the chemical pathway to dust in C–star shells (Keller 1987, Gail & Sedlmayr 1987a, Allamandola et al. 1989). The physical properties of dust have been and are still extensively studied in CSEs. On the other hand, there are few studies concerning the physical properties of PAHs in stellar shells (Omont 1986, Cherchneff et al. 1991,1992).

One of the aims of this chapter is to propose a description of the effects of gas particles on PAHs under the physical conditions relevant to the interstellar medium, and especially to circumstellar environments. The calculations are achieved with the simple assumption that PAHs can be considered as large and flat plates. Using this modelization, analytical expressions are derived in Sect. 4.2 for the collision rate, drag force and energy input of gas particles to PAHs. Applying these analytical relations to PAHs in CSEs enables us to determine PAH drift velocities and temperatures, as shown by calculations presented in Sects. 4.3 and 4.4, respectively. These results are used in Sect. 4.5 to examine the formation and growth processes of PAHs and the role of PAHs in the formation of dust particles in the CSEs of C–stars.

## 4.2 Particles, Momentum and Energy flux onto PAHs

### 4.2.1 Collision rate

Assuming that PAHs are the carriers of the interstellar UIR bands, Léger et al. (1989b) have concluded, by comparison of the IR spectra of compact PAHs and PAHs with protuberant rings, that interstellar PAHs should be rather compact molecules. Moreover, using the relative intensities of the spectra of the UIR bands and models for the excitation of PAHs, Allamandola et al. (1987, 1989) have estimated that the molecular size of interstellar PAHs should be of about 50 carbon atoms. Such compact PAHs containing 50 carbon atoms have a typical diameter of about 1.2 nm. Since hydrogen atoms and molecules and helium atoms, which are the most abundant species in the circumstellar winds of C–stars have characteristic dimensions smaller than 0.2 nm, interstellar PAHs can be regarded in a first approximation as large and flat molecules.

However, this description may prove incorrect in the case of circumstellar environments where it is expected that the chemical pathway for the formation of PAHs from acetylene favors the formation of PAHs containing rings with five carbon atoms (Keller 1987, Cherchneff et al. 1992, Goeres 1993). Such molecules should be non planar by the combination of five and six carbon atom rings. An extreme case corresponds to the predicted formation of fullerene–like molecules as in the case of R Coronae Borealis stars (Goeres & Sedlmayr 1992). In the case of C–giants which we consider here, molecules like corannulene, which is constituted by a five carbon atom ring surrounded by five fused 6–membered aromatic rings, are expected to form. However, the exact nature of circumstellar PAHs is still under investigation (Goeres 1993). Due to these uncertainties we describe PAHs as large flat molecules in the following. Moreover, we consider only pericondensed PAHs which are the most stable PAHs under the conditions of pressure and temperature encountered in CSEs (Keller 1987).

In all the calculations presented here we therefore assimilate PAHs to flat plates with

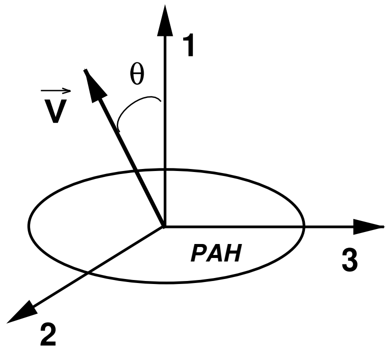


Figure 4.1: Coordinate system for PAHs.

surface $A$. Furthermore, we suppose that PAHs are moving with a drift velocity $V$ relative to the gas, which is mainly composed of atomic and molecular hydrogen and of helium atoms as it is the case in all astrophysically relevant media. The gas is assumed to be in Maxwellian equilibrium, with density $n$, temperature $T$ and thermal velocity $v_{\rm th}$:

$$v_{\rm th} = \sqrt{\frac{2k_{\rm B}T}{\mu}}\ , \tag{4.1}$$

where $\mu$ is the mean particle mass and $k_{\rm B}$ the Boltzmann constant.

The number flux $N_\theta$ incident on a PAH at angle of attack $\theta$ is given by:

$$N_\theta = \int_{-\infty}^{+\infty}\int_{-\infty}^{+\infty}\int_{-\infty}^{+\infty} v_1 A f\ dv_1 dv_2 dv_3 \tag{4.2}$$

with the geometric parameters defined in Fig. 4.1 and the distribution function $f$ given by:

$$\begin{aligned} f &= \frac{n}{\left(\sqrt{\pi}v_{\rm th}\right)^3} \times \\ &\quad \exp\left[-\frac{\left(v_1 - V\cos\theta\right)^2 + \left(v_2 - V\sin\theta\right)^2 + v_3^2}{v_{\rm th}^2}\right]\ . \end{aligned} \tag{4.3}$$

To account for all the possible orientations, we calculate the flux averaged over the angles:

$$\begin{aligned} N_{\rm PAH} &= \int\int N_\theta \frac{d\Omega}{4\pi} \\ &= nAv_{\rm th}\left[\ \frac{2S^2+1}{4S}\ {\rm erf}(S) + \frac{\exp\left(-S^2\right)}{2\sqrt{\pi}}\ \right]\ , \end{aligned} \tag{4.4}$$

where we have defined:

$$S = \frac{V}{v_{\rm th}} \tag{4.5}$$

and used the notation erf for the error function.

The result of Eq. (4.4) can be compared to that obtained from a similar calculation applied to a sphere (see Dominik et al. 1989):

$$\frac{N_{\rm PAH}}{2A} = \frac{N_{\rm sphere}}{4\pi r^2} \tag{4.6}$$

where $N_{\rm sphere}$ is the number flux of gas particles incident onto a sphere with radius $r$. An excellent approximation of Eq. (4.4) is provided by:

$$N_{\rm PAH} = nAv_{\rm th}\frac{1}{\sqrt{\pi}}\sqrt{1+\frac{\pi}{4}S^2}\ , \tag{4.7}$$

which is exact in the limits $S \gg 1$ and $S \ll 1$ and is accurate to within 2.5 % in all cases.

The limiting case for small velocities $V$ provides good results in C-star envelopes where the drift velocity of PAHs is negligible (see Sect. 4.3). On the other hand, in the case of C-type shocks propagating in molecular clouds the magnetic field leads to drift velocity of molecules relative to ions of some km.s$^{-1}$ (Flower et al. 1990). This may enhance the collisional rate of PAHs with gas particles and thereby modify some reaction rates.

Equation (4.4) can be also used when one considers the contribution of only one type of particle ($i$) impinging onto the PAH. One has then to substitute $n_i$ and $v_{{\rm th}\ i}$ the density and thermal velocity of the considered particles to $n$ and $v_{\rm th}$ in Eq. (4.4).

Both atomic hydrogen and acetylene molecules are involved in the chemical process of PAH growth (Keller 1987; Gail & Sedlmayr 1987a; Frenklach & Feigelson 1989, Cherchneff et al. 1992) and it is therefore of interest to study their interaction with PAHs. Considering first the case of hydrogen atoms impinging onto PAHs, we deduce from Eq. (4.4) a collision rate with a PAH containing $N_{\rm C}$ carbon atoms:

$$k_{\rm H}^{\rm col} = 3.5\ 10^{-10}\ \left(\frac{N_{\rm C}}{6}\right)\left(\frac{T}{1000\ {\rm K}}\right)^{1/2}\quad {\rm cm}^3\ {\rm s}^{-1} \tag{4.8}$$

where we have supposed that $S \ll 1$ and used the relation of Omont (1986) for the radius of a typical interstellar PAH:

$$R_{\rm PAH} = 0.9\ N_{\rm C}^{1/2}\quad {\rm \AA}\ . \tag{4.9}$$

Applying Eq. (4.4) to the case of molecules of acetylene incident on a PAH we obtain a collision rate of acetylene with a PAH containing $N_{\rm C}$ carbon atoms equal to:

$$k_{\rm C_2H_2}^{\rm col} = 6.9\ 10^{-11}\ \left(\frac{N_{\rm C}}{6}\right)\left(\frac{T}{1000\ {\rm K}}\right)^{1/2}\quad {\rm cm}^3\ {\rm s}^{-1}\ . \tag{4.10}$$

The collision rates obtained in Eqs. (4.8) and (4.10) provide upper limit for the chemical reaction rates of acetylene and atomic hydrogen with PAHs, which are more precisely discussed in Sect. 4.5.1.

### 4.2.2 Momentum transfer to PAHs

The flux of momentum $\mathbf{F}_{\theta_\mathrm{i}}$ incident on a PAH at an angle of attack $\theta$ is given by:

$$\mathbf{F}_{\theta_\mathrm{i}} = \int_{-\infty}^{+\infty}\int_{-\infty}^{+\infty}\int_{-\infty}^{+\infty} \mu \mathbf{v} v_1 A f \; dv_1 dv_2 dv_3 \; . \tag{4.11}$$

The net flux also includes the momentum of the re–emitted particles.

The most abundant particles are, on the one hand, hydrogen molecules and helium atoms, which do not attach or react with PAHs and are therefore likely to be re–emitted, and on the other hand, hydrogen atoms which may on the contrary attach and react. At low temperatures ($T < 100$K) the trapping fraction of atomic hydrogen interacting with PAHs is indeed likely to be near unity (see for instance the study of Burke & Hollenbach (1983) about the interactions of hydrogen atoms with amorphous carbon). However, the trapping fraction of atomic hydrogen on PAHs probably rapidly decreases with temperature and is probably very low in the regions of interest surrounding stars. Moreover, we shall show in Sect. 4.5.1 that less than 1 % of the impinging hydrogen atoms actually react with PAHs in the CSEs of C–stars. We consequently neglect the effect of possible interactions between PAHs and atomic hydrogen in the present calculation. The other molecules interacting with PAHs have all abundances lower than $10^{-4}$ relative to hydrogen and can be therefore neglected here. In the calculation presented here we therefore consider that gas particles are all re–emitted. In order to simplify the calculation we furthermore assume that PAHs act as a specularly reflecting surface. A more exact treatment of the problem taking precisely into account all PAH–gas interactions (sticking, accomodation) would probably not lead to extremely different results, as in the case of dust particles (Dominik et al. 1989).

The flux of momentum from re–emitted particles $\mathbf{F}_{\theta_\mathrm{r}}$ has the same form as $\mathbf{F}_{\theta_\mathrm{i}}$ with a velocity $\mathbf{v}'$ for the re–emitted particles equal to:

$$\mathbf{v}' = \mathbf{v} - \frac{2\;\mu\; m_\mathrm{PAH}}{\mu\; + \; m_\mathrm{PAH}} \left[\mathbf{n_1}.\left(\mathbf{V} - \mathbf{v}\right)\right] \mathbf{n_1} \; , \tag{4.12}$$

where $m_\mathrm{PAH}$ is the mass of the PAH. Adding the contributions of $\mathbf{F}_{\theta_\mathrm{i}}$ and $\mathbf{F}_{\theta_\mathrm{r}}$ and averaging over the angles leads to the following expression of the drag force of gas $\mathbf{F}_\mathrm{g}$:

$$\begin{aligned} \mathbf{F}_\mathrm{g} \;\; = \;\; & -A n v_\mathrm{th}^2 \, \frac{\mu\; m_\mathrm{PAH}}{\mu + m_\mathrm{PAH}} \, \frac{\mathbf{V}}{V} \;\; \times \\ & \left[ \frac{\mathrm{erf}(S)}{4S^2} \left(4S^4 + 8S^2 - 3\right) + \frac{\exp\left(-S^2\right)}{2\sqrt{\pi}S} \left(2S^2 + 3\right)\right] \; . \end{aligned} \tag{4.13}$$

In the limiting cases of small and large velocity $V$, Eq. (4.13) reduces to:

$$\mathbf{F}_\mathrm{g} = \begin{cases} -\;\dfrac{4}{\sqrt{\pi}}\; A\; n\; v_\mathrm{th}\; \dfrac{\mu\; m_\mathrm{PAH}}{\mu + m_\mathrm{PAH}}\; \mathbf{V} & S \ll 1 \\[2ex] -\; A\; n\; v_\mathrm{th}\; \dfrac{\mu\; m_\mathrm{PAH}}{\mu + m_\mathrm{PAH}}\; V\, \mathbf{V} & S \gg 1 \end{cases} \tag{4.14}$$

The following expression gives an approximation of Eq. (4.13) to better than 1 % in all cases:

$$\mathbf{F}_{\rm g} = -Anv_{\rm th}^2 \, \frac{\mu \, m_{\rm PAH}}{\mu + m_{\rm PAH}} \, \frac{\mathbf{V}}{V} \, S \, \frac{4}{\sqrt{\pi}} \, \sqrt{1 + \frac{\pi}{16} S^2} \; . \tag{4.15}$$

In the envelopes of C-giants the drag force acts against the radiation pressure which is responsible for the acceleration of PAHs (Cherchneff et al. 1991). A drift velocity of PAHs relative to the gas occurs as a result of this competition. This point is discussed in detail in Sect. 4.3.

### 4.2.3 Energy transfer to PAHs

The flux of energy (kinetik and internal) $E_{\theta_{\rm i}}$ transferred from the gas to a PAH at an angle of attack $\theta$ is given by:

$$E_{\theta_{\rm i}} = \int_{-\infty}^{+\infty} \int_{-\infty}^{+\infty} \int_{-\infty}^{+\infty} \left[ u + \frac{1}{2} \mu v^2 \right] v_1 A f \; dv_1 dv_2 dv_3 \; . \tag{4.16}$$

where $u$ is the internal energy of the gas particles, which we assume equal to $j/2 \; k_{\rm B} T$ for a gas with $j$ internal degrees of freedom. [1] After averaging over the angles, one obtains the following expression:

$$\begin{aligned} E_{\rm i} \;\; = \;\; & N_{\rm PAH} \; u \; + \; A \; n \; k_{\rm B} T \; v_{\rm th} \; \times \\ & \left[ \frac{{\rm erf}(S)}{8S} \left( 4S^4 + 12 S^2 + 3 \right) + \frac{\exp\left(-S^2\right)}{4\sqrt{\pi}} \left( 2S^2 + 5 \right) \right] \; , \end{aligned} \tag{4.17}$$

which may be approximated to:

$$E_{\rm i} = \frac{j}{2} \; k_{\rm B} T \; N_{\rm PAH} \;\; + \;\; \begin{cases} \dfrac{2}{\sqrt{\pi}} \; A n k_{\rm B} T v_{\rm th} & S \ll 1 \\[2ex] \left( \dfrac{1}{2} \mu V^2 \right) \; \dfrac{1}{2} A n V & S \gg 1 \end{cases} \tag{4.18}$$

in the respective limits $S \gg 1$ and $S \ll 1$.

To estimate the energy flux due to the re–emitted particles $E_{\rm r}$, an energy accomodation coefficient $\alpha$ is usually introduced as follows:

$$E_{\rm r} = \left(1 - \alpha\right) E_{\rm i} + \alpha E_{\rm eq} \; , \tag{4.19}$$

where $E_{\rm eq}$ is the flux of energy that would correspond to reemited particles in complete equilibrium with the PAH at temperature $T_{\rm PAH}$, $E_{\rm eq} = \left( \frac{j}{2} + 2 \right) k_{\rm B} T_{\rm PAH} N_{\rm PAH}$. The net

[1] In the regions surrounding C–stars considered in the following sections, only the rotational degree of freedom of molecular hydrogen has to be taken into account.

energy flux $E_g$ from the gas to the PAH is equal to $E_i - E_r$. In the case of low drift velocities the energy flux reduces to:

$$E_g = \alpha N_{\rm PAH} \left[ \left( \frac{j}{2} + 2 \right) k_{\rm B} T - \left( \frac{j}{2} + 2 \right) k_{\rm B} T_{\rm PAH} \right] , \qquad (4.20)$$

which is analogous to the expression adopted by Burke & Hollenbach (1983) in their study of gas–grain interactions in the ISM.

Hollenbach & McKee (1979) have proposed the following type of expression for the energy accomodation coefficient $\alpha$ in a case with no drift velocity:

$$\alpha = \left(1 - \alpha^0\right) \exp \left[ - \frac{2 k_{\rm B} \left(T_{\rm PAH} + T\right)}{D} \right] + \alpha^0 , \qquad (4.21)$$

where $\alpha^0$ is the high–temperature hard–sphere limit defined as:

$$\alpha^0 = \frac{2 m_{\rm X} m_{\rm C}}{\left(m_{\rm X} + m_{\rm C}\right)^2} . \qquad (4.22)$$

In the expression for $\alpha^0$, $m_{\rm X}$ is the mass of the impinging particles while $m_{\rm C}$ is the mass of a carbon atom. In Eq. (4.21) $D$ represents the surface absorption energy for the particles colliding with the PAH. Burke & Hollenbach (1983) have successfully applied the model to graphite and we anticipate that we will not commit large errors by applying the results of this model to PAHs.

For the calculations carried out in Sect. 4.4 the species we consider are helium atoms, atomic and molecular hydrogen. For the adsorption energy of hydrogen atoms on a PAH, whose value has been much discussed so far (see Omont 1986), we adopt the most recently published value equal to 0.3 eV (Klose 1992). For helium atoms and hydrogen molecules we use the adsorption energies of Burke & Hollenbach (1983).

## 4.3 Drift of PAHs in circumstellar envelopes

### 4.3.1 Equilibrium drift velocities of PAHs

In the envelopes of C–giants PAHs are accelerated by radiation pressure (Cherchneff et al. 1991). To limit the acceleration, a drag force due to gas particles appears which introduces a drift velocity between PAHs and the gas particles. An upper–estimate of this drift velocity can be reached by calculating the equilibrium drift velocity $V_0$ where both radiation and gas pressure are equal.

The radiation force on a PAH at distance $R$ from the star may be written:

$$F_{\rm rad}(R) = A \int_0^\infty Q_{\rm pr} \frac{F_\nu(R)}{c} d\nu , \qquad (4.23)$$

where $F_\nu$, $c$ and $Q_{\rm pr}$ represent the radiation flux from the star, the velocity of light and the radiation pressure efficiency of the considered PAH, respectively.

Following the method of Lucy (1971,1976) for the treatment of radiative transfer in an extended stellar atmosphere, we write the radiation flux:

$$F_\nu(R) = F_\nu(R_\star)\ \left(\frac{R_\star}{R}\right)^2 \ , \tag{4.24}$$

where $F_\nu(R_\star)$ is the flux at the photosphere of the star, which we assume equal to $\pi B_\nu(T_\star)$, the flux of a sphere of uniform brightness emitting as a blackbody at the effective temperature $T_\star$ of the star. $B_\nu(T_\star)$ represents the well–known Planck function $B_\nu(T_\star) = 2h\nu^3/c^2[\exp(h\nu/k_\mathrm{B}T_\star) - 1]$. A more exact treatment of the radiative transfer using the code of Winters (1994) for the radiative flux in circumstellar envelopes has not been used here because it would not provide much different results and, furthermore, would prevent the use of meaningful analytic expressions.

In order to estimate $F_\mathrm{rad}$, we use the expressions of the Planck mean of the radiation pressure cross–section of PAHs from Cherchneff et al. (1991):

$$\begin{aligned}\overline{K(T_\star)} &= \frac{1}{\sigma T_\star^4}\int_0^\infty A\ Q_\mathrm{pr}\ \pi B_\nu(T_\star)\ d\nu \\ &= \mathrm{Max}(\ \overline{K^-(T_\star)}\ ,\ \overline{K^+(T_\star)}\ )\ ,\end{aligned} \tag{4.25}$$

where $\sigma$ is the Stefan constant. The quantities $\overline{K^-(T)}$ and $\overline{K^+(T)}$ represent the contributions to $\overline{K(T)}$ at low and high radiative temperatures, respectively, and are defined as functions of temperature and of $N_\mathrm{C}$, the number of carbon atoms of the PAH, according to Cherchneff et al. (1991):

$$\begin{aligned}\log \overline{K^-(T)} &= -13.24 - 2.7\ N_\mathrm{C}^{-0.113} \log T \\ &\qquad - \exp\left(-2.7(\log T - 2.33)\right)\ , \\ \log \overline{K^+(T)} &= -8.59 \left[\ \frac{\log T - 3.28\ N_\mathrm{C}^{-0.096}}{17.47}\ \right]^{-0.282} .\end{aligned} \tag{4.26}$$

Combining Eqs. (4.23) to (4.25), we obtain the following expression for the radiative force on a PAH:

$$F_\mathrm{rad}(R) = \frac{\sigma T_\star^4}{c}\left(\frac{R_\star}{R}\right)^2\ \overline{K(T_\star)}\ . \tag{4.27}$$

Equating the radiative force $F_\mathrm{rad}$ to the drag force $F_\mathrm{g}$ at a given position in the envelope allows the calculation of the equilibrium drift velocity of PAHs. We have carried out this calculation for the stationary models of C–star envelopes of Winters et al. (1994) (henceforth WDS).

We have used a model characterized by the stellar parameters $M_\star = 0.7\ M_\odot$, $L_\star = 2.4\ 10^4\ L_\odot$, $\dot{M}_\star = 8.10^{-5}\ \dot{M}_\odot\mathrm{yr}^{-1}$, where $M_\star$, $L_\star$ and $\dot{M}_\star$ are the stellar mass, luminosity and mass loss, respectively. The model moreover assumes a carbon to oxygen ratio of

$\epsilon_C/\epsilon_O = 1.40$ and yields a reliable description for the carbon star IRC+10216. Some information about the WDS model is given in Appendix A.

The drift velocity of some PAHs are plotted as a function of distance from the star in Fig. 4.2 for this circumstellar shell. The values of some thousand cm/s obtained for the equilibrium drift velocities are always 2 orders of magnitude lower than the value of the gas thermal velocity $v_{\rm th}$. Applying the limiting case of $S \ll 1$ for the expression of the drag force $F_{\rm g}$ we obtain from the equality of $F_{\rm rad}$ and $F_{\rm g}$ the following estimate of the equilibrium drift velocity of PAHs in circumstellar envelopes:

$$V_0 \simeq 3.10^{-2}\, v_{\rm th} \left(\frac{R}{3R_\star}\right)^{-2} \left(\frac{T_\star}{2500\ \rm K}\right)^{4} \left(\frac{N_{\rm C}}{50}\right)^{-1} \times \left(\frac{\overline{K(T_\star)}}{10^{-19}\ \rm cm^2}\right) \left(\frac{n}{10^{7}\ \rm cm^{-3}}\right)^{-1} \left(\frac{T}{1000\ \rm K}\right)^{-1} . \qquad (4.28)$$

From Fig 4.2 and Eq. (4.28) it is clear that drift of PAHs can be neglected to a very good approximation in C–star CSEs.

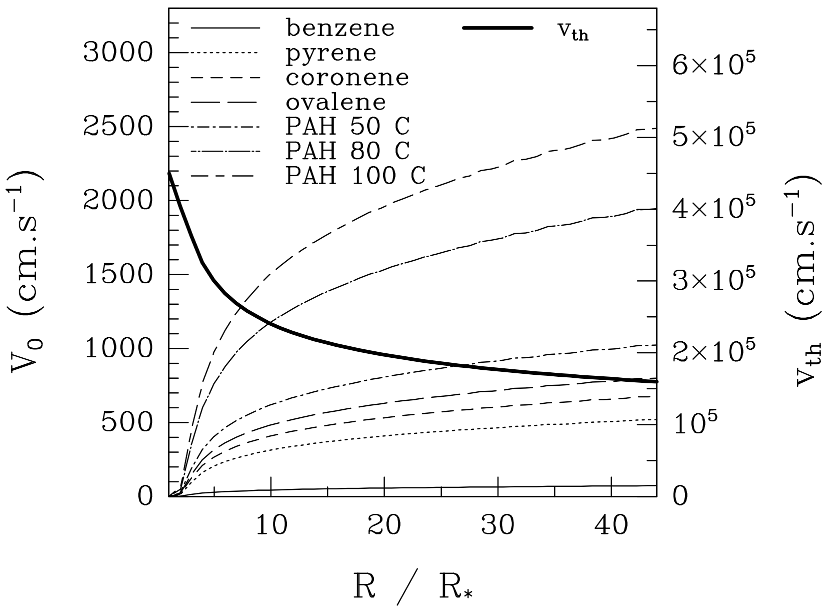


Figure 4.2: Equilibrium drift velocity of some PAHs in the envelope of a typical C–giant [WDS model for IRC+10216] as a function of distance from the star.

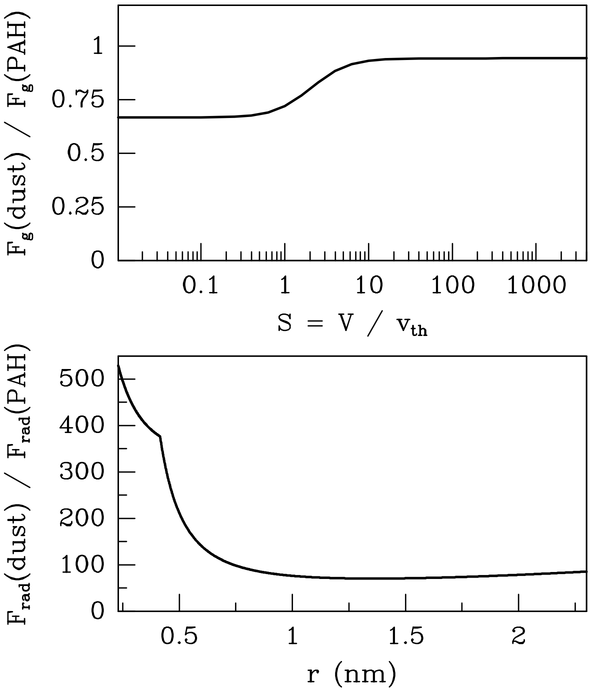


Figure 4.3: Upper diagram: Dust particle to PAH ratio of the gas drag force as a function of parameter S for a PAH and a dust particle of same radius in the envelope of a typical C–giant.
Lower diagram: Dust particle to PAH ratio of the radiative force as a function of radius for a PAH and a dust particle of same radius in the envelope of a typical C–giant.

### 4.3.2 Comparison between PAHs and dust particles

In contrast to the low PAH drift velocities, Dominik et al. (1989) have obtained drift velocities of a few km s$^{-1}$ for spherical dust particles with a radius of 1 nm in the envelope of C–giants stars. Such a radius is comparable to that of a pericondensed PAH with about 100 carbon atoms (see Eq. (4.9)). It is therefore worth looking at the reason explaining the differences of drift velocities between PAHs and dust particles. For this purpose, let us compare the radiative and drag forces undergone by a PAH and by a dust particle with same radius $r$.

The drag force on a dust particle can be obtained from a calculation similar to that performed in Sect. 4.2.2 for a PAH and leads to:

$$\begin{aligned} \mathbf{F}_{\mathrm{g}} \;=\; & -\pi r^2 n v_{\mathrm{th}}^2 \, \frac{\mu \, m_{\mathrm{dust}}}{\mu + m_{\mathrm{dust}}} \, \frac{\mathbf{V}}{V} \times \\ & \left[ \frac{\mathrm{erf}(S)}{4S^2} \left( 4S^4 + 4S^2 - 1 \right) + \frac{\exp\left(-S^2\right)}{2\sqrt{\pi} S} \left( 2S^2 + 1 \right) \right] , \end{aligned} \tag{4.29}$$

where $m_{\mathrm{dust}}$ is the mass of the dust particle and $r$ its radius (Dominik et al. 1989).

Figure 4.3 (upper diagram) shows the ratio $F_{\rm g}(\text{dust})/F_{\rm g}(\text{PAH})$ as a function of parameter $S$. This ratio does not depend on the position in the envelope and on the radius chosen for the comparison. It can be seen in Fig. 4.3 that the drag force on a dust particle and on a PAH of the same radius are always comparable. This result therefore provides no explanation for the difference of several orders of magnitude between the drift velocities of dust particles and PAHs in C–star CSEs.

The radiative force on a dust particle at a distance $R$ from the star has been estimated by Dominik et al. (1989) as:

$$F_{\rm rad}(R) = \frac{1}{2}\left(\frac{R_\star}{R}\right)^2 \frac{\sigma T_\star^4}{c}\,\pi r^2\ \mathrm{Min}\left(1, \frac{2\pi r}{1\mu}\right)\ . \qquad (4.30)$$

The ratio $F_{\rm rad}(\text{dust})/F_{\rm rad}(\text{PAH})$ is represented in Fig. 4.3 (lower diagram) as a function of radius $r$ in the envelope of a typical C–giant star. This ratio does not depend on the position in the envelope. We observe that the ratio decreases with increasing radius but is always of the order of $10^2$. This proves that PAHs are not accelerated by stellar radiation as efficiently as dust particles of comparable size. A similar result has already been derived by Cherchneff et al. (1991) to demonstrate that PAHs have a negligible role in the acceleration process of stellar winds.

Since PAHs are less accelerated than dust particles but undergo similar gas drag force for comparable size, PAHs have drift velocities much smaller than dust particles.

## 4.4 Temperature of PAHs in circumstellar envelopes

In order to use Eq. (4.20) for determining net energy flux, one has to know the temperature of PAHs. Alternatively, PAH temperatures may be reached by using Eq. (4.20) and balancing the energy gains to the energy loss of PAHs.

Heating of PAHs proceeds via collisions with gas particles (see above) and absorption of radiation from the neighbouring star (Cherchneff et al. 1991) and/or the interstellar radiation field. In the case of C–star envelopes, the ultraviolet photons from the ISM are absorbed by dust grains before reaching the region near the star, so that only collisions and absorption of stellar emission contribute to the heating of PAHs. Moreover since C–stars are thought to have a very weak chromospheric activity (Johnson & Luttermoser 1987) we restrain the stellar emission to the contribution of the photosphere.

Cooling of PAHs occurs via emission from their rotationally and vibrationally excited states (Cherchneff et al. 1991) and possibly by ionization (Verstraete et al. 1990) and ejection of hydrogen. As far as concerns photoionization and hydrogen photoejection, they are negligible because of the weak UV stellar radiation. The value of about 8 eV or the PAH ionization potential probably much hinders PAH thermoionization. On the other hand, the loss of hydrogen from PAHs has an activation energy of some eV and could occur at the temperatures prevailing near the star. However, since we have not taken into account the effects of chemical reactions on the heating of PAHs via collisions, and in particular the energy gained by recombination of PAHs radicals with hydrogen and of PAHs ions with electrons, we also neglect hydrogen ejection and ionization as a cooling process for PAHs.

The heating rate of PAHs via absorption of stellar radiation may be written:

$$H_{\rm PAH} = \int_0^\infty \sigma_\nu^{\rm abs}\ J_\nu(R)\ d\nu\ , \tag{4.31}$$

where $J_\nu$ is the mean specific intensity. To perform the calculations we have used the results of the radiative transfer code of Winters (1994) who kindly provided us with the values of $J_\nu$ as a function of frequency $\nu$ for various distances $R$ from star centre. The values of $J_\nu(R)$ were then fitted by a modified Planck distribution $W(R)\ B_\nu[T_{\rm rad}(R)]$, where $W$ and $T_{\rm rad}$ represent a dilution factor and a radiative temperature, respectively. We note that the dilution factor we have obtained for the best fit is different from the quantity $(R/R_\star)^2$ or $1/2(1\text{-}\sqrt{1-(R/R_\star)^2})$ usually introduced for the calculation of the temperature of molecular species in CSEs (MacCabe 1982, Cherchneff et al. 1991). Similarly $T_{\rm rad}$ is not equal to $T_\star$ as assumed by MacCabe (1982) and Cherchneff et al. (1991). Figure 4.4 shows the results obtained for $J_\nu$ from the radiative transfer code and from the fit formula as function of frequency $\nu$ at various positions in the envelope. From Fig. 4.4 it can be seen that both the maximum and the corresponding value of $\nu$ are well reproduced by the fit formula. The fitting procedure therefore provides a good estimate of $J_\nu$ in the frequency range of the maximum intensity, which is also the frequency range in the infrared where PAHs most absorb ($3\ \mu m < \lambda < 30 \mu m$).

In Eq. (4.31), $\sigma_\nu^{\rm abs}$ is the PAH absorption cross–section. As in the study of Cherchneff et al. (1991) we use the Eqs. (4.25) for the Planck mean of the absorption cross–sections, so that the heating rate for one PAH can be finally written:

$$H_{\rm PAH}(R) = \overline{K(T_{\rm rad})}\ W(R)\ \sigma T_{\rm rad}(R)^4\ . \tag{4.32}$$

The cooling rate of PAHs via emission is equal to:

$$C = 4\pi\ \int_0^\infty j_\nu\ d\nu\ , \tag{4.33}$$

where $j_\nu$ represents the emission coefficient of PAHs in units of erg cm$^{-3}$ s$^{-1}$ ster$^{-1}$ Hz$^{-1}$. Applying Kirchhoff's law for thermal emission of PAHs, we obtain $j_\nu = n_{\rm PAH}\ \sigma_\nu^{\rm abs}\ B_\nu(T_{\rm PAH})$ where $n_{\rm PAH}$ is the PAH density. Rewriting Eq. (4.33) for one PAH and using Eq. (4.25) we deduce:

$$C_{\rm PAH} = 4\ \overline{K(T_{\rm PAH})}\ \sigma {T_{\rm PAH}}^4\ . \tag{4.34}$$

The temperature of a PAH can finally be obtained from the equality:

$$E_{\rm g}\ (\ T_{\rm gas}\ ,\ T_{\rm PAH}\ ) + H_{\rm PAH}\ (\ T_{\rm rad}\ ) = C_{\rm PAH}\ (\ T_{\rm PAH}\ )\ . \tag{4.35}$$

The results obtained for some PAHs in the envelope of IRC+10216 described by the WDS model are presented in Fig. 4.5. As already noticed by Cherchneff et al. (1991) PAH temperatures are much lower than the gas temperature.

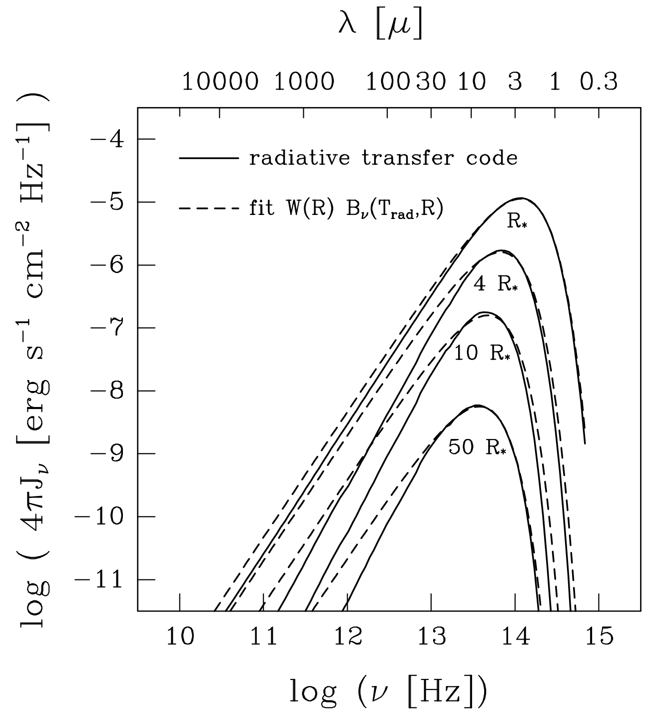


Figure 4.4: Mean specific intensity $J_\nu$ as a function of frequency $\nu$ at various distances from the star centre for the WDS model of the IRC+10216 envelope. The fit by a diluted blackbody field $W(R)\ B_\nu(T_{\rm rad}, R)$ is also represented.

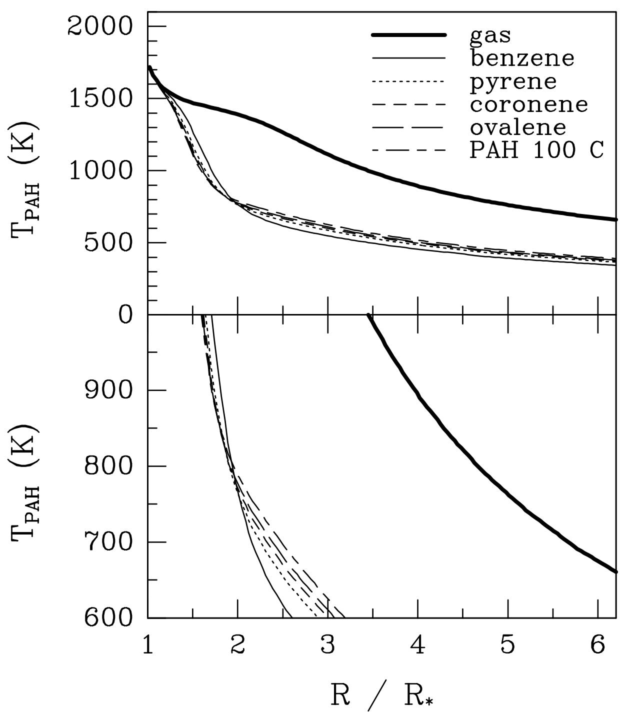


Figure 4.5: Temperatures of some PAHs as a function of distance from the star in the model of WDS for IRC+10216. The lower panel presents the curves in more detail.

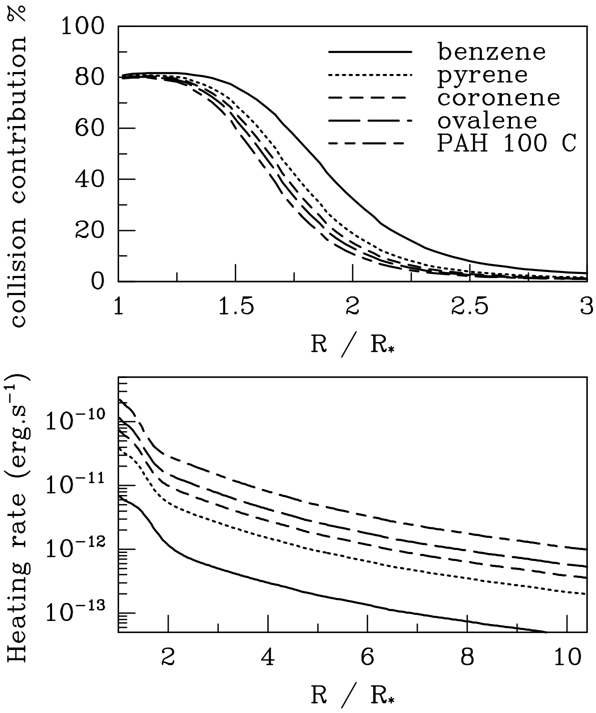


Figure 4.6: Upper diagram: Relative contribution of collisions for the heating of PAHs in the envelope of IRC+10216 as a function of distance from the star.
Lower diagram: Heating rates of PAHs in the envelope as a function of distance from the star.

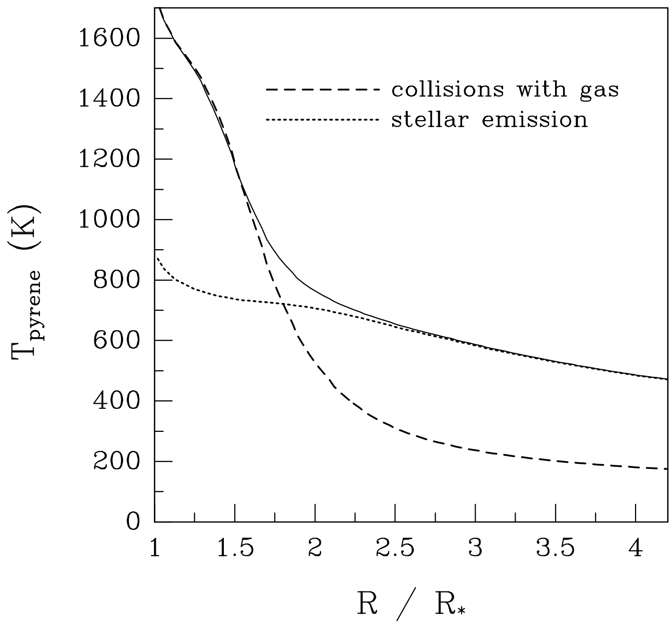


Figure 4.7: Determination of the temperature of pyrene molecules as a function of distance from the star. The solid curve shows the temperature obtained by taking into account both collisions and absorption of stellar emission for the heating. The other curves present the results obtained by considering separately each heating process. This calculation has been done for the WDS model for IRC+10216.

Figure 4.6 shows the heating rates in the envelope (upper diagram) and the relative contribution of collisions with gas particles for the heating (lower diagram) for various PAHs . The larger the PAH, the smaller is the part of collisions compared to the part of absorption in the heating process. However, absolute values of collisional heating increase with PAH molecular size, as well as the total heating rates (see lower diagram of Fig. 4.6).

Figure 4.6 also shows that heating rates have higher values near the star where both collisions and radiation are more abundant. Near the star, however, collisions dominate over absorption of stellar radiation for the heating of all PAHs. In contrast, for distances from the star greater than 2 stellar radii, absorption of stellar emission is the main heating process.

In the studies of Cherchneff et al. (1991, 1992) the two heating processes have not been treated simultaneously. Figure 4.7 presents the temperatures that one would obtain by considering only one of the heating mechanisms for pyrene molecules taken as an example (a similar result is obtained for all PAHs). In the region near the star, collisional heating alone provides a good approximation of PAH temperatures. On the other hand, heating by absorption of radiation from the star and the dust layer provides good values of the PAH temperatures for distances greater than 2 stellar radii. For distances greater than 2 $R_\star$, PAH temperatures are therefore much higher than those assumed by Cherchneff et al. (1992) who only considered collisional heating. This allows PAHs to stay longer in the temperature window (1000–800 K) favourable to their formation and growth. To conclude, we note that the determination of PAH temperatures in the whole envelope imperatively requires to take into account both heating processes simultaneously.

## 4.5 Growth of PAHs in circumstellar envelopes

### 4.5.1 Chemical reactions

The reactions of hydrogen abstraction from PAH molecules and addition of acetylene on the formed PAH radicals are the basic chemical reactions in the process of PAH growth in circumstellar environments (Keller 1987; Gail & Sedlmayr 1987a; Frenklach & Feigelson 1989, Cherchneff et al. 1992). Unfortunately, no experimental data concerning these chemical reactions for PAHs larger than benzene is available in the literature. Applying these results to larger PAHs is still relatively uncertain and requires the introduction of some modifications with respect to the case of benzene.

The reaction of hydrogen abstraction has a rate given by the modified Arrhenius expressions introduced in Chap. 3:

$$\text{for} \qquad \mathrm{T} \geq 1000 \text{ K}, \tag{4.36}$$
$$k_{\mathrm{H}}^{\mathrm{abs}} = 4.15\ 10^{-10} \left(\frac{N_{\mathrm{C}}}{6}\right)^{\frac{1}{2}} \exp\left(-\frac{8060}{T}\right) \ \mathrm{cm}^3\ \mathrm{s}^{-1},$$

for $\quad T < 1000$ K,

$$k_{\rm H}^{\rm abs} = 5\ 10^{-12}\ \left(\frac{N_{\rm C}}{6}\right)^{\frac{1}{2}} \exp\left(-\frac{4080}{T}\right) \quad {\rm cm}^3\ {\rm s}^{-1}.$$

The factor $(N_{\rm C}/6)^{1/2}$ accounts for the increasing number of hydrogen atoms at the edge of PAHs for increasing PAH molecular size. The efficiency of the hydrogen abstraction reaction may be defined as the ratio of the reaction rate to the collision rate. The values of the efficiency for a PAH with 50 carbon atoms are plotted in the upper diagram of Fig 4.8 as a function of temperature for the temperature range observed in late type star envelopes. The efficiency is less than 1 % for temperatures lower than 2000 K and rapidly decreases with decreasing temperature.

Fahr & Stein (1989) have obtained a rate for the reaction of addition of acetylene to the radical phenyl. From their results we derive the following expression of the Arrhenius law:

$$k_{\rm C_2H_2}^{\rm add} = 6.6\ 10^{-11}\ \exp\left(-\frac{5090}{T}\right)\ {\rm cm}^3\ {\rm s}^{-1}\ . \tag{4.37}$$

We assume that this rate also gives valid results for the addition of acetylene to PAH radicals larger than phenyl. However, this may prove incorrect when the addition of acetylene leads to the formation of a new ring, as for instance in the formation of naphthalene from phenylacetylene. There is unfortunately no experimental data for the rate of such reactions. We therefore also use the result of Eq. (4.37) in this case.

Using Eq. (4.37) we can calculate the efficiency of the acetylene addition reaction as for the case of hydrogen abstraction. The result is plotted in Fig 4.8 for a PAH radical with 50 carbon atoms as a function of temperature. For temperatures lower than 2000 K the efficiency is less than 1 % and decreases with temperature down to $10^{-6}$ at 500 K. These values are comparable to the experimental efficiency measured by Wehrer et al. (1983) for the decomposition of acetylene on carbon.

The low efficiency of PAH chemical reactions with hydrogen and acetylene could constitute a severe hindrance for their realization in some astrophysical environments. In order to study this question in the special case of CSEs, we have represented in the lower diagram of Fig. 4.8 the rates of the processes of hydrogen abstraction from PAH molecules, $n_{\rm H} k_{\rm H}^{\rm abs}$, and of addition of acetylene on PAH radicals, $n_{\rm C_2H_2} k_{\rm C_2H_2}^{\rm add}$, for a PAH with 50 carbon atoms as a function of temperature in a C–star envelope described by the WDS model. The densities of atomic hydrogen and of acetylene have been obtained from the kinetic calculation presented in Sect. 4.5.5.

The inverse of the chemical rates $1/n_{\rm H}\ k_{\rm H}^{\rm abs}$ and $1/n_{\rm C_2H_2}\ k_{\rm C_2H_2}^{\rm add}$ provide the characteristic timescales for reaction of typical circumstellar PAHs with hydrogen and acetylene, respectively. We have compared the chemical timescales to the characteristic timescale for the dynamical changes of the physical parameters in the envelope. This timescale is simply stated as being equal to $R/v$, where $v$ is the gas velocity in the envelope and $R$ the distance from the star (see Appendix B for a more detailed description of timescale discussion in CSEs). The inverse of the dynamical timescale is plotted in Fig. 4.8.

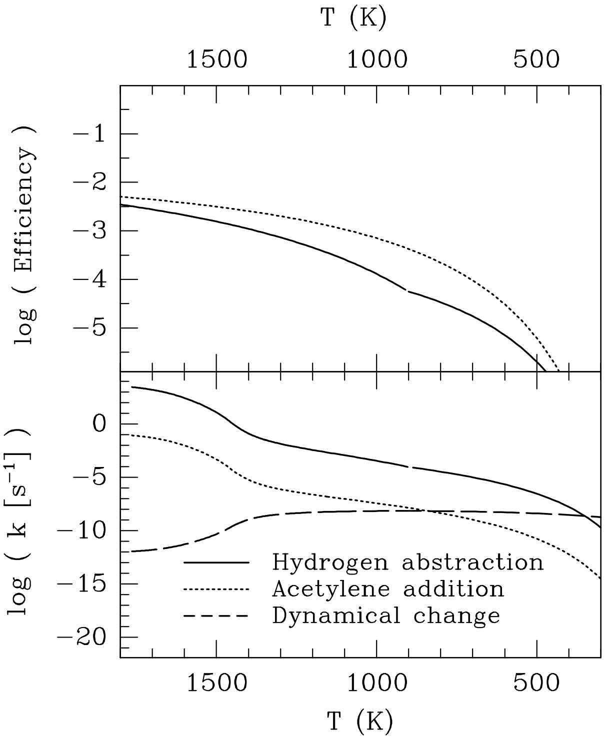


Figure 4.8: Upper panel: Efficiency of hydrogen abstraction and acetylene addition for a PAH with 50 carbon atoms as a function of temperature.
Lower panel: Rates for hydrogen abstraction and acetylene addition for a PAH with 50 carbon atoms and dynamical changes as a function of gas temperature in a typical C–giant envelope [WDS model for IRC+10216] (see text for the definition of the rates).

We can infer from Fig. 4.8 that in the inner part of the envelope the chemical reactions have the smallest timescales. They are therefore the quickest processes until the temperature and densities have dropped to values where the chemistry is frozen due to rapid dynamic evolution of the shell physical properties. The freezing out of chemistry occurs for temperatures lower than 800–600 K which correspond to a distance to the centre of the star greater than 5 stellar radii. If one considers that the reaction temperatures are mainly governed by the PAH temperatures (Cherchneff et al. 1992), the reactions may be frozen out for distances larger than 3 stellar radii. We finally conclude that the chemical reactions of hydrogen abtraction from PAHs and acetylene addition to PAH radicals can take place within a distance of a few stellar radii from the star although their efficiencies are lower than 1 %.

### 4.5.2 Growth rate of PAHs in circumstellar envelopes

We know of only two studies taking into account the growth of large PAHs ($N_{\rm C} > 18$) by addition of acetylene in CSEs (Frenklach & Feigelson 1989, Cadwell et al. 1994). However, these authors have performed their calculation for PAHs larger than naphthalene without taking into consideration the various temperatures of PAHs and under the assumption that the chemical reaction rates for larger PAHs are all equal to those of benzene. We propose here some simple arguments to describe more adequately the growth of PAHs in CSEs.

PAHs can grow by addition of acetylene when they have a radical site at their edge. To describe the growth of a given PAH we therefore introduce the following growth rate:

$$k^{\mathrm{gr}}_{\mathrm{C_2H_2}} = p_{\mathrm{rad}}\; n_{\mathrm{C_2H_2}}\; k^{\mathrm{add}}_{\mathrm{C_2H_2}} \;, \tag{4.38}$$

where $p_{\mathrm{rad}}$ represents the probability for the considered PAH to have a radical site (Keller 1987). In Eq. (4.38) $k^{\mathrm{add}}_{\mathrm{C_2H_2}}$ is the rate already presented in Eq. (4.37) for the addition of acetylene to the phenyl radical.

The probability $p_{\mathrm{rad}}$ can be obtained approximately from the expression:

$$p_{\mathrm{rad}} \simeq N_{\mathrm{H}}\, \frac{n_{\mathrm{PA\bullet}}}{n_{\mathrm{PA\bullet}} + n_{\mathrm{PAH}}} \;, \tag{4.39}$$

where $n_{\mathrm{PA\bullet}}$ and $n_{\mathrm{PAH}}$ are the densities of PAHs having one radical site, and as a molecule, respectively, while $N_{\mathrm{H}}$ is the number of hydrogen atoms at the edge of the PAH. The fraction in Eq. (4.39) provides the probability to be a radical site for a carbon atom bound to an hydrogen atom at the edge of the PAH carbon skeleton. To establish Eq. (4.39) we have implicitly assumed that all hydrogen atoms at the edge of a PAH molecule are equivalent and simply multiply by $N_{\mathrm{H}}$ the probability relative to a carbon atom at the edge. The number of hydrogen atoms increases with the length of the edge and, for compact PAHs, may be estimated as:

$$N_{\mathrm{H}} \simeq \sqrt{6 N_{\mathrm{C}}} \;. \tag{4.40}$$

The reaction of hydrogen abstraction is more rapid than the dynamical change in the region of the envelope where acetylene addition is effective (see Fig. 4.8) and therefore remains at chemical equilibrium in the region where acetylene addition occurs efficiently. This point is confirmed by the kinetic calculation presented in Sect. 4.5.5. Hence, by use of the law of mass action we can deduce the radical to molecule density ratio for a given PAH:

$$\frac{n_{\mathrm{PA\bullet}}}{n_{\mathrm{PAH}}} = \frac{k^{\mathrm{abs}}_{\mathrm{H}}}{k^{\mathrm{r}}} \frac{n_{\mathrm{H}}}{n_{\mathrm{H_2}}} \tag{4.41}$$

$$k^{\mathrm{r}}(T) = k^{\mathrm{abs}}_{\mathrm{H}}(T) \exp\left( -\frac{\Delta G^0_{\mathrm{PA\bullet}} + \Delta G^0_{\mathrm{H_2}} - \Delta G^0_{\mathrm{PAH}} - \Delta G^0_{\mathrm{H}}}{RT} \right) \;, \tag{4.42}$$

where $k^{\mathrm{r}}$ denotes the reverse reaction to the hydrogen abstraction. In Eq. (4.42) the difference of the standard free enthalpies, $\Delta G^0_{\mathrm{PA\bullet}} - \Delta G^0_{\mathrm{PAH}}$, has been estimated by using the group additivity theory of Benson (1976).

The temperature in Eq. (4.42) is a reaction temperature, which depends on the temperatures of the hydrogen molecules and of the PAH. For such a reaction involving two species A and B we define the following chemical reaction temperature $T_{\rm r}$:

$$T_{\rm r} = \frac{s_{\rm A}T_{\rm A} + s_{\rm B}T_{\rm B}}{s_{\rm A} + s_{\rm B}} \; , \tag{4.43}$$

where $T_{\rm X}$ represents the temperature of species X, while $s_{\rm X}$ is its number of vibrational degrees of freedom, equal to $3N - 6$ for a PAH with $N$ atoms and to $3N - 5$ for linear molecules ($H_2$, $C_2H_2$). By using Eq. (4.43) we assume that the vibrational energy of the reactive species is redistributed over the vibrational modes of both species during the reaction. This treatment of the reaction temperature seems to be more realistic than that proposed by Cherchneff et al. (1992), who assumed that reactions always occur at the PAH temperature when PAHs are involved. However, a theoretical study of this question is still required for future work on PAH chemistry in CSEs.

Combining Eqs. (4.39) to (4.43) enables the calculation of the growth rate of a given PAH by addition of acetylene in circumstellar environments taking into account both the size and the temperature of the PAH. The results for some PAHs are presented in Fig. 4.9 as a function of distance from the star centre in the WDS model for IRC+10216. The growth rate increases with molecular size and is nearly two orders of magnitude greater for a PAH with 100 carbon atoms than for benzene. For a given PAH the growth rate decreases with decreasing PAH temperature and acetylene density and, consequently, with distance from the star. For distances greater than 3 star radii the growth rate of PAHs is lower than the dynamical change rate in the envelope so that the growth process freezes out.

### 4.5.3 Thermodestruction of PAHs

In the region near the star where temperatures have higher values, PAHs may dissociate by the reverse reaction to the growth process. An estimate for the rate of this thermodissociation process can be obtained by the following expression:

$$k^{\rm diss} = \int_0^{\infty} k(E)\rho(E)p(E)dE \; , \tag{4.44}$$

where $E$, $k(E)$, $\rho(E)$ and $p(E)$ are the internal energy of the PAH, its dissociation rate, its density of states and its probability for having the internal energy $E$, respectively.

The density of states can be approximated by the semi–empirical expression of Whitten & Rabinovitch (1963):

$$\rho(E) = (E + aE_{\rm z})^{s-1}\left[s!\,\prod_{i=1}^{s} h\nu_i\right]^{-1} \; , \tag{4.45}$$

where $\nu_i$ are the vibrational frequencies of the molecular modes and $s$ their number, while $a$ is a correction factor ($0 < a < 1$) that varies with $E$ according to an empirical law given by Forst (1973). For the calculations we use the same set of vibrational frequencies as in

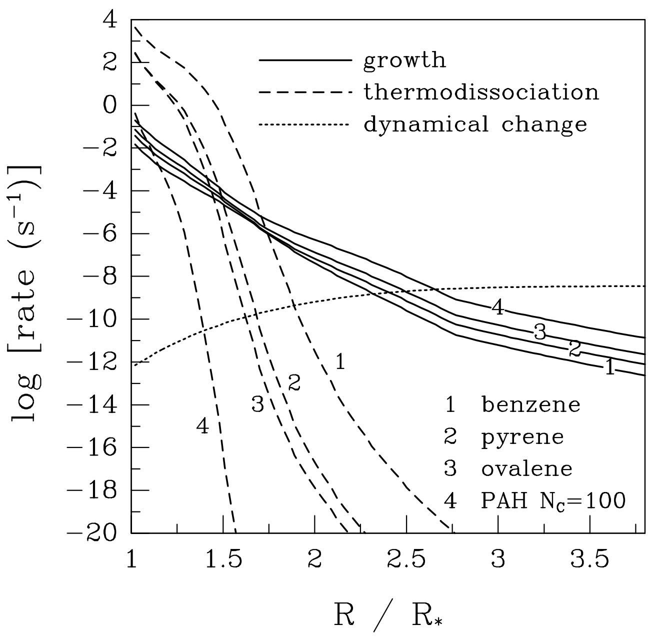


Figure 4.9: Rate of growth by acetylene addition and rate of acetylene thermoejection of some PAHs as a function of distance from the star centre in the envelope of IRC+10216 modelized by WDS.

Chap. 2. We furthermore assume that the probability $p(E)$ is of a Boltzmann type and write:

$$p(E) = \frac{\exp\left(-\frac{E}{kT_{\rm PAH}}\right)}{\int_0^\infty \rho(E)\ \exp\left(-\frac{E}{kT_{\rm PAH}}\right) dE} \ . \tag{4.46}$$

The dissociation rate in Eq. (4.44) is estimated by RRK theory using the parameters presented in Chap. 2 for the loss of an acetylene molecule.

The thermodissociation rates $k^{\rm diss}_{\rm C_2H_2}$ calculated according to Eq. (4.44) are plotted in Fig. 4.9 for some PAHs in the circumstellar shell of IRC+10216 described by the WDS model. Figure 4.9 confirms that thermodissociation dominates over growth in the region near the star.

The thermodissociation rate rapidly decreases with molecular size. PAHs with 100 carbon atoms and more are already stable against thermodissociation at 1.1 $R_\star$, whereas benzene molecules are stable only for distances greater than 1.9 $R_\star$. At a given position in the envelope, we call critical PAH the smallest PAH for which the growth rate is greater than the thermodissociation rate. Near the star, the critical PAH contains at least 100 carbon atoms, while for distances greater than 2 stellar radii the critical PAH is as small as benzene.

The concept of a critical PAH along the PAH chemical pathway has been developed by Keller (1987), Gail & Sedlmayr (1987a) and Goeres (1993). For PAHs smaller than the critical PAH the chemistry can probably be correctly described by equilibrium calculations. PAHs larger than the critical PAH grow under kinetical equilibrium and may be correctly described by moment equations similar to those used by Gail & Sedlmayr (1988) to describe the growth of dust particles.

Additionally, we note that for PAHs larger than benzene the thermodissociation rate is lower than the typical rate for infrared emission ($10^2$–$10^3$ $s^{-1}$) (see Léger et al. 1989b, Jochims et al. 1994). This partially justifies that we have neglected thermoejection processes in the cooling process of circumstellar PAHs (see Sect. 4.4).

### 4.5.4 Efficiency of PAH growth processes

Although some work has been devoted to the question of the growth process of PAHs up to macroscopic size, the exact pathway from PAHs to large macromolecules is still unknown. According to Allamandola et al. (1989) and more recently Cadwell et al. (1994), the growth may proceed via coagulation of PAHs. On the other hand, Keller (1987) and Frenklach & Feigelson (1989) have considered growth of PAHs by reaction with acetylene and hydrogen.

In order to study quantitatively the hypothesis concerning the growth of PAHs in circumstellar envelopes, we define characteristic timescales for the growth of a pyrene molecule ($N_{\rm C} = 16$) up to a large PAH with 100 carbon atoms. For the growth process via acetylene addition we define:

$$\tau^{\rm add}_{\rm C_2H_2} = \sum_{N_{\rm C}=16,18,\ldots,100} \frac{1}{\tilde{k}^{\rm gr}_{\rm C_2H_2}(N_{\rm C})} \, . \tag{4.47}$$

In Eq. (4.47) we have introduced a net growth rate $\tilde{k}^{\rm gr}_{\rm C_2H_2}$ defined by:

$$\tilde{k}^{\rm gr}_{\rm C_2H_2} = {\rm Max}\left(0 \, , \; k^{\rm gr}_{\rm C_2H_2} - k^{\rm diss}\right) \, , \tag{4.48}$$

where $k^{\rm gr}_{\rm C_2H_2}$ is defined according to Eq. (4.38) and $k^{\rm diss}$ is the thermodissociation rate.

In the case of coagulation, we define a timescale by considering the growth by succesive additions of pyrene molecules:

$$\tau^{\rm coag}_{\rm C_{16}H_{10}} = \frac{N_{\rm coll}}{\alpha_{\rm s} \; A^{\rm pyr} \; v^{\rm pyr}_{\rm th} \; n^{\rm pyr}} \, , \tag{4.49}$$

where $A^{\rm pyr}$, $v^{\rm pyr}_{\rm th}$ and $n^{\rm pyr}$ represent the surface, thermal velocity and density of pyrene molecules, respectively. The factor $\alpha_{\rm s}$ is a sticking coefficient which is unknown and set here equal to unity. $N_{\rm coll}$ represents the number of collisions necessary to obtain a PAH with 100 carbon atoms from pyrene molecules. In agreement with our assumption that each colliding pyrene molecule sticks onto the growing PAH, we deduce a value of 5 for $N_{\rm coll}$. We note that this assumption corresponds to the best efficiency for coagulation. The density of pyrene molecules in Eq. (4.49) has been obtained from the kinetic calculation presented in Sect. 4.5.5.

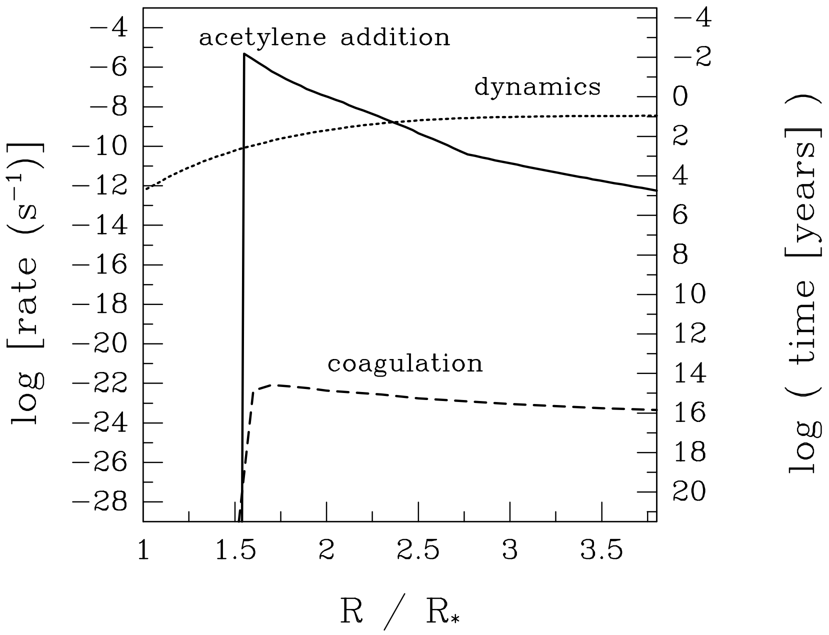


Figure 4.10: Rates for growth of a pyrene molecule up to a PAH with 100 carbon atoms by acetylene addition and by coagulation of pyrene molecules as function of distance from the star centre in the envelope of IRC+10216 modelized by WDS.

Figure 4.10 shows the values obtained for these timescales in the envelope of IRC+10216. The timescale for coagulation is several orders of magnitude greater than the timescale for acetylene addition. The large difference would probably not be changed by a more exact calculation of coagulation based on the Smoluchowski equation (Cadwell et al. 1994). Moreover, coagulation processes are probably too slow to take place in the envelope since the coagulation timescale is much larger than the time for dynamical changes in the envelope. On the other hand, growth of large PAHs via addition of acetylene is quick enough to take place in the first stellar radii of the shell. We therefore conclude that small PAHs probably grow up to large size preferentially via addition of acetylene molecules in the inner part of C–star CSEs.

### 4.5.5 Nucleation rate of PAHs

The previous results confirm that PAHs can favourably grow in the circumstellar envelopes of C–stars, probably up to macroscopic size. It has already been suggested by Keller & Sedlmayr (1983), Keller (1987), Gail & Sedlmayr (1987a) and Allamandola et al. (1989) that PAH formation constitutes the first step in the chemical pathway to dust in C–star shells. Unfortunately, the approach developed in the previous sections does not allow to estimate the abundance of PAHs which form in the envelope and, therefore, does not allow to test quantitatively the hypothesis of PAHs as seed particles for dust. An alternative way to study the formation of PAHs is to solve the kinetic equations of a chemical reaction network which takes into account all the species involved in PAH formation. Such calculations have already been performed by Frenklach & Feigelson (1989) and Cherchneff et al. (1992). We use this approach here to evaluate the nucleation rate of dust particles via PAHs.

In the present calculations we use the networks of Frenklach & Feigelson (1989) and Cherchneff et al. (1992) with the following modifications: (i) the reactions of PAHs with acetylene are described by the coefficient rate of Eq. (4.37), (ii) the reverse reaction of the reaction of formation of acenaphthalene from the naphthalene radical (reaction 100 of Frenklach & Feigelson 1989), which was artificially omitted by Frenklach & Feigelson (1989) for the sake of their computing procedure, is introduced, (iii) the set of reactions to pyrene is corrected (since one acetylene molecule is needed to form pyrene from anthracene and not two !), (iv) the formation of corannulene is implemented, (v) for distances greater than $R^{\rm gr} = 1.6 R_\star$ we have added to the set of reactions the growth reaction of pyrene and corannulene to take into account the growth of larger PAHs.

For distances greater than $R^{\rm gr} = 1.6 R_\star$ pyrene and corannulene indeed grow more rapidly than they eject acetylene (see Fig. 4.9). Hence, pyrene and corannulene molecules are consumed by the PAH growth process and their densities are thereby diminished. The above modification (v) accounts for this diminution. Since PAHs larger than pyrene and corannulene also grow faster than they dissociate, we can moreover neglect the increase of pyrene and corannulene densities due to the dissociation of larger PAHs. On the other hand, at distances smaller than $R^{\rm gr}$, pyrene and corannulene eject acetylene rather than grow and we can therefore omit the growth reaction of these species. For distances smaller than $R^{\rm gr}$, some PAHs larger than pyrene and corannulene may also dissociate rather than grow and thereby enhance the densities of pyrene and corannulene. With the present reaction network we cannot take into account the influence of those larger PAHs.

Some reactions in the chemical network involve species with different temperatures. The same procedure as in Eq. (4.43) has been used for the reaction temperature $T_{\rm r}$ in order to calculate the rate coefficients of the forward and reverse reactions. As did Cherchneff et al. (1992) we have also performed the calculation by setting all reaction temperatures equal to the gas temperature. In this case the distance $R^{\rm gr}$, where pyrene and corannulene grow more rapidly than they dissociate, is equal to 2.75 $R_\star$

To estimate the formation rate of large PAHs, $J_{\rm PAH}$, we have calculated the flux of PAHs growing from pyrene and corannulene molecules to larger molecular sizes, according to the following relations:

$$
\begin{aligned}
R \ \leq \ & R^{\rm gr} : \\
& J_{\rm PAH} = 0 \ , \qquad (4.50) \\
R \ > \ & R^{\rm gr} : \\
& J_{\rm PAH} = k^{\rm gr,pyr}_{\rm C_2H_2} \ n^{\rm pyr} + k^{\rm gr,cor}_{\rm C_2H_2} \ n^{\rm cor} \ , \qquad (4.51)
\end{aligned}
$$

where $k^{\rm gr,pyr}_{\rm C_2H_2}$ and $k^{\rm gr,cor}_{\rm C_2H_2}$ represent the rates for addition of acetylene defined in Eq. (4.38)

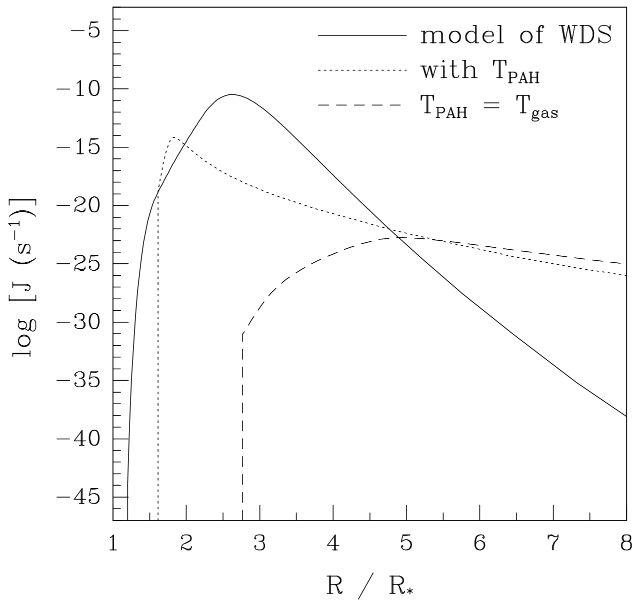


Figure 4.11: Formation rate of PAHs (i) including PAH temperatures; (ii) with reaction temperatures set equal to the gas temperature, and (iii) dust nucleation rate used in the WDS model.

for pyrene and corannulene, respectively, while $n^{\rm pyr}$ and $n^{\rm cor}$ are the corresponding PAH densities. Figure 4.11 shows the results we have obtained for the PAH formation rate by solving the kinetic reaction network.

The results presented in Fig. 4.11 correspond to the calculation carried out at gas temperature and to the calculation including PAH temperatures. The introduction of PAH temperatures leads to a displacement of the maximum value of the PAH formation rate nearer to the star and to an enhancement of nine orders of magnitude for the maximum of the PAH formation rate. This result is in qualitative agreement with the results of Cherchneff et al. (1992). We consider that this phenomenon is a crucial point for the study of circumstellar PAHs. The nucleation rate calculated by Cadwell et al. (1994), who did not take into account this effect, would probably be considerably changed by introducing the PAH temperatures.

To test the hypothesis of PAHs as seed for the dust particles, we have compared the PAH formation rate to the dust nucleation rate. We have reported in Fig. 4.11 the nucleation rate used by WDS to describe the formation of dust particles. In the model of WDS the condensation of carbon grains is described by classical nucleation theory according to the equations given in Gail & Sedlmayr (1984) and extended to heteromolecular, homogeneous growth of the dust particles (Gail & Sedlmayr 1988). The PAH formation rate reaches its maximum nearer to the star than the dust nucleation rate of WDS. However, the maximum values obtained with the PAH chemistry are 4 orders of magnitude lower than the rate obtained by WDS. This could suggest that the present PAH formation path is not sufficient to produce the amount of dust capable of driving the stellar wind. Nevertheless, the self–consistency of the envelope model of WDS makes the dynamical structure very dependent on the dust nucleation rate. As shown in Appendix A introducing another nucleation rate would induce other temperature and pressure profiles. The new profiles in turn would affect the concentration of the condensating species and the value of the nucleation rate. As a consequence, a stellar wind could also develop for an apparently lower nucleation rate. For that reason any conclusion from the previous comparison remains delicate.

Some additional criticism must be adressed to the present kinetic description of the PAH chemistry. The chemical pathway in the network is based on study of terrestrial gas flame chemistry and there may exist other more efficient routes for PAH formation in the case of circumstellar envelopes, for which no kinetic data are now available (see for instance the proposal of Goeres 1993). Moreover, as already pointed out by Goeres (1993) a correct description of PAH formation with a chemical network should include species up to the critical cluster size. Near the star the critical cluster contains about 100 carbon atoms, which is much more than the larger PAHs considered in the network ($N_C$=20). Finally, our theoretical aproach of chemical reactions involving partners with different temperatures probably needs some improvement. Consequently, it seems with the present results difficult to draw any definite quantitative conclusion about the role of PAHs in the formation of dust particles. However, it is qualitatively confirmed that PAHs, due to their low temperatures, are potentially a good candidate as seeds for dust nucleation in C–star CSEs.

## 4.6 Discussion

The chemical reactions of PAHs with hydrogen atoms and acetylene molecules have proved to be rapid enough to enable the formation and growth of PAHs in carbon–star envelopes (Keller 1987; Frenklach & Feigelson 1989; Cherchneff et al. 1992). Although these reactions have efficiencies lower than one per cent, their characteristic timescales indeed are smaller than the timescale for the dynamical change of the physical parameters in the envelope. These reactions ensure a rapid and efficient growth of PAHs up to large molecular size. This growth via acetylene addition proceeds quicker than growth via coagulation of PAHs in the region near the star.

Generally, growth processes are considerably favoured by differential drift velocities between the growing species and the gas reacting species. Dominik et al. (1989) and more recently Krüger & Sedlmayr (1994) have for instance investigated the influence of drift velocity of dust grains in their study of the structure of carbon–star envelopes. They have shown that the efficiency of dust growth and consequently the structure of the envelope actually depend on dust grain drift. In the case of PAHs, the drift velocities of some thousand cm.s$^{-1}$ we have obtained are much smaller than the gas thermal velocity. Thus, the PAH drift velocities do not lead to any modifications of the chemical reaction rates involving PAHs and can therefore be neglected in the study of PAH growth in CSEs.

In contrast, PAH temperatures have a strong influence on the PAH growth process. Cherchneff et al. (1991, 1992) first estimated the temperatures of PAHs in carbon–star envelopes and investigated their influence on PAH chemistry. They have shown that the yield of formation of small PAHs ($N_C < 20$) is enhanced by several orders of magnitude when one introduces temperatures for PAHs lower than the gas temperature. Because of their lower temperatures, PAHs indeed reach the temperature range (800 K $\leq T \leq$ 1000 K) favourable to their formation nearer to the star than when they are assumed to be at gas temperature. Near the star, the density is much greater and the growth of PAHs is therefore more effective. However, Cherchneff et al. (1992) have considered only heating of PAHs via collisions with the gas and used a simple model of CSE. Their yield for PAH formation is therefore somewhat uncertain. In the present study, we have introduced heating via absorption of stellar emission and shown that this heating process is important at distances greater than $\simeq 1.5\ R_\star$. Hence, PAHs stay olonger in the favourable temperature range and thereby grow more efficiently than estimated by Cherchneff et al. (1992).

In the model of Gail & Sedlmayr (1987b) and WDS for C–stars, the onset of dust formation occurs at a distance from the star where the gas temperature has dropped to a value of about 1300 K. Gail & Sedlmayr (1987a) have shown that, at such temperatures, the efficiency of PAH formation is not high enough to induce a dust nucleation rate and consequently a dust formation which allows to drive a stellar wind. These results seem to be in contradiction with the picture of PAHs as seeds for the formation of dust grains. The lower temperatures of PAHs compared to the gas temperature may provide an explanation of this discrepancy. Near the star PAHs may indeed have temperatures lower than 1000 K and therefore favourably grow, while the gas temperature remains at higher values. The formation rate of PAHs calculated using a chemical reaction network is considerably increased when one takes into account PAH temperatures. The study of PAHs as possible seeds for dust particles has therefore to be carried on more precisely. Compared to SiC, which has also been proposed as seed particle (Cadwell et al. 1994) but for which no convincing thermodynamical data exist, and to purely carbon particles, whose nucleation described according to classical nucleation theory is still discussed (Donn & Nuth 1983, Keller 1987), PAHs indeed constitute a promising candidate which should be introduced in models of dust formation.

However, the question of a dust nucleation rate based on PAH chemistry deserves a careful analysis. The formation rate calculated from PAH chemistry has indeed a high dependence on the reaction rates and chemical pathway used to describe the formation and growth of PAHs. The data used in the present chapter are derived from laboratory experiments whose physical conditions are far from those of circumstellar environments. Most of these experiments have been furthermore performed with benzene, which is not a characteristic PAH. More experimental data concerning the reactions of PAHs with acetylene and hydrogen are presently needed to have a better understanding of the chemical pathway from acetylene to PAHs and dust grains. Moreover, the PAH chemistry is based on reactions involving partners with different temperatures for which no reliable theoretical description exists. The situation is furthermore complicated by the presence of shock waves in the envelopes of C–stars (Fleischer et al. 1992) which have not been taken into account in the present chapter. Cherchneff (1991, 1995) has qualitatively shown that PAH formation rate could be enhanced under the pressure and temperature conditions of the shocks developing near the star. Finally, we note that the introduction of a nucleation rate based on the PAH chemistry in a self–consistent model of carbon–star envelopes is a difficult task which nevertheless requires further investigation.

## 4.7 Conclusion

We have studied the interaction of gas particles with PAHs, regarded in this chapter as large and flat plates. This modelization enables the calculation to be carried out of collision rates of PAHs with gas particles and of the momentum and energy exchange rates from gas particles to PAHs. The results have been applied to the case of C–star envelopes where PAHs can form and grow. The results of the self–consistent models of C–star envelopes of Winters et al. (1994) have been used to provide reliable estimates of the temperature and density profiles and of radiative transfer in the envelope.

The reaction rates of the chemical reactions involved in PAH formation and growth are shown to be high enough to ensure a rapid growth of PAHs, although the efficiencies of these reactions do not exceed some per cent. These reaction rates are not enhanced by the drift velocity of some thousand cm.s$^{-1}$ affecting PAHs in the envelope.

The temperature of PAHs have been determined by balancing their heating via collisions with gas particles and absorption of stellar emission and their cooling via emission from the rotational and vibrational levels of PAHs. The PAH temperatures are lower than the gas temperature and enable an efficient formation and growth of PAHs in the circumstellar envelopes of C–stars. The PAH formation rate is large enough to support the idea that PAHs could constitute the first step in the formation of dust grain.

Dust particles have a crucial role in circumstellar envelopes because they partly drive the stellar wind and therefore influence the structure of the shells where PAHs form. The study of the growth of PAHs and dust is consequently closely coupled with that of the structure of the C–star shells. A complete treatment of the whole problem, now far from being obtained, provides the only possibility to accurately determine both the structure of carbon–star envelopes and the nature of circumstellar PAHs.

Tout ainsi que les femmes [...] s'embellissent d'une beauté fausse et empruntée: ainsi fait la science; [...]elle nous donne en payement et en présupposition les choses qu'elle même nous apprend être inventées: car ces épicycles, excentriques, concentriques, de quoi l'Astrologie s'aide à conduire le branle des étoiles, elle nous le donne pour le mieux qu'elle ait su inventer en ce sujet.

Montaigne, *Apologie de Raymond Sebond* .

# Chapter 5

# PAHs and photochemistry in circumstellar envelopes

**abstract**

Dust and molecular shielding are evaluated in a typical C–star envelope in order to calculate reliable rates for the photoprocesses undergone by polycyclic aromatic hydrocarbons (PAHs) in the outer part of the circumstellar shell. PAH photoionization and photoejection of hydrogen and acetylene are considered. The densities of electron, of atomic hydrogen and of carbon cation, $C^+$, are determined in order to calculate the rates for electron recombination, for hydrogenation and for carbon accretion. Taking into account photoionization, electron photodetachment and reactions with electrons enables to estimate the fraction of PAH cations and anions in the circumstellar envelope. A similar calculation accounting for hydrogenation and photoejection of hydrogen leads to the estimate of the hydrogen coverage of PAHs in the circumstellar shell. It is shown that collisions of PAHs with $C^+$ are frequent enough to modify the size–distribution of the PAHs formed near the star. However, lack of knowledge about the rate for carbon accretion onto PAHs prevents making any definitive estimate of the size distribution of the PAHs ejected into the interstellar medium by C–stars.

———————————————

## 5.1 Introduction

The generally assumed existence of large quantities of polycyclic aromatic hydrocarbons (PAHs) in the interstellar medium (ISM) stimulates the search for the mechanisms responsible for PAH formation and growth under interstellar conditions. If PAHs are really the carriers of the so–called unidentified infrared (UIR) bands observed in carbon–rich protoplanetary and planetary nebula, the circumstellar envelopes (CSEs) of C–stars probably constitute a most favourable place for PAH formation and growth (see e.g. Waters et al. (1989), Buss et al. (1990,1991,1993) and references therein). The chemical formation of PAHs from acetylene has been therefore extensively investigated in the region of carbon–rich CSEs within the first ten stellar radii (Keller & Sedlmayr 1983, Keller 1987; Gail

& Sedlmayr 1987a; Frenklach & Feigelson 1989, Cherchneff et al. 1992, Chap. 4 of this thesis). In contrast, no attention has been paid so far to the outer part of the envelopes where photoprocesses are likely to play an important role in the evolution of the PAHs formed near the star.

In the external region of CSEs outwards to the transition region with the ISM, PAHs are indeed exposed to the radiation of the interstellar ultraviolet photon fied which can penetrate the envelope. After the absorption of such a photon, PAHs can easily ionize or eject hydrogen (see Chap. 2 and 3). A fraction of the PAHs ejected into the ISM is therefore ionized and partially dehydrogenated. Moreover, photodestruction and growth via addition of carbon cation are much enhanced in the outer region of the CSEs. The size distribution of the PAHs formed near the star is hence probably modified before PAHs reach the ISM. A study of PAH photoprocesses in stellar winds could therefore provide precious information about the nature of the PAHs ejected into the ISM by carbon–rich stars.

In this investigation the evaluation of the yields for the PAH photoionization and photoejection of hydrogen and acetylene (see Chap. 2 and 3) represents useful results. Especially the precise estimate of the dependence of these yields on photon frequency allows a detailed analysis of PAH photoprocesses in CSEs. However, the precision in the frequency dependence of the PAH photoprocess yields is much better than that usually used in the photochemical model of CSEs ( Huggins & Glassgold 1982; Morris & Jura 1983; Glassgold & Huggins 1983; Huggins et al. 1984; Glassgold et al. 1986; Glassgold et al. 1987, Nejad & Millar 1987, Mamon et al. 1988, Howe & Millar 1990, Cherchneff et al. 1993, Millar & Herbst 1994). In these models monochromaticity of the photoreaction yields and of the dust shielding are generally assumed. In this context, the recent study of Cherchneff et al. (1993), who split the ultraviolet frequency range of the interstellar radiation in sub–regions with different values of the dust optical depth and of the photochemical rates, constitutes an interesting improvement. However, more precision in the frequency dependence of dust shielding is still required to take advantage of the detailed knowledge of PAH photoprocesses. Moreover, in most all studies of photochemistry in CSEs only dust particles are considered for the shielding process. Jura & Morris (1981), Glassgold & Huggins (1983) and Morris & Jura (1983) showed that molecular shielding and/or self–shielding by $H_2$ and CO molecules have also to be taken into account in the study of the photodestruction of $H_2$ and CO. However, no comparison of the relative contribution of dust and molecular shielding has been done so far to justify the omission of molecular shielding in most of the studies of CSE photochemistry.

The next section of this chapter deals precisely with dust and molecular shielding in CSEs and gives some general results, which will be useful for future investigation of photochemistry in circumstellar environments. These results are applied in Sects. 5.3 and 5.4, which concern the shielding of PAHs and the PAH states of ionization and hydrogenation in CSEs, respectively. Finally, Sect. 5.5 investigates the influence of photodestruction and growth process on the size–distribution of PAHs in the outer part of CSEs.

## 5.2 Shielding by dust and molecules in CSEs

There has been much work done to study the photochemistry in the outer region of C–star envelopes ( Huggins & Glassgold 1982; Morris & Jura 1983; Glassgold & Huggins 1983; Huggins et al. 1984; Glassgold et al. 1986; Glassgold et al. 1987, Nejad & Millar 1987, Mamon et al. 1988, Howe & Millar 1990, Cherchneff et al. 1993, Millar & Herbst 1994). In all of these studies the envelopes are characterized by constant gas flow and mass–loss rate and the chemical composition at the beginning of the calculation is fixed to values deduced from the observations or from calculations assuming chemical equilibrium in the inner part of the envelope. These assumptions provide the inner boundary conditions for the description of the complex photochemistry which develops under the influence of the interstellar ultraviolet photons penetrating the envelope.

These models show that, on the one hand, dust particles and, on the other hand, $H_2$ and CO molecules ensure an efficient shielding of the species present in the envelope.

### 5.2.1 Dust shielding

For the shielding by dust Morris & Jura (1983) have proposed to use the following approximation based on the Sobolev approximation for the radiation transfer:

$$\begin{aligned} k(R) &= k_0\ \gamma^{\rm dust}(R) \\ &= k_0\ \exp\left[-1.664\left(\tau^{\rm dust}\right)^{0.86}\right]\ . \end{aligned} \tag{5.1}$$

Equation (5.1) provides an estimate for the photorate $k$ of a chemical reaction at the distance $R$ from the star centre as functions of the photorate $k_0$ calculated in the ISM and of an attenuation factor $\gamma^{\rm dust}$. In Eq. (5.1) $\tau^{\rm dust}$ is the radial optical depth for continuum aborption by dust grain, which is usually approximated by:

$$\tau^{\rm dust} = \frac{d}{R}\ , \tag{5.2}$$

where the distance $d$ is introduced as a parameter, whose value is determined either by assuming dust abundance and dust optical properties or by trying to fit the observations. This treatement of the dust optical depth does not allow to account for any dependence of photoprocesses on photon wavelength.

In their recent work Cherchneff et al. (1993) therefore proposed to split the energy range of the interstellar UV–photons [4–13.6 eV] in 6 sub–regions. For these sub–regions they introduced different values of the photorate $k_0$ to take account of the variation of the photoprocess rate with photon frequency $\nu$. In a given energy sub–region however, the photorate $k_0$ has a constant value. Cherchneff et al (1993) also used for each energy sub–region different values of the parameter $d$ in order to account for the variation of the optical grain properties with photon frequency $\nu$. To determine the values of $d_\nu$ Cherchneff

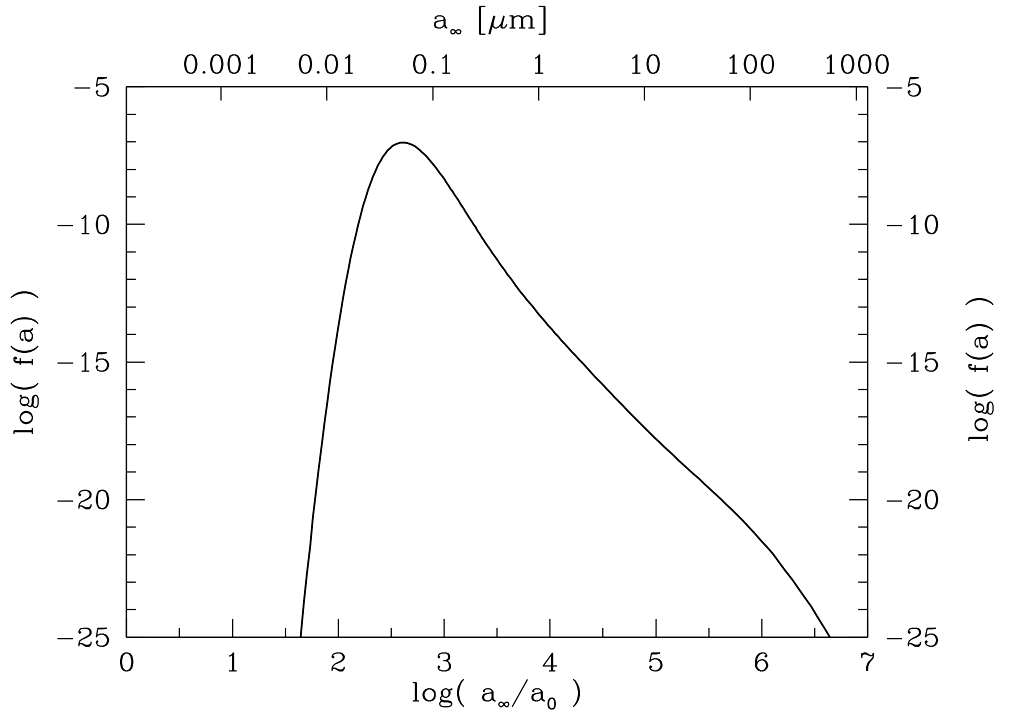


Figure 5.1: Grain–size distribution function normalized to the number of hydrogen nuclei $n_{<\mathrm{H}>}$ for the model of IRC+10216 (from Winters 1994). $\mathrm{a}_0$ represents the hypothetical radius of a monomer, equal to 0.0128 $\mu m$ for amorphous carbon, while $\mathrm{a}_\infty$ denotes the particle size of the dust grain in the region of the envelope where formation and growth of dust have stopped.

et al. (1993) have assumed that dust particles have the extinction properties of 0.05 $\mu m$ size amorphous carbon particles.

In the following, we reconsider this approach by using a realistic grain–size distribution of amorphous carbon grains for the envelopes of C–stars. The dust size distribution has been determined by Winters (1994) for the envelopes of C–stars using the approach of Dominik et al. (1989). Figure 5.1 shows the dust size distribution function obtained for the model of the well–studied carbon–rich red giant IRC+10216. In Fig. 5.1 the size distribution function is normalized to the number of hydrogen nuclei $n_{<\mathrm{H}>}$ and is represented for a distance of the star where both formation and growth of dust have stopped. For larger distances the evolution of the size distribution is therefore entirely determined by the dilution of the outflow in the envelope, so that the normalized size distribution remains constant.

Combining the size distribution of Winters (1994) to the data of Rouleau & Martin (1991) for the UV extinction of amorphous carbon enables us to calculate the dust optical depth in the envelopes of C–stars. For the present calculation we have used the model of Winters et al. (1994) (henceforth WDS) which describes the envelope of the C–star

IRC+10216 (see Appendix A for detailed information) and the model AC1 of Rouleau & Martin (1991) for the properties of amorphous carbon. Figures 5.2 and 5.3 present the results obtained for the optical depth as functions of photon energy and of distance from the star, respectively. In the region near the star ($R < 3R_\star$) dust does not condense because of the high temperatures and, therefore, the dust optical depth does not depend on distance. In contrast, in the region near the star the optical depth is very dependent on photon energy (see Fig. 5.3) because the whole dust shell contributes to the extinction. On the other hand, for distances larger than 10 stellar radii the optical depth has a relatively constant value for all photon energies greater than 5 eV but rapidly decreases with distance from the star due to the dilution effect in the envelope.

In the calculations presented in Fig. 5.2 and 5.3 only the model AC1 of Rouleau & Martin (1991) has been used. The other theoretical models of Rouleau & Martin (1991) for amorphous carbon provide other dependences on wavelength, especially for distances smaller than 3 stellar radii. However, we note that for distances larger than 10 stellar radii the choice of the model used for amorphous carbon has practically no incidence on the results. For all of these models we indeed obtain, within a few per cent, the same values as those presented in Fig. 5.3 and 5.2 for the optical depth. Moreover, for all the models for amorphous carbon the optical depth is relatively independent of wavelength in the energy range 5–13.6 eV and for distances larger than 10 stellar radii. In a sense, this is a positive validation of the previous studies of circumstellar photochemistry which do not explicitly take into account the dependence of dust optical depth with wavelength.

Combining Eqs. (5.1) and (5.2) we introduce the following fit formula for the values of the attenuation factor $\gamma^{\rm dust}$ in the envelope of IRC+10216:

$$\gamma_\nu^{\rm dust} = \exp\left[-1.664\left(\frac{d_\nu}{R}\right)^{0.86}\right] . \tag{5.3}$$

Figure 5.4 shows the values of $\gamma^{\rm dust}$ calculated, on the one hand, with the dust optical depth based on the results of WDS and Rouleau & Martin (1991) and, on the other hand, with the fit formula (5.3) in the envelope of IRC+10216 for a photon energy $h\nu$=8 eV. A good fit is obtained for a value $d_\nu$=176$R_\star$. However, such a fit is dependent on the photon energy. We give in Table 5.1 the values of $d_\nu$ for some photon energies in the range 3–13.6 eV. These values provide estimates of $\gamma_\nu^{\rm dust}$ with 10 % accuracy in the whole part of the envelope where dust particules are present. For a treatment which does not take the wavelength dependence of the optical depth into account the value:

$$d_0 = 177\ R_\star\ , \tag{5.4}$$

gives an approximation of $\gamma^{\rm dust}$ better than to 40 % for all photon energies greater than 4 eV and all distances greater than 50 $R_\star$. In Eq. (5.4) $R_\star$ is the stellar radius whose value is set equal to 9.24 $10^{13}$ cm according to the WDS model.

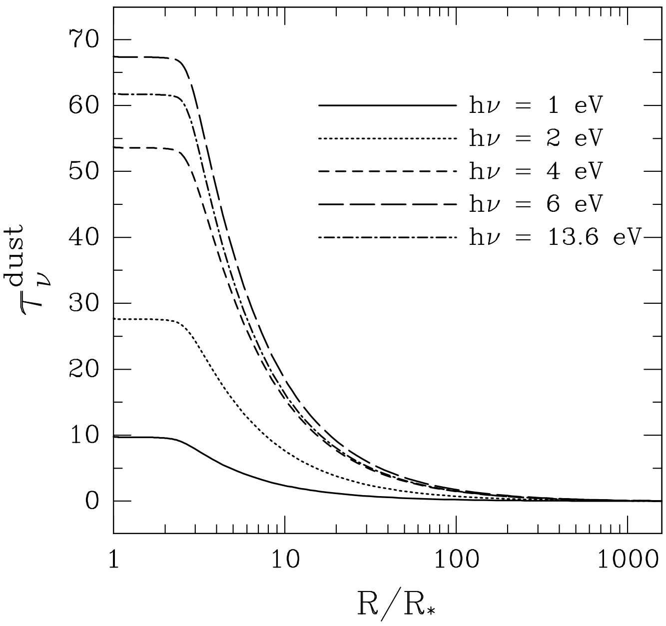


Figure 5.2: Dust optical depth as a function of distance from the star in the WDS model for the envelope of IRC+10216. The results have been obtained for the grain–size distribution of Winters (1994) and the optical constant from the model AC1 of Rouleau & Martin (1991) and are presented for various values of the UV–photon energy.

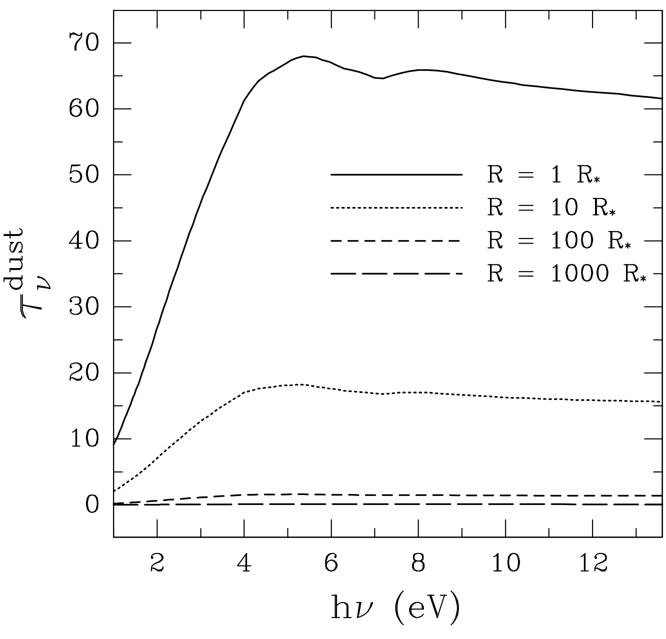


Figure 5.3: Dust optical depth as a function of photon energy in the WDS model for the envelope of IRC+10216. The results have been obtained for the grain–size distribution of Winters (1994) and the optical constant from the model AC1 of Rouleau & Martin (1991) and are presented for various distances R from the star center.

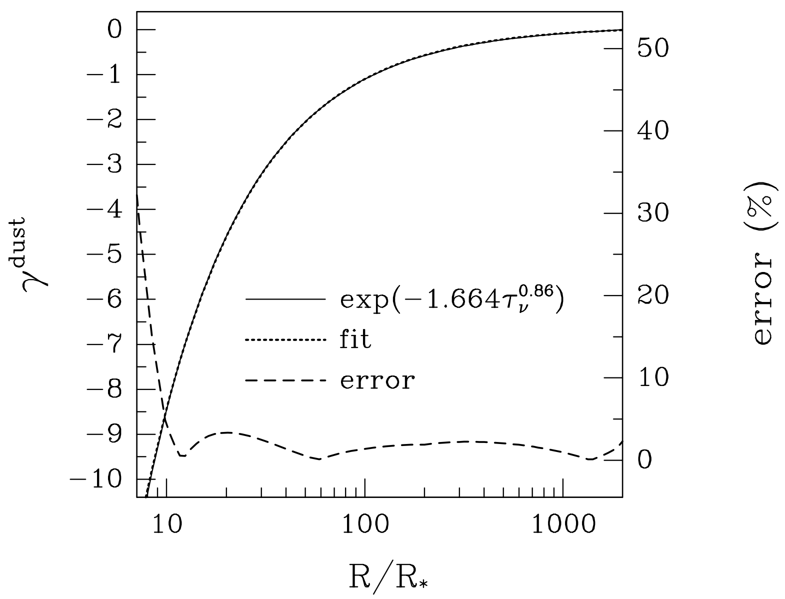


Figure 5.4: Attenuation factor of the photon flux as a function of distance from the star in the WDS model for IRC+10216. The value of the photon energy considered in this figure is 8 eV. The fit function (see text) with parameters $d_\nu$=176 $R_\star$ is also plotted. To visualize the difference the relative error made by using the fit function is also represented.

Table 5.1: Parameters for the fit function of the attenuation factor $\gamma^{\rm dust}$.

| photon energy [eV] | $d_\nu$ $[R_\star^a]$ |
|---|---|
| 3 | 134 |
| 4 | 179 |
| 5 | 186 |
| 6 | 185 |
| 7 | 176 |
| 8 | 176 |
| 9 | 174 |
| 10 | 169 |
| 11 | 166 |
| 12 | 164 |
| 13 | 163 |
| 13.6 | 162 |

(a) The stellar radius $R_\star$ is equal to 9.24 $10^{13}$ cm in the WDS model

### 5.2.2 Molecular shielding by $H_2$ and CO

A precise description of shielding and/or self–shielding by $H_2$ and CO has already been done and has been succesfully applied to the study of the photodissociation of $H_2$ and CO (Jura & Morris 1981; Glassgold & Huggins 1983, Morris & Jura 1983). However, $H_2$ and CO photodissociation processes follow line absorption and therefore require a different treatment than processes following absorption in the continuum. To our knowledge, there is no study in the literature of the contribution of molecular shielding compared to that of dust in the case of continuous photoprocesses.

The absorption cross–section of a molecule may be written (e.g. Eidelsberg et al. (1991)):

$$\sigma_\nu^{\mathrm{abs}} = \sum_{J"} \left[ \left( \frac{n_{J"}}{\sum_{J"} n_{J"}} \right) \sum_{J'} \left( \frac{\pi e^2}{m_{\mathrm{e}} c} \right) f_{v"J",v'J'} \Phi(\nu) \right] \tag{5.5}$$

where $J$ and $v$ denote rotation and vibration states, respectively. In Eq. (5.5) $f_{v"J",v'J'}$ is the oscillator strengh of the transition $(J',v') \longrightarrow (J",v")$, while $n_J$ is the occupation level of the rotational state $J$, which we assume to follow a Boltzmann distribution. For the normalized profile function, $\Phi$, of the vibration line corresponding to the transition $v"$ $\longrightarrow v'$ we use a Voigt–profile with width $\nu_{v",v'}\sqrt{2k_{\mathrm{B}}T/m_{\mathrm{e}}c^2}$. To simplify the calculations, we define integrated cross–section by:

$$\overline{\sigma^{\mathrm{abs}}_{\nu_{v',v"}}}\ \Delta\nu_{\nu_{v',v"}} = \int_{\mathrm{line}} \sigma_\nu^{\mathrm{abs}} d\nu \ . \tag{5.6}$$

Patzer (1992) has shown that the integrated cross–sections, $\overline{\sigma^{\mathrm{abs}}_{\nu_{v',v"}}}$, are nearly independent of temperature in the temperature range relevant for the outer part of C–star envelopes. In the remainder of this chapter, we use the integrated cross–sections for $H_2$ and CO tabulated in Appendix C and a line width $\Delta\nu_{\nu_{v',v"}}$ corresponding to a wavelength width of 1Å.

At a distance $R$ from star the optical depth for a molecular species X in the stellar envelope is equal to:

$$\tau^{\mathrm{X}}_{\nu_{v',v"}}(R) = \overline{\sigma^{\mathrm{abs}}_{\nu_{v',v"}}} \int_R^\infty n_{\mathrm{X}}(r) dr = \overline{\sigma^{\mathrm{abs}}_{\nu_{v',v"}}}\ \overline{n_{\mathrm{X}}} \ , \tag{5.7}$$

where $n_{\mathrm{X}}$ and $\overline{n_{\mathrm{X}}}$ are the density and column density of species X, respectively. The column densities used for the calculations have been estimated by using the calculations of chemical kinetics developed in Sect. 5.4.1. Figure 5.5 shows the results we have obtained for the optical depths of $H_2$ and CO at a distance of 10 stellar radii from the star. Lines of $H_2$ are almost regularly distributed in the energy range 11.3–13.6 eV, whereas CO molecules have lines between 10.7 and 13.6 eV with a higher wavelength density for the higher values of the energy. The difference of 3 orders of magnitude between the values of the optical depths of $H_2$ and CO is mainly due to the difference in the number densities of those molecules in the envelope. However, for both molecules the values of the optical depth in the lines are several orders of magnitude greater than the dust optical depth. Absorption by $H_2$ and

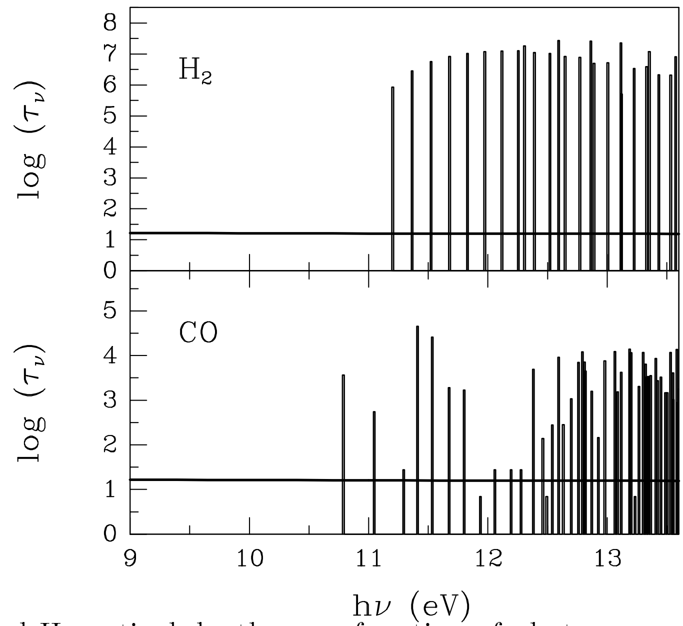


Figure 5.5: CO and $H_2$ optical depths as a function of photon energy at a distance 10 $R_\star$ compared with the dust optical depth (continuous line).

CO may therefore efficiently shield species such as PAHs which absorb in the continuum between 10.7 and 13.6 eV.

The molecular optical depth may be introduced as follows in the calculation of reaction rates. For a species with absorption cross–section, $\sigma_\nu^{\rm abs}$, which undergoes a photoprocess with yield, $Y_\nu$, the rate is given by:

$$k = \int_{h\nu=0}^{h\nu=13.6eV} Y_\nu \; \sigma_\nu^{\rm abs} \; \gamma_\nu \; N_\nu \; d\nu \; , \tag{5.8}$$

where $N_\nu$ and $\gamma_\nu$ are the mean interstellar photon flux in unit cm$^{-2}$s$^{-1}$Hz$^{-1}$ and the attenuation factor, respectively. To simplify the discussion we define $k_\nu$ the interstellar photorate at frequency $\nu$ by:

$$k_\nu = Y_\nu \sigma_\nu^{\rm abs} N_\nu \tag{5.9}$$

To take into account both dust and molecular shielding we calculate the photorate $k$ according to the following equation:

$$\begin{aligned} k \;\; &= \;\; \int_0^{13.6\ eV} k_\nu \gamma_\nu^{\rm dust} d\nu - \sum_i^{\rm H_2,CO} \Delta\nu_i k_{\nu_i} \gamma_{\nu_i}^{\rm dust} \qquad (5.10) \\ &+ \;\; \sum_i^{\rm H_2,CO} \Delta\nu_i k_{\nu_i} \exp\left[-1.664 \left(\tau_{\nu_i}^{\rm dust} + \tau_{\nu_i}^{\rm H_2,CO}\right)^{0.86}\right] \; , \end{aligned}$$

where $i$ denote the lines of CO and $H_2$. This equation is used in Sect. 5.3.2 to estimate the photoprocess rates of PAHs in a typical CSE.

## 5.3 Shielding of PAHs in circumstellar envelopes

### 5.3.1 PAH self–shielding

If PAH formation from acetylene molecules is efficient enough in C–star envelopes, many acetylene molecules are converted into PAHs. Since large PAHs absorb intensively and almost continuously in the ultraviolet (Verstraete & Léger 1992), PAHs may be self–shielded in CSEs as it is the case for $H_2$ and CO molecules. In order to estimate the importance of this process we calculate the optical depth of PAHs. For this purpose we first define the PAH formation yield, $Y_{\mathrm{PAH}}$, following Cherchneff et al. (1992), as:

$$Y_{\mathrm{PAH}} = \frac{N_{\mathrm{C}}^{\mathrm{PAH}}}{\breve{N}_{\mathrm{C}}^{\mathrm{C_2H_2}}} \,, \tag{5.11}$$

where $N_{\mathrm{C}}^{\mathrm{PAH}}$ and $\breve{N}_{\mathrm{C}}^{\mathrm{C_2H_2}}$ represent the number of carbon atoms in PAHs and the number of carbon atoms contained in acetylene molecules at the stellar photosphere, respectively. Denoting $\sigma_{/\mathrm{C}}^{\mathrm{abs}}$ the PAH ultraviolet absorption cross–section per carbon atom, we evaluate the PAH optical depth, $\tau_{\mathrm{PAH}}$, at a distance $R$ from the star to be:

$$\begin{aligned} \tau_{\mathrm{PAH}}(R) &\simeq \int_R^{\infty} \sigma_{/\mathrm{C}}^{\mathrm{abs}} \; 2 \; Y_{\mathrm{PAH}}(R) \; \breve{n}_{\mathrm{C_2H_2}} \left(\frac{R}{r}\right)^2 dr & (5.12) \\ &\simeq 2 \; \sigma_{/\mathrm{C}}^{\mathrm{abs}} \; Y_{\mathrm{PAH}}(R) \; R \; \breve{n}_{\mathrm{C_2H_2}} & (5.13) \end{aligned}$$

where $\breve{n}_{\mathrm{C_2H_2}}$ is the photospheric density of acetylene. Equation (5.12) is based on the assumption that the PAH density is decreasing in the envelope with distance $R$ simply because of the dilution, which is described by the $(R/r)^2$ factor. In fact, this is true only for distances where PAH formation and growth have stopped. According to the calculations presented in Chap. 4, chemical formation of small PAHs has ceased at distances equal or greater than $R = 10R_\star$. However, we shall see in Sect. 5.5.3 that PAH growth probably still occurs in the outer part of the envelope via acretion of $C^+$ cations. Since no data is available concerning the effectiveness of this process, we continue to use Eq. (5.12) to evaluate the PAH optical depth.

Figure 5.6 shows the results obtained at a distance $R = 10R_\star$. In the calculations we have used the absorption cross–section per carbon atom given by Verstraete & Léger (1992). The results are presented for two values of the PAH formation yield, 0.1 and 0.01. These values are much higher than the PAH formation yields estimated by Cherchneff et al. (1992). These values of the PAH yield are also probably larger than that obtained by considering the accretion with $C^+$ in the external part of the envelope. Such values therefore provide over–estimates of the PAH formation yield and consequently of the PAH optical depth. A comparison of the PAH optical depth with the dust optical depth shows that absorption by PAHs is probably always less effective than absorption by dust. We therefore neglect PAH self–shielding in the remainder of this chapter. We note, however, that PAH self–shielding will have to be taken into account in future investigations if the PAH yield is proved to reach values as large as 10 %.

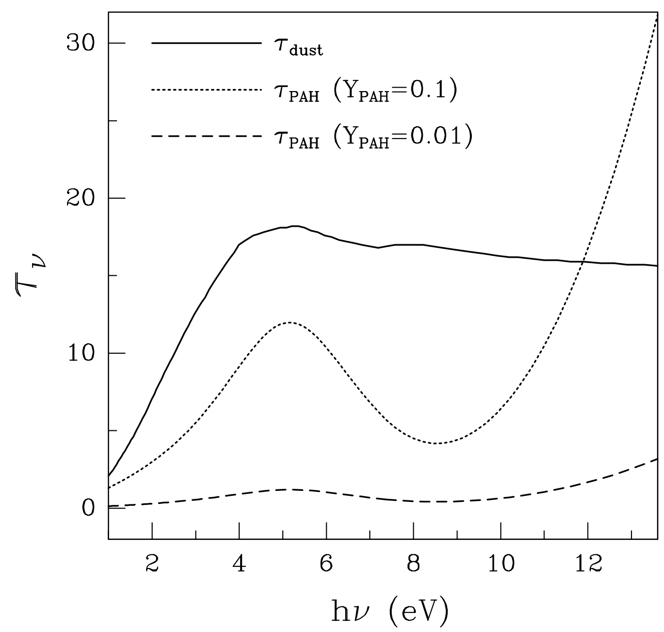


Figure 5.6: PAH optical depth as a function of photon energy at a distance 10 $R_\star$. The curves are drawn for two PAH yields corresponding to extremely high values (0.1 and 0.01) to allow for comparison with the dust optical depth at the same distance from the star.

### 5.3.2 Rates of PAH photoprocesses

In this section we apply Eqs. (5.8) to (5.10) to the determination of PAH photoionization and photoejection of hydrogen in the CSE of IRC+10216 described by the WDS model. We use the photoionization and hydrogen photoejection yields estimated in Chap. 2 and Chap. 3. For the mean interstellar photon flux in Eq. (5.8) we take the estimate of Draine (1978). The densities of CO and $H_2$ necessary for the calculation of the molecular optical depths are discussed in Sect. 5.4.1.

The upper panel of Fig. 5.7 presents the photoionization rate of pyrene molecules as a function of distance from the star. The rate has a constant value in the region near the star, which is dust free, and increases with distance up to its value of about $10^{-9}$ $s^{-1}$ in the ISM (see Chap. 2). The upper panel of Fig. 5.7 shows that taking into account molecular shielding leads to a decrease of the photoionization rate by about 25 % compared to a calculation with only dust shielding. Consequently, the molecular shielding of PAHs is really efficient in the CSEs of C–stars.

It was shown in Chap. 2 that all PAHs have similar ionization yields and photoionization rates in the ISM. The results and conclusions presented for pyrene are therefore valid for all PAHs. This is different in the case of hydrogen photoejection for which the photorate considerably varies with PAH molecular size. This may be observed in Fig. 5.8 where the hydrogen photoejection rate has been represented in the CSE of IRC+10216 for benzene molecules and PAH cations containing 50 carbon atoms.

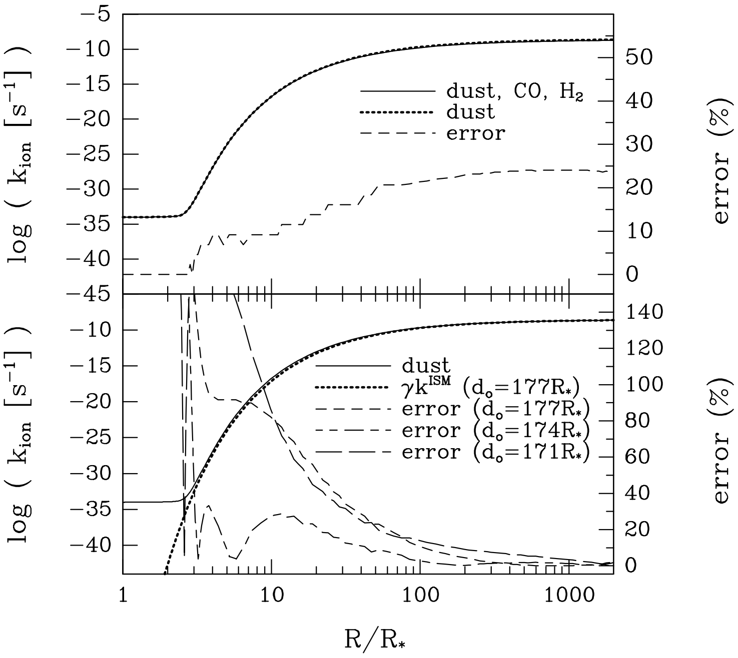


Figure 5.7: Ionization rate of pyrene molecules in the WDS model for the envelope of IRC+10216. Upper panel: Results taking into account dust and molecular shielding (continuous line) and results only for dust shielding (dotted line). The error obtained by omitting molecular shielding is also plotted.
Lower panel: Results with dust shielding and with the fit formula for dust optical depth. The error obtained by using the fit formula and various values of parameter $d_o$ is also plotted.

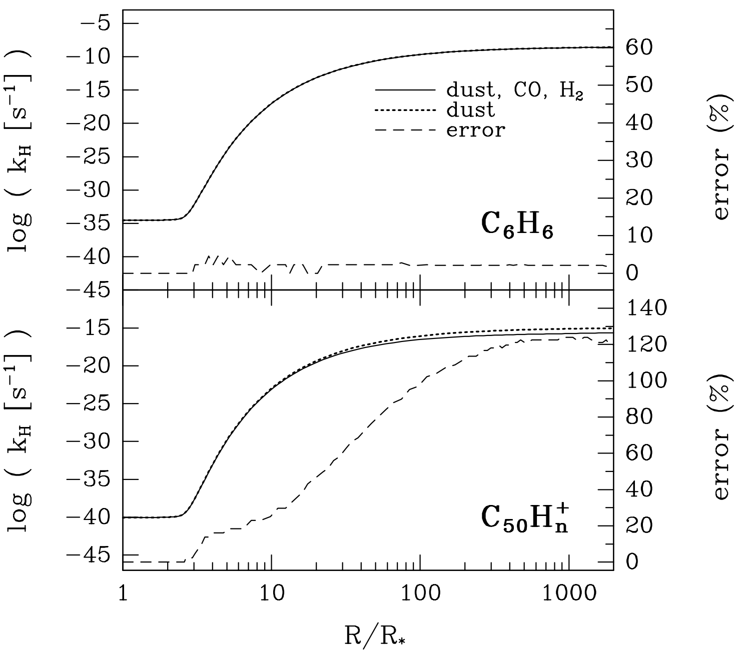


Figure 5.8: Upper panel: Hydrogen ejection rate for the benzene molecule in the WDS model for the envelope of IRC+10216. The calculations take into account dust and molecular shielding. The error obtained by omitting molecular shielding is also plotted.
Lower panel: same as the upper panel for PAH cations with 50 carbon atoms.

Figure 5.8 shows that omitting molecular shielding has no consequence for the calculation of the hydrogen photoejection rate of benzene, but leads to an error of a factor 2 (error of 100 %) for large PAH cations. This is due to the fact that the benzene photoejection yield reaches its highest values in the energy range 5–10 eV (see Chap. 2) where $H_2$ and CO do not absorb. On the contrary, for a large PAH cation the photoejection yield is maximal for the photon energies where $H_2$ and CO most absorb. In conclusion, molecular shielding should be introduced in photorate calculations as soon as the yield of the considered photoprocess has high values in the absorption region of $H_2$ and CO. In C–star CSEs the densities of CO and $H_2$ molecules have indeed proved to be great enough compared to dust density to dominate over dust in the shielding process.

The lower panel of Fig. 5.7 presents the results obtained for the photoionization rate of pyrene molecules by using the fit formula (5.3) and the monochromatic approximation of Eq. (5.4) ($d_o = 177R_\star$) for the dust optical depth. In the region where dust is present ($R > 3R_\star$) this approximation is correct to within to a factor of 2 and over 30 orders of magnitude. Furthermore, the error introduced by the approximation decreases for increasing values of distance from the star down to some per cent for distances greater than 100 stellar radii. Nethertheless, it fails to describe the constant value of the photorate near the star and leads to errors of several orders of magnitude in this region.

In the lower pannel of Fig. 5.7 it is shown that better agreement between exact calculation and approximation is obtained in the case of pyrene ionization for a parameter $d_o$ of 174 $R_\star$ instead of 177 $R_\star$ in Eq. (5.3). In general, for a good approximation the distance $d_o$ should be chosen according to Table 5.1 for the photon energy at which the rate $k_\nu$ of Eq. (5.9) reaches its maximum. According to Table 5.1 the distance of 177 $R_\star$ corresponds to a photon energy between 6 and 7 eV. However, for such energies PAH ionization yield and, consequently, the rate $k_\nu$ are equal to zero (see Chap. 2 or Verstraete et al. 1990). PAH ionization yields have non-zero values for energies larger than their ionization potential, which is about 8 eV. The value of $174R_\star$ corresponds in Table 5.1 to a photon energy of about 9 eV, at which the rate $k_\nu$ is maximal. The value of $174R_\star$ for $d_o$ is therefore better appropriate for PAH photoionization. The present discussion and the various curves in the lower pannel of Fig. 5.7 illustrate the sensitivity of the fit formula with $d_o$ and, consequently, the necessity to adopt the choice of $d_o$ for an accurate estimate with the monochromatic approximation of Eq. (5.3).

# 5.4 PAH ionization and hydrogenation in CSEs

## 5.4.1 Electron and atomic hydrogen densities

Studying the evolution of the PAH ionization fraction and the PAH hydrogen coverage in stellar shells enables estimates to be made of the ionization and hydrogenation states of the PAHs ejected by C–stars into the ISM. Moreover, knowledge of the PAH ionization and hydrogenation states is necessary to evaluate the photodestruction of PAHs in CSEs since the process of acetylene photoejection is much dependent on the PAH hydrogenation and ionization states (see Chap. 3). As in Chap 3., the hydrogenation and ionization states of PAHs are mainly determined by the gas temperature and by the densities of electron and atomic hydrogen. The temperature profile in the envelope is obtained as a result of the model calculations of WDS (see Appendix A). In this section we therefore restrict our investigation to calculations of the electronic and atomic hydrogen densities in the CSE. For this purpose, we solve the equations of a kinetic reaction network based on the structure of the CSE of IRC+10216 modelized by WDS.

The influence of PAHs on the chemistry has been studied by Lepp & Dalgarno (1988) and Lepp et al. (1988) in the case of interstellar clouds. Lepp & Dalgarno (1988) have compared chemical calculations without PAHs and calculations assuming a PAH abundance relative to hydrogen of $10^{-7}$. They found differences by one order of magnitude for the density of electrons and on average 2 orders of magnitude for carbon bearing molecules. On the other hand, the calculations of the PAH chemistry in the WDS model for IRC+10216 presented in Chap. 4 have led to abundances of small PAHs ($N_{\rm C} \leq 20$) less than $10^{-16}$. We therefore assume in the following that, in the envelope of IRC+10216, PAHs do not strongly modify the chemistry of the more abundant species. Furthermore, we note that the greatest abundance reported by Cherchneff et al. (1992) for small PAHs in CSEs is $3\ 10^{-9}$ and is hence still lower than the abundance assumed in the calculation of Lepp & Dalgarno (1988).

An extensive work on atomic and molecular hydrogen in CSEs has been carried out by Glassgold & Huggins (1983). We follow the approach of these authors to describe the photodissociation of $H_2$ in the outer part of the stellar shell. More detailed results concerning the photodissociation rates of $H_2$ are now available (see Abgrall et al. 1992) but have not been used here for sake of simplicity and because the more accurate rates of Abgrall et al. (1992) would probably not modify too much the results obtained with the approach of Glassgold & Huggins (1983).

In the description of Glassgold & Huggins (1983) the external limit of the CSE has to be introduced. We therefore assume that the envelope expands up to the distance where the local pressure of the stellar wind equals the pressure of the ISM. Using the results of Woitke et al. (1993) we obtain a distance of $8.48\ 10^{18}$ cm for our model of IRC+12016, that is to say $\simeq 9.2\ 10^4 R_\star$.

The density of atomic hydrogen obtained by solving the equations for the reaction network is represented in Fig. 5.9. Near the star its value is determined by chemical equilibrium. The chemical reactions involving H and $H_2$ however rapidly freeze out and the concentration of atomic hydrogen is constant from a distance of 1.5 $R_\star$ to a distance of about $2.10^4$ $R_\star$ where photodissociation of $H_2$ begins.

The electron density is governed, on the one hand, by the photodissociation of the more abundant carbon bearing molecules (CO and $C_2H_2$) and by the subsequent ionization of atomic carbon, and on the other hand, by direct photoionization of metals (Si, Mg, Fe, S, Na). The photodestruction rates of the $C_2H_2$ chain have been taken from Cherchneff et al. (1993). To describe CO photodissociation we follow the approach of Mamon et al. (1988), which takes into account self–shielding and shielding by $H_2$, and we use the photodissociation rates in CO lines determined by Patzer (1992). The ionization and

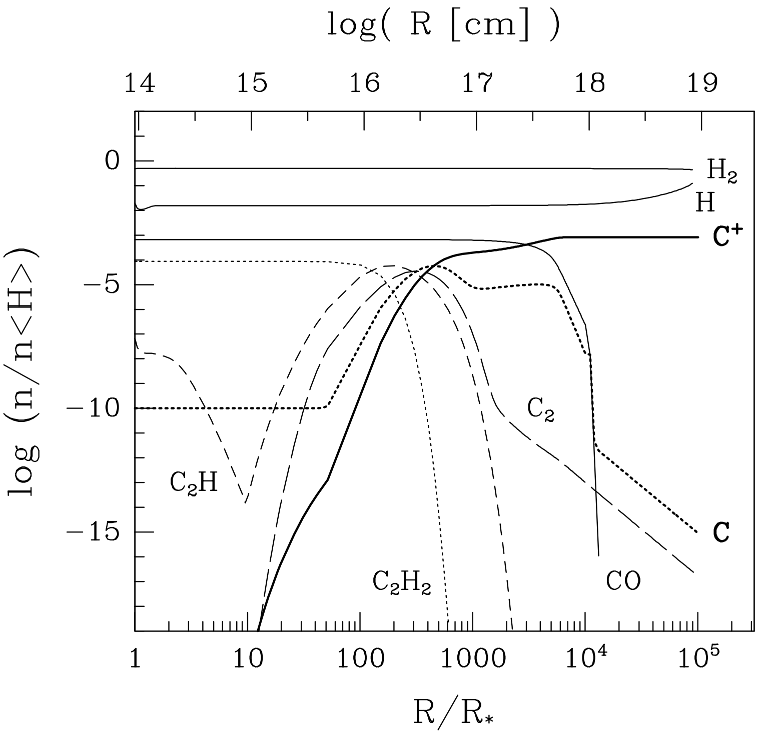


Figure 5.9: Concentration profiles of (i) atomic and (ii) molecular hydrogen, and (iii) of the carbon bearing species in the envelope of IRC+10216 described by the WDS model.

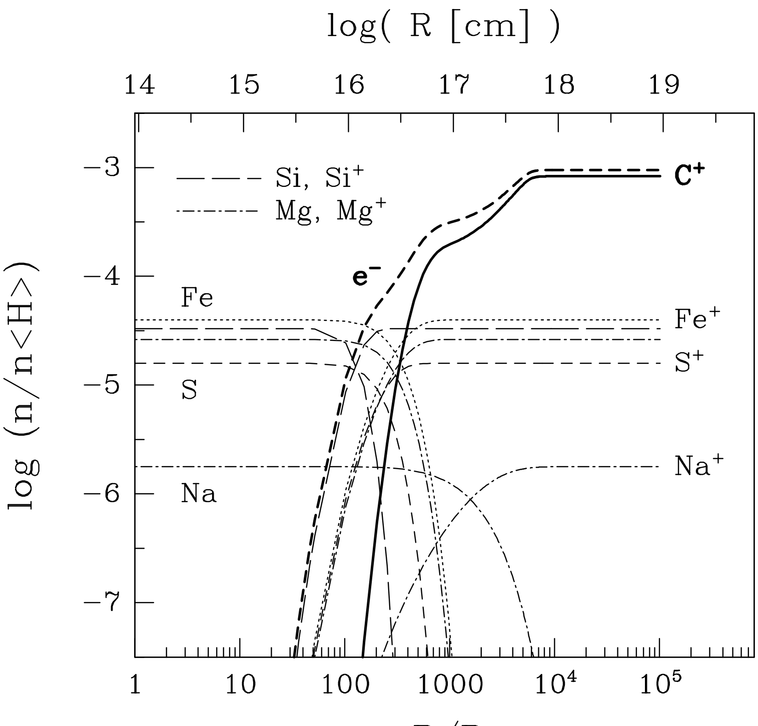


Figure 5.10: Concentration profiles of metallic ion and atom and of electrons in the envelope of IRC+10216 described by the WDS model.

electron recombination rates of metals have been obtained from the compilation of Millar et al. (1991).

The concentrations of the carbon bearing molecules are presented in Fig. 5.9. The concentration of $C^+$ originates mainly from ionization of the carbon atoms released by the photodissociation of the molecular chain $C_2H_2$, $C_2H$ and $C_2$ for distances between 10 and 1000 $R_\star$. From $R \simeq 2000 R_\star$ outwards, $C^+$ is mainly produced via photodissociation of CO molecules. Figure 5.10 shows the concentrations of the electrons and of the metal atoms and cations. In the region between 10 and $200 R_\star$, electrons are produced by the ionization of metals, especially silicon. For distances greater than $200 R_\star$ the ionization of carbon atoms is the main source of electrons.

## 5.4.2 Ionization state of PAHs

### PAH cations

In C–stars CSEs ionization of PAHs proceeds via photoionization and possibly via charge transfer reactions with $C^+$ and metallic cations. The reverse process is dominated by recombination with electrons. The PAH photoionization rates and the PAH electron recombination rate have been extensively discussed in Sect. 5.3.2 and in Chap. 3, respectively. For the same reasons as in Chap. 3, we neglect here the dissociative character of PAH recombination with electrons.

The reaction of PAHs with $C^+$ is known at present only for the benzene molecule. Bohme et al. (1982) have measured a reaction rate coefficient of 2.4 $10^{-9}$ $\mathrm{cm^3 s^{-1}}$ for the collision of benzene and $C^+$ at 296 K. We assume here that, for benzene and for all PAH cations, this rate coefficient is well described by the so–called Langevin rate (in memory of his pionneering work (Langevin 1905)). We therefore consider the coefficient as temperature independent and assume that it varies linearly with the square root of the PAH polarisability (see e.g. Ridge (1986) and references therein). Omont (1986) has shown that the polarisability of compact PAHs may be approximated by 0.9 $N_\mathrm{C}^{3/2}$ Å$^3$ where $N_\mathrm{C}$ is the number of carbon atoms of the PAH. Combining these results we estimate the collision rate of PAHs with $C^+$ to:

$$k^{\mathrm{col}}_{\mathrm{C^+}} = 2.4\ 10^{-9} \left(\frac{N_\mathrm{C}}{6}\right)^{3/4} \quad \mathrm{cm^3 s^{-1}} \tag{5.14}$$

The rate coefficient for charge exchange with $C^+$ has been measured for the benzene molecule by Bohme et al. (1982). They obtained a yield of 67 % for this reaction at 296 K. Since PAHs all have similar values of the ionization potential and similar molecular dynamics it is likely that the yield for PAH charge exchange with $C^+$ has also a similar relatively high value for other PAHs. However, further experimental investigation is needed to clarify this point. In the case of metallic cations, charge transfer seems to be less important than for $C^+$. For silicon cations Bohme et al. (1989) have reported a yield for charge exchange 7 times smaller than the yield for capture of $Si^+$. Serra et al. (1992) have assumed a yield of 100 % for the formation of organometallic complexes after collision between PAHs and iron cations. Consequently, we do not take into account the charge exchange process between PAHs and metallic cations in the present calculation.

In order to evaluate the importance of charge exchange reaction in the ionization process of circumstellar PAHs, we have plotted in Fig. 5.11 the collision rate with $C^+$, the photoionization rate and the electron recombination rate for a coronene molecule in the envelope of IRC+10216.

The rate for dynamical change is also represented in Fig. 5.11. As in Chap. 4 the dynamical timescale is stated as being equal to $R/v$ where $v$ denotes the stellar wind velocity at distance $R$ from the star (see also Appendix B). A physical or chemical process can be significant in the envelope only if its characteristic timescale has a value lower than that of the timescale for dynamical change. This is the case for collisions with $C^+$, photoionization and electron recombination at distances $R > 100R_\star$. Moreover, Fig. 5.11 shows that the most rapid process in practically the whole envelope is the electron recombination. However, near the transition region with the ISM, photoionization becomes the dominating process.

Charge exchange with $C^+$, whose rate is lower than that of collisions with $C^+$, is never the most rapid process and can be neglected in the calculation. The lack of knowledge concerning the exact value of the charge exchange rate is therefore of no importance for the determination of the PAH ionization state. We furthermore argue that the effect of charge exchange with metallic cations can also be neglected in the study of PAH ionization. Finally, we can infer from Fig. 5.11 that PAHs are not positively ionized in the main part of the envelope. In the outer part however, ionization probably occurs via photoionization.

### PAH anions

There is little knowledge about the reactions involving PAH anions in space. In CSEs PAHs may negatively ionize by electron attachment. On the same basis as in the discussion about reactions between PAHs and $C^+$, Omont (1986) proposed the following numerical expression for the electron attachment rate coefficient:

$$k_{\rm e}^{\rm att} = Y\ 1.8\ 10^{-6}\ \left(\frac{N_{\rm C}}{50}\right)^{3/4} \quad {\rm cm^3 s^{-1}}\ . \tag{5.15}$$

This rate coefficient has been adopted by Lepp & Dalgarno (1988) and Lepp et al. (1988) in their study of the chemistry of interstellar clouds with the value 0.3 for the reaction yield $Y$. On the other hand, the experimental results of Tobita et al. (1992) lead to values of the thermal electron attachment rate coefficient 2 or 3 orders of magnitude lower (0.9 $10^{-9}$ $\rm cm^3s^{-1}$ and 0.2 $10^{-9}$ $\rm cm^3s^{-1}$ for anthracene and pyrene, respectively). To reproduce the experimental value for pyrene with Eq. 5.15, we adopt the value $Y = 3\ 10^{-4}$.

Tobita et al. (1992) also noted an increase of the electron photoattachment rate for fast electrons with energies of some eV. Such electrons could be released by the the photoionization processes of metal atoms and PAHs. However, since we have not considered nonthermal electron in the calculations, we have not taken into account this phenomenon in the treatment of electron photoattachment. Moreover, Tobita et al. (1992) observed

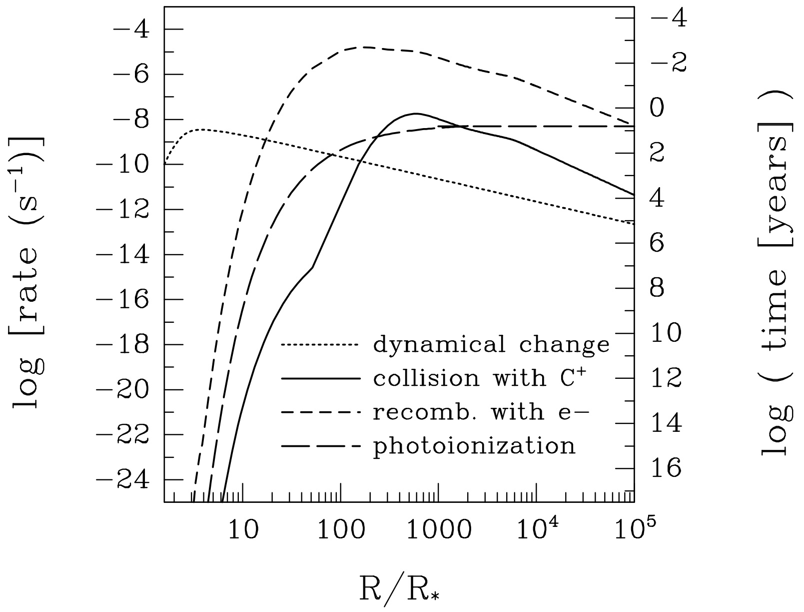


Figure 5.11: Rates for (i) dynamical change in the CSE and, for a coronene molecule, (ii) collision with $C^+$, (iii) electron recombination, (iv) photoionization. The rates are defined in the text and are represented for the WDS model describing the CSE of IRC+10216.

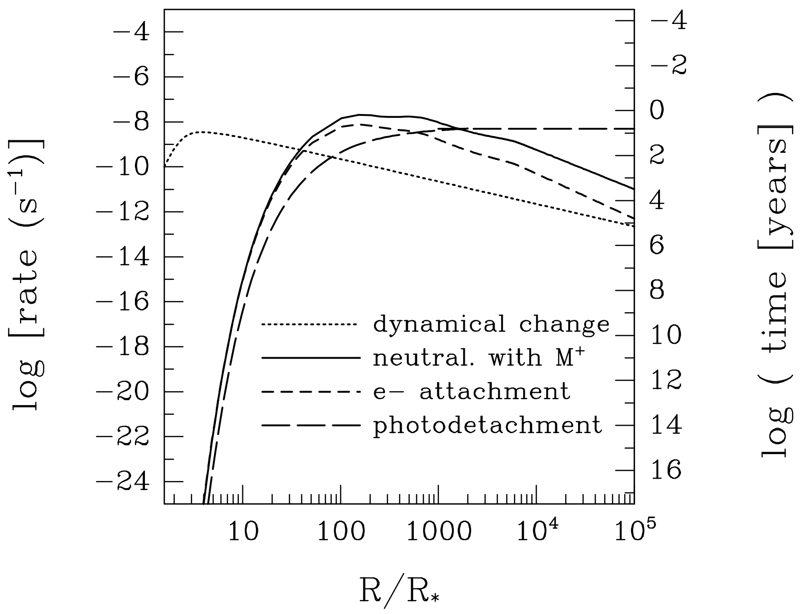


Figure 5.12: Rates for (i) dynamical change in the CSE and (ii) mutual neutralization of coronene anion with metal cations, (iii) electron attachment to coronene molecule, (iv) photodetachment for a coronene anion. The rates are defined in the text and are represented for the WDS model describing the CSE of IRC+10216.

dissociative electron attachment for small PAHs. As for electron recombination, we have nethertheless neglected dissociation processes for electron attachment to PAHs.

The reverse process is the neutralization of PAH anions and occurs via photodetachment or mutual neutralization with metal cations including $C^+$. For the photodetachment, we follow the suggestion of Omont (1986) and use the rate for photoionization of neutral PAHs. For the mutual neutralization:

$$\mathrm{M}^+ \ + \ \mathrm{PAH}^- \longrightarrow \mathrm{M} \ + \ \mathrm{PAH} \tag{5.16}$$

we adopt the same analytical expression for the rate coefficient as in the case of electron recombination (see Chap. 3) and replace the mass of the electron with that of the involved metal atom M, so that the mutual neutralization rate coefficient is given by:

$$k_{\mathrm{M}}^{\mathrm{neu}} = 1.7\ 10^{-7}\ Y N_{\mathrm{C}}^{1/2}\ T^{-1/2}\ A_{\mathrm{M}}^{-1/2} \left[1 \ + \ 3.82\ 10^{-3} \left(\frac{T}{100}\right) \left(\frac{N_{\mathrm{C}}}{50}\right)^{1/2}\right] \ \mathrm{cm^3 s^{-1}} \ , \tag{5.17}$$

where $A_{\mathrm{M}}$ designates the atomic mass of the metal, while $Y$ is the probability that reaction (5.16) occurs after collision between PAH anions and metallic cations, which we set equal to 0.3 as in the case of electron recombination.

Figure 5.12 shows the various rates for coronene. Between 50 and about 500 stellar radii, electron attachment and mutual neutralization with metal cations are competing. We therefore deduce that a fraction of PAHs are likely to be negatively charged in this distance range. For greater values of the distance, photodetachment is more effective and leads to the neutralization of PAH anions. However, we note that the results concerning PAH anions will have to be revised when more experimental data is available.

### Electric charge of PAHs in CSEs

As pointed out by Omont (1986) the charge of PAHs is probably always limited to a single elementary charge. The presence of doubly charged PAH cations have been already mentioned by several authors (Leach 1986, Millar 1992, Leach et al. 1989) but we have neglected them in the calculations for the same reason as in Chap. 3, namely the high ionization potential of the cations $\mathrm{PAH}^+$ (about 11–13 eV according to Tobita et al. (1994)).

To determine more precisely the charge of PAHs in CSEs we define the PAH cation and anion fraction, $\alpha^+$ and $\alpha^-$ respectively, by:

$$\alpha^+ \ = \ \frac{n_{\mathrm{PAH}^+}}{n_{\mathrm{PAH}^+} + n_{\mathrm{PAH}^0} + n_{\mathrm{PAH}^-}} \ , \tag{5.18}$$

$$\alpha^- \ = \ \frac{n_{\mathrm{PAH}^-}}{n_{\mathrm{PAH}^+} + n_{\mathrm{PAH}^0} + n_{\mathrm{PAH}^-}} \ , \tag{5.19}$$

where $n_{\mathrm{PAH}^+}$, $n_{\mathrm{PAH}^0}$ and $n_{\mathrm{PAH}^-}$ represent, for a given type of PAH, the densities of positively charged, neutral and negatively charged PAHs, respectively. To study the evolution of the quantities $\alpha^+$ and $\alpha^-$ in a circumstellar shell we consider a Lagrange volume element moving outwards with the same velocity, $v$, as the stellar wind. For a given type of PAH in this volume element at a distance $R$ from the star centre, $\alpha^+$ and $\alpha^-$ follow the system of equations:

$$\frac{\partial \alpha^+}{\partial t} = -2\alpha^+ \frac{v}{R} - \alpha^+ \frac{\partial v}{\partial R} - \alpha^+ n_{\rm e} k^{\rm rec} + \left(1 - \alpha^+ - \alpha^-\right) \left[k^{\rm ion} + n_{\rm C+} k^{\rm ex}_{\rm C+}\right] \,, \quad (5.20)$$

$$\frac{\partial \alpha^-}{\partial t} = -2\alpha^- \frac{v}{R} - \alpha^- \frac{\partial v}{\partial R} - \alpha^- \left[k^{\rm det} + \sum_i^{\rm metal} n_{{\rm M}_i} k^{\rm neu}_{{\rm M}_i}\right] + \left(1 - \alpha^+ - \alpha^-\right) n_{\rm e} k^{\rm att} \,, \quad (5.21)$$

where $n_{\rm X}$ denotes the density of species X and $k^{\rm rec}$, $k^{\rm ion}$, $k^{\rm ex}_{\rm C+}$, $k^{\rm det}$, $k^{\rm neu}_{\rm M}$, $k^{\rm att}$ the rates for electron recombination, photoionization, charge exchange with $C^+$, photodetachment, neutralization with metal cation and electron attachment, respectively.

We present in the lower panel of Fig. 5.13 the results obtained by solving Eqs. (5.20) and (5.21) for the envelope of IRC+10216. Near the star, PAHs appear as neutral molecules. For distances greater than $20 R_\star$ the increasing density of electrons rapidly convert about 50 % of PAHs into anions. PAHs anions keep their negative charge up to a distance of about $10^4 R_\star$, where they have all undergone neutralization by photodetachment. At the transition region with the ISM, PAH anions have totally disappeared. On the other hand, the fraction of positively charged PAHs increases with distance from a value less than 1 % between the star and a distance of $10^4$ stellar radii up to some 60 % at the transition region with the ISM. Larger PAHs have greater photoionization rates (see Chap. 2) and are therefore more rapidly ionized. However, the fractions of PAH anions and cations are practically the same for all PAHs as it was already observed in the calculations at ionization equilibrium in Chap. 3.

### 5.4.3 Hydrogenation state of PAHs

To study the hydrogenation state of PAHs in a circumstellar environment we adopt the same approach as for the PAH ionization state. Figure 5.14 shows the rate for hydrogenation, $k^{\rm hyd}_{\rm H}$, (see Chap. 3) and the rate of photoejection of hydrogen, $k^{\rm UV}_{\rm H}$, for some neutral PAHs (see Chap. 2 and Chap. 3). We have omitted in Fig. 5.14 to mention the hydrogen abstraction after collision with atomic hydrogen. It has been shown in Chap. 4 that abstraction is effective only very near to the star. When the temperature is lower than about 500 K, that is to say for distances greater than $10 R_\star$, the abstraction rate is indeed lower than the rate for dynamical change and the reaction of hydrogen abstraction freezes out.

According to Figure 5.14, hydrogenation is the most rapid process in the region between 10 and $10^3 R_\star$. PAHs are therefore probably well hydrogenated in this region of the envelope. In contrast, for distances greater than $10^3 R_\star$, the hydrogen photoejection rates become greater than hydrogenation in the case of small PAHs ($N_{\rm C} < 32$). The smaller the PAH, the

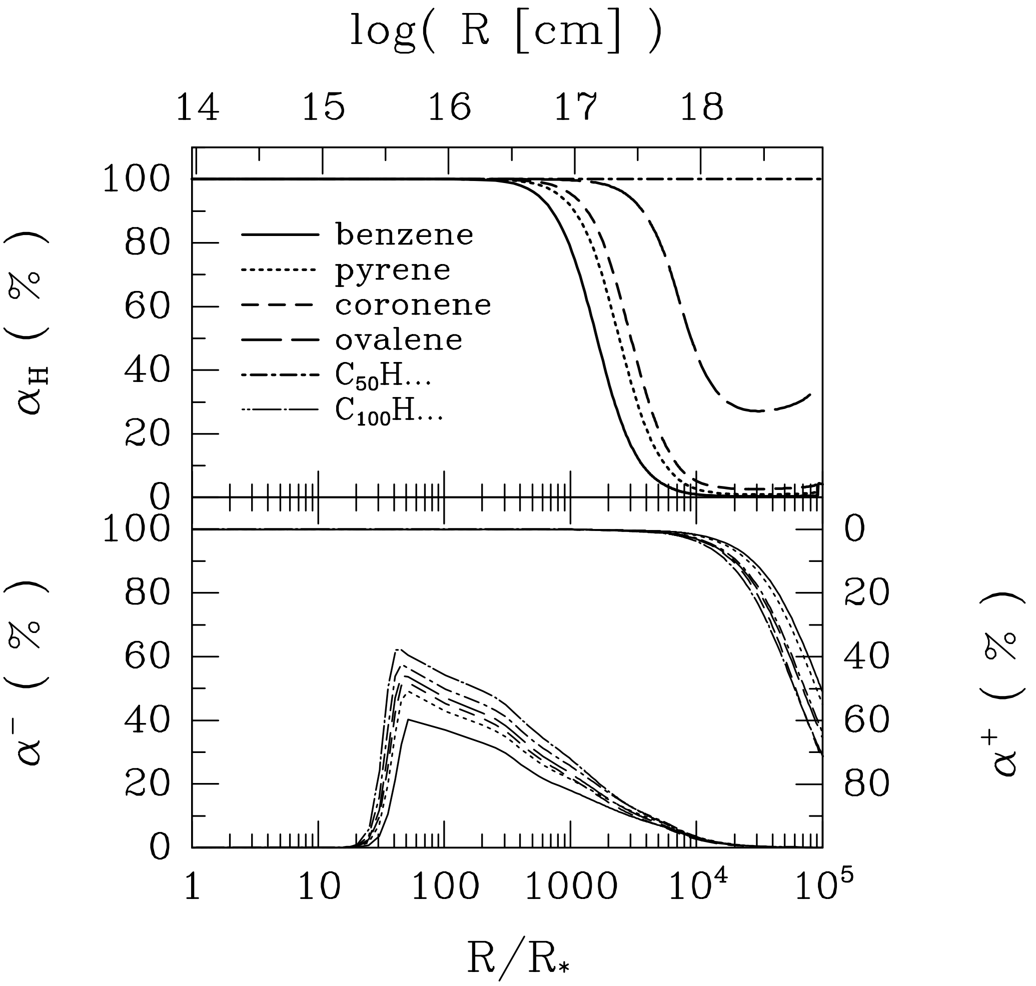


Figure 5.13: Upper panel: Hydrogen coverage of PAHs in the WDS model for the envelope of IRC+10216.
Lower panel: Fraction of neutral and ionic PAHs in the envelope of IRC+10216.

sooner it reaches the region where dehydrogenation dominates. On the other hand, PAHs containing 50 carbon atoms and more are not dehydrogenated in the envelope because their rate for hydrogen photoejection are always smaller than the rate for dynamical change.

A more precise calculation of the PAH hydrogenation state can be performed by solving the equation for the hydrogen coverage, $\alpha_H$, defined as:

$$\alpha_H = \frac{N_H}{N_H^o} \tag{5.22}$$

where $N_H$ is the number of hydrogen atoms on the PAH in the envelope and $N_H^o$ the number of hydrogen atoms of the corresponding fully hydrogenated PAH.

Similarly as for the ionization fractions, the equation for the hydrogen coverage can be writen:

$$\frac{\partial \alpha_{\rm H}}{\partial t} = -2\alpha_{\rm H}\frac{v}{R} - \alpha_{\rm H}\frac{\partial v}{\partial R} - \alpha_{\rm H}\ k_{\rm H}^{\rm UV} + (1-\alpha_{\rm H})\ n_{\rm H} k_{\rm H}^{\rm hyd}\ . \tag{5.23}$$

The photoejection rate of hydrogen depends on the state of ionization of the PAH (see Chap. 3) and is defined by:

$$\begin{aligned} k_{\rm H}^{\rm UV} &= \alpha^+\left[k_{\rm H}^{\rm UV}({\rm cation}) + 2k_{\rm H_2}^{\rm UV}({\rm cation})\right] + \alpha^-\left[k_{\rm H}^{\rm UV}({\rm anion}) + 2k_{\rm H_2}^{\rm UV}({\rm anion})\right] \\ &+ \left(1-\alpha^+-\alpha^+\right)\left[k_{\rm H}^{\rm UV}({\rm mol}) + 2k_{\rm H_2}^{\rm UV}({\rm mol})\right]\ , \end{aligned} \tag{5.24}$$

where $k_{\rm X}^{\rm UV}$(state) is the rate for the photoejection of species X from a PAH in ionic or molecular state. The rate of hydrogen ejection from PAH anions is assumed to be equal to that for PAH molecules. It was shown in Chap. 3 that the rates for PAH cations and molecules only differ by a factor of about 4. This is probably also not very different in the case of PAH anions.

The rate of hydrogenation also depends on the PAH degree of ionization and we therefore write:

$$k^{\rm hyd} = \left(\alpha^+ + \alpha^-\right) k^{\rm hyd}({\rm ion}) + \left(1-\alpha^+-\alpha^-\right) k^{\rm hyd}({\rm mol})\ , \tag{5.25}$$

where we have used, as in Chap. 3, the values 1.7 $10^{-11}$ cm$^3$s$^{-1}$ and $10^{-9}$ cm$^3$s$^{-1}$ for the hydrogenation rate coefficient of PAH ions, $k^{\rm hyd}$(ion), and of PAH molecules, $k^{\rm hyd}$(mol), respectively.

Hydrogenation may also occur during collision with $H_2$ molecules. For a PAH molecule, the corresponding reaction can be regarded as the reverse reaction to the hydrogen abstraction discussed in Chap. 4. Hence, the coefficient rate for hydrogenation can be obtained from the relation $k_{\rm H_2}^{\rm hyd} = k_{\rm H}^{\rm abs}/K_{\rm e}$, where $k_{\rm H}^{\rm abs}$ and and $K_{\rm e}$ denote the rate coefficient and the equilibrium constant for hydrogen abstraction, respectively. Using the Arrhenius expression (Eq. (4.36)) and typical thermodynamical values for PAHs (Benson 1976) we obtain the numerical expression $k_{\rm H_2}^{\rm hyd} = 6.5\ 10^{-12}{\rm exp}(-4693/T(K))$ cm$^3$s$^{-1}$, which is always more than 5 orders of magnitude lower than $k^{\rm hyd}$ calculated from Eq. (5.25) for $T < 500K$, that is to say for $R > 10R_\star$. Since the abundance of $H_2$ is never more than 2 order of magnitude greater than the abundance of atomic hydrogen, hydrogenation after collision with $H_2$ can be neglected to a good approximation.

The solution of Eq. (5.23) obtained for some PAHs are presented in the upper panel of Fig. 5.13 and confirm the results deduced from the previous discussion of the rates. PAHs smaller than ovalene are totally dehydrogenated at distances greater than $10^4 R_\star$, whereas larger PAHs are stable against photoejection of hydrogen in the whole envelope. Ovalene is partially dehydrogenated. The hydrogen coverage of ovalene is very sentitive to the density of hydrogen near the transition region with the ISM. Hence, the increase of hydrogen density following the photodissociation of $H_2$ leads to a slight increase of the ovalene hydrogen coverage.

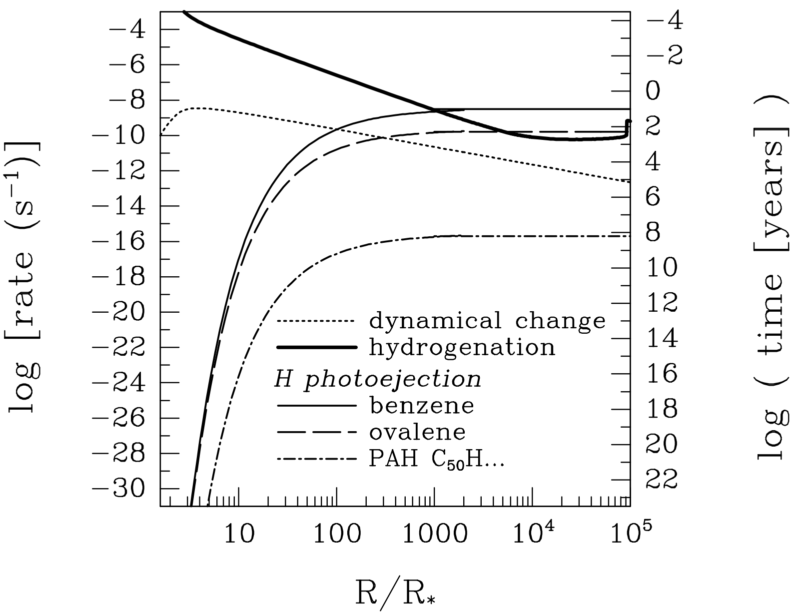


Figure 5.14: Rates for (i) dynamical change in the CSE and (ii) hydrogenation, (iii) hydrogen photoejection from some PAHs. The rates are defined in the text and are represented for the WDS model describing the CSE of IRC+10216.

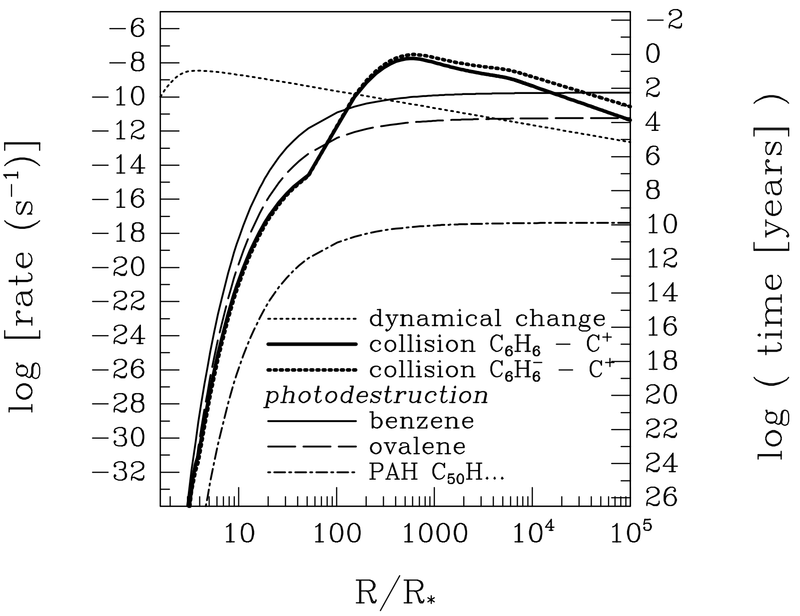


Figure 5.15: Rates (i) for dynamical changes and (ii) for collision of benzene molecule and anion with $C^+$ and (iii) for carbon photoejection from some PAHs. The rates are defined in the text and are represented for the WDS model describing the CSE of IRC+10216

## 5.5 PAH ejected into the ISM

PAH photoionization, electron attachment and neutralization, on the one hand, hydrogen photoejection and hydrogenation, on the other hand, have proved to be rapid enough to modify the ionization and hydrogenation states of PAHs in the outer part of CSEs. It is therefore also likely that carbon photoejection from PAHs and accretion of carbon particles to PAHs occur in the external part of CSEs and thereby change the size distribution of the PAHs formed near the stars. In order to test this hypothesis, we apply the same procedure as in the previous sections and first pay attention to the timescales of the involved processes.

### 5.5.1 Timescale discussion

In Fig. 5.15, the rate for collision with $C^+$ and the rate for carbon photoejection from some PAHs are represented. These rates are compared to the rate accounting for dynamical change in the envelope. The corresponding dynamical timescale is the smallest timescale near the star. Carbon photoejection and accretion are therefore ineffective in this region. However, for distances from the star greater than 100 stellar radii, the timescale for collision is the smallest one and collisions with $C^+$ effectively occur. Unfortunately, the exact yields for accretion, charge exchange and sputtering after collision with $C^+$ are still unknown for PAHs larger than benzene. In the absence of experimental data, simple assumptions could, however, help further investigation. An attempt in this direction is presented in Sect. 5.5.2.

According to Fig. 5.15 the timescale for carbon photoejection is, in the case of PAHs smaller than ovalene, lower than that for dynamic change in the external part of the envelope; carbon photoejection is therefore effective in this part of the envelope for small PAHs. Moreover, in agreement with the results of Chap. 2 and 3, Fig. 5.15 shows that the smaller the PAH, the greater is the probability to lose carbon atoms after the absorption of an ultraviolet photon. In contrast, PAHs larger than ovalene have timescales for carbon photoejection greater than the dynamic timescale in the whole envelope and are therefore always stable against carbon loss.

Since the timescale for carbon photoejection from small PAHs ($N_{\mathrm{C}} < 32$) is smaller than that of carbon accretion in the outer part of the shell, we deduce that a small PAH gradually loses all its carbon atoms before reaching the ISM. However, for a type of PAH the decrease of density due to photoejection processes may be compensated by the increase following the photodestruction of larger PAHs and carbon accretion on smaller ones. A definite conclusion concerning the decrease of the density for small PAHs is therefore *a priori* not straightforward and requires a careful examination of the PAH size–distribution.

As a consequence, no result concerning the exact processing of the PAH size distribution in the outer part of CSEs can be gained definitely from the present discussion. However, the effectiveness of both collision with $C^+$ and carbon photoejection have been stressed on the basis of simple timescale arguments.

### 5.5.2 Model used in the calculation

#### Condensation yield

In order to estimate the importance of carbon accretion onto PAHs in CSEs, we propose some simple assumptions for the yields of the processes following collision of $C^+$ with a PAH. These yields have been so far measured only for benzene molecules at a temperature of 296 K by Bohme et al. (1982). After collision these authors obtained the following results: charge exchange (67 %), accretion (10 %) with emission of atomic hydrogen, destruction with product $C_5H_3^+ + C_2H_3$ (17 %) and $C_3H_3^+ + C_4H_3$ (6 %).

As mentioned in Sect. 5.4.2, charge exchange is also probably the main process after collision between $C^+$ and PAHs larger than benzene. In the present calculations we assume the yield for charge exchange to be equal to 67 % for all PAH molecules. When charge exchange does not occur, formation of an excited complex (PAH–C), which dissociates or stabilizes via infrared emission, follows the collision. The larger the PAH, the greater is the probability of stabilizing the complex and therefore of accreting carbon. To describe the dependence of dissociation and accretion on PAH size, we assume that the yield for accretion increases linearly with the number of carbon atoms up to $\tilde{N}_\mathrm{C}$, for which dissociation processes are negligible. $\tilde{N}_\mathrm{C}$ is a parameter whose value will be varied to test its influence on the results. Figure 5.16 illustrates the assumptions made here for the yield following collision with $C^+$.

To fix a standard value of $\tilde{N}_\mathrm{C}$ we first note that the energy liberated in charge exchange reactions between PAHs and $C^+$ is about 4 eV (Omont 1986). Following Omont (1986) we consider that, if a complex $(\mathrm{PAH{-}C})^+$ forms after collision between a PAH and a cation $C^+$, the situation of this excited complex is similar to that following absorption of a photon of energy $E = 4\mathrm{eV}$. Hence, the rate for photoejection can be expressed as a function of the number of carbon atoms, $N_\mathrm{C}$, of the complex by the RRK expression discussed in Chap. 2 and deduced from the experimental results of Jochims et al. (1994). As did Jochims et al. (1994) we can compare the rate of photoejection to the typical rate for infrared emission $k^\mathrm{IR} \simeq 10^2\mathrm{s}^{-1}$. At 4 eV equality is obtained for $N_\mathrm{C} \simeq 10$. In our model of linearly increasing accretion yield (see Fig 5.16), this imply a value of 35 for $\tilde{N}_\mathrm{C} \simeq 35$. In the case of a PAH anion, the energy liberated in neutralization with $C^+$ is about 9 eV (Omont 1986). For such an energy, the size corresponding to the equality between destruction and infrared emission is $N_\mathrm{C} \simeq 35$, which leads to $\tilde{N}_\mathrm{C} \simeq 100$ for $\mathrm{PAH}^-$–$C^+$ collisions.

Two additional assumptions have been made in the following calculations: (i) destruction after collision with a carbon particle leads to the loss of 2 carbon atoms, as has been observed after photoabsorption (Joachims et al. 1994); (ii) the reaction $\mathrm{PAH}^+ + \mathrm{C}$ and $\mathrm{PAH}^- + \mathrm{C}$ have been attributed the same rate as the reaction $\mathrm{PAH} + \mathrm{C}^+$.

#### PAH size distribution

The PAH size distribution $f(N_\mathrm{C}, R)$ provides the density of PAHs with $N_\mathrm{C}$ carbon atoms at distance $R$ from the star. We know of no determination of the PAH size distribution in CSEs in the literature. However, two proposals have been made for the size distribution

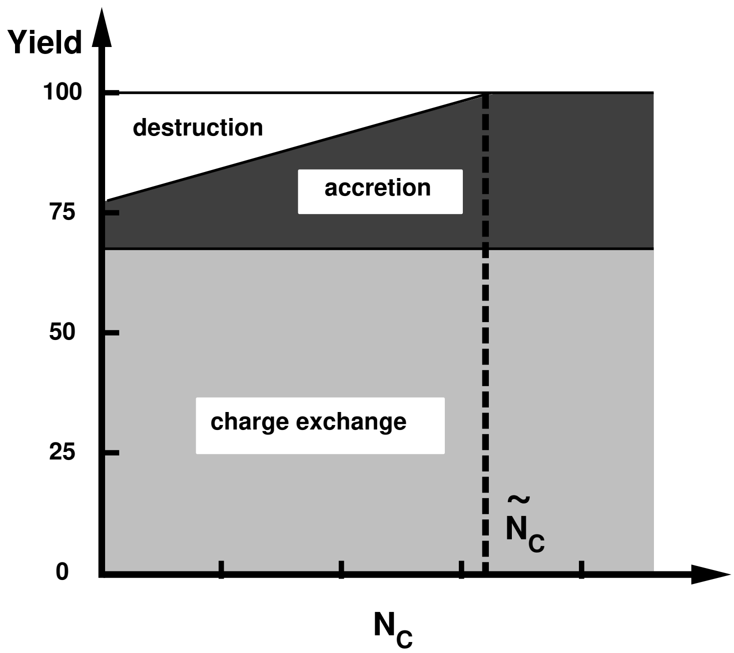


Figure 5.16: Model for the reaction of $C^+$ with a PAH: the yields for charge exchange, accretion and destruction are represented as a fonction of the number of carbon atoms, $N_C$ of the PAH (see text for more precision).

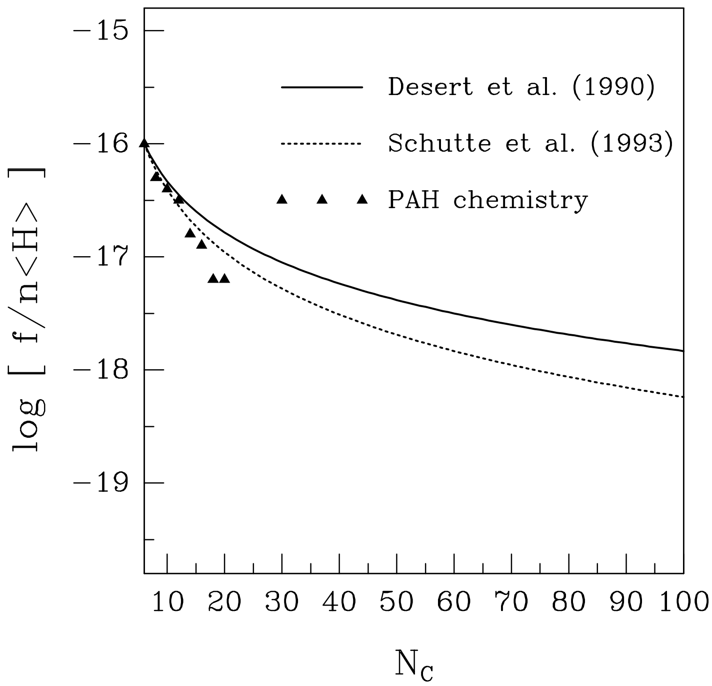


Figure 5.17: PAH size distribution after PAH formation near the star (adapted from Désert et al. (1990) and Shuttle et al. (1993)) and concentrations of some PAHs obtained from chemical calculations.

of interstellar PAHs by Désert et al. (1990) and Schutte et al. (1993). These PAH size–distributions have been calculated with the aim of reproducing the unidentified infrared emission bands, whose carriers are assumed to be PAHs alone. In both studies it is also assumed that the PAH size distribution is given by a power law:

$$f(N_{\rm C}) = B\ n_{<{\rm H}>}\ N_{\rm C}^{-\beta}\ , \tag{5.26}$$

where $\beta$ is the exponent of the power law equal to 1.5 for Désert et al. (1990) and to 1.833 for Schutte et al. (1993), while B is a constant which fixes the PAH abundance.

The calculation of PAH chemistry in the envelope of IRC+10216 presented in Chap. 4 provides estimates of abundance for the PAHs containing $N_{\rm C} \leq 20$ carbon atoms. These results are reproduced in Fig. 5.17 at a distance $R = 10R_\star$, where PAH formation has stopped. Also represented are the size distribution of Désert et al. (1990) and Schutte et al. (1993), for which we have used the benzene density $f(6, 10R_\star)$ to fix the value of $B$. For PAHs with $N_{\rm C} \leq 20$ carbon atoms the results of the chemical calculation are quite similar to that obtained with the power law distributions. In the remainder of this chapter. we therefore assume that the initial (at $R = 10R_\star$) size distribution of circumstellar PAHs can also be given by a power law function. We use the value of 2.2 for the exponent $\beta$, which provides the best fit of the results obtained by the chemical calculation.

The evolution of the PAH size-distribution in the CSE is governed by the equation:

$$\begin{aligned} \frac{\partial f(N_{\rm C},R)}{\partial t} = & - \ 2f(N_{\rm C},R)\frac{v}{R} - f(N_{\rm C},R)\frac{\partial v}{\partial R} - f(N_{\rm C},R)\left[k_{\rm C}^{\rm acc} + k_{\rm C}^{\rm dest} + k_{\rm C}^{\rm UV}\right] \\ & + \ f(N_{\rm C}+2,R)\ k_{\rm C}^{\rm UV} + f(N_{\rm C}+1,R)\ k_{\rm C}^{\rm dest} \\ & + \ f(N_{\rm C}-1,R)\ k_{\rm C}^{\rm acc} + J_{\rm form}\ , \end{aligned} \tag{5.27}$$

where $k_{\rm C}^{\rm UV}$, $k_{\rm C}^{\rm acc}$ and $k_{\rm C}^{\rm dest}$ are the rates for carbon photoejection, carbon accretion and destruction after collision with carbon, respectively. For photoejection we take account of the PAH hydrogen coverage and degree of ionization and write:

$$k_{\rm C}^{\rm UV} = \alpha^+ k_{\rm C}^{\rm UV}({\rm cation},\alpha_{\rm H}) + \alpha^- k_{\rm C}^{\rm UV}({\rm anion},\alpha_{\rm H}) + \left(1-\alpha^+-\alpha^-\right) k_{\rm C}^{\rm UV}({\rm mol},\alpha_{\rm H})\ . \tag{5.28}$$

In Eq. (5.28), $k_{\rm C}^{\rm UV}({\rm state},\alpha_{\rm H})$ denotes the rate for photoejection of a carbon particle from a PAH with hydrogen coverage $\alpha_{\rm H}$ and in a molecular or ionic state. These rates have been estimated in Chap. 3. As in the case of hydrogen photoejection, we use the same rate for carbon photoejection from PAH molecules and from PAH anions. The rates for accretion and destruction after collision with carbon particles include the rate for collisions of $C^+$ with neutral and negative PAHs and of C with PAH cations and are expressed as:

$$k_{\rm C}^{\rm p} = \left[\alpha^+ n_{\rm C} + \left(1-\alpha^+-\alpha^-\right) n_{\rm C^+} + \alpha^- n_{\rm C}\right] k^{\rm col+} Y_{35}^{\rm p} + \alpha^- n_{\rm C^+} k^{\rm col-} Y_{100}^{\rm p} \tag{5.29}$$

In Eq. (5.29), p denotes accretion or destruction and $Y^{\mathrm{p}}_{N_{\mathrm{C}}}$ is the corresponding yield calculated according to Sect. 5.5.2, while $k^{\mathrm{col}+}$ and $k^{\mathrm{col}-}$ are the collisional rates defined in Eqs. (5.14) and (5.17), respectively.

In Eqs. (5.27), $J_{\mathrm{form}}$ denotes the formation rate of new PAHs by ion/molecule reactions between species in the gas phase. This formation rate has been introduced in the case of benzene and naphthalene.

There is indeed some evidence for the formation of benzene–like cations in ion/molecule reactions involving three–carbon units, whereas the synthesis of benzene–like cations is less certain in the case of two–carbon units (Bohme 1992). To describe the formation of new benzene cations, we have used the following set of reactions:

$$\mathrm{C_3H_4} + \mathrm{h}\nu \longrightarrow \mathrm{C_3H_4^+} \tag{5.30}$$
$$\mathrm{C_3H_4^+} + \mathrm{e^-} \longrightarrow \mathrm{destruction} \tag{5.31}$$
$$\mathrm{C_3H_4} + \mathrm{C_3H_4^+} \longrightarrow \mathrm{C_6H_7^+} + \mathrm{H} \tag{5.32}$$

$$\mathrm{C_2H_2} + \mathrm{C_2H_2^+} \longrightarrow \mathrm{C_4H_2^+} + \mathrm{H_2} \tag{5.33}$$
$$\mathrm{C_2H_2} + \mathrm{C_2H_2^+} \longrightarrow \mathrm{C_4H_3^+} + \mathrm{H} \tag{5.34}$$
$$\mathrm{C_4H_2^+} + \mathrm{e^-} \longrightarrow \mathrm{destruction} \tag{5.35}$$
$$\mathrm{C_4H_3^+} + \mathrm{e^-} \longrightarrow \mathrm{destruction} \tag{5.36}$$
$$\mathrm{C_4H_2^+} + \mathrm{C_2H_2} \longrightarrow \mathrm{C_6H_4^+} + \mathrm{h}\nu \tag{5.37}$$
$$\mathrm{C_4H_3^+} + \mathrm{C_2H_2} \longrightarrow \mathrm{C_6H_5^+} + \mathrm{h}\nu \tag{5.38}$$

In Reactions (5.30) to (5.32) $\mathrm{C_6H_7^+}$ is the benzenium cation and $\mathrm{C_3H_4}$ the molecule of allene, for which we set an initial abundance of $10^{-12}$ equal to that of the radical propargyl $\mathrm{H_2C_3H}\bullet$ calculated in the chemical kinetic study of Chap. 4 (see also the reaction network of Cherchneff et al. 1992). In Reaction (5.37) the identity of the $\mathrm{C_6H_4^+}$ has not been established (Anicich et al. 1986) and we assumed that 10 % of the ions could be benzyne cations. In Reaction (5.38), we have made the same assumption for $\mathrm{C_6H_5^+}$ which could be phenyl cations. For the dissociative recombination of the cations with electrons we have used the coefficient rates of Mitchell (1990). For Reaction (5.32) the coefficient rate is taken from Lias & Ausloos (1982) and for Reactions (5.37) and (5.38) from Anicich et al. (1986).

In the case of naphthalene cations, the formation from benzene cations and diacetylene has been investigated by Bohme et al. (1991). We have integrated these reactions in the set of chemical reactions. Moreover, Bohme et al. (1991) have observed that further growth of naphthalene cations via addition of acetylene and diacetylene is negligible. We have hence not considered PAH growth by addition of acetylene or diacetylene. We furthermore argue that, at distances greater than $500R_\star$, C and $\mathrm{C^+}$ are the most abundant carbon bearing species besides CO molecules (see Fig. 5.9) and we therefore only consider C and $\mathrm{C^+}$ for the growth process of PAHs.

### 5.5.3 Results

Figure 5.18 presents the results obtained for the evolution of the PAH size distribution in the envelope of IRC+10216 modelized by WDS. The value $\tilde{N}_{\rm C} = 35$ has been adopted for the yields of the processes following the collisions PAH + $C^+$, $PAH^+$ + C, $PAH^-$ + C, and $\tilde{N}_{\rm C} = 100$ for the collision $PAH^-$ + $C^+$. A power law with exponent $\beta = 2.2$ has been used for the PAH size distribution. Although the calculations are performed for PAHs with up to 500 carbon atoms, we will restrict here the discussion mainly to PAHs containing less than 100 carbon atoms since nothing is known concerning the exact structure of larger PAHs. The results of Chap. 4 have shown that PAHs with less than 100 carbon atoms are effectively formed near the star by addition of acetylene molecules. Moreover, the size range between 6 and 100 carbon atoms contains the sizes generally deduced for the interstellar PAHs from observations of the UIR bands (Allamandola et al. 1989).

As shown in Fig. 5.18 the densities of PAHs relative to hydrogen nuclei dramatically diminish between the region near the star and the outer part of the CSE. This decrease is mainly due to the destruction of small PAHs ($N_{\rm C} < 35$) and to the accretion of $C^+$ and C to PAHs with $35 \leq N_{\rm C} \leq 150$, which hence grow to larger molecular sizes. Since accretion dominates over destruction for most of the PAHs, the number of carbon atoms locked up into PAHs probably increases efficiently with distance in the envelope, even if the abundances of the PAHs considered here are decreasing.

The synthesis of new small PAH molecules or cations by ion/molecule reactions involving species in the gas phase contributes to an increase of the number of PAHs at distances less than some hundred stellar radii. However, the synthesis of benzene cations cannot prevent the depletion of PAHs at greater distances. The calculations show that the density of electrons ensures a rapid dissociative recombination of the molecular cations involved in the formation of new benzene–like cations. This is illustrated in Fig. 5.20 where the rates of formation for benzene–like cations are represented. The pathway via $C_4H^+_{\ldots}$ cations is more efficient than that involving $C_3H^+_{\ldots}$ cations. However, at distances greater than $150 R_\star$, the formation of new benzene-like cations is always slower than the destruction of benzene PAH in collision with $C^+$ and can therefore no longer limit the depletion of PAHs. Although we have not performed exact calculations, we expect that this may also be the case for other possible synthesis pathways, for instance via propyne cations (see Bohme(1992) and references therein).

Only another formation process of new PAHs could slow down the consumption of PAHs observed in Fig. 5.18. PAHs could eventually form via sputtering of amorphous carbon grains or via grain–grain collisions (Omont 1986). Since no experimental data exist about these processes we have not considered them here.

At distances smaller than $10^4 R_\star$ collisions with carbon particles constitute the dominant process for the evolution of the PAH size distribution. In the rest of the envelope ($R > 10^4 R_\star$), PAH photodestruction becomes increasingly efficient and is the determining process for the evolution of the smallest PAHs. As already pointed out, the smaller the PAH, the more effective is the photodestruction process. As a result, the abundances of small PAHs ($N_{\rm C} \leq 40$) diminishes more rapidly in the outer part of the circumstellar shell than the

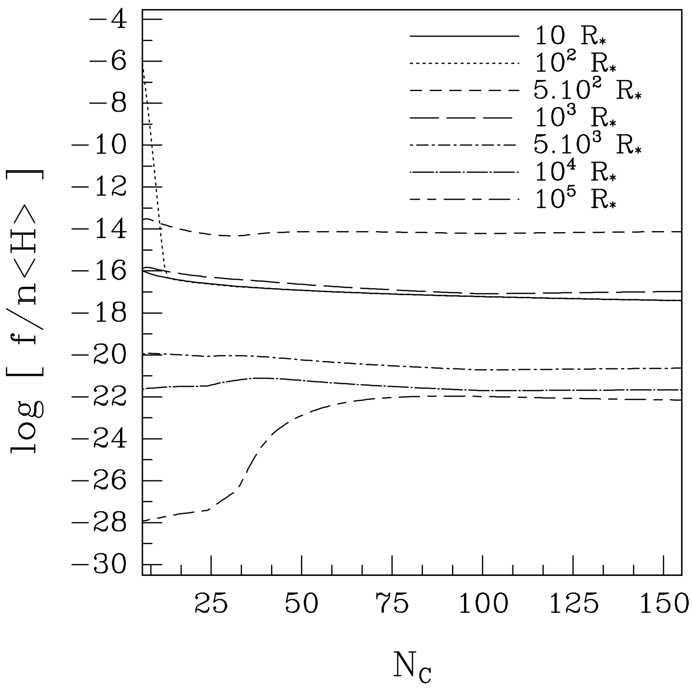


Figure 5.18: PAH size distribution at various distances from the star

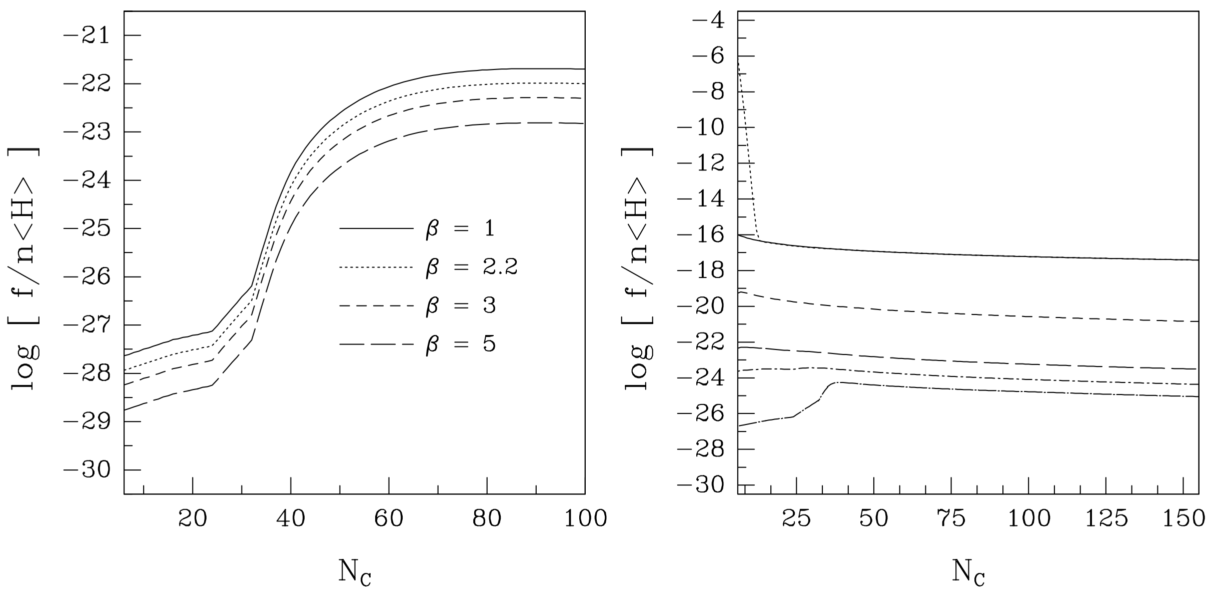


Figure 5.19: (left) Same as Fig. 5.18 at a distance $10^5 R_\star$ for various values of the exponent $\beta$; (right) Same as Fig. 5.18 for $\tilde{N}_{\rm C} = 500$ (the distance corresponding to a given curve is the same that corresponding to the curve with the same type of plot as in Fig. 5.18).

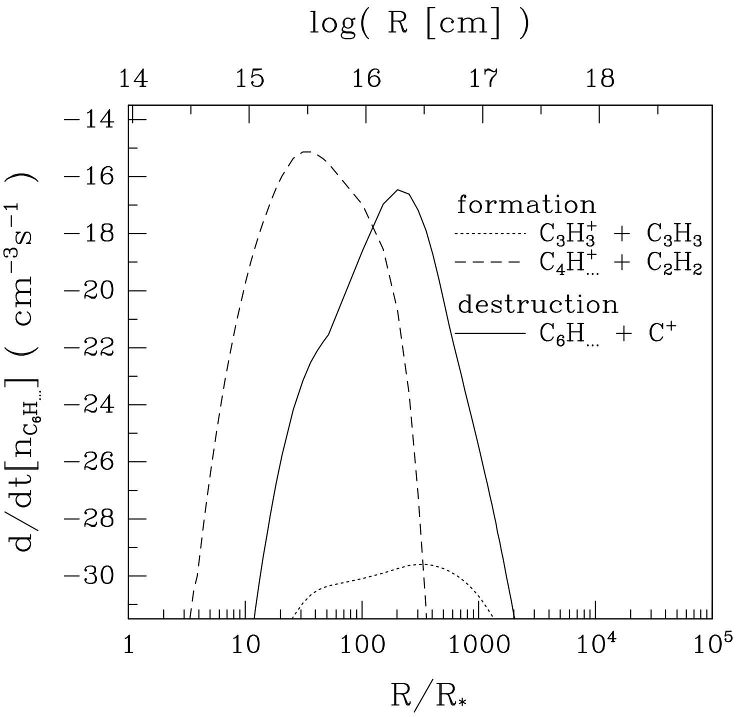


Figure 5.20: Formation and destruction rates of benzene–like PAHs

densities of larger PAHs. At the transition region with the ISM the densities of PAHs with $N_C \le 30$ are found to be six orders of magnitude lower than those of larger PAHs.

However, the model presented here is based on several speculative assumptions: more reliable results are actually needed for the initial size distribution of the PAHs formed near the star and for the yields of the reactions involving PAHs and $C^+$. Some insight into the influence of these elements can be gained by varying the parameter $\tilde{N}_C$ introduced in Sect. 5.5.2 and the exponent $\beta$ of the power law for the PAH size distribution.

The left hand figure of Fig. 5.19 shows the results obtained for the terminal PAH size distribution and various values of the exponent $\beta$. A remarkable result is that the form of the terminal PAH size distribution is not very sensitive to the value of the exponent used for the initial size distribution. It seems that the form of the PAH size distribution rather undergoes a self–tuning in the CSE under the combined effect of collisions and photodestruction. We note, however, that we have given no reliable justification for our choice of a power law for the initial size distribution and that the previous result therefore holds only in the limits of this model.

The terminal size distribution may also depend on the accretion process. In the right hand figure of Fig. 5.19 we have modified the values of $\tilde{N}_C$ as compared to the values used in the case of Fig. 5.18, which probably corresponds to a relatively efficient accretion. Indeed, it is likely that the PAH growth via accretion of $C^+$ proceeds by the formation of side chains which subsequently form rings. Such side chains could be less stable against destruction and, thus, the PAH growth could be slower than assumed in the case of Fig.

5.18 (Omont 1986). It is therefore worth calculating the evolution of the size distribution with a less efficient accretion.

In the calculations presented in the right hand panel of Fig. 5.19 we have set $\tilde{N}_{\rm C} = 500$ for all collisions between PAHs and carbon particles, which implies, in our model, that accretion is slower than carbon ejection for PAHs containing less than 140 carbon atoms. In this case we observe that (i) the formation of new benzene–like cations does not lead to an increase of PAH abundances because the PAH growth process is too slow, and that (ii) the abundances of PAHs also decrease with distance but less rapidly than in Fig. 5.18. We extrapolate that, if accretion of $C^+$ were proved by experiment to be less effective than assumed in Fig. 5.19 (right hand panel), the depletion of PAHs would be correspondingly decreased. Moreover, it can be seen in Fig. 5.19 (right hand panel) that, at the transition region with the ISM, the size distribution shows a smooth maximum at about 40 carbon atoms. If experiment would prove that accretion of carbon onto PAHs is as effective as assumed in Fig. 5.19 (right hand panel) or even less effective, this could imply the presence of PAHs with a size distribution showing a smooth maximum at about 40 carbon atoms in the external part of C–stars CSEs.

The value of 40 carbon atoms is indeed comparable with that obtained for the molecular size of the UIR bands carriers by Allamandola et al. (1989) from observations of the planetary nebula NGC 7027. Since late–type red giants constitute the progenitor of planetary nebulae, circumstellar PAHs are often thought to be responsible for the UIR bands (Waters et al. 1989, Buss et al. 1990, 1991, 1993). In this case the conclusions of Allamandola et al. (1989) could support the idea of a less effective carbon accretion onto PAHs in C–stars CSEs than assumed in Fig. 5.18.

However, the large depletion of PAHs obtained in all our calculations puts into question the previous conclusion. Moreover, Woodward et al. (1989) have deduced a size between 13 and 27 carbon atoms for the species emiting the UIR bands in NGC 7027. Our calculations show, in contrast, that PAHs with less than 30 carbon atoms have in all cases an abundance several orders of magnitude lower than PAHs bearing more than 40 carbon atoms. The recent observations of Buss et al. (1993) could provide an explanation to the apparently contradictory results presented here. Indeed, Buss et al. (1993) have shown that the UIR bands are not always present in the transition objects between red giants and planetary nebulae. These authors have therefore suggested that PAHs could be formed during the processing of dust particles and PAH clusters in the terminal shocks of stellar winds.

This proposition is compatible with our results. We indeed argue that (i), in the external part of circumstellar shells of C–stars, collisions between PAHs and $C^+$ probably lead to a large depletion of PAHs with less than $\simeq 150$ carbon atoms and to the appearance of larger PAH–like structures [1]; and that, (ii) photodestruction processes efficiently reduce the abundances of PAHs bearing less than 40 carbon atoms in the outer part of C–star envelopes, so that only a very small amount of such PAHs can be ejected into the ISM by C–stars. Finally, (iii) we conclude that, if PAHs with $N_{\rm C} \leq 40$ are really the carriers

[1]This is actually only true if PAH formation via dust grain destruction or via other molecule/ion reaction pathway as those considered in Reactions (5.30) to (5.38) are proved to be negligible

of the UIR bands observed in protoplanetary and planetary nebulae, there must be an efficient mechanism responsible for their formation; probably these PAHs originate from the destruction of large PAH–like structures in the terminal shock of stellar winds.

## 5.6 Discussion

New aspects of the photochemistry in CSEs has been developed in this chapter. In particular, the treatment of the shielding for the species present in the circumstellar shell has been much improved. The shielding by dust has been revised by taking precisely account of the dust size distribution. As a result, the dependence of the dust optical depth with wavelength has been obtained. The results support the previous models of circumstellar photochemistry which have neglected the variation of the dust shielding with wavelength. However, the new numerical values obtained for the dust optical depth could have consequences for the photochemical models, which show some sensitivity to the value of the dust optical depth (Cherchneff et al. 1993). Moreover, an estimate for the shielding by $H_2$ and CO molecules has been presented, which can lead to a diminution by a factor of 2 for some photorates. A revision of CSE photochemistry in view of these new results would be worth doing. Such a study was beyong the scope of this chapter. We have indeed restricted here our investigation to the species which influence the processing of PAHs in CSEs. For these species, we have only considered dust shielding since the uncertainties in the rates for the processes involving PAHs are probably greater than those introduced by neglecting the shielding by $H_2$ and CO.

Using the rates for the PAH photoprocesses enables us to estimate the hydrogen coverage and the ionization fractions of PAHs in CSEs. The state of hydrogenation and ionization of PAHs have been already estimated in Chap. 3 for the media showing the UIR bands. In these astrophysical environments, however, the PAH state at the time of their formation is unknown and an equilibrium approach has been used for the calculation. In CSEs, the initial state of PAHs are known (see Chap. 4). Moreover, exact knowledge of the conditions of pressure and temperature allows us to estimate the densities of electron and atomic hydrogen, which play an important role in the PAH state of ionization and hydrogenation. As a consequence, the evolution with time of the PAH hydrogenation and ionization states can be calculated within the whole envelope. At the transition region between the CSE and the ISM, (i) an ionization fraction of about 60 % is obtained, (ii) the hydrogen coverage of PAHs smaller than ovalene is found to be negligible, whereas (iii) PAHs with more than 50 carbon atoms are totally hydrogenated. These results could constitute initial values for a dynamical study of the processing of PAHs in the ISM.

The growth and destruction of PAHs in the outer part of CSEs has been also studied. It was thought so far that a study of the PAH chemical formation near the star could provide an estimate of the amount of PAHs ejected into the ISM by C–stars (Frenklach & Feigelson 1989; Latter 1991; Cherchneff et al. 1992). On the contrary, it has been demonstrated that the collision rate of PAHs with $C^+$ and the rate for carbon photoejection are large enough to modify the PAH size distribution in the stellar wind. We have furthermore observed that PAH growth via accretion of $C^+$ is effective enough to enhance the quantity of carbon locked up into PAHs. This could be an explanation for the low PAH formation yield obtained by Cherchneff et al. (1992). The PAH formation yields of Cherchneff et al. (1992) were indeed several orders of magnitude lower than the less realistic yields of Frenklach & Feigelson (1989), which were shown to be barely sufficient to explain the PAH abundance deduced from observations (Latter 1991). We note that Cadwell et al. (1994) recently present another solution to this problem by introducing PAH nucleation, coagulation and surface growth on grains. Although some points in the study of Cadwell et al. (1994) are still questionable (the non–determination of the amount of SiC seeds, the elementary description of the C–star envelope, the non-consideration of the PAH temperature – see Chap. 4), their proposal constitutes an alternative solution. Both explanations probably contribute to the formation of large quantities of PAHs in C–stars envelopes.

The present approach for PAH growth however suffers from lack of knowledge concerning the yields of the processes following collision of PAHs with $C^+$ (charge exchange, accretion, destruction). Experimental results are therefore crucially needed, since they could help to better modelize the formation and growth of PAHs in CSEs and more generally in the ISM. More experimental information is also necessary for a good estimate of the size distribution of the PAHs formed near the star (see Chap. 4) and for a reliable description of PAH formation by molecule/ion reactions. With the help of all these new experimental results, it will be possible to precisely study the evolution of the PAH size distribution between their formation near the star and their release into the ISM. In such studies a better mathematical approach than the simple and computer time consuming set of differential equations presented here will be required for treatment of the PAH size distribution. The moment equations of Gail & Sedlmayr (1984) and the methods developed by Dominik et al. (1989) and Krüger et al. (1995) to estimate size distributions could be precious tools in order to follow the evolution of the PAH size distribution in the stellar wind.

Before circumstellar PAHs are released into the ISM, they have to pass through the shock front where the CSE joins the ISM. In the shock front PAHs probably behave similar to small graphitic grains (Omont 1986). The influence of the terminal shock wave of circumstellar winds on such dust particles have been already studied by Woitke et al. (1994). These authors concluded that the destruction yields across the shock front including evaporation, sputtering and collision with dust grains does not exceed 20 %. However, the calculations have not been performed for PAHs and should be therefore considered with some precaution. The behaviour of PAHs in shocked regions has been investigated however by Duley & Williams (1986), Brown et al. (1989) and Flower et al. (1990) in the case of molecular clouds. They observed that the lack of exact chemical data once more leads to contradictory results concluding that PAHs either are totally destroyed or remain unchanged in the shock. Finally, we note that the destruction of dust grains or PAH clusters in the terminal shock of CSEs could also eventually produce new PAHs and thereby modify the PAH size distribution. In conclusion, knowledge about PAHs in CSE shocks is still relatively uncertain and further investigation is required.

## 5.7 Conclusion

New estimates of the shielding by dust, $H_2$ and CO molecules in circumstellar envelopes of C–stars have been presented and applied to the study of PAH photoprocesses. The results point to an efficient and complex processing of PAHs occuring in the outer part of circumstellar shells.

PAHs are found to be ionized by the ultraviolet interstellar radiation. When PAHs reach the transition region between the circumstellar envelope and the interstellar medium, about 60 % of the PAHs are indeed positively ionized. However, a fraction of PAHs are also negatively charged in the region of the circumstellar envelope between 10 and $10^4$ stellar radii. Moreover, PAHs smaller than ovalene ($N_C < 32$) are totally dehydrogenated at the outer limit of the circumstellar envelope, whereas PAHs with more than 50 carbon atoms are stable against hydrogen photoejection in the whole envelope.

Collisions of PAHs with $C^+$ are frequent and influence the evolution of the PAH size distribution in the stellar wind. Unfortunately, lack of data about the relative yields of charge exchange, accretion and destruction after collision with $C^+$ prevents the presentation of definite conclusions. However, accretion is likely to be efficient enough to ensure a rapid growth of PAHs and thereby to enhance the amount of carbon locked up in large PAHs. As a consequence, PAHs bearing less than $\simeq 150$ carbon atoms are much depleted in the CSEs. This depletion is even enhanced by photodestruction for PAHs with less than 30 carbon atoms. If PAHs are the carriers of the UIR bands observed in protoplanetary and planetary nebula, the present results indicate that the PAHs emitting the UIR bands are probably not directly ejected into the ISM by C–stars but are produced during destruction processes in the terminal stellar shocks. This result is confirmed by recent observations.

However, only new experimental investigations could help to get a definite picture of the evolution of the PAH size distribution in the circumstellar envelopes of C–stars. Such experiments would also be of great interest for the study of growth and destruction of PAHs in molecular clouds, and in general for the estimate of PAH abundances in the interstellar medium.

Ma fille, disait la Raison à la Vérité, voici, je crois, notre règne qui pourrait bien commencer à advenir après notre longue prison. [...] Il nous arrivera ce qui est arrivé à la Nature: elle a été couverte d'un méchant voile, et toute défigurée pendant des siècles innombrables. A la fin il est venu un Galilée, un Copernic, un Newton, qui l'ont montrée presque nue, et qui en ont rendu les hommes amoureux.

Voltaire, *Eloge historique de la Raison*, 1774.

# Chapter 6

# Conclusions and Outlook

The presence of large amounts of PAHs in space is still a matter of debate in the astrophysical community. The assignement of the unidentified infrared (UIR) bands to the vibrational modes of free PAHs is indeed still questioned, although the PAH abundance deduced from the observations of the UIR bands is astonishingly generally assumed. Besides the UIR bands, PAHs have also been assessed as candidates for the carriers of the diffuse interstellar bands (DIBs) in the visible (Léger & d'Hendecourt 1985, van der Zwet & Allamandola 1985, van der Zwet 1987). The extended red emission (ERE) in reflexion nebulae has also been tentatively attributed to visible luminescence of PAHs (d'Hendecourt et al. 1986). However, the assignement of these observations to PAHs is still discussed (see Miles & Sarre (1993) and the general discussion which follows). Consequently, we note that no definite evidence exists at the present time to support undoubtedly the PAH hypothesis, which assumes the existence of large quantities of interstellar PAHs. In this context, the philosophy of the present thesis is to get new information about interstellar PAHs independently of astronomical observations. Indeed, in this work, use is made only of experimental results and of theoretical calculations, with the purpose to determine the characteristic properties of the PAHs capable of surviving in the ISM.

This thesis can be divided into two parts. In the first part (Chap. 2 and Chap. 3) we study the chance of survival for PAHs in the media showing the UIR bands. It seems indeed contradictory that these media which should reveal some evidence for the presence of PAHs are also the media where PAHs are most exposed to destructive ultraviolet radiation fields. An estimate of the minimal molecular size of the PAHs which can possibly survive in these regions is made. The second part (Chap. 4 and Chap. 5) concentrates on the circumstellar envelopes of C–stars, where probably most of the interstellar PAHs form. Special emphasis is put on the PAH formation and growth and on the evolution of the PAH size distribution in the well defined physical conditions of the circumstellar environment. The aim is thereby to estimate the properties of the PAHs ejected into the ISM by C–stars.

**In the first part** PAH photodestruction rates in the ISM have been calculated by use of the experimental results of Jochims et al. (1994). Such computations are only made possible by careful analysis and comparison of the processes following the absorption of a photon: ionization, photodestruction, infrared emission and luminescence from the electronic excited state. As a result, astrophysically relevant rates – that is to say, integrated over the interstellar radiation field – have been presented for the photoejection of hydrogen and acetylene from PAH molecules. Comparing the rate for photoejection of acetylene to that of the reverse process, accretion of carbon particles, leads to the conclusion that only PAHs containing more than 50 carbon atoms are able to resist the ultraviolet radiation field in the regions showing the UIR bands.

It is usually argued that PAHs are probably ionized and partially dehydrogenated under the conditions of the ISM. A method for evaluating simultaneously the hydrogen coverage and degree of ionization of interstellar PAHs has been developed and applied to the astrophysical media where the UIR bands are observed. The calculations have shown that various degrees of ionization are encountered in the media showing the UIR bands. For a given medium, the degree of ionization is, however, almost the same for all PAH sizes. In contrast, the PAH hydrogenation state is rather independent on the medium but depends on the PAH size. In most cases, PAHs with less than 50 carbon atoms are totally dehydrogenated, whereas the larger ones are fully hydrogenated.

In order to study the photoejection rates of these ionized and partially dehydrogenated PAHs, a model has been developed by extending the approach used for PAH molecules to PAHs cations and to PAH with low hydrogen coverage. The rates for photoejection of hydrogen and carbon particles from ionized and partially dehydrogenated PAHs have been proved to be higher that those of their parent molecules, especially for the partially dehydrogenated PAHs which are very unstable against photodestruction. However, since PAHs with more than 50 carbon atoms are fully hydrogenated, the previous conclusions concerning the minimal size of surviving PAHs remain practically unchanged. Only PAHs containing more than 50 carbon atoms are therefore eventually able to resist the strong ultraviolet radiation field of the regions exhibiting the UIR bands.

Since PAHs with more than 50 carbon atoms can possibly survive in the ISM, it is worth studying the regions where they form and grow. Hence, this is the object of **the second part** of this thesis to deal with PAHs in circumstellar environments. The envelopes of the cool carbon–rich red giant stars, the so–called C–stars, indeed provide the most favourable conditions of temperature and density for an effective formation of PAHs from acetylene molecules. For this purpose, the stationary models for dust forming circumstellar shells of C–giants developed at the Institute of Astrophysics in Berlin have been used. In these models, the detailed and self–consistent treatment of hydrodynamics, thermodynamics and dust processing ensures reliable estimates of the temperature, density and stellar radiation field and provides a precise description of the radial structure of the envelope necessary for the present investigation. The model for the shell of the carbon–rich star IRC+10216, which is the nearest and most studied carbon–rich red giant, is taken as an example for C–star envelopes.

All the physical processes which could favour PAH formation have been carefully analyzed. PAH drift velocities relative to the gas phase have been determined and proved to have no influence on PAH formation. In contrast, the low PAH temperatures compared to that of the gas are favourable to formation and growth of PAHs. On the basis of these results, the density of small PAHs have been evaluated near the star by solving the kinetic equations for the reaction network describing PAH formation. It has also been established that PAHs rapidly grow by succesive hydrogen abstraction and addition of acetylene molecules, up to macroscopic sizes. For the first time, the link between PAHs and dust particles has been numerically studied, with the result that PAHs could possibly be the seeds for dust grains.

The processes undergone by PAHs when they reach the outer part of the circumstellar envelopes have also been investigated. To allow for reliable calculations, the shielding from interstellar ultraviolet radiation by dust, $H_2$ and CO molecules has been precisely analyzed. New values have been calculated for the dust and molecular optical depths in the envelopes of C–stars. Using these results, the PAH ionization and hydrogenation states have been estimated in the envelope of IRC+10216. The PAHs released to the ISM are shown to have a degree of ionization of about 60 % and a hydrogen coverage of 100 % for PAHs larger than ovalene ($N_C > 32$).

The growth via $C^+$ accretion and the photodestruction of PAHs have also been studied with the aim of estimating the size distribution of the PAHs ejected into the ISM. Although it is demonstrated that the growth and destruction processes are rapid enough to modify the PAH size distribution along their way from the star outwards to the ISM, no definite conclusions have been drawn because of the lack of data concerning the yields of the processes occuring after collision between PAHs and $C^+$. However, $C^+$ accretion is likely to lead to the depletion of PAHs with less than $\simeq 150$ carbon atoms and to enhance the amount of carbon locked up in larger PAH–like structures. The present results could indicate that the PAHs usually assumed to be the carriers of the UIR bands are probably not directly ejected into the ISM by C–stars but are produced during destruction processes of these larger structures in the terminal stellar shocks.

In view of these last results, we strongly encourage further experimental investigation. Only a reliable value for the accretion rate of $C^+$ onto PAHs could indeed provide estimates of the amount of PAHs released to the ISM by C–stars. In the present thesis, we have also noted the lack of experimental data on PAHs for the reactions of hydrogenation, reactions with electrons and addition with acetylene. The exact pathway from acetylene to large PAHs is also uncertain in circumstellar envelopes and needs to be precisely investigated in the laboratory. Part of these chemical problems have been recently submitted to the specialists of astrophysical chemistry by colleagues of our group (Patzer et al. 1994). The difficulty in such experimental studies consists in reproducing the physical conditions of temperature and pressure relevant for astrophysical situations in the laboratory. However, large hopes are put in the new cooperation between astrophysicists and experimental chemists.

The results presented in this thesis are based on experimental and theoretical analysis and no assumption derived from astronomical observations has been made. Conversely, some insight into the interpretation of observations could be gained by applying the results of the present work. Let us discuss an example. Recently, Giard et al. (1994) observed in the 3.3 $\mu m$ feature the photodissociation region of the ionization/shock front in the Orion bar. They found a strong emission in the neutral/molecular gas just behind the front but no significant emission in the ionized gas, and therefore concluded that the 3.3 $\mu m$ emitting particles are destroyed in this ionized region but survive in the neutral one. Assuming that the emitting species are PAHs, Giard et al. (1994) analyzed qualitatively the possible destruction mechanisms. One of their propositions is that the photodestruction processes are compensated by efficient growth in the dense neutral/molecular gas but not in the ionized gas. Our numerical results could help to test precisely such an hypothesis. More generally, the increasing number of observations of the UIR bands provides a large field of application for the photodestruction and growth rates investigated in this thesis.

A goal of the present work was to study the physical properties (ionization, hydrogenation) and the size distribution of the PAHs ejected into the ISM by C–stars. As was shortly pointed out, shock waves are present in the stellar wind, where PAHs form and grow, both in the region near the star and in the transition region with the ISM. Although PAH chemistry in shock fronts have not been considered in this thesis for the sake of simplicity, shock waves probably modify the properties and size distribution of PAHs and therefore need to be investigated in the future. For this purpose, the time dependent models of pulsating cool red giants developed in our group could provide good structures of the circumstellar shocks (Fleischer et al. 1992, Fleischer 1994). The destruction processes acting on dust grains in the terminal shock of the stellar wind has been also studied by colleagues of us (Woitke et al. 1994) and could be applied to the case of PAHs with appropriate modifications. Moreover, the analytical expressions obtained in Chap. 4 for the interactions of PAHs with gas particles could be introduced in the study of the dynamics and energy exchange of PAHs in shock waves. This future analysis of the behaviour of PAHs in circumstellar shock waves, combined with the results of this thesis, will provide a realistic picture of circumstellar PAHs and will help to determine the exact nature of the PAHs ejected into the ISM by C–stars.

The ultimate aim is to propose an estimate of the density of PAHs in the ISM. Such a goal supposes that the physical conditions of the considered medium are well–known, and that all the processes contributing to the input of PAHs (formation and growth in situ, contribution of C–stars, of shock waves) and to the disappearance of PAHs (photodestruction, collision with gas particles, sputtering) are correctly estimated. Solving the conservation equation for PAHs will then provide a value for the PAH density. A similar approach has already been adopted by Latter (1991) in order to test the hypothesis that the PAH formation in the stellar winds of carbon stars is sufficient to explain the abundance of $10^{-7}$ generally admitted for PAHs. However, Latter (1991) based his results on the formation yield of PAHs in circumstellar envelopes determined by Frenklach & Feigelson (1989). Many new results prove now that the PAH yield of Frenklach & Feigelson (1989) is not reliable. Compared to the paper of Frenklach & Feigelson (1989), many improvements have been achieved in this thesis: the introduction of realistic circumstellar envelope structure, the determination of PAH temperatures, the estimates of the growth process by addition of $C^+$. Each of these points separatly modifies by several orders of magnitude the results of Frenklach & Feigelson (1989). Consequently, a revision of the study by Latter (1991) is necessary.

Such a study would definitely address the question of the presence of PAHs in the ISM and, hence, enables to test whether PAHs are as ubiquitous and abundant as observations seem to imply. A complete answer to these interrogations is still far from being reached and constitutes an ambitious challenge to the success of which the present work will hopefully contribute.

# Appendix A

# Self–consistent model of dust driven circumstellar winds

The self–consistent model for the dust–forming winds surrounding late–type C–stars presented in this Appendix has been recently developed by Winters et al. (1994) and Winters (1994), from which the two figures of this Appendix are extracted and to which the reader is referred to for more information. The aim is here to sketch the main features of the complex physical problem of dust forming winds in circumstellar envelopes and to explicit the results used in Chap. 4 and Chap. 5.

A picture of the physical problem of dust forming atmospheres around late–type stars is presented in Fig. A.1. As shown in this figure the high complexity of the problem arises from the coupling of hydrodynamics, thermodynamics, chemistry and, finally, of dust formation and growth. Before trying to analyze Fig. A.1, it may be interesting to present a stationary solution of the problem, which will help in the understanding. The first calculations of Gail & Sedlmayr (1987b), Dominik et al. (1989) and the recent computations of Winters et al. (1994) and Winters (1994) have shown that a stationary solution of the problem is entirely determined by the choice of 4 stellar parameters: $M_\star$, the stellar mass; $L_\star$ the stellar luminosity; $\dot{M}_\star$, the stellar mass loss rate and $\epsilon_{\rm C}/\epsilon_{\rm O}$, the stellar carbon to oxygen abundance ratio. Figure A.2 presents some of the results obtained for the set of parameters given in Table A.1. These parameters have been chosen in order to approximate the observed spectrum and visibilities of the well–studied carbon star IRC+10216. In Fig. A.2 the radial structure of the envelope is shown. More precisely, the profiles of the following quantities are represented: $\rho$, the mass density; $\chi_{\rm H} = \int \chi_\nu H_\nu d\nu / \int H_\nu d\nu$ ($H_\nu$ is the monochromatic Eddington flux) the flux–mean of the dust extinction coefficient; $v$, the wind velocity; $c_{\rm T}$, the sound velocity; $v_{\rm esc}$, the escape velocity; $\alpha$, the radiative acceleration; $T^{\rm g}$ and $T^{\rm d}$, the gas and dust temperature, respectively.

Due to the decreasing temperature in the stellar atmosphere, an increasingly complex chemistry develops as the material outflow expands in the envelope (see Chap. 4 concerning the PAH chemistry for instance). Solving the chemical equations for the species present in the envelope provides estimates of their local densities and, consequently, of the gas composition. In the region near the star, which is free of dust, the hydrodynamic and

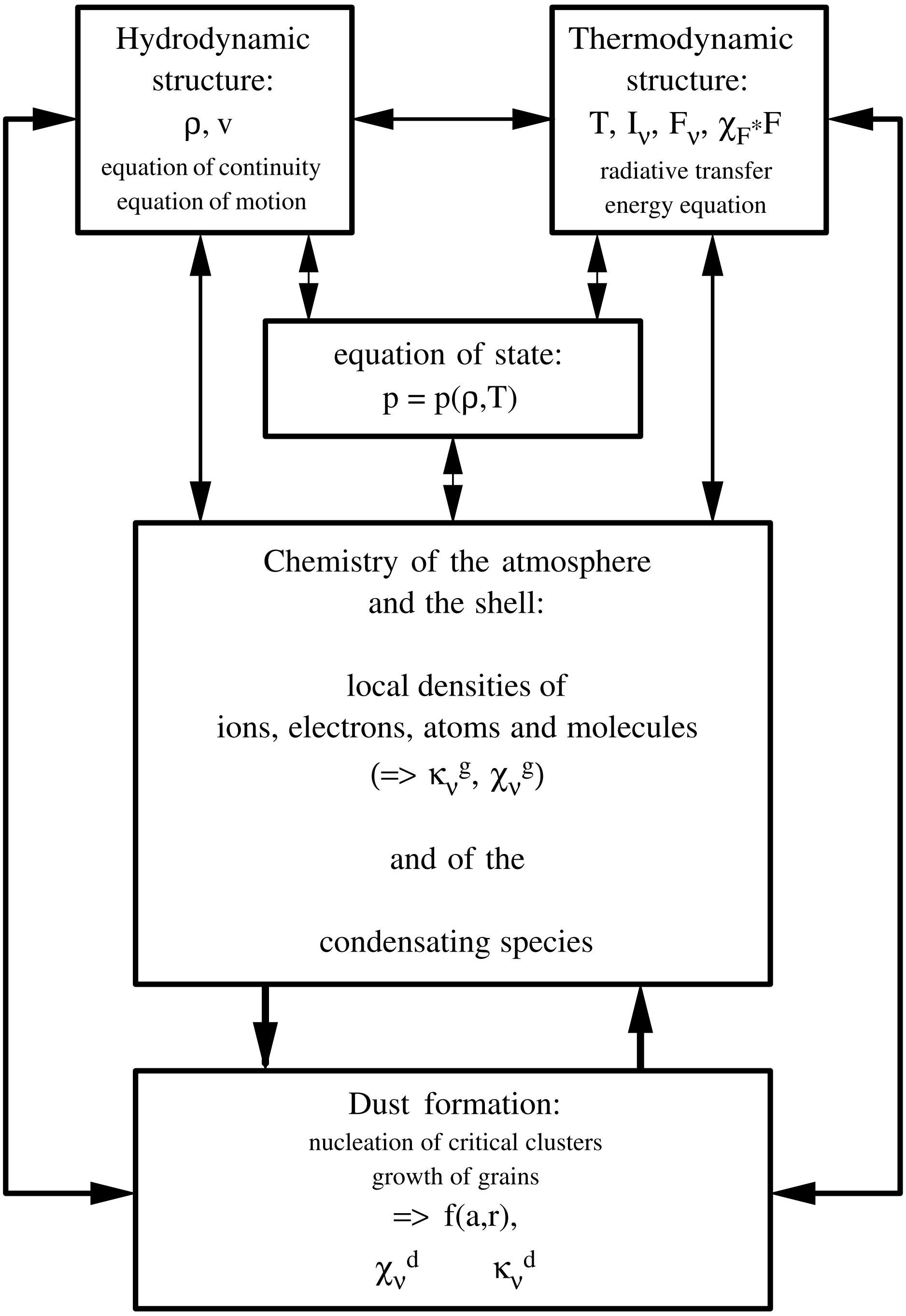


Figure A.1: Physical problem of dust forming circumstellar envelopes (from Winters 1994)

Table A.1: Stellar parameters for the model of IRC+10216.

| | |
|---|---|
| Mass | 0.7 $M_{\odot}$ |
| Luminosity | 2.4 $10^4$ $L_{\odot}$ |
| Mass loss rate | $8.10^{-5}$ $\dot{M}_{\odot}\mathrm{yr}^{-1}$ |
| Carbon to oxygen ratio | 1.40 |

thermodynamic structure of the envelope are strongly influenced by the gas density and composition since the transport of radiation through the atmosphere is entirely determined by the gas extinction coefficient, $\chi_{\nu}^{\rm g}$, and by the gas absorption coefficient, $\kappa_{\nu}^{\rm g}$. The situation changes dramatically when the temperature has dropped to a value such that dust begins to condense.

This process of dust nucleation involves some of the species forming in the inner envelope (e.g. small PAHs, see Chap. 4). Combining the densities of the condensing species into the equations for the dust nucleation rate and using the moment equations developed by Gail et al. (1984), Gail & Sedlmayr (1988) and Gauger et al. (1990) for the description of dust growth, leads to a complete determination of the dust component. The dust size–distribution f(a,r), which gives the density of dust particles with radius a in the size interval (a,a+da) at distance r from the star, can be calculated with the equations developed by Dominik et al. (1989). A picture of this size–distribution is presented in Fig. 5.1. The knowledge of the dust component enables calculation of the dust extinction coefficient, $\chi_{\nu}^{\rm d}$, and the dust absorption coefficient, $\kappa_{\nu}^{\rm d}$. The peak of the flux–mean extinction coefficient, $\chi_{\rm H}$, of the dust component between 2 and 3 stellar radii illustrates the massive formation and growth of dust particles in this region (see Fig. A.2).

Dust has a tremendous impact on the hydrodynamic structure of the stellar wind. After absorbing stellar radiation, dust particles indeed transfer the photon momentum to the gas phase by collision and hence give rise to acceleration of the circumstellar material. The profile of the acceleration factor, $\alpha$, presented in Fig. A.2 gives an impression of this mechanism. Exact knowledge of the hydrodynamic structure is gained by the solution of the equations of continuity and of motion, which provide the density $\rho$ and the velocity field $v$, respectively. In the region of dust formation, the wind velocity rapidly increases and exceeds the local velocity of sound and the local escape velocity in the first stellar radii before reaching its terminal velocity, whose value of some 20 km/s is confirmed by observations of the envelopes of C–stars.

Dust also plays a large role in the transfer of stellar radiation to the infrared spectral region. The infrared emission of dust grains is known to cause the observed infrared excess of the dust forming circumstellar shells. An exact calculation of the radiative transfer allows to determine the specific intensity, $I_{\nu}$, at each place in the envelope, and the various

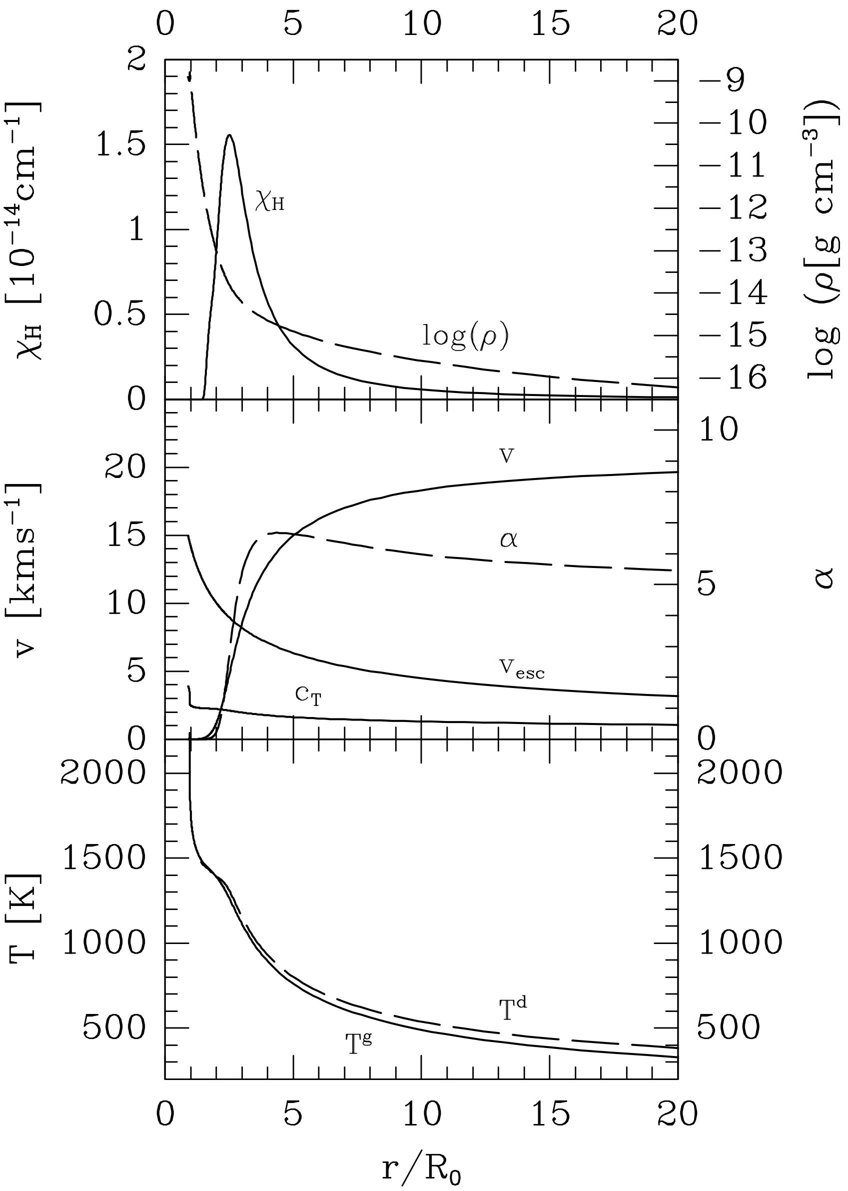


Figure A.2: Radial structure of the circumstellar shell of IRC+10216 (from Winters et al. 1994)
**Upper panel:** flux–mean extinction coefficient, $\chi_H$ of the dust component and logarithm of the mass density $\rho$;
**middle panel:** wind velocity $v$, velocity of sound $c_T$, escape velocity $v_{esc}$ and radiative acceleration in units of the local gravitational deceleration, $\alpha$;
**lower panel:** temperature of the gas, $T^g$, and of the dust component, $T^d$.

moments of the specific intensity: the mean intensity, $J_\nu$, which is represented in Fig. 4.4, and the energy flux, $F_\nu$, which is directly related to the observational results. Moreover, the thermalization of the photon energy from the stellar radiation within the internal degrees of freedom of dust grains ensures cooling of the circumstellar material and therefore influences the thermodynamic structure of the envelope. As a result of the large dust opacity, the dust particles decouple from the gas and reach a higher internal temperature than the gas phase.

Both the temperature and the density of the circumstellar material determine the pressure in the envelope via the equation of state. The pressure in turn acts on the chemical structure of the shell, which was mentioned at the beginning of the discussion. This last remark closes the present description of the model for dust–forming circumstellar envelopes. In this short view of the problem, the leading part of dust has been several times emphasized and justifies the appellation of dust driven wind encountered in the literature.

In contrast with the linear description in this Appendix, the system of equations used for modelling dust–driven stellar winds leads to a strongly coupled non–linear problem where hydrodynamics, thermodynamics and chemistry simultaneously interact with the complex process of dust formation and growth. Only a self–consistent approach such as that used in the model of Winters et al. (1994) and Winters (1994) can ensure a realistic picture of the local and global structure of dust–forming circumstellar envelopes.

# Appendix B

# Timescale discussion in circumstellar envelopes

The aim of this Appendix is to give the basis for a discussion on timescales in the study of non-equilibrium chemistry in circumstellar envelopes. The results presented here have been applied in Chap. 4 and Chap. 5

For a given chemical system containing $N$ reacting species the problem of non equilibrium chemistry consists in finding the solution of the system of equations describing the evolution with time of the density of each species. In the present case we consider a chemical system constituted by a Lagrange volume element moving outwards in a stellar wind. The system of equations can be written under the form of the following equations of continuity:

$$\frac{\partial n_{\rm i}}{\partial t} = -div(n_{\rm i}\mathbf{v}) + S_{\rm Gi}^{\rm chem} - S_{\rm Li}^{\rm chem} + S_{\rm Gi}^{\rm UV} - S_{\rm Li}^{\rm UV} \qquad i = 1, ..., N \tag{B.1}$$

where $n_{\rm i}$ denotes the particle density of species i and $\mathbf{v}$ the velocity field. The source terms $S_{\rm Gi}^{\rm chem}$ and $S_{\rm Li}^{\rm chem}$ represent the gain and loss by chemical reactions, respectively. $S_{\rm Gi}^{\rm UV}$ and $S_{\rm Li}^{\rm UV}$ account for gain and loss during photophysical processes. In the model of circumstellar envelopes we have considered in Chap. 4 and Chap. 5, spherical symmetry is assumed. For a volume element at distance $R$ from the star centre, Eq. (B.1) therefore reduces to:

$$\frac{\partial n_{\rm i}}{\partial t} = -2n_{\rm i}\frac{v}{R} - n_{\rm i}\frac{\partial v}{\partial R} + S_{\rm Gi}^{\rm chem} - S_{\rm Li}^{\rm chem} + S_{\rm Gi}^{\rm UV} - S_{\rm Li}^{\rm UV} \qquad i = 1, ..., N \tag{B.2}$$

By dividing each of the Eqs. (B.2) by $n_{\rm i}$ we obtain equations where each term can be expressed in units of s$^{-1}$, that is to say as the inverse of a timescale. Considering these timescales we recognize a timescale for dilution, $\tau^{\rm dil}$, a timescale for acceleration, $\tau^{\rm acc}$ and for each species a timescale for chemical reaction, $\tau_{\rm i}^{\rm chem}$, and a timescale for photophysical processes, $\tau_{\rm i}^{\rm UV}$, which we define as follows:

$$\tau^{\mathrm{dil}} = \frac{R}{v} \tag{B.3}$$

$$\tau^{\mathrm{acc}} = \left(\frac{\partial v}{\partial R}\right)^{-1} \tag{B.4}$$

$$\tau_{\mathrm{i}}^{\mathrm{chem}} = \min\left[\frac{n_{\mathrm{i}}}{S_{\mathrm{Gi}}^{\mathrm{chem}}}, \frac{n_{\mathrm{i}}}{S_{\mathrm{Li}}^{\mathrm{chem}}}\right] \tag{B.5}$$

$$\tau_{\mathrm{i}}^{\mathrm{UV}} = \min\left[\frac{n_{\mathrm{i}}}{S_{\mathrm{Gi}}^{\mathrm{UV}}}, \frac{n_{\mathrm{i}}}{S_{\mathrm{Li}}^{\mathrm{UV}}}\right] \tag{B.6}$$

A process is considered as being dominating when the corresponding timescale is the smallest. Physically, this means that the dominating process needs less time than the others to occur; it is the quickest process. Mathematically, if a timescale is the smallest one, the corresponding term in Eq. (B.2) is greater than the others, which can therefore be neglected. Hence, the dominating process provides the main contribution to the evolution of the density in Eq. (B.2).

An other interesting comparison to make is that between the timescale of a given chemical process ($\tau^{\mathrm{chem}}$ or $\tau^{\mathrm{UV}}$) and the timescales for dilution and for acceleration, which only concern the physical properties of the envelope. If one of the timescales $\tau^{\mathrm{dil}}$ or $\tau^{\mathrm{acc}}$ is lower than that for the considered chemical process, this chemical process cannot occur effectively. On the contrary, if the chemical timescale is lower than both $\tau^{\mathrm{dil}}$ and $\tau^{\mathrm{acc}}$, this chemical process does occur, even if it is not necessarily the dominating one.

To illustrate the discussion we have ploted in Figure B.1 the timescale for dilution, for acceleration and, in the case of pyrene molecule, the timescales for chemical formation and for photodestruction. These later timescales are simply stated as being equal to:

$$\begin{aligned} \tau_{\mathrm{pyr}}^{\mathrm{chem}} &= \frac{n_{\mathrm{pyr}}}{\sum_m k_m n_p n_q n_s} \\ \tau_{\mathrm{pyr}}^{\mathrm{UV}} &= \frac{n_{\mathrm{pyr}}}{k_{\mathrm{C_2H_2}}^{\mathrm{UV}}} \end{aligned} \tag{B.7}$$

where $k_{\mathrm{C_2H_2}}^{\mathrm{UV}}$ is the acetylene photoejection rate and the summation in the expression for $\tau_{\mathrm{pyr}}^{\mathrm{chem}}$ is over all chemical reactions $m$ in which the species $p$, $q$ and $s$ react to produce pyrene with the forward rate $k_m$.

Both the times $\tau^{\mathrm{dil}}$ and $\tau^{\mathrm{acc}}$ describe the physics of the envelope. Since these timescales directly depend on the wind velocity, they are indicator of the evolution of the physical properties of the stellar wind. The timescale for dilution is in most of the envelope the smaller of the two timescales and is therefore the more important. For that reason $\tau^{\mathrm{dil}}$ is often considered as the dynamical timescale in the envelope. This is the timescale used in Chap. 4 and Chap. 5 to describe the dynamical change.

Figure B.1 shows that the envelope can be divided in three different parts. For $R \leq 2R_\star$ the timescale for chemical formation is smaller than the timescales for dynamical

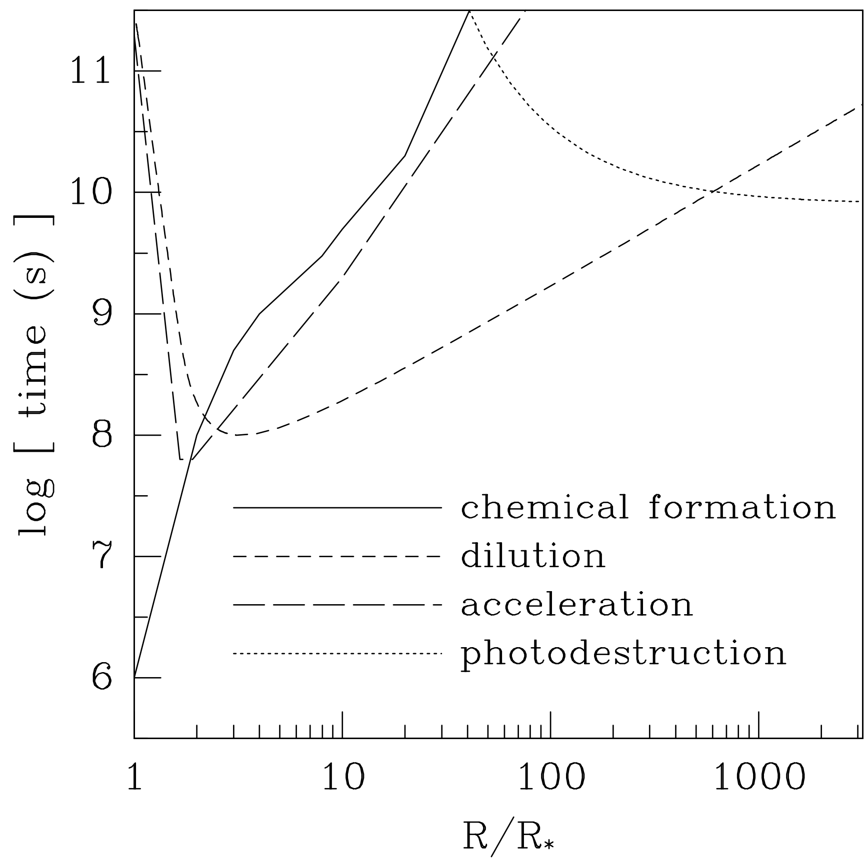


Figure B.1: Charactistical timescales in the envelope

evolution of the envelope and than the timescale for photodestruction. The growth of pyrene molecules does effectively take place in this region. For $2R_\star \le R \le 800R_\star$ the chemical reactions gradually freeze out due to the rapid dilution of the shell. Finally, for $R \ge 800R_\star$ the photodestruction becomes the more rapid process and leads to the disparition of pyrene molecules.

When many processes are simultaneously involved in the evolution of a system, timescale evaluation constitutes an useful method for estimating the dominating process and, hence, enables one to deduce the behaviour of the system without solving the equations describing its evolution.

# Appendix C

# Integrated absorption cross–sections of CO and $H_2$

Tables C.2 and C.1 present the integrated ultraviolet absorption cross–sections of the CO and $H_2$ molecules defined in Eq. (5.6). We have only retained the lines with a wavelenght greater than 912.7 Å (Lyman limit), which are used in the calculations of the molecular optical depths.

The integrated absorption cross–section, $\overline{\sigma^{\rm abs}_{\lambda_{v',v"}}}$, for the transition $v" \longrightarrow v'$ at wavelength $\lambda$ can be obtained from the band oscillator strength $f_{v',v"}$:

$$\overline{\sigma^{\rm abs}_{\lambda_{v',v"}}} = f_{v',v"}\ \lambda^2\ \left(\frac{\pi e^2}{m_{\rm e} c^2}\right) \tag{C.1}$$

The values for $f_{v',v"}$ of CO lines are taken from Eidelsberg et al. (1991, 1992). In fact, more recent data are available (Stark et al. 1991, 1992, 1993) but they are not expected to change much the overall rates (van Dishoeck 1994). The oscillators strenghts for the Lyman and Werner band system of $H_2$ are taken from Abgrall & Roueff (1989). The data in Tables C.2 and C.1 have been kindly provided to us by B. Patzer. For more detail the reader is refered to Patzer (1992).

Table C.1: Integrated absorption cross–sections of CO. Only the lines corresponding to the wavelenght $\lambda > 912.7$ Å (Lyman limit) are considered.

| $\lambda$ [Å] | $\overline{\sigma^{\rm abs}}$ [cm$^{-2}$] | $\lambda$ [Å] | $\overline{\sigma^{\rm abs}}$ [cm$^{-2}$] |
|---|---|---|---|
| 1150.534 | 5.28999 (-17) | 956.245 | 1.09000 (-16) |
| 1123.617 | 7.99999 (-18) | 950.047 | 1.75997 (-16) |
| 1099.044 | 3.99996 (-19) | 948.394 | 2.21997 (-17) |
| 1087.913 | 6.48001 (-16) | 946.293 | 6.03999 (-17) |
| 1076.079 | 3.73996 (-16) | 941.177 | 2.01997 (-16) |
| 1063.088 | 2.76998 (-17) | 940.203 | 1.67002 (-16) |
| 1051.714 | 2.42001 (-17) | 937.985 | 1.00003 (-19) |
| 1039.750 | 1.00005 (-19) | 935.673 | 2.92001 (-17) |
| 1029.295 | 4.00003 (-19) | 933.061 | 1.69899 (-16) |
| 1017.869 | 4.00001 (-19) | 931.663 | 9.26989 (-17) |
| 1010.921 | 4.00003 (-19) | 931.082 | 4.63001 (-17) |
| 1002.590 | 7.05997 (-17) | 930.069 | 4.86000 (-17) |
| 996.105 | 1.99999 (-18) | 928.666 | 5.09996 (-17) |
| 993.523 | 1.00002 (-19) | 925.818 | 1.23997 (-16) |
| 989.783 | 4.00000 (-18) | 924.639 | 3.89997 (-17) |
| 985.600 | 1.32000 (-16) | 922.765 | 4.76001 (-17) |
| 982.591 | 4.09998 (-18) | 920.149 | 2.11002 (-17) |
| 977.418 | 1.53997 (-17) | 919.219 | 2.11002 (-17) |
| 972.702 | 1.01004 (-16) | 917.281 | 1.69003 (-16) |
| 970.364 | 1.74997 (-16) | 915.979 | 5.88003 (-17) |
| 968.887 | 1.03004 (-16) | 915.734 | 1.47002 (-17) |
| 968.323 | 6.41999 (-17) | 913.675 | 1.99001 (-16) |
| 964.403 | 2.30000 (-17) | 913.436 | 1.24010 (-17) |
| 960.301 | 2.10004 (-18) | 912.712 | 2.48999 (-17) |

Table C.2: Integrated absorption cross–sections of $H_2$. Only the lines corresponding to the wavelenght $\lambda > 912.7$ Å (Lyman limit) are considered.

| Werner band system | | | |
|---|---|---|---|
| $\lambda$ [Å] | $\overline{\sigma^{\rm abs}}$ [cm$^{-2}$] | $\lambda$ [Å] | $\overline{\sigma^{\rm abs}}$ [cm$^{-2}$] |
| 1008.551 | 3.96068 (16) | 929.535 | 2.59975 (16) |
| 985.629 | 5.93195 (16) | 914.397 | 1.77583 (16) |
| 964.977 | 5.68597 (16) | 900.801 | 1.22075 (16) |
| 946.424 | 4.91456 (16) | 888.656 | 8.38630 (17) |

| Lyman band system | | | |
|---|---|---|---|
| $\lambda$ [Å] | $\overline{\sigma^{\rm abs}}$ [cm$^{-2}$] | $\lambda$ [Å] | $\overline{\sigma^{\rm abs}}$ [cm$^{-2}$] |
| 1108.130 | 1.84736 (17) | 981.443 | 1.79007 (16) |
| 1092.200 | 6.12285 (17) | 971.989 | 1.67215 (16) |
| 1077.142 | 1.23211 (16) | 962.980 | 1.06684 (16) |
| 1062.883 | 1.79955 (16) | 954.417 | 1.12856 (16) |
| 1049.367 | 2.24132 (16) | 946.174 | 1.10915 (17) |
| 1036.546 | 2.56722 (16) | 938.471 | 7.32641 (17) |
| 1024.376 | 2.69301 (16) | 931.065 | 8.43867 (17) |
| 1012.817 | 2.72336 (16) | 923.985 | 4.60873 (17) |
| 1001.828 | 2.39812 (16) | 917.250 | 4.54179 (17) |
| 991.384 | 2.26141 (16) | 910.820 | 2.78978 (17) |

# Bibliography

[Abgrall and Roueff 1989] Abgrall, H. and Roueff, E., 1989. Wavelengths, oscillator strengths and transition probabilities of the $H_2$ molecule for Lyman and Werner systems. *A&AS*, **78**, 313–328.

[Abgrall *et al.* 1991] Abgrall, H., Le Bourlot, J., Pineau des Forêts, G., Roueff, E., Flower, D. R., and Heck, L., 1991. Photodissociation of $H_2$ and the $H/H_2$ transition in interstellar clouds. *A&A*, **253**, 525–536.

[Abouelaziz *et al.* 1993] Abouelaziz, H., Gomet, J. C., Pasquerault, D., Rowe, B. R., and Mitchell, J. B. A., 1993. Measurements of $C_3H_3^+$, $C_5H_3^+$, $C_6H_6^+$, $C_7H_5^+$ and $C_{10}H_8^+$ dissociative recombination rate coefficients. *J. Chem. Phys.*, **99**, 237–243.

[Aitken 1981] Aitken, D. K., 1981. Spectrophotometry of dust. In Wynn-Williams, C. G. and Cruikshank, D. P., editors, *Infrared Astronomy*, pages 207–221.

[Allamandola 1991] Allamandola, L. J., 1991. PAHs in space: the evidence and implications. In Bussoletti, E. and Strazzulla, G., editors, *Solid–State Astrophysics*, pages 1–28. North–Holland.

[Allamandola *et al.* 1985] Allamandola, L. J., Tielens, A. G. G. M., and Barker, J. R., 1985. PAHs and the UIR bands: auto exhaust along the Milky Way ! *ApJ*, **290**, L25–L28.

[Allamandola *et al.* 1987] Allamandola, L. J., Tielens, A. G. G. M., and Barker, J. R., 1987. The IR emission feature: emission from PAH molecules and amorphous carbon particles. In Léger, A., d'Hendecourt, L. B., and Boccarra, N., editors, *Polycyclic Aromatic Hydrocarbons and Astrophysics*, pages 255–271. Reidel Publ. Comp.

[Allamandola *et al.* 1989] Allamandola, L. J., Tielens, A. G. G. M., and Barker, J. R., 1989. Interstellar PAHs: the IR emission bands, the excitation/emission mechanism, and the astrophysical implications. *ApJS*, **71**, 733–775.

[Allen 1973] Allen, C. W., 1973. *Astrophysical Quantities*. The Athlone Press, London.

[Anicich *et al.* 1986] Anicich, V. G., Wesley, T. H., and McEwan, M. J., 1986. Ion–Molecule Reaction of Hydrocarbon Ions in $C_2H_2$ and HCN. *J. Phys. Chem.*, **90**, 2446–2450.

[Avouris *et al.* 1977] Avouris, P., Gelbart, W. M., and El-Sayed, M. A., 1977. Nonradiative Electronic Relaxation under Collision-free Conditions. *Chem. Rev.*, **77**, 793–833.

[Barker 1983] Barker, J. R., 1983. Monte Carlo calculations on unimolecular reactions energy transfer, and IR-multiphoton decomposition. *Chem. Phys.*, **77**, 301–318.

[Barlow and Silk 1977] Barlow, M. J. and Silk, J., 1977. Graphite Grain Surface Reactions in Interstellar and Protostellar Environments. *ApJ*, **215**, 800–804.

[Bellamy 1966] Bellamy, L. J., 1966. *The Infrared Spectra of Complex Molecules.* Wiley, New–York.

[Benson 1976] Benson, S. W., 1976. *Thermochemical kinetics.* Wiley-Interscience.

[Bermudez and Chan 1986] Bermudez, G. and Chan, I. Y., 1986. Excitation and Fluorescence Spectra of Coronene in a jet. *J. Phys. Chem.*, **90**, 5029–5034.

[Birks 1970] Birks, J., 1970. *Photophysics of Aromatic Molecules.* Willey Interscience.

[Bishop and Cheung 1982] Bishop, D. M. and Cheung, L. M., 1982. Vibrational Contributions to Molecular Dipole Polarizabilities. *J. Phys. Chem. Ref. Data*, **11**, 119–133.

[Bohme 1992] Bohme, D. K., 1992. PAH and Fullerene Ions and Ion/Molecule Reactions in Interstellar and Circumstellar Chemistry. *Chem. Rev.*, **92**, 1487–1508.

[Bohme *et al.* 1982] Bohme, D. K., Rakshit, A. B., and Schiff, H. I., 1982. Reaction of $^{12}C^{+}$ with hydrocarbons at 296K: carbon–carbon bond formation. *Chem. Phys. Let.*, **93**, 592–597.

[Bohme *et al.* 1989] Bohme, D. K., Wlodek, S., and Wincel, H., 1989. Novel chemical role for polycyclic aromatic molecules in the synthesis of interstellar molecules. *ApJ*, **342**, L91–L93.

[Bohme *et al.* 1991] Bohme, D. K., Wlodek, S., Zimmermann, J. A., and Eyler, J. R., 1991. Formation of $C_{10}H_8^+$ from the benzene radical cation: a case for the growth of PAH ions by ion/molecule reactions in the gas phase ? *Int. J. Mass Spect. Ion Proc.*, **109**, 31–47.

[Borghesi *et al.* 1987] Borghesi, A., Bussoletti, E., and Colangi, L., 1987. amorphous carbon and the UIR bands. *ApJ*, **314**, 422–428.

[Bree *et al.* 1971] Bree, A., Kydd, R. A., Misra, T. N., and Vilkos, V. V. B., 1971. The fundamental frequencies of pyrene and pyrene–$d_{10}$. *Spectrochemica Acta*, **27A**, 2315–2332.

[Bregman *et al.* 1989] Bregman, J. D., Allamandola, L. J., Tielens, A. G. G. M., Geballe, T. R., and Witteborn, F. C., 1989. The IR emission bands: II. A spatial and spectral study of the Orion Bar. *ApJ*, **344**, 791–798.

[Brown *et al.* 1989] Brown, P. D., Duley, W. W., Jones, A. P., and Williams, D. A., 1989. HAC coated silicate grains and PAHs in diffuse clouds and low–velocity shocks. *MNRAS*, **241**, 753–767.

[Buch 1989] Buch, V., 1989. Direct photodissociation of CH bonds in PAHs: implications for the IR emission bands. *ApJ*, **343**, 208–211.

[Burke and Hollenbach 1983] Burke, J. R. and Hollenbach, D. J., 1983. The gas–grain interaction in the interstellar medium: thermal accomodation and trapping. *ApJ*, **265**, 223–234.

[Buss *et al.* 1990] Buss, R. H., Tielens, A. G. G. M., Cohen, M., Werner, M. W., Bregman, J. D., Witteborg, F. C., Rank, D., and Sandford, S. A., 1990. Hydrocarbon emission features in the infrared spectra of warm supergiants. *ApJ*, **365**, L23–L26.

[Buss *et al.* 1991] Buss, R. H., Tielens, A. G. G. M., and Snow, T. P., 1991. The mid–infrared spectrum of the carbon star HD 38218 and its possible relations to PAHs. *ApJ*, **372**, 281–290.

[Buss *et al.* 1993] Buss, R. H., Tielens, A. G. G. M., Cohen, M., Werner, M. W., Bregman, J. D., and Witteborg, F. C., 1993. Infrared spectra of transition objects and the composition and evolution of carbon dust. *ApJ*, **415**, 250–257.

[Cadwell *et al.* 1994] Cadwell, B. J., Wang, H., Feigelson, E. D., and Frenklach, M., 1994. Induced nucleation of carbon dust in red giants stars. *ApJ*, **429**, 285–299.

[Cherchneff 1991] Cherchneff, I., 1991. *PAH radiative properties and formation in carbon–rich stellar outflows*. PhD thesis, University of Michigan.

[Cherchneff 1995] Cherchneff, I., 1995. Forming Dust precursors in the inner envelopes of Carbon–rich AGB stars. *Ap&SS*, **224**, 379–382.

[Cherchneff *et al.* 1991] Cherchneff, I., Barker, J. R., and Tielens, A. G. G. M., 1991. PAH optical properties and contribution to the acceleration of stellar outflows. *ApJ*, **394**, 703–716.

[Cherchneff *et al.* 1992] Cherchneff, I., Barker, J. R., and Tielens, A. G. G. M., 1992. PAH formation in carbon–rich stellar envelopes. *ApJ*, **401**, 269–287.

[Cherchneff *et al.* 1993] Cherchneff, I., Glassgold, E., and Mamon, G. A., 1993. The Formation of Cyanopolyyne Molecules in IRC+10216. *ApJ*, **410**, 188–201.

[Chokski *et al.* 1988] Chokski, A., Tielens, A. G. G. M., Werner, M. W., and Castelaz, M. W., 1988. CII 158 micron and OI 63 micron observations of NGC 7023: a model for its photodissociation region. *ApJ*, **334**, 803–814.

[Cohen *et al.* 1985] Cohen, M., Tielens, A. G. G. M., and Allamandola, L., 1985. a new emission in IRAS spectra and the PAH spectrum. *ApJ*, **299**, L93–L97.

[Cohen *et al.* 1986] Cohen, M., Allamandola, L. J., Tielens, A. G. G. M., Bregman, J. D., Simpson, J. P., Witteborg, F. C., Wooden, D., and Rank, D., 1986. The infrared emission bands. I: Correlations studies and the dependence on C/O ratio. *ApJ*, **302**, 737–749.

[Cohen *et al.* 1989] Cohen, M., Tielens, A. G. G. M., Bregman, J. D., Witteborg, F. C., Rank, D., Allamandola, L., Wooden, D., and de Muizon, M., 1989. The infrared emission bands. III: Southern IRAS Sources. *ApJ*, **341**, 246–269.

[Csàszàr and Fogarasi 1989] Csàszàr, A. G. and Fogarasi, G., 1989. Theoretical Prediction of the Vibrational Spectrum, Geometry and Scaled Quantum Mechanical Force Field for Phenylacetylene. *J. Phys. Chem.*, **93**, 7644–7651.

[Cyvin 1982] Cyvin, S. J., 1982. Molecular vibrations of condensed Aromatic Hydrocarbons. *J. Mol. Struct.*, **79**, 423–442.

[Cyvin *et al.* 1979] Cyvin, S. J., Cyvin, B. N., Brunvoll, J., Whitmer, J. C., Klaboe, P., and Gustavsen, J. E., 1979. Condensed Aromatics. Part III. In-plane Molecular Vibrations of Pyrene. *Zeit. Naturforsch.*, **34a**, 876–886.

[Cyvin *et al.* 1984] Cyvin, B. N., Brunvoll, J., and Cyvin, S. J., 1984. a simple force-field approximation applied to the in-plane vibrations of some condensed aromatics. *Spec. Let.*, **17**(9), 559–567.

[De Frees *et al.* 1993] De Frees, D. J., Miller, M. D., D., T., Pauzat, F., and Ellinger, Y., 1993. Theoretical IR spectra of some model PAHs: effect of ionization. *ApJ*, **408**, 530–538.

[Désert *et al.* 1990] Désert, F. X., Boulanger, F., and Puget, J. L., 1990. Interstellar dust model for extinction and emission. *A&A*, **237**, 215–236.

[d'Hendecourt *et al.* 1986] d'Hendecourt, L. B., Léger, A., Olofsson, G., and Schmidt, W., 1986. The Red Rectangle: a possible case of visible luminescence from PAHs. *A&A*, **170**, 91–96.

[Dominik *et al.* 1989] Dominik, C., Gail, H. P., Sedlmayr, E., and Winters, J. M., 1989. The size distribution of dust particles in a dust–driven wind. *A&A*, **223**, 227–236.

[Donn 1968] Donn, B., 1968. Polycyclic hydrocarbons, Platt particles and interstellar extinction. *ApJ*, **152**, L129–L133.

[Donn *et al.* 1989] Donn, B. D., Allen, J. E., and Khanna, R. K., 1989. A critical assessement of the PAH hypothesis. In Allamandola, L. J. and Tielens, A. G. G. M., editors, *Interstellar Dust*, pages 181–189. Kluwer: Dordrecht.

[Draine 1978] Draine, B. T., 1978. Photoelectric Heating of interstellar gas. *ApJ*, **36**, 595–619.

[Draine 1979] Draine, B. T., 1979. On the Chemisputtering of Interstellar Graphite Grains. *ApJ*, **230**, 106–115.

[Duley 1987] Duley, W. W., 1987. Interstellar extinction and the composition of dust grains. *MNRAS*, **229**, 203–212.

[Duley 1988] Duley, W. W., 1988. Amorphous Carbon and Interstellar Emission Excesses. *MNRAS*, **234**, 61p–65p.

[Duley 1994] Duley, W., 1994. *Carbonaceous Grains*, chapter 5, pages 71–102. The Graduate Series in Astronomy. Institute of Physics Publishing, London.

[Duley and Jones 1990] Duley, W. W. and Jones, A. P., 1990. Simple Linear PAH molecules and the IR emission features: mothballs in the Orion Ridge ? *ApJ*, **351**, L49–L52.

[Duley and Williams 1981] Duley, W. W. and Williams, D. A., 1981. The infrared spectrum of interstellar dust: Surface fonctional groups on carbon. *MNRAS*, **196**, 269–274.

[Duley and Williams 1986] Duley, W. W. and Williams, D. A., 1986. PAH molecules and carbon dust in interstellar clouds. *MNRAS*, **219**, 859–864.

[Duley and Williams 1988] Duley, W. W. and Williams, D. A., 1988. Excess IR emission from large interstellar grains. *MNRAS*, **231**, 969–975.

[Dunbar 1986] Dunbar, R. C., 1986. Collisionless Relaxation of Photoexcited Benzene Ions. *Chem. Phys. Let.*, **125**, 543–546.

[Dunbar *et al.* 1987] Dunbar, R. C., Chen, J. H., So, H. Y., and Asamoto, B., 1987. Infrared fluorescence of photoexcited gas-phase ions by chopped-laser two-photon dissociation. *J. Chem. Phys.*, **86**, 2081–2086.

[Eidelsberg *et al.* 1991] Eidelsberg, M., Benayoun, J. J., Viala, Y., and Rostas, F., 1991. Atlas of the absorption/dissociation spectra of CO and its isotopes between 91.2 nm and 115.2 nm. *A&AS*, **90**, 231–282.

[Eidelsberg *et al.* 1992] Eidelsberg, M., Benayoun, J. J., Viala, Y., Rostas, F., Smith, P. L., Yoshino, K., Stark, G., and Shettle, C. A., 1992. Recalibration of the absorption/dissociation spectra of CO and its isotopes between 91 nm and 115 nm. *A&A*, **265**, 839–842.

[Eilfeld and Schmidt 1981] Eilfeld, P. and Schmidt, W., 1981. Resonance theoretical approach to the calculation of the first IP's of PAHs. *J. Elec. Spec. Rel. Phen.*, **24**, 101–120.

[Evans and Scully 1964] Evans, D. J. and Scully, D. B., 1964. Non-planar vibration frequencies of anthracene. *Spectr. Acta*, **20**, 891–900.

[Fahr and Stein 1989] Fahr, A. and Stein, S. E., 1989. Reactions of vinyl and phenyl radicals with ethyne, ethenen and benzene. In *22*$^{\mathrm{nd}}$ *Symposium (International) on Combustion*, pages 1023–1029. Pittsburgh: The Combustion Institute.

[Fischer *et al.* 1971] Fischer, S., Schlag, E. W., and Schneider, S., 1971. Communicating states models for ISC of isolated molecules. *Chem. Phys. Let.*, **11**, 583–588.

[Fleischer 1994] Fleischer, A. J., 1994. *Hydrodynamics and Dust Formation in the Circumstellar Shells of Miras and Long–Period Variables.* PhD thesis, Technische Universität, Berlin, FRG.

[Fleischer *et al.* 1992] Fleischer, A. J., Gauger, A., and Sedlmayr, E., 1992. Circumstellar Dust shells around Long–Period Variables. I. Dynamical models of C–stars including dust formation, growth and evaporation. *A&A*, **266**, 321–339.

[Flower *et al.* 1990] Flower, D. R., Heck, L., Pineau des Forêts, G., and Millar, T. J., 1990. The erosion of PAH molecules within shocks in dark clouds. *MNRAS*, **242**, 512–516.

[Forst 1973] Forst, W., 1973. *Theory of Unimolecular Reaction.* Ac. Press. New York.

[Frenklach and Feigelson 1989] Frenklach, M. and Feigelson, E. D., 1989. Formation of PAH molecules in circumstellar envelopes. *ApJ*, **341**, 372–384.

[Frenklach *et al.* 1984] Frenklach, M., Clary, D. W., Gardiner, W. C. J., and Stein, S. E., 1984. Detailed kinetic modeling of soot formation in shock–tube pyrolysis of acetylene. In *20*$^{\mathrm{th}}$ *Symposium (International) on Combustion*, pages 887–901. Pittsburgh: The Combustion Institute.

[Gail and Sedlmayr 1985] Gail, H. P. and Sedlmayr, E., 1985. Dust formation in stellar winds. II. Carbon condensation in stationary, sphrically expandind winds. *A&A*, **148**, 320–190.

[Gail and Sedlmayr 1987a] Gail, H.-P. and Sedlmayr, E., 1987. Dust formation in stellar winds. In Morfill, G. E. and Scholer, M., editors, *Physical Processes in Interstellar Clouds*, pages 275–303. D. Reidel Publ. Comp.

[Gail and Sedlmayr 1987b] Gail, H. P. and Sedlmayr, E., 1987. Dust formation in stellar winds. III. Self-consistent models for dust driven winds around C–stars. *A&A*, **171**, 197.

[Gail and Sedlmayr 1988] Gail, H. P. and Sedlmayr, E., 1988. Dust formation in stellar winds. IV. Heteromolecular carbon grain formation and growth. *A&A*, **206**, 153–168.

[Gail *et al.* 1984] Gail, H. P., Keller, R., and Sedlmayr, E., 1984. Dust formation in stellar winds. I. a rapid computational method and application to graphite condensation. *A&A*, **133**, 183–332.

[Gauger *et al.* 1990] Gauger, A., Gail, H.-P., and Sedlmayr, E., 1990. Dust formation, growth and evaporation in a cool pulsating circumstellar shell. *A&A*, **235**, 345–361.

[Geballe *et al.* 1989] Geballe, T. R., Tielens, A. G. G. M., Moorhouse, A., and Brand, P. W., 1989. Spatial variations of the 3 Micron Emission Features within UV-excited Nebulae: Photochemical Evolution of Interstellar PAHs. *ApJ*, **341**, 278–287.

[Geballe *et al.* 1992] Geballe, T. R., Tielens, A. G. G. M., Kwock, S., and Hrivnak, B. J., 1992. Unusual 3 micron emission features in three proto– planetary nebulae. *ApJ*, **387**, L89–L91.

[Giard *et al.* 1988] Giard, M., Pajot, F., Lamarre, J. M., Serra, G., Caux, E., Gispert, R., Léger, A., and Rouan, D., 1988. First detection of the aromatic 3.3 $\mu m$ feature in the diffuse emission of the galactic disk. *A&A*, **201**, L1–L4.

[Giard *et al.* 1994] Giard, M., Bernard, J. P., Normand, P., and Rouan, D., 1994. PAH destruction at ionization fronts. *A&A*, **291**, 239–249.

[Gillet *et al.* 1973] Gillet, F. C., Forrest, W., and Merrill, K. M., 1973. 8–13 micron spectra of NGC 7027, BD+30°3639, and NGC 6572. *ApJ*, **183**, 87–93.

[Glassgold and Huggins 1983] Glassgold, A. E. and Huggins, P. J., 1983. Atomic and Molecular hydrogen in the circumstellar envelope of late–type stars. *MNRAS*, **203**, 517–532.

[Glassgold *et al.* 1986] Glassgold, A. E., Lucas, R., and Omont, A., 1986. Molecular ions in the circumstellar envelope of IRC+10216. *A&A*, **157**, 35–48.

[Glassgold *et al.* 1987] Glassgold, A. E., Mamon, G. A., Omont, A., and Lucas, R., 1987. Photochemistry and molecular ions in carbon–rich circumstellar envelopes. *A&A*, **180**, 183–190.

[Goeres 1993] Goeres, A., 1993. The formation of PAHs in C–type star environments. *Rev.Mod.Astron.*, **6**, 165–177.

[Goeres and Sedlmayr 1992] Goeres, A. and Sedlmayr, E., 1992. The envelopes of R Coronae Borealis stars. I. A physical model of the decline events due to dust formation. *A&A*, **265**, 216–236.

[Gondhalekar *et al.* 1980] Gondhalekar, P. M., Phillips, A. P., and Wilson, R., 1980. Observations of the Interstellar Radiation Field from the S2/68 Sky–survey Telescope. *A&A*, **128**, 272–280.

[Habing 1968] Habing, H. J., 1968. The Interstellar Radiation Density between 912 Åand 2400 Å. *Bull.Astr.Inst.Neth.*, **19**, 421–431.

[Herbst 1991] Herbst, E., 1991. The in–situ formation of large molecules in dense interstellar clouds. *ApJ*, **133**, 133–140.

[Hermine 1994] Hermine, P., 1994. *Etude de molécules aromatiques polycycliques en jet supersonique par fluorescence induite par laser et applications astrophysiques.* PhD thesis, Université Paris–Sud.

[Hollenbach and McKee 1979] Hollenbach, D. and McKee, F., 1979. Molecule formation and infrared emission in fast interstellar shocks. I. Physical processes. *ApJS*, **41**, 555–592.

[Howe and Millar 1990] Howe, D. A. and Millar, T. J., 1990. The formation of carbon chain molecules in IRC+10216. *MNRAS*, **244**, 444–449.

[Hsieh *et al.* 1974] Hsieh, J. C., Huang, C. S., and Lim, E. C., 1974. Radiationless singlet deactivation in isolated large molecule. I. Naphthalene, naphthol, and naphthylamine. *J. Chem. Phys.*, **60**, 4345–4353.

[Huggins and Glassgold 1982] Huggins, P. J. and Glassgold, A. E., 1982. The Photochemistry of Carbon–Rich Circumstellar Shells. *ApJ*, **252**, 201–207.

[Huggins *et al.* 1984] Huggins, P. J., Glassgold, A. E., and Morris, M., 1984. CN and $C_2H$ in IRC+10216. *ApJ*, **279**, 284–290.

[Joblin 1992] Joblin, C., 1992. *Spectroscopie de molécules aromatiques. Test du modele PAH en astrophysique.* PhD thesis, Université Paris–7.

[Jochims *et al.* 1994] Jochims, H. W., Rűhl, E., Baumgärtel, H., Tobita, S., and Leach, S., 1994. Size effects on dissociation rates of PAH cations: laboratory studies and astrophysical implications. *ApJ*, **420**, 307–317.

[Jochims *et al.* 1995] Jochims, H. W., Baumgärtel, H., and Leach, S., 1995. Photoionization quantum yields of PAHs. *A&A*, **in preparation**.

[Johnson and Luttermoser 1987] Johnson, H. R. and Luttermoser, D. G., 1987. Ultraviolet spectra and chromospheres of cool carbon stars. *ApJ*, **314**, 329–340.

[Jura 1974] Jura, M., 1974. Formation and Destruction rates of interstellar $H_2$. *ApJ*, **191**, 375–379.

[Jura and Morris 1981] Jura, M. and Morris, M., 1981. Model for the circumstellar gas around $\alpha$ Orionis. *ApJ*, **251**, 181–189.

[Keller 1987] Keller, R., 1987. Polyaromatic hydrocarbons and the condensation of carbon in stellar winds. In Léger, A., d'Hendecourt, L., and Boccara, N., editors, *Polycyclic Aromatic Hydrocarbons and Astrophysics*, pages 387–397. Reidel Publ. Comp.

[Keller and Sedlmayr 1983] Keller, R. and Sedlmayr, E., 1983. Entstehung von Kohlenstaub in Sternhüllen. *Mitt. Astron. Ges.*, **60**, 312.

[Kiefer *et al.* 1985] Kiefer, J. H., Mizerka, L. J., Patel, M. R., and Wei, H. C., 1985. a Shock Tube Investigation of Major Pathways in the High–Temperature Pyrolysis of Benzene. *J. Phys. Chem.*, **89**, 2013–2019.

[King and So 1970] King, G. W. and So, S. P., 1970. Ethynylbenzene; The vibrational Spectra of Some Deuterated Isomers. *J. molec. Spectrosc.*, **36**, 468–487.

[Klippenstein *et al.* 1993] Klippenstein, S. J., Faulk, J. D., and Dunbar, R. C., 1993. a combined theoretical and experimental study of the dissociation for benzene cation. *J. Chem. Phys.*, **98**, 243–256.

[Klose 1992] Klose, S., 1992. Hydrogen chemisorption on a graphite surface. *A&A*, **260**, 321–328.

[Koch and Otto 1972] Koch, E. E. and Otto, A., 1972. Optical absorption of benzene vapour for photon energies from 6 eV to 35 eV. *Chem. Phys. Lett.*, **12**, 476–480.

[Koch *et al.* 1972] Koch, E. E., Otto, A., and Radler, E., 1972. The vacuum UV spectrum of naphthalene vapour for photon energies from 5 to 30 eV. *Chem. Phys. Lett.*, **16**, 131–135.

[Krüger *et al.* 1996] Krüger, D., Woitke, P., and Sedlmayr, E., 1996. a general multi–component method for the description of dust grain processing. *A&A*, **in press**.

[Langevin 1905] Langevin, M. P., 1905. Une formule fondamentale de théorie cinétique. *Ann. Chim. Phys. Ser. 8*, **5**, 245–288.

[Latter 1991] Latter, W. B., 1991. Large Molecule Production by Mass–losing Carbon Stars: The Primary Source of Interstellar PAHs ? *ApJ*, **377**, 187–191.

[Leach 1985] Leach, S., 1985. Molecular ions in Astrophysics and in the Laboratory. In Dierksen, G. H. e. a., editor, *Molecular Astrophysics*, pages 353–374. D. Reidel Publish. Comp.

[Leach 1986] Leach, S., 1986. The formation and Destruction of Doubly-charged PAH cations in the ISM. *J. Electr. Spect. Rel. Phen.*, **41**, 427–438.

[Leach 1987] Leach, S., 1987. Photophysics, Electronic Spectroscopy and Relaxation of Molecular Ions and Radicals with Special Reference to PAHs. In Léger, A., d'Hendecourt, L. B., and Boccarra, N., editors, *Polycyclic Aromatic Hydrocarbons and Astrophysics*, pages 99–127. Reidel Publ. Comp.

[Leach *et al.* 1989] Leach, S., Eland, J. H. D., and Price, S. D., 1989. Formation and Dissociation of Dications of Naphthalene Azulene and Related Heterocyclic Compounds. *J. Phys. Chem.*, **93**(22), 7575–7583.

[Lee and Wdowiak 1993a] Lee, W. and Wdowiak, T. J., 1993. Laboratory spectra of PAH ions and the interstellar extinction curve. *ApJ*, **410**, L127–L130.

[Lee and Wdowiak 1993b] Lee, W. and Wdowiak, T. J., 1993. Origin of the hydrocarbon component of carbonaceous chondrites: The star–meteorite connection. *ApJ*, **417**, L49–L51.

[Léger and d'Hendecourt 1985] Léger, A. and d'Hendecourt, L., 1985. are PAHs the carriers of the diffuse interstellar bands in the visible ? *A&A*, **146**, 81–85.

[Léger and Puget 1984] Léger, A. and Puget, J. L., 1984. Identification of the UIR features of interstellar dust ? *A&A*, **137**, L5–L8.

[Léger *et al.* 1988] Léger, A., Boissel, P., and d'Hendecourt, L., 1988. Predicted Fluorescence Mechanism in Highly Isolated Molecules: The Poincaré Fluorescence. *Phys. Rev. Let.*, **60**, 921–924.

[Léger *et al.* 1989a] Léger, A., Boissel, P., Desert, F. X., and d'Hendecourt, L., 1989. Photo–thermo–dissociation. *A&A*, **213**, 351–359.

[Léger *et al.* 1989b] Léger, A., d'Hendecourt, L., and Defourneau, D., 1989. Physics of IR emission by interstellar PAH molecules. *A&A*, **216**, 148–164.

[Lepp and Dalgarno 1988] Lepp, S. and Dalgarno, A., 1988. PAHs in interstellar chemistry. *ApJ*, **324**, 553–556.

[Lepp *et al.* 1988] Lepp, S., Dalgarno, A., van Dishoeck, E. F., and Black, J. H., 1988. Large molecules in diffuse interstellar clouds. *ApJ*, **329**, 418–429.

[Lias and Ausloos 1982]
Lias, S. G. and Ausloos, P., 1982. The reaction $C_3H_4^+(C_3H_4,H)C_6H_7^+$. *J. Chem. Phys.*, **77**, 2383–2386.

[Lim 1985] Lim, E. C., 1985. Excess Energy Dependence of Vibrational Relaxation and Photophysical Branching Ratios in Isolated Aromatic Molecules: Relevance to Vacuum Ultraviolet Photochemistry. In Mc Glynn, S. P., Findley, G. L., and Huebner, R. H., editors, *Photophysics and Photochemistry in the Vacuum Ultra-Violet*, pages 855–873. Dordrecht: Reidel.

[Lucy 1971] Lucy, L. B., 1971. The formation of resonance lines in extended atmospheres. *ApJ*, **163**, 95–110.

[Lucy 1976] Lucy, L. B., 1976. Mass loss by cool carbon stars. *ApJ*, **205**, 482–491.

[Mamon *et al.* 1987] Mamon, G. A., Glassgold, A. E., and Omont, A., 1987. Photochemistry and Molecular Ions in Oxygen–Rich Circumstellar Envelopes. *ApJ*, **323**, 306–315.

[Mamon *et al.* 1988] Mamon, G. A., Glassgold, A. E., and Huggins, P. J., 1988. The Photodissociation of CO in Circumstellar Envelopes. *ApJ*, **328**, 797–808.

[Mathis *et al.* 1977] Mathis, J. S., Rumpl, W., and Nordsieck, K. H., 1977. The size–distribution of interstellar grains. *ApJ*, **217**, 425–433.

[Mathis *et al.* 1978] Mathis, J. S., Metzger, P. S., and Panagia, N., 1978. Interstellar radiation field and dust temperature. *A&A*, **128**, 212–229.

[McCabe 1982] McCabe, E. M., 1982. Dust and molecules in the shells of carbon stars – the inverse greenhouse effect. *MNRAS*, **200**, 71–82.

[Miles and Sarre 1993] Miles, J. R. and Sarre, P. J., 1993. On the Diffuse Interstellar Bands. *J. Chem. Soc. Faraday Trans.*, **89**, 2269–2276.

[Millar 1992] Millar, T. J., 1992. The chemistry of PAH and fullerene molecules in interstellar clouds. *MNRAS*, **259**, 35p–39p.

[Millar and Herbst 1994] Millar, T. J. and Herbst, E., 1994. A new chemical model of the circumstellar envelope surrounding IRC +10216. *A&A*, **288**, 561–571.

[Millar *et al.* 1991] Millar, T. J., Rawlings, J. M. C., Bennet, A., Brown, P. D., and Charley, S. B., 1991. Gas phase reactions and rate coefficients for use in Astrophysics. *A&AS*, **87**, 585–619.

[Mitchell 1990] Mitchell, J. B. A., 1990. The dissociative recombination of molecular ions. *Phys. Reports*, **186**, 215–248.

[Morris and Jura 1983] Morris, M. and Jura, M., 1983. Molecular Self–Shielding in the Outflows from Late–type Stars. *ApJ*, **264**, 546–553.

[Nejad and Millar 1987] Nejad, L. A. M. and Millar, T. J., 1987. Chemical modelling of molecular sources V. IRC + 10216. *A&A*, **183**, 279–286.

[Nicovich and Ravishankara 1984] Nicovich, J. M. and Ravishankara, A. R., 1984. Reaction of Hydrogen Atom with Benzene: Kinetics and Mechanism. *J. Phys. Chem.*, **88**, 2534–2541.

[Omont 1986] Omont, A., 1986. Physics and chemistry of interstellar polycyclic aromatic molecules. *Astr. Astr.*, **164**, 159–178.

[Palmő *et al.* 1986] Palmő, K., Mannfors, B., and Pietilă, L. O., 1986. an out–of–plane force field for some benzene derivatives having unsaturated substituents. *Spectrochim. Acta*, **42A**, 1265–1276.

[Pantos *et al.* 1978] Pantos, E., Philis, J., and Bolovinos, A., 1978. The extinction Coefficient of Benzene Vapor in the Region 4.6 to 36 eV. *J. Mol. Spect.*, **72**, 36–43.

[Papoular *et al.* 1989] Papoular, R., Conard, J., Giuliano, M., and Mille, G., 1989. a coal model for the carriers of the UIR bands. *A&A*, **217**, 204–208.

[Patzer 1992] Patzer, B., 1992. Einfluß äußerer Strahlungsfelder auf die Chemie zirkumstellarer Staubhüllen. Master's thesis, Technische Universität, Berlin, FRG.

[Patzer *et al.* 1995] Patzer, A. B. C., Kőhler, T. M., and Sedlmayr, E., 1995. Primary Astrophysical Dust Formation: Laboratory Desiderata. *Planetary and Space Science*, **in press**.

[Pietilä *et al.* 1988] Pietilä, L. O., Mannfors, B., and Palmő, K., 1988. an in–plane force field for some benzene derivatives having unsaturated substituents. *Spectrochim. Acta*, **44A**(2), 141–156.

[Platt 1956] Platt, J. R., 1956. On the optical properties of interstellar dust. *ApJ*, **123**, 486–490.

[Pujet and Léger 1989] Pujet, J. L. and Léger, A., 1989. a new component of the interstellar Matter: small grains and Large Aromatic Molecules. *ARA&A*, **27**, 161–198.

[Pulay *et al.* 1981] Pulay, P., Fogarasi, G., and Boggs, J. E., 1981. Force field, dipole moment derivatives, and vibronic constants of benzene from a combination of experimental and *ab initio* quantum chemical information . *J. Chem. Phys.*, **74**, 3999–4014.

[Ridge 1986] Ridge, D. P., 1986. Capture collision therie. In Ausloos, P. and Lias, S. G., editors, *Structure/ Reactivity and Thermochemistry of Ions*, pages 15–22, Reidel Pub. Comp., Dordrecht.

[Robertson 1986] Robertson, J., 1986. amorphous carbon. *Advanced in Physics*, **35**, 317–371.

[Rouan *et al.* 1992] Rouan, D., Léger, A., Omont, A., and Giard, M., 1992. Physics of the rotation of a PAH molecule in interstellar environments. *A&A*, **253**, 498–514.

[Rouleau and Martin 1991] Rouleau, F. and Martin, P. G., 1991. Shape and Clustering Effects on the Optical Properties of Amorphous Carbon. *ApJ*, **377**, 526–540.

[Sakata *et al.* 1984] Sakata, A., Wada, S., Tanabe, T., and Onaka, T., 1984. IR spectrum of the laboratory–synthesized quenched carbonaceous composite (QCC): comparison with the UIR bands. *ApJ*, **287**, L51–L54.

[Sakata *et al.* 1987] Sakata, A., Wada, S., Tanabe, T., and Tokunaga, A. T., 1987. IR spectrum of the laboratory–synthesized quenched carbonaceous composite (QCC) II: a new identification of the 7.7 and 8.6 micron UIR band. *ApJ*, **320**, L63–L67.

[Salama and Allamandola 1991] Salama, F. and Allamandola, L. J., 1991. Electronic absorption spectroscopy of matrix-isolated PAH cations. I. The naphthalene cation. *J. Chem. Phys.*, **94**, 6964–6977.

[Salama and Allamandola 1992] Salama, F. and Allamandola, L. J., 1992. The UV and Visible spectrum of the PAH $C_{10}H_8^+$: possible contributions to the Diffuse Interstellar Bands and to the UV–Visible Extinction. *ApJ*, **395**, 301–306.

[Schutte *et al.* 1993] Schutte, W. A., Tielens, A. G. G. M., and Allamandola, L. J., 1993. Theoretical modeling of the IR fluorescence from interstellar PAHs. *ApJ*, **415**, 397–414.

[Sellgren 1984] Sellgren, K., 1984. The near IR continuum emission of visual reflection nebulae. *ApJ*, **277**, 397–414.

[Sellgren *et al.* 1985] Sellgren, K., Allamandola, L. J., Bregman, J. D., Werner, M. W., and Wooden, D. H., 1985. Emission features in the 4–13 micron Spectra of the Reflection Nebulae NGC 7023 and NGC 2023. *ApJ*, **299**, 416–423.

[Serra *et al.* 1992] Serra, G., Chaudret, B., Saillard, Y., Le Beuze, A., Rabaa, H., Ristorcelli, I., and Klotz, A., 1992. Organometallic chemistry in the interstellar medium. I. Are organometallic reactions efficient processes in astrochemistry ? . *A&A*, **260**, 489–493.

[Spears and Rice 1971] Spears, K. G. and Rice, S. A., 1971. Study of the Lifetimes of Individual Vibronic States of the Isolated Benzene Molecule. *J. Chem. Phys.*, **55**, 5561–5581.

[Spizer 1978] Spizer, L., 1978. *Physical Processes in the Interstellar Medium.* Wiley, New–York.

[Stark *et al.* 1991] Stark, G., Yoshino, K., Smith, P. L., Ito, K., and Parkinson, W. H., 1991. High–resolution absorption cross sections of carbon monoxide bands at 295 K between 91.7 and 100.4 nanometers. *ApJ*, **369**, 574–580.

[Stark *et al.* 1992] Stark, G., Smith, P. L., Ito, K., and Yoshino, K., 1992. High–resolution photoabsorption cross sections of $E^1\Pi - X^1\Sigma^+$ vibrational bands of $^{12}CO$ and $^{13}CO$. *ApJ*, **395**, 705–709.

[Stark *et al.* 1993] Stark, G., Yoshino, K., Smith, P. L., Esmond, J. R., Ito, K., and Stevens, M. H., 1993. High–resolution absorption cross section measurements of carbon monoxide at 20 K between 96.7 and 98.8 nanometers. *ApJ*, **410**, 837–842.

[Tielens 1990] Tielens, A. G. G. M., 1990. . In Watt, G. D. and Webster, A. S., editors, *Submillimeter Astronomy*, page 13. Kluwer: Dordrecht.

[Tielens and Hollenbach 1985a] Tielens, A. G. G. M. and Hollenbach, D. J., 1985. Photodissociation Regions. I. Basic Model. *ApJ*, **291**, 722–746.

[Tielens and Hollenbach 1985b] Tielens, A. G. G. M. and Hollenbach, D. J., 1985. Photodissociation Regions. II. A Model for Orion Photodissociation Region. *ApJ*, **291**, 747–754.

[Tielens *et al.* 1987] Tielens, A. G. G. M., Allamandola, L. J., Barker, J. R., and Cohen, M., 1987. The hydrogen coverage of interstellar PAHs. In Léger, A., d'Hendecourt, L. B., and Boccarra, N., editors, *Polycyclic Aromatic Hydrocarbons and Astrophysics*, pages 273–286. Dordrecht: Reidel.

[Tobita *et al.* 1992] Tobita, S., Meinke, M., Illenberger, E., Chritophorou, L. G., Baumgärtel, H., and Leach, S., 1992. PAHs: negative ion formation following low energy (0–15 eV) electron impact. *Chem. Phys.*, **161**, 501–508.

[Tobita *et al.* 1994] Tobita, S., Leach, S., Jochims, H. W., Rűhl, E., Illenberger, E., and Baumgärtel, H., 1994. Single and Double Ionization Potentials of PAHs and Fullerenes by Photon and Electron Impact. *Can. J. Phys.*, **72**, 1060–1069.

[van der Zwet 1987] van der Zwet, G. P., 1987. Possible Carriers of the Diffuse Interstellar Bands. In Léger, A., d'Hendecourt, L. B., and Boccarra, N., editors, *Polycyclic Aromatic Hydrocarbons and Astrophysics*, pages 351–366. Dordrecht: Reidel.

[van der Zwet and Allamandola 1985] van der Zwet, G. P. and Allamandola, L. J., 1985. PAHs and the diffuse interstellar bands. *A&A*, **146**, 76–80.

[van Dishoeck 1988] van Dishoeck, E. F., 1988. Photodissociation and Photoionization Processes. In Millar, T. J. and Williams, D. A., editors, *Rate Coefficients in Astrochemistry*, pages 49–72. Kluwer Acad. Publ.

[van Dishoeck 1994] van Dishoeck, E. F., 1994. Continous Molecular Opacities and Photodissociation. In Jørgensen, U. G., editor, *IAU Colloquium 146: Molecules in the Stellar Environment*, pages 223–233, Springer–Verlag, Berlin.

[Vestraete and Léger 1992] Vestraete, L. and Léger, A., 1992. The visible and ultraviolet absorption of large PAHs. *A&A*, **266**, 513–519.

[Vestraete *et al.* 1990] Vestraete, L., Léger, A., d'Hendecourt, L., Dutuit, O., and Defourneau, D., 1990. Ionization cross–section measurements for two PAH molecules: implication for the heating of diffuse interstellar gas. *A&A*, **237**, 436–444.

[Waters *et al.* 1989] Waters, L. B. F. M., Lamers, H. J. G. L. M., Snow, T. P., Mathlener, E., Trams, N. R., van Hoff, P. A. M., and Waelkens, C., 1989. Circumstellar dust around HR 4049: a critical test for theories of interstellar dust. *A&A*, **211**, 208–216.

[Wehrer *et al.* 1983] Wehrer, A., Wehrer, P., and Duval, X., 1983. Decomposition de l'acétylène, de l'éthylène et du benzène sur le carbone aux très hautes températures et sous de basses pressions. *Carbon*, **21**, 247–253.

[Werkhoven *et al.* 1975a] Werkhoven, C. J., Denum, T., Langelaar, J., Rettschnick, R. P. H., and Van Voorst, J. D. W., 1975. Energy dependence of the radiative and non-radiative decay constants of the S1 fluorescence of pyrene vapour. *Chem. Phys. Let.*, **32**, 328–331.

[Werkhoven *et al.* 1975b] Werkhoven, C. J., Denum, T., Langelaar, J., Rettschnick, R. P. H., and Van Voorst, J. D. W., 1975. Vibrational redistribution effects in the time resolved emission of isolated pyrene molecules. *Chem. Phys. Let.*, **30**, 504–509.

[Whitten and Rabinovitch 1963] Whitten, G. Z. and Rabinovitch, B. S., 1963. accurate and Facile Approximation for Vibrational Energy–Level Sums. *J. Chem. Phys.*, **38**, 2466–2473.

[Willner 1984] Willner, S. P., 1984. Observed spectral features of dust. In Kessler, M. F. and Phillips, J. P., editors, *Galactic and Extragalactic Infrared Spectroscopy*, pages 37–57. Reidel Publ. Comp.

[Willner *et al.* 1977] Willner, S. P., Soifer, B. T., Russell, R. W., Joyce, R. R., and Gillet, F. C., 1977. 2 to 8 micron Spectrophotometry of M82. *ApJ*, **217**, L121–L124.

[Winters 1994] Winters, J. M., 1994. *Internal structure and optical appearence of circumstellar dust shells around cool carbon giants.* PhD thesis, Technische Universität, Berlin, FRG.

[Winters *et al.* 1994] Winters, J. M., Dominik, C., and Sedlmayr, E., 1994. Theoretical spectra of circumstellar dust shells around carbon–rich asymptotic giant branch stars. *A&A*, **288**, 255–272.

[Witt and Johnson 1973] Witt, A. N. and Johnson, M. W., 1973. The interstellar radiation density between 1250 and 4250 Å. *ApJ*, **181**, 363–368.

[Woitke *et al.* 1993] Woitke, P., Dominik, C., and Sedlmayr, E., 1993. Dust destruction in the transition region between stellar wind and interstellar medium. *A&A*, **274**, 451–464.

[Wolfire *et al.* 1988] Wolfire, M., Tielens, A. G. G. M., and Hollenbach, D. J., 1988. Physical Conditions in Photodissociation Regions: Application to Galactic Nuclei. *ApJ*, **358**, 116–131.

[Woodward *et al.* 1989] Woodward, C. E., Pipher, J. L., Shure, M., Forrest, W. J., and Sellgren, K., 1989. Spectroscopic Images of NGC 7027 in the Near IR Dust Emission Feature. *ApJ*, **342**, 860–870.

# Danksagung

Mein größter Dank gilt meinen beiden Lehrern: Prof. E. Sedlmayr, der mich vor 4 Jahre in seine Arbeitsgruppe aufnahm und mir die Gelegenheit gab, an einem großen Forschungsprojekt teilzunehmen und dabei viel Spaß zu haben und Dr. S. Leach, der mit Kompetenz, Interesse und Geduld meine Arbeit betreute und mir erlaubte, seine Erfahrung und ständige Hilfbereitschaft zu genießen.

Priv. Doz. Dr. J. P. Kaufmann bin ich sehr dankbar für unsere zahlreichen Diskusionnen und für das Erstellen des Zweitgutachtens.

Des weiteren danke ich Prof. W. Richter, der sich bereit erklärte, den Prüfungvorsitz zu übernehmen sowie Prof. P. Bréchignac für die Erstellung eines Berichtes für die Universität Paris-Sud.

Allen Mitarbeiterinnen und Mitarbeitern des Institutes möchte ich für die schönen 4 Jahre im 8. Stock des Physikgebäude danken. Ich denke da besonders an Holger, der vor 4 Jahre mein erster Ansprechpartner war, an Uwe für seine freundliche Unterstützung und Hilfbereitschaft, an Jan-Martin für seine große Hilfe und für die Berechnungen, die er für mich erstellt hat, an Beate und Daniel für unsere Zusammenarbeit über die Chemie der zirkumstellaren Hüllen und an Jürgen, Carsten S., Peter, Kyung, Beate, Daniel, Carsten D., Achim für die fachlichen Unterhaltungen und noch mehr für die *unfachlichen* und für unsere gemeinsamen Erlebnisse. Axel danke ich noch zusätzlich für die deutsche Übersetzung des Abstracts und Christine für die nette Stimmung im Zimmer PN 803.

Großen Dank schulde ich auch Dr. A. Canossa aus Rennes, Dr. G. Pineau des Forêts aus Paris-Meudon, Prof. H. Baumgärtel, Dr. H. W. Jochims aus Berlin für ihr Interesse und ihre Anregungen, sowie Dr. C. Joblin und Dr. P. Hermine, die mir ihre experimentellen Ergebnisse zur Verfügung gestellt haben.

# Lebenslauf

Persönliche Daten

| | |
|---|---|
| geboren am | 13. Juni 1966 in Oran (Algerien) |
| Familienstand | verheiratet, 1 Kind |
| Staatsangehörigkeit | französisch |
| Eltern | Jean und Odette Allain |

Zivildienst

| | |
|---|---|
| 1989-1991 | Lehrer für Physik und Chemie am Französischen Gymnasium in Berlin |

Ausbildungsdaten

| | |
|---|---|
| 1981-1984 | Gymnasium Gaspart Monge in Nantes |
| Juni 1984 | Baccalauréat C (Abitur mit Schwerpunkt Mathematik und Physik) |
| 1984-1986 | 'Classes préparatoires' in Nantes (französische Vorbereitungsklasse für die Hochschule) |
| 1986-1992 | *Ecole Normale Supérieure de Cachan* (Hochschule für Wissenschaft und Unterricht) |
| 1986-1987 | 'Licence de physique' an der Universität von Paris 11 |
| 1987-1988 | 'Maîtrise de physique' an der Universität von Paris 11 |
| 1988-1989 | 'Agrégation de physique' (Erstes Staatsexamen der Lehramtsprüfung) |
| 1891-1992 | 'Diplôme d'étude approfondie' Thema: Astrophysik an der *Observatoire de Meudon* (Universität von Paris 11) Beendung der Diplomarbeit am Institut für Astronomie und Astrophysik an der Technischen Universität Berlin |

Berufliche Werdegang

| | |
|---|---|
| 1991-1992 | Wissenschaftlicher Assistent an den 'Classes Préparatoires' in Paris (Lycée Lakanal) |
| 1992-1995 | Wissenschaftlischer Mitarbeiter am *Département Atomes et Molécules en Astrophysique* (DAMAp) an der *Observatoire de Meudon* Zusammenarbeit mit der Arbeitsgruppe von Professor Sedlmayr am Institut für Astronomie und Astrophysik an der Technischen Universität Berlin |
| 1992-1995 | Zusammenarbeit mit der physikalischen Abteilung des naturwissentschaflichen Museums *Palais de la Découverte* in Paris und mit der Abteilung Spektrum des *Museums für Verkehr und Technik* in Berlin |